NASA Contractor Report 165813

NASA-CR-165813
19820008197

TURBOPROP CARGO AIRCRAFT SYSTEMS STUDY

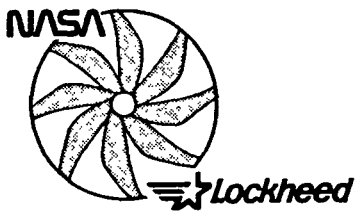

J.C. Muehlbauer; J.G. Hewell, Jr.;
S.P. Lindenbaum; C.C. Randall;
N. Searle; F.R. Stone, Jr.

LOCKHEED-GEORGIA COMPANY
A Division of Lockheed Corporation
Marietta, Georgia

Contract No. NAS1-15708
NOVEMBER 1981

National Aeronautics and
Space Administration

Langley Research Center
Hampton, Virginia 23665

Lewis Research Center
Cleveland, Ohio 44135

NASA Contractor Report 165813

TURBOPROP CARGO AIRCRAFT SYSTEMS STUDY

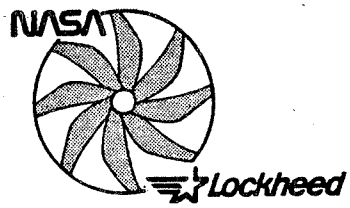

J.C. Muehlbauer; J.G. Hewell, Jr.;
S.P. Lindenbaum; C.C. Randall;
N. Searle; F.R. Stone, Jr.

LOCKHEED-GEORGIA COMPANY
A Division of Lockheed Corporation
Marietta, Georgia

Contract No. NAS1-15708
NOVEMBER 1981

NASA
National Aeronautics and
Space Administration

Langley Research Center
Hampton, Virginia 23665

Lewis Research Center
Cleveland, Ohio 44135

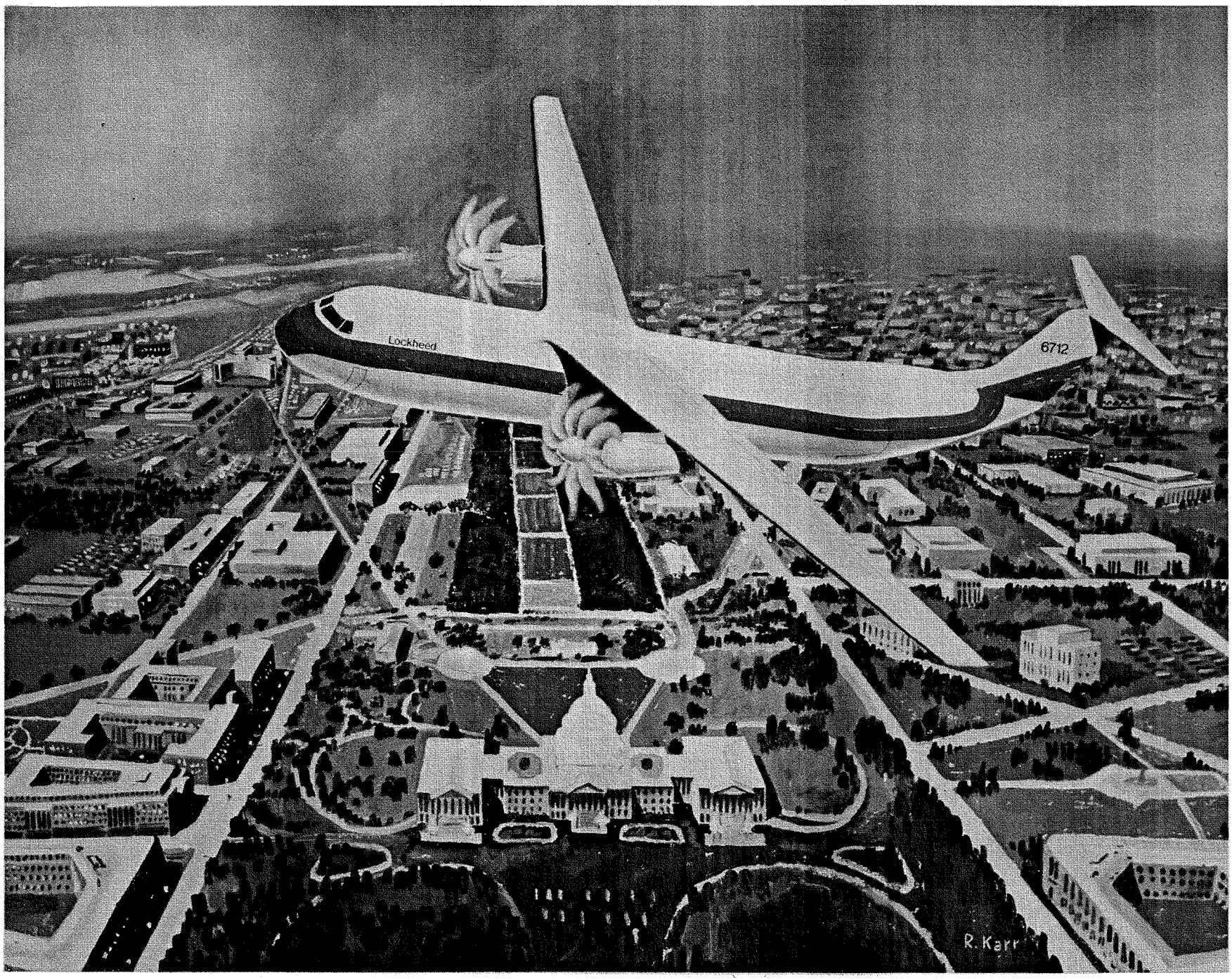
Lockheed
6712
R. Karr

FOREWORD

This report presents the results of a study on Turboprop Cargo Aircraft Systems by the Lockheed-Georgia Company for the National Aeronautics and Space Administration Langley Research Center at Hampton, Virginia and Lewis Research Center in Cleveland, Ohio.

This study was jointly supported by NASA Contract No. NAS1-15708 and by Lockheed's Independent Research and Development Program. The latter was used to assemble propulsion data bases for turboshaft (Appendix E) and turbofan (Appendix J) engines, to develop the noise methodology (Appendix C) used in the aircraft parametric studies, and to define the competitive turbofan-powered aircraft (Reference Turbofan Aircraft Studies Section).

Mr. Atwood R. Heath, Jr. served as the NASA-Langley technical monitor of this study until his retirement in December 1979. He has been ably succeeded by Mr. S. Jack Morris. During 1981, Mr. Gerald A. Kraft of NASA-Lewis served as a co-monitor.

Dr. John C. Muehlbauer directed the Lockheed effort on this study which was performed as part of a continuing preliminary design investigation of new aircraft concepts by the Lockheed-Georgia Company's Advanced Concepts Department - Mr. Roy H. Lange, Manager. Other major Lockheed contributors to this study were:

C. Lee Bowden, Jr.	William A. French	James G. Hewell, Jr.
Stephen P. Lindenbaum	Robert T. Meyer	R. Dennis O'Brien
Anthony P. Pennock	Charles C. Randall	Norm Searle
R. Ernest Stephens	F. Robert Stone, Jr.	Sterling G. Thompson
James E. Viney	L. Richard Woodward	Carl E. Izurieta

The Hamilton Standard Division of United Technologies Corporation, under subcontract to Lockheed, provided data on their advanced propeller concept - the propfan, and furnished the propeller noise levels of the selected aircraft for the prediction correlation discussed in Appendix G. Mr. Bernard S. Gatzen served as the Hamilton Standard study manager.

Special recognition and our appreciation are extended to the Commercial Products Division of Pratt & Whitney Aircraft Company for their cooperation and contributions concerning the turboshaft and turbofan engines used in this study.

Numbers contained in this report are in both SI and customary units, with the former stated first and the latter in parentheses. All of the calculations were made in the customary system of units and then converted to SI units.

TABLE OF CONTENTS

TABLE OF CONTENTS (CONT'D)

TABLE OF CONTENTS (CONT'D)

LIST OF FIGURES

LIST OF FIGURES (Cont'd)

LIST OF FIGURES (Cont'd)

LIST OF FIGURES (Cont'd)

LIST OF FIGURES (Cont'd)

LIST OF FIGURES (Cont'd)

LIST OF FIGURES (Cont'd)

LIST OF FIGURES (Cont'd)

LIST OF FIGURES (Cont'd)

LIST OF FIGURES (Cont'd)

LIST OF FIGURES (Cont'd)

LIST OF FIGURES (Cont'd)

LIST OF TABLES

LIST OF TABLES (Cont'd)

LIST OF TABLES (Cont'd)

SUMMARY

Future air transportation faces two serious threats: the rising cost and uncertain availability of fuel and curtailed operations due to noise regulations around airports. This report presents the results of a Lockheed study of an advanced turboprop (propfan) propulsion system concept that has been proposed as a means of reducing the impact of these two threats. The propfan is a highly-loaded, multi-blade turboprop system that incorporates advanced aerodynamic and structures technology in the propeller to provide high aerodynamic efficiency and low noise at flight speeds up to 0.8 Mach number for altitudes of 9.1 km (30,000 ft) and above.

Current federal regulations specify that noise certification measurements for aircraft be taken at three discrete locations for a type of flight profile that is considerably different from that typically flown in normal commercial operation. Consequently, two aircraft may satisfy the regulations equally, but they may be perceived by the neighboring community as radically different, because one is heard throughout a much larger area around the airport than the other. The extent of the area affected by the aircraft noise at a specified or higher level, the noiseprint area, is probably a better measure than the federal regulations for determining if a new aircraft will be a quiet neighbor that will not face operational curfews due to noise. This is not a recommendation that aircraft noiseprint areas be incorporated into any federal regulations; such action is unnecessary because public and commercial demands will force aircraft manufacturers to minimize noiseprint areas in the design of future transport aircraft if they are to be bought and flown.

The objective of this study was to explore the effects of using advanced turboprop propulsion systems to reduce the fuel consumption and direct operating costs of cargo aircraft and to determine the impact of these systems on aircraft noise and noiseprints around a terminal area. To accomplish this, parametric variations of aircraft and propeller characteristics were investigated to determine their effects on noiseprint areas, fuel consumption, and direct operating costs (DOC). From these results, three aircraft designs were selected and subjected to design refinements and sensitivity analyses. Three competitive turbofan aircraft were also defined from parametric studies to provide a basis for comparing the two types of propulsion.

That comparison showed that advanced turboprop aircraft offer the potential for impressive performance benefits relative to advanced turbofan aircraft. The turboprop aircraft experienced a fuel saving of 17 to 21 percent, better fuel efficiency of 21 to 26 percent, and lower DOCs by 8 to 15 percent. Equally significant, 20 to 25 percent shorter field lengths of the turboprop aircraft mean that they can service small airports that are inaccessible to turbofan aircraft. Relative to current turbofan aircraft, the fuel saving can be as high as 40 percent.

Noisewise, both the turboprop and turbofan aircraft easily comply with current regulations. The turboprop aircraft have smaller noiseprint areas at a 90 EPNdB level than the turbofan aircraft, approximately equal areas at 80 EPNdB, but larger areas at 70 EPNdB. The latter two levels bracket the range that is typically suggested as low enough for curfew-free operation.

Several other results were identified:

- Accuracy of the predicted noise levels is critical to the study results. Sensitivity study results show that a 3-dB increase in the predicted noise levels of the aircraft produces 100 and 40 percent increases in the noiseprints for the turboprop and turbofan aircraft, respectively.

- Operation at cruise Mach numbers below 0.8 becomes increasingly attractive as fuel price increases and becomes a greater percentage of aircraft direct operating cost.

- A propeller speed of about 229 m/s (750 fps) provides a compromise for minimizing cost and noiseprint. Parametric study results show that propeller speeds greater than 229 m/s (750 ft/s) offer only minimal reductions in operating costs while substantially increasing the noiseprint area. Lower speeds offer slightly smaller noiseprints but at severe economic penalties.

- An installed sea-level disk loading* of about 402 kW/m^2 (50 hp/ft^2) for the propeller gives aircraft designs that effectively compromise the conflicting design goals to minimize noiseprint area and direct operating cost. At lower values, the propeller diameters become excessively large and the aircraft are more expensive to operate. Conversely, with higher values the aircraft noiseprints become large.

- Changing the takeoff climb procedure produced greater noiseprint reductions for the turboprop aircraft than for the competitive turbofan aircraft. Noiseprints for the turboprop aircraft were reduced by 40 to 60 perceent, while those for the turbofan aircraft dropped by less than 20 percent. The turboprop aircraft benefits because of its better takeoff power features.

- The effect on noiseprints of reducing the propeller tip speed on takeoff is dependent upon the noise level defining the noiseprint. Reducing the propeller tip speed during takeoff climb from 229 m/s (750 ft/s) to 204 m/s (670 ft/s), increased the 90-EPNdB noiseprint by 2.4 percent but decreased the 80 and 70-EPNdB noiseprints by 17.5 and 36.7 percent, respectively.

- An advanced turboprop aircraft can serve as a joint civil/military airlifter with minimal modifications and penalties. A turboprop aircraft, when modified to meet the C-X requirements, experiences less than a 12.6 percent penalty in block fuel, ramp weight, and costs.

Considerable research and development will be required before an advanced turboprop propulsion system can be flown on a new aircraft in the forseeable future. New propulsion systems typically require a minimum of five to seven years for technology development and demonstration. Currently, plans are just being prepared to develop a turboshaft engine and gearbox of the size required. With there being less than five years between now and 1985, the 1985 technology level for the system, as specified in a guideline for this study, is not likely to be attained. However, every effort should be made to accelerate all propfan-related technology development so that it will be available as soon as possible for commercial applications because of the potential fuel saving.

Several specific recommendations are made to overcome shortcomings encountered during this study and to provide design improvements suggested by some of the study results. These recommendations include: a determination of propeller effects on wing aerodynamics and structure, verification of propulsion system performance and noise characteristics by an engine manufacturer, initiation of design studies for large-size turboshaft engines and gearboxes, establishment of desired noise levels and areas for existing airports, and assessment of military applications.

*The corresponding disk loading during cruise is about one half the value at sea level.

INTRODUCTION

Future air cargo faces two serious threats: the rising cost and uncertain availability of fuel and restricted airport use through noise regulations which may include night time curfews.

An advanced turboprop (propfan) propulsion system concept has been proposed* as a means of reducing the possible impact of these threats to cargo carried in new aircraft, and is now being investigated as part of the NASA Aircraft Energy Efficiency program. The propfan concept, as described by Dugan et al.** and shown in Figure 1, is a highly-loaded, multi-blade turboprop system that incorporates advanced aerodynamics and structures technology that has largely been developed for other aircraft propulsion components to achieve high aerodynamic efficiency and low noise levels at flight speeds up to 0.8 Mach number for altitudes of 9.1 km (30,000 ft) and above. For example, swept leading edges are used on the wings of high-speed transport aircraft to improve performance; this aerodynamic concept is being applied to the propfan blade. The swept blade shape and the integrated shape of the spinner and nacelle combine to produce a propulsion efficiency that is projected in Figure 2 to be higher than that of typical high-bypass-ratio turbofan engines.

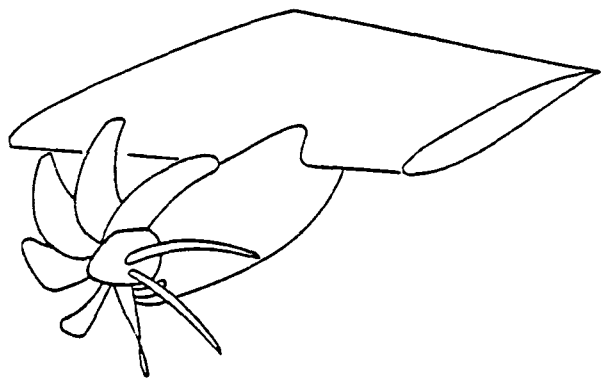

Figure 1. Propfan Propulsion System

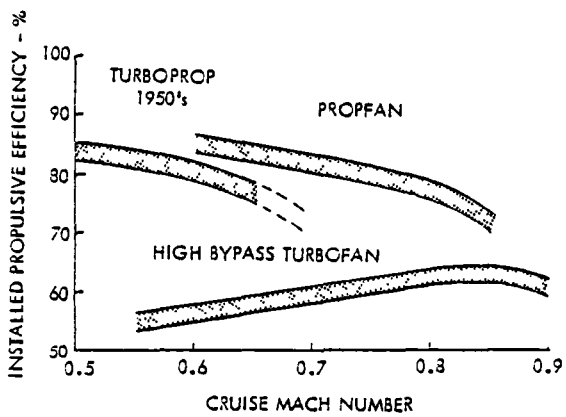

Figure 2. Comparison of Cruise Efficiencies for Different Types of Aircraft Propulsion

---

* C. Rohrbach and F. B. Metzer, "The Prop-fan - A New Look in Propulsors," AIAA Paper 75-1208, Hamilton Standard, October 1975 (Ref. 1)

A. H. Jackson, Jr. and B. S. Gatzen, "Multi-Mission Uses for Prop-fan Propulsion," AGARD Paper, Hamilton Standard, September 1976 (Ref. 2)

B. S. Gatzen and S. M. Hudson, "General Characteristics of Fuel Conservative Prop-fan Propulsion System," SAE Paper 751085, Hamilton Standard and Detroit Diesel Allison, November 1975 (Ref. 3)

** J. F. Dugan, Jr., B. S. Gatzen and W. M. Adamson, "Prop-fan Propulsion - Its Status and Potential," SAE Paper 780995, NASA-Lewis and Hamilton Standard, November 1978 (Ref. 4)

Numerous aircraft system studies* from as early as 1974 have predicted that the propfan system will reduce fuel consumption by 15 to 30 percent compared with aircraft equipped with turbofan engines of equivalent technology. Subsequently, since 1976, research programs have been underway to analyze the propfan and to establish a data base through wind-tunnel tests on several models.**

More recently, attention has been focused on the noise characteristics of this advanced turboprop.‡ Analytical noise prediction methods, acoustic test results of scale models, and aircraft studies show that the noise of propfan-powered aircraft will be below the levels specified by the Federal Aviation Regulations‡‡ (FAR)+ for new certified aircraft. Figure 3 by Dugan et al[4] compares the regulatory requirements at the three measuring points with the noise levels of current wide-body transports and with those expected from a four-engine, propfan aircraft.++

---

* E. F. Kraus and J. C. Van Abkoude, "Cost/Benefit Tradeoffs for Reducing the Energy Consumption of the Commercial Air Transportation System," NASA CR-137923, 137924, 137925, Douglas Aircraft, June 1976 (Ref. 5)

J. P. Hopkins and H. E. Wharton, "Study of the Cost/Benefit Tradeoffs for Reducing the Energy Consumption of the Commercial Air Transportation System," NASA CR-137926, 137927, Lockheed-California, August 1976 (Ref. 6)

"Energy Consumption Characteristics of Transports Using the Prop-fan Concept," NASA CR-137937, 137938, Boeing Commercial Airplane Co., October 1976 (Ref. 7)

J. D. Revell and R. H. Tullis, "Fuel Conservation Merits of Advanced Turboprop Transport Aircraft," NASA CR-152096, Lockheed-California, August 1977 (Ref. 8)

** C. Rohrbach, "A Report on the Aerodynamic Design and Wind Tunnel Test of a Prop-fan Model," AIAA Paper 76-667, Hamilton Standard, July 1976 (Ref. 9)

D. C. Mikkelson et al, "Design and Performance of Energy Efficient Propeller for Mach 0.8 Cruise," SAE Paper 770458, NASA-Lewis, 1977 (Ref. 10)

J. F. Dugan, D. P. Bencze, and L. F. Williams, "Advanced Turboprop Technology Development," AIAA Paper 77-1223, NASA-Lewis and Ames, August 1977 (Ref. 11)

J. A. Baum et al, "Prop-fan Data Support Study," NASA CR-152141, Hamilton Standard, February 1978 (Ref. 12)

H. R. Welge and J. P. Crowder, "Simulated Propeller Slipstream Effects on a Supercritical Wing," NASA CR-152138, Douglas Aircraft, June 1978 (Ref. 13)

M. L. Boctor et al, "An Analysis of Prop-fan/Airframe Aerodynamic Integration," NASA CR-152186, Boeing Commercial Airplane Co., October 1978 (Ref. 14)

J. V. Bowles, T. L. Galloway and L. J. Williams, "Turboprop/Propfan Performance and Installation Considerations for Advanced Transport Aircraft," SAE Paper 780996, NASA-Ames, November 1978 (Ref. 15)

D. P. Bencze, R. C. Smith, H. R. Welge, and J. P. Crowder, "Propeller Slipstream/Wing Interaction at M = 0.8," SAE Paper 780997, NASA-Ames and Douglas Aircraft, November 1978 (Ref. 16)

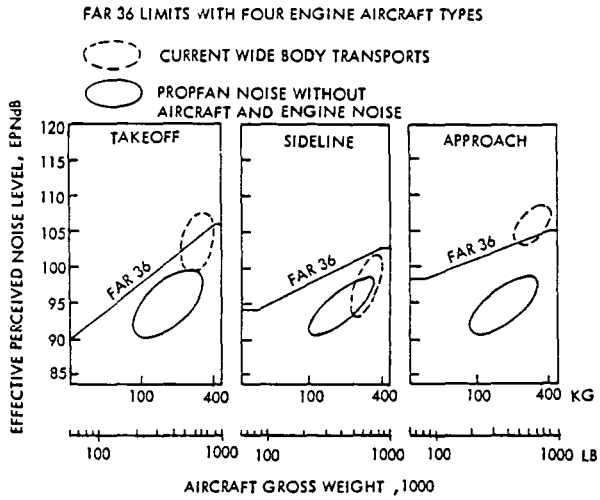

Figure 3. Far Field Noise Limits Compared to Current and Future Aircraft Noise Levels

Current federal regulations specify that the noise certification measurements be taken at three discrete locations for a type of flight profile that is considerably different from that typically flown in normal airline operation. Consequently, two aircraft may satisfy the regulations equally, but they may be perceived by the neighboring community as radically different because one is heard throughout a large area surrounding the airport, while the second may affect a much smaller area. Thus, the extent of the area affected by aircraft noise at some perceived level, the noiseprint area, is probably a better measure than those of the regulations when trying to determine how well an aircraft will do relative to possible operational curfews that may be imposed at airports to reduce noise. Obviously, any new aircraft will still have to be designed to satisfy the federal regulations. But, and perhaps equally important to the airlines, consideration will also have to be given to reducing the noiseprint area of future aircraft to avoid locally-imposed operational curfews at airports that could have an adverse economic impact on air cargo. The effect of this additional design consideration is addressed in this study.

---

* F. B. Metzger and C. Rohrbach, "Aeroacoustic Design of the Prop-fan," AIAA Paper 79-0610, Hamilton Standard, March 1979 (Ref. 17)

D. B. Hanson, "The Influence of Propeller Design Parameters on Far Field Harmonic Noise in Forward Flight," AIAA Paper 79-0609, Hamilton Standard, March 1979 (Ref. 18)

D. B. Hanson, "Near Field Noise of High Tip Speed Propellers in Forward Flight," AIAA Paper 76-565, Hamilton Standard, July 1976 (Ref. 19)

D. B. Hanson and M. R. Fink, "The Importance of Quadrupole Source in Prediction of Transonic Tip Speed Propeller Noise," Journal of Sound and Vibration, Vol. 62, January 1979 (Ref. 20)

F. Farassat, "Theory of Noise Generation from Moving Helicopter Blades with an Application to Helicopter Rotors," NASA TR-R-451, NASA, December 1975 (Ref. 42)

F. Farassat, "Linear Acoustic Formulas for Calculation of Rotating Blade Noise," AIAA Journal, Vol. 19, September 1981 (Ref. 43)

** "Noise Standards: Aircraft Type Certification," Federal Aviation Regulations, Part 36 (FAR 36), Federal Aviation Administration, Department of Transportation (Ref. 21)

\+ All abbreviations and symbols are listed in Appendix A.

++ Superscript numbers in the text corresponds to those of the references.

Lest there be any confusion, we are not advocating any federal regulations on aircraft noiseprints but are recognizing that public and commercial demands will result in future transport aircraft that are quieter than today's aircraft. The impact of noise considerations on aircraft designs in the future is directly analogous to the current influence of economics. Airlines are buying and flying only those aircraft that minimize direct operating costs and maximize return-on-investment for their route structure, because the airlines want to stay in business. If the airlines are to survive in the future, they will buy new aircraft that provide both maximum economics and minimum noiseprints so that their airport operations will not be restricted by local communities who refuse to tolerate excessive noise and who, therefore, pass legislation that curtails operations or even closes airports during certain daily periods.

The objective of this study is to explore the effects of using advanced turboprop propulsion systems to reduce the fuel consumption and direct operating costs of cargo aircraft and to determine the impact of these systems on aircraft noise and noiseprints around a terminal area. To accomplish this, the sensitivities of performance, fuel consumption, productivity, and economics are identified for various levels of noise reduction for turboprop aircraft and are compared with those for competitive turbofan aircraft designs.

The overall plan, shown in Figure 4, for achieving the study objective is composed of five major tasks that are discussed in more detail in the remaining sections. To review briefly, in the first task parametric variations of aircraft and propeller characteristics were investigated to determine their effects on noiseprint areas and direct operating costs. From these results, three aircraft designs were selected and subjected to refinement and design sensitivity analysis in the second task. In the third task, parametric analyses were performed to define three turbofan aircraft with the same mission capabilities as the selected turboprop aircraft. These three turbofan aircraft provide a basis for comparing the two types of propulsion in the fourth task. The fifth task was to identify potential problem areas, several of which were investigated. As a separate supportive task, analytical noise prediction methods were developed for use in the parametric studies of both the turboprop and turbofan powered aircraft.

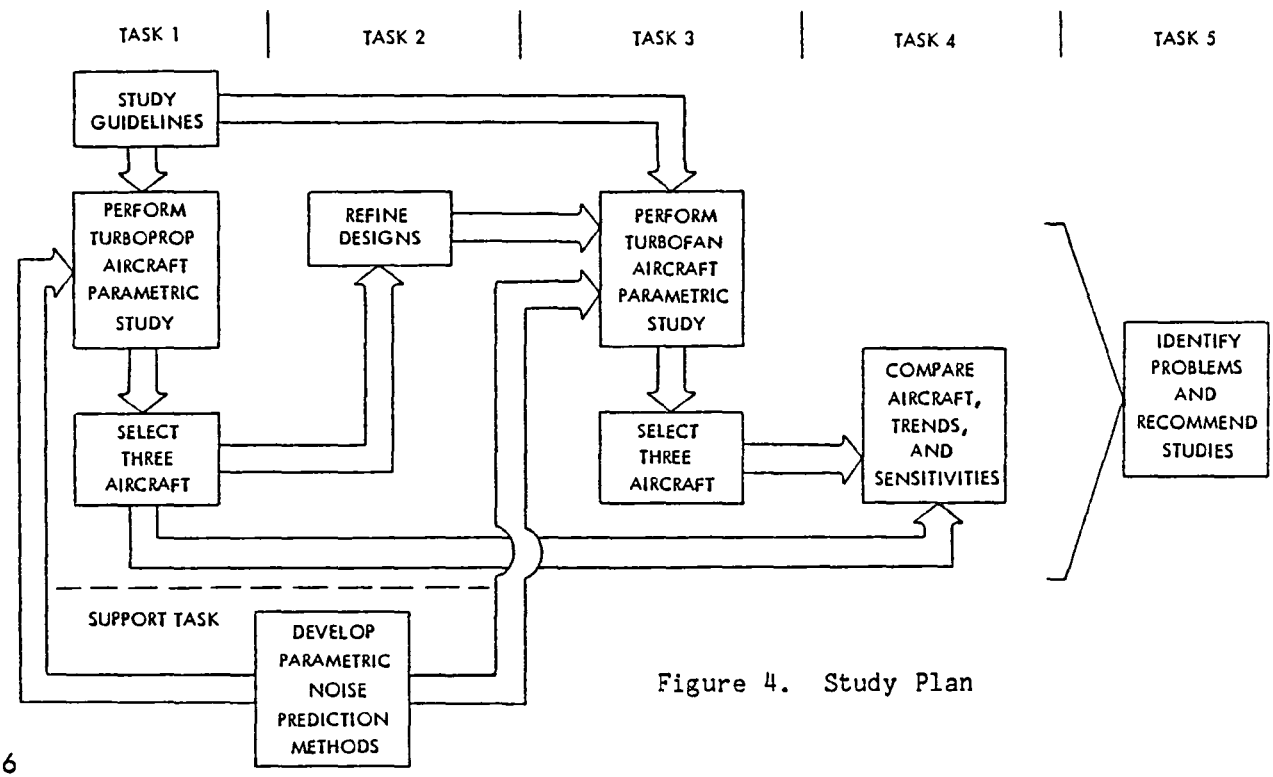

Figure 4. Study Plan

GUIDELINES

Guidelines for the conduct of this study were defined by NASA in the statement of work or were adopted by Lockheed based on experience in transport aircraft design. For ease of presentation, they have been grouped according to whether they apply to the study in general or are limited in that they help only to define the mission, to constrain the aircraft configuration, to delineate applicable advanced technologies, to direct the economic evaluation, or to establish noise goals.

GENERAL CONSTRAINTS

The aircraft configurations generated in this study could be ready for introduction into service between 1990 and 1995. The configurations include those elements of advanced technology that may be ready for production application in 1985 with the exception of the turboprop system, and that have the potential for improving performance, reducing noise and costs, and solving design or operational problems. Current requirements of the Federal Aviation Regulations for Transport Category Aircraft are assumed to be applicable to aircraft with an initial operational capability in the early 1990s, and are satisfied by the aircraft configurations designed in this study.

MISSION DEFINITION

A single-leg, domestic flight serves as the design mission for this study. While the mission definition is restricted to a single range and flight profile, various cruise speeds and payloads are considered.

Range

The design mission range for all configurations is 4250 km (2295 n. mi. or 2640 s. mi.).

Speed

Three cruise Mach numbers of 0.6, 0.7, and 0.8 are considered for the three smaller payloads. For the largest payload, the values are 0.7, 0.75, and 0.8.

Payload

The design payloads for the design range consist of 2, 4, 6, and 9 fully loaded containers. Nominally, the container size is 2.44 m high by 2.44 m wide by 6.1 m long, (8 ft by 8 ft by 20 ft) while the densities of the payload and the container are 160 and 24 kg/m^3 (10 and 1.5 lb/ft^3), respectively. Gross payload values, that is net payload plus container tare, for this study are 13,650 kg (30,000 lb), 27,300 kg (60,000 lb), 40,950 kg (90,000 lb), and 61,425 kg (135,000 lb).

Flight Profile

Details of the mission flight profile are depicted in Figure 5. The minimum initial cruise altitude is 9,144 m (30,000 ft) for the configurations designed for the 0.7 and 0.8 cruise Mach numbers. For those configurations with a 0.6 cruise Mach number, the initial cruise altitude is at least 7600 m (25,000 ft).

All of the configurations may be operated from airports used by current transport aircraft designed for a comparable mission. For this study, all of the aircraft comply with a maximum FAA balanced or factored field length limit of 2440 m (8000 ft). During landing, approach is on a 0.05-rad (3-deg) glideslope with a maximum approach speed limited to 69 m/s (135 kt).

CONFIGURATION CONSTRAINTS

Cargo Compartment Environment

The cargo compartments are designed to maintain a minimum pressure equivalent to an altitude of 5.5 km (18,000

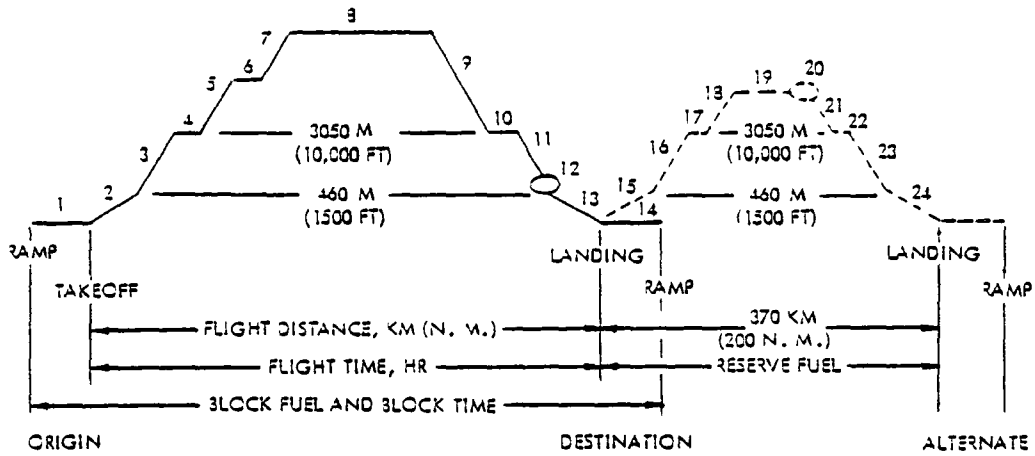

SEGMENT CODE

1. START, TAXI, AND GROUND HOLD; 9 MINUTES
2. TAKEOFF TO 460 M (1500 FT) V_2 + ΔV, CLEAN UP ABOVE 120 M (400 FT)
3. CLIMB TO 3050 M (10,000 FT) ALTITUDE AT BEST RATE OF CLIMB, 130 M/S (250 KT) MAX.
4. ACCELERATE
5. CLIMB TO INITIAL CRUISE ALTITUDE AT BEST RATE OF CLIMB
6. INITIAL CRUISE AT CONSTANT ALTITUDE
7. STEP CLIMB } REPEAT AS REQUIRED
8. CRUISE AT CONSTANT ALT }
9. DESCEND TO 3050 M (10,000 FT)
10. DECELERATE
11. DESCENT TO 460 M (1500 FT), 130 M/S (250 KT) MAX.
12. AIR MANEUVER AT 460 M (1500 FT) FOR 3 MINS.
13. APPROACH 0.05 RAD (3 DEG) GLIDESLOPE, 69 M/S (135 KT) MAX.
14. TAXI, STOP, AND SHUTDOWN, 3 MINS.
15. MISSED APPROACH, TAKEOFF AT 460 M (1500 FT) V_2 + ΔV, CLEAN UP ABOVE 120 M (400 FT)
16. CLIMB TO 3050 M (10,000 FT) ALTITUDE AT BEST RATE OF CLIMB, 130 M/S (250 KT) MAX.
17. ACCELERATE
18. CLIMB
19. CRUISE AT ALTITUDE
20. HOLD AT ALTITUDE, 45 MINUTES
21. DESCEND TO 3050 M (10,000 FT)
22. DECELERATE
23. DESCEND TO 460 M (1500 FT), 130 M/S (250 KT) MAX.
24. APPROACH, 0.05 RAD (3 DEG) GLIDESLOPE, 69 M/S (135 KT) MAX.

Figure 5. Mission Flight Profile

ft) at maximum cruise altitude. The temperature control system is designed to maintain a minimum cargo compartment temperature of 283°K (50°F) or greater at maximum cruise altitude.

Cargo Compartment Capacity

The cargo compartment structure is designed to carry approximately 20 percent larger payloads (volume and/or mass) at a reduced range.

Configuration Sizing Variables

The variables considered in sizing the configurations include wing angle, wing aspect ratio, wing loading, wing thickness ratio, and thrust-to-weight ratio.

ADVANCED TECHNOLOGY APPLICATIONS

The advanced technology items and levels included in all of the aircraft configurations are expected to achieve state-of-the-art status and be ready for production application by 1985 except for the propulsion system, which will probably not be ready until later. Specifically, the configurations have supercritical airfoils, composite mate-

rials, advanced engines, a Hamilton Standard advanced propfan+, and active controls. Graphite/epoxy composite materials are used for the secondary structure of the wing, fuselage, nacelles, and landing gear; for the nacelle and pylon skins; and for both primary and secondary structures of the empennage. Pratt & Whitney STF477 turbofan* and STS487 turboshaft** engines are used as the baseline powerplants in the configurations to ensure a high degree of commonality for the comparative analysis. These two engines are of the same family of designs by one manufacturer and have equivalent technology levels.

ECONOMIC GUIDELINES

The 1967 Air Transport Association (ATA)[Δ] equations with coefficients updated to January 1980 levels are used to calculate direct operating cost (DOC). Likewise, pricing and other costs are based on January 1980 dollar values.

Aircraft manufacturing and development costs, as well as propulsion system acquisition and maintenance costs, are estimated by Lockheed's in-house methods. Details of the propulsion system costing approach are presented in Appendix B.

Aircraft production runs to meet the productivity, or throughput, requirement of 26 revenue kilogram-petameters (15.4 billion revenue ton-nautical miles) are listed in Table I for load factors of 100 and 85 percent of the gross payload for variations in payload and cruise speed. Calculations of the DOCs for each of these runs are based on an average annual utilization of 3000 hours per aircraft, a crew of 3, a 15-year straight-line depreciation with a 10-percent residual salvage value, and a hull insurance rate of 2 percent. Fuel prices of 132, 198, and 264 $/m^3 (50, 75, and 100 ¢/gal) are considered in the parametric studies; and additional prices of 518 and 792 $/m^3 (200 and 300 ¢/gal) are included in some of the sensitivity studies.

Table I. Production Fleet Sizes for Load Factors of 100(85) Percent for Variations of Cruise Mach Number and Payload

PAYLOAD, 1000		CRUISE MACH NUMBER		
KG	LB	0 6	0 7	0 8
13 6	30	951 (1118)	843 (992)	738 (868)
27 2	60	475 (559)	422 (496)	369 (434)
40 8	90	317 (373)	281 (331)	246 (289)
61 2	135	*	188 (222)	164 (193)

* For the largest payload, a closer range of Mach numbers was selected with M = 0 75 being the third value The fleet sizes for this third speed are 175 (206)

NOISE GOAL

The noise goal is to minimize the area at airports that is subjected to high noise levels from aircraft on takeoff and landing, while maintaining aircraft economic viability. State-of-the-art noise prediction methods are used for source intensity and directivity. The elements in these methods are discussed in Appendix C along with a description of the simplified parametric noise prediction method that was developed under Lockheed's Independent Research and Development Program for use on this study.

+ Performance and noise data for this propfan are those in Reference 12. This propfan is similar in external appearance to that version designated SR-5 by Hamilton Standard, but it encompasses projected technology advances beyond those attainable with the SR-5 version.

* "Preliminary Performance and Installation Data for the STF477 Turbofan Engine," CDS-6, Pratt & Whitney Aircraft Corporation, February 1976 (Ref. 22)

** "Preliminary Performance and Installation Data for the STS487 Turboshaft Engine," CDS-11, Pratt & Whitney Aircraft Corporation, March 1976 (Ref. 23)

Δ "Standard Method of Estimating Direct Operating Costs of Turbine Powered Transport Aircraft," Air Transport Association, 1967 (Ref. 24)

TURBOPROP AIRCRAFT PARAMETRIC STUDIES

Wing geometry and propulsion system characteristics for three turboprop aircraft point designs were selected based on the results of design, cost, and noise studies. These studies included a preliminary design investigation of cargo compartment layouts for four mission payload values and a parametric analysis of aircraft sizing effects on cost, noise, and performance. The approach followed in these studies and the rationale for selecting the three designs for further refinement are described in this section.

BASIC CONFIGURATION DESCRIPTION

The basic aircraft configuration used in this study, as shown in Figure 6, encompasses many features of today's aircraft. All of the payload is carried in the fuselage and is loaded straight-in through either a nose visor door or an aft fuselage door. The wing is mounted sufficiently high on the fuselage at approximately mid-fuselage length so that it does not compromise the cargo compartment design. Other pertinent features of the basic configuration include conventional fuselage-mounted landing gear and engines attached to the underside of the wing. Although only two engines are shown on the aircraft in Figure 6, four engines are used for the largest payload cases. Pitch and directional flight controls are provided by a T-tail empennage mounted on the aft fuselage.

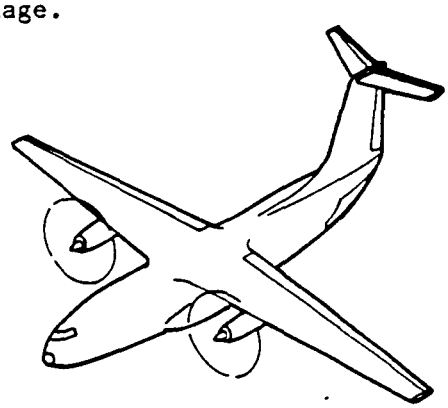

Figure 6. Basic Aircraft Configuration

Standard design criteria and data were used in the parametric studies to size the various aircraft configurations. The data base and the pertinent criteria in the areas of structures and materials, aerodynamics, propulsion, and flight controls are reviewed under these headings.

Structures and Materials

Basic structural design criteria were applied in determining the weights of the aircraft configurations and in computing the structural loads, rigidity requirements, and sizes for the point design refinements. These criteria are consistent with current civil specifications*. Specific criteria include limit load factors between +2.5 and -1.0 g's for maneuvers and +1.5 g's for landing and taxi. Structural design speed criteria are 180 m/s (350 kt) in cruise and 211 m/s (410 kt) in a dive.

In addition to the design criteria, certain assumptions were required concerning permissible stress levels in the structural materials. Current cargo aircraft wings, using conventional aluminum and construction techniques, are designed with tensile strength limits between 290 and 379 MN/m^2 (42,000 and 55,000 psi), depending upon the design lifetime. The relatively low limits are due primarily to fracture and fatigue properties at long operational lifetimes exceeding 30,000 hours. With the operational lifetime fixed at 45,000 hours for the aircraft in this study (3000 hours annual utilization for a 15-year lifetime), the lower limit is applicable in this case.

High levels of composite materials will be used in future aircraft because of improvements they offer in relative economics, coupled with the higher strength-to-weight ratios of composites compared with conventional metals. Unfortunately, the maximum level of com-

* "Airworthiness Standards: Transport Category Airplanes," Federal Aviation Regulations, Part 25 (FAR 25), Federal Aviation Administration, Department of Transportation, 1974 (Ref. 25)

posite usage is not likely to be reached until near the end of this century. By the technology readiness data of 1985 for this study, the level of composites used will be relatively low and will vary from one structural subsystem to another . Characteristically for this period, only the secondary structure of the wing, fuselage, nacelles, and landing gear will be constructed of composite materials. In addition, the nacelle skins and both the primary and secondary structure in the empennage will be made of composites.

Aerodynamics

The basic airfoils used in this study have supercritical technology levels envisioned for application in 1985. Lockheed has defined and wind-tunnel tested supercritical airfoil sections with thickness ratios between 10 and 21 percent, which is the basis for the airfoil performance characteristics that are used in this study. Typical variations in cruise Mach number and lift capability for the basic airfoils are shown in Figure 7 for two scaling variables, sweep angle and thickness-to-chord ratio. These curves depict the optimum thickness ratio values at a drag rise of 10 counts.

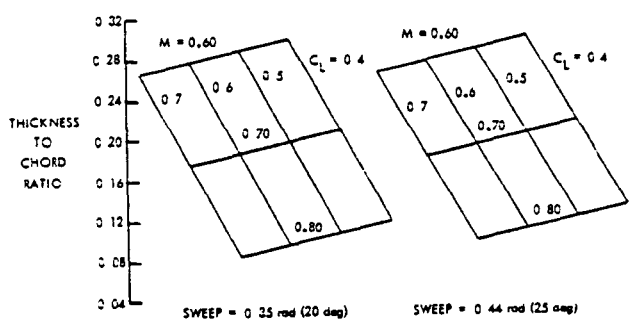

Figure 7. Typical Airfoil Characteristics

Drag characteristics of the aircraft are estimated on a component buildup basis, that is, the wing, fuselage, horizontal tail, etc. are treated individually. The skin friction drag is determined for the wetted area and the characteristic Reynolds number for each component, and is then referenced to the wing area. Next, shape factors are applied to the skin friction drag to obtain the profile drag for each component, and these are combined to obtain the basic profile drag. The drag penalties listed in Table II are then added to obtain the total profile drag.

Table II. Drag Penalties

ELEMENT	VALUATION
ROUGHNESS	3% OF BASIC PROFILE DRAG
INTERFERENCE	5% OF BASIC PROFILE DRAG
TRIM	12 COUNTS
COMPRESSIBILITY	5 - 10 COUNTS
MISCELLANEOUS	4 COUNTS
PROP/AIRFRAME INTEGRATION	SEE APPENDIX D

The installation of propellers or propfans on an aircraft introduces additional drag that is not experienced by a turbofan-powered aircraft. Unfortunately, a standard approach for defining and quantifying the elements of this added drag does not exist. As may be observed by comparing the reports of recent studies [6,7,13] on propeller-driven aircraft, each investigator seems to have a different method for categorizing, accounting for, and measuring the elements that contribute to this added drag. For this study, we have attempted to augment the best from these previous studies with our own experience on the C-130 aircraft to produce a method for estimating propeller/airframe integration drag. This method is described in Appendix D.

The high lift system on all of the aircraft consists of a 30-percent-chord, double-slotted flap arrangement. This system is augmented by a 10-percent-chord, leading-edge device to keep approach speeds down.

Flight Controls

Design criteria for sizing the directional, lateral, and longitudinal flight control surfaces are based on the requirements of FAR 25. Directional control is provided by a vertical tail with a 25-percent-chord rudder. The vertical tail is sized to provide adequate static directional

stability, while the rudder size is regulated by cross-wind landing and critical-engine-out conditions. Ailerons extended over the trailing edge of the outboard 25-percent of the wing furnish lateral control capability. Pitch control is provided by a horizontal tail with a 25-percent-chord elevator. The horizontal tail size insures at least a negative 5-percent static stability margin at the most aft center-of-gravity position, and the elevator is designed for the nose wheel lift-off condition at the most forward center-of-gravity position.

Propulsion

The turboprop propulsion system is composed of three major elements: the engine, the gearbox, and the propeller. The basic engine is the Pratt & Whitney STS487 turboshaft engine which has a companion turbofan engine, the STF477, that is used in developing designs of competitive turbofan-powered aircraft. Both engines were defined under NASA's Advanced Turbofan Engines Designed for Low Energy Consumption study. Although these engines were optimized for minimum fuel consumption instead of minimum direct operating cost and noise, these engines are scalable over the range of sizes needed in this study, are of appropriate technology levels, and are of the same family, which should enhance the comparison between the two propulsion concepts.

The STS487 engine is a three-spool, free-turbine, shaft engine. As noted in Reference 23, the basic engine is flat rated to 302°K (84°F) at 15.2 MW (20,424 hp) and has a mass of 970 kg (2134 lb).

Six, eight and ten-blade versions of an advanced Hamilton Standard Propfan are candidate propellers. Propfan performance used in this study and data on the gearbox are based on that defined in Reference 12. The data are for a propfan that is similar in external appearance to the SR-5 version of a 2-ft diameter model that was tested by Hamilton Standard; however, the data include advances beyond those of the SR-5.

Lockheed's engine cycle analysis program was used to generate a base set of installed thrust and thrust specific fuel consumption data for the base size STS487 engine in combination with the propfan. This set includes takeoff, climb, and cruise performance for variations in the number of blades, tip speed, and sea-level-installed disk loading of the propfan.

The propulsion system data base of performance, weight, and cost characteristics for the range of power requirements in this study was assembled as part of Lockheed's Independent Research and Development Program. Although this data base* is proprietary and is not included in this report, the results obtained from using the data are provided. Examples of the data are contained in Appendix E.

FUSELAGE SIZING

In developing the design of an aircraft, the first task is to design accommodations for whatever is to be carried, subject to constraints imposed by the application. The guidelines for this study specify four payloads that are to be carried and explicitly define each payload mass and size. The latter is fixed by requiring the four payloads to be in 2, 4, 6, and 9 standard 2.44 m by 2.44 m by 6.1 m (8 ft by 8 ft by 20 ft) containers, respectively.

The three major considerations in this task are: a cargo compartment layout to efficiently house the containers, a minimum-sized fuselage to encapsulate the cargo compartment, and the impact of loading and unloading on both the fuselage and the cargo compartment. Although these three considerations are strongly interrelated, they will be discussed separately for ease of presentation.

* F. R. Stone, "Propfan Data Base for Parametric Aircraft Studies," LG79-ER0128, Lockheed-Georgia, August 1979 (Ref. 26)

Cargo Compartment Layout

The selection of cargo compartment designs for this study is based on analysis of several floor plan layouts and cross-sectional area arrangements and their effects on the fuselage. A rule-of-thumb guideline used in the analysis is that the cargo compartment fineness ratio (length/equivalent diameter) should be between 2 and 8. This leads to an efficient fineness ratio between 6 and 12 for the encapsulating fuselage when allowance is made for the tapered fore and aft ends. Experience has shown that this guideline provides aerodynamically and structurally efficient fuselages without excessive frontal area, pressure volume, or surface area per unit volume. Generally, it precludes any ground clearance problems for typical landing gear lengths.

For the 2 and 4-container payloads, the fineness ratio falls within the guideline when all of the containers are placed end to end in a single row. However, for the 6 and 9-container payloads the fineness ratio for a single row of containers exceeds the guideline by a considerable margin. Necessarly then, alternate floor plan arrangements must be considered that have two rows of containers for some portion of their length. Three two-row alternate arrangements are presented in Table III, along with the single-row layout for the 6-container payload. The table also contains comparative data which illustrate the effects of the layout on their fuselages, assuming a constant cross-sectional area. Choosing between the three alternates is deferred pending other considerations. For the 9-container payload, as will become obvious later, 8 of the containers are in a two-row arrangement, and the last container is positioned along the centerline of the aft fuselage.

Loading

Only forward and aft fuselage apertures are considered for loading the aircraft in this study. Furthermore, only one aperture is provided in each particular point design.

Table III. Comparison of Cargo Compartment Layouts for 6-Container Payload

LAYOUT ARRANGEMENT	1 	2. 	3 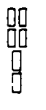	4. 
FUSELAGE LENGTH, M (FT)	54(178)	39(128)	42(138)	38(124)
FUSELAGE DIAMETER, M (FT)	3 9(12 8)	6 3(20 6)	6 3(20 6)	6 3(20 6)
FUSELAGE FINENESS RATIO	13 8	6 2	6.7	6.0
PRESSURE VOLUME, M^3 (FT^3)	564(19,900)	1149(40,600)	960(33,900)	802(28,300)
SURFACE AREA, M^2 (FT^2)	606(6500)	804(8700)	684(7400)	595(6400)
FRONTAL AREA, M^2 (FT^2)	12(130)	31(334)	31(334)	31(334)

The idea of using doors in the side of the fuselage for loading containers is discarded as impractical and/or inefficient for the candidate cases. To load containers that are 6.1 m (20 ft) long through the side of the fuselage requires that the opening be at least 6.3 m (20.5 ft) wide because the containers cannot be rotated to achieve correct directional alignment once they are inside the cargo compartment. Such a wide opening in the side of the fuselage would impose substantial structural weight penalties that are not warranted relative to forward or aft fuselage doors. Also, in a two-container-sized aircraft, a side door would interfer with the main structural frames connecting the wing and landing gear.

Both the forward and aft fuselage openings permit straight-in loading of the containers, which tends to minimize ground handling time and to simplify the cargo handling system. An aft fuselage door and ramp are used for cargo loading in all of the 2 and 4-container aircraft designs. This allows the crew compartment to be placed ahead of the cargo compartment without affecting the frontal area of the fuselage; that is, no bubble is required on the top of the fuselages, as on a 747 aircraft, to accommodate the crew.

A nose visor door is provided for cargo loading on the 6 and 9-container aircraft designs. Furthermore, the door is made sufficiently wide to permit simultaneous loading of two containers side by side. Although there is no requirement for a door this wide, contacts with commercial operators indicate that such a feature is very desirable. By using a door this wide, cargo floor plan layout number 4 in Table III is eliminated from further consideration because it is configured for a single-row door width. Revisions to this layout for the wider door would result in considerable wasted space and a longer and heavier aircraft.

The penalty for raising the crew flight station above the cargo compartment to allow straight-in nose loading is smaller on a two-row wide arrangement than on a single-row design. This occurs because there is considerably more unused space between the top of the two-row cargo compartment and the circular fuselage arc above it. Consequently, the crew compartment can be accommodated with only a relatively small increase in the fuselage frontal area, and this is largely compensated for by a shorter overall length of the aircraft.

Of the two remaining candidate layouts in Table III, namely layouts 2 and 3, both use a visor nose that is wide enough for two rows. Thus, the final selection of a preferred design is based on minimizing the fuselage size, which is indicated by the values of the surface area and pressure volume. A comparison of these two parameters clearly shows that layout 3 is to be preferred.

Fuselage Cross-Section

The initial fuselage cross-sections, as shown in Figure 8 for both the one and two-row cases, provide only minimal clearances for loading the containers consistent with standard commercial practices. Recently, attention has been focused on the concept of a common civil-military aircraft*. This trend for the future dictates that the applicability of the fuselage cross-section for military transportation be evaluated, particularly for the single-row design.

* D. L. Bouquet, "Strategic Airlift Aircraft Design Study, (Issues of Commonality)," Lockheed-Georgia Company Final Report on Air Force Contract F33615-79-C-0115, December 1979 (Ref. 27)

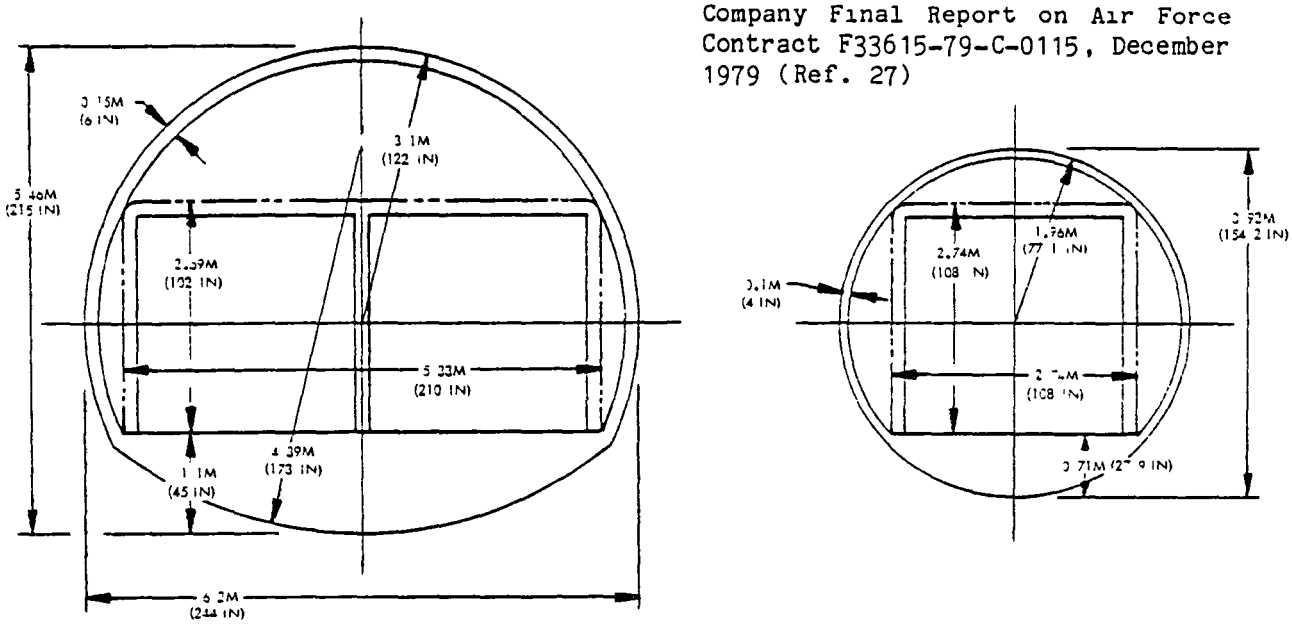

Figure 8. Initial Fuselage Cross-Sections

To aid in this evaluation, Lockheed's Cargo Loading Program was used with its extensive data base, which includes the number, dimensions, and weights of all the vehicles and equipment in the inventory of the various types of U.S. Army divisions. Specifically, the program was used to determine the effects on the percentages of the various divisions that can be transported by particular aircraft designs with different cargo compartment sizes. Limitations on the maximum weight, length, width, and height of the items to be carried were applied individually and collectively to the Army division inventories to obtain the results in Table IV. The first part of the table shows the effects of load and length limits that correspond to those of a two-container payload. These two limits do not severely restrict the transportable inventory percentage. More than 88 percent of the total inventory is transportable in all cases; in only one case is less than 90 percent transportable, and in 7 of the 15 cases less than 3 percent of the inventory is excluded.

The second grouping in the table shows the effect of imposing only a height restriction. The heights listed are the limits on the inventory items and do not include the 0.15 m (6 in.) clearance that is allotted between the items and the top of the cargo compartment. From the results in the table, it is evident that little is to be gained by increasing the height by 0.15 m over the basic container height of 2.44 m (8 ft). However, considerably greater benefits accrue when the height is increased 0.3 m (1 ft) above the basic container height.

The third grouping in the table shows the effect of imposing only a width limitation on the inventory items, while maintaining a requirement that there be a lateral clearance of 0.075 m (3 in.) between the items and the sides of the cargo compartment. Substantial benefits are realized for a 0.15 m (6 in.) increase over the basic container width of 2.44 m (8 ft), but only negligible benefits accrue for further increases.

The bottom section of the table shows the effect of collectively applying various height and width limits for a particular load and length limit. The results at the beginning of this group, that is for a height of 2.75 m and a width of 2.59 m, indicate that between 84 and 95 percent of the inventory of the five divisions can be transported. A comparison of these results with those on the third line of the first grouping, where only load and length limits are imposed, suggest that very little is to be gained through further increases in the width and height restrictions.

Based on these results, the cargo compartment cross-section is increased to accommodate items up to 8.59 m (8.5 ft) wide by 2.75 m (9 ft) high. Quite coincidently, these dimensions are compatible with the projected trend of containers to larger cross sections. Furthermore, the increased volume in the cargo compartment will provide space for carrying 20 percent more payload at the same density, a requirement of the study guidelines. Figure 9 shows the fuselage cross-sections enlarged slightly for items or containers with these larger widths and heights.

Table IV. Percentage of Inventory of U.S. Army Divisions that is Transportable for Variations in Cargo Compartment Cross-Section Size

SIZING CRITERIA	DIVISIONS				
	ARMORED	MECHANIZED	INFANTRY	AIRBORNE	AIRMOBLE
LOAD ≤ 6800 KG (30,000 LB)	90.4	92.0	96.9	97.9	99.5
LENGTH ≤ 12.7 M (500 IN)	98.0	97.9	97.7	97.0	93.2
LOAD ≤ 6800 KG AND LENGTH ≤ 12.7 M	88.8	90.4	94.6	94.9	92.8
HEIGHT ≤ 2.75 M (108 IN)	89.5	91.1	95.1	99.5	98.1
≤ 2.59 M (102 IN)	83.8	85.4	90.3	95.7	92.0
≤ 2.44 M (96 IN)	80.5	82.2	89.3	94.3	91.2
WIDTH ≤ 2.75 M (108 IN)	88.1	89.7	96.1	98.8	97.9
≤ 2.59 M (102 IN)	87.2	88.8	94.4	96.6	93.9
≤ 2.44 M (96 IN)	66.1	66.4	83.3	92.9	90.2
LOAD ≤ 6800 KG, LENGTH ≤ 12.7 M, AND HEIGHT ≤ 2.75 M, AND					
WIDTH ≤ 2.59 M	84.0	85.6	88.3	94.5	91.9
≤ 2.44 M	64.7	65.1	79.8	92.0	88.8
HEIGHT ≤ 2.59 M, AND					
WIDTH ≤ 2.59 M	80.4	82.1	86.4	94.4	91.8
≤ 2.44 M	63.8	64.2	78.0	92.0	88.8
HEIGHT ≤ 2.44 M, AND					
WIDTH ≤ 2.59 M	80.4	82.0	85.8	94.3	91.2
≤ 2.44 M	63.7	64.2	78.0	91.9	88.2

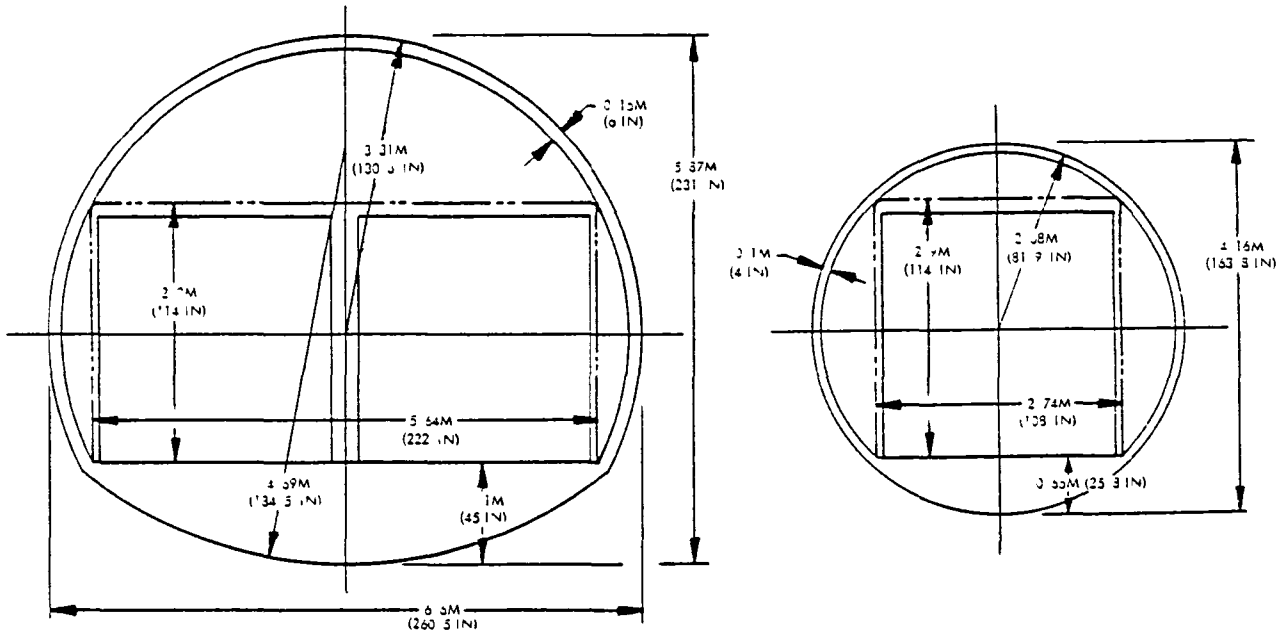

Figure 9. Revised Fuselage Cross-Sections

Fuselage Nose

For the range of cruise speeds in this study, different shapes for the forward fuselage are essential to obtain the most efficient designs. A short, blunt nose, similar to that on a C-130 aircraft, is best for the 0.6 Mach number case. A longer and more streamlined nose like that on the L-1011 aircraft is better for the higher cruise Mach numbers of 0.7 and 0.8. Figure 10 provides a comparison of the contours that are used for the forward fuselage for these two speed conditions.

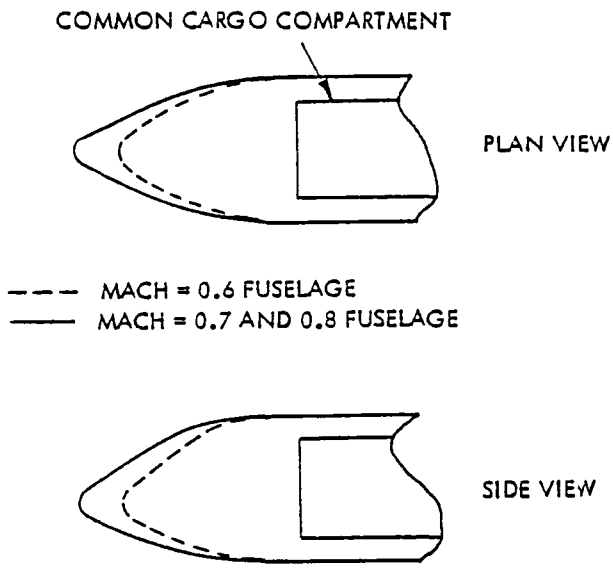

Figure 10. Forward Fuselage Contours

PARAMETRIC STUDY

Parametric studies were conducted for turboprop-powered aircraft to identify the sensitivity of direct operating costs, fuel consumption, and noiseprint areas to variations in performance, geometry, fuel price, and propulsion system characteristics. Although some of the study variables were discussed throughout the section on study guidelines, all of the variables and the extent of variation are consolidated into Table V for conciseness.

When parametric studies are undertaken with a large number of variables, schedule and budget constraints usually dictate that an approach be adopted of using engineering judgment to select combinations that will illustrate the sensitivity of the specified measures of effectiveness to the different variables, and if required, will provide any desired opti-

Table V. Turboprop Aircraft Parametric Study Variables

MISSION	
CRUISE MACH NUMBER	0.6, 0.7, 0.75, 0.8
PAYLOAD CONTAINERS	2, 4, 6, 9*
INITIAL CRUISE ALTITUDE, 1000 M	7.6, 8.2, 9.1, 10.1, 11.0
FT	25, 27, 30, 33, 36
AIRCRAFT WING GEOMETRY	
SWEEP ANGLE, RAD	0.17, 0.26, 0.35, 0.44
DEG	10, 15, 20, 25
LOADING, N/M^2	4310, 5270, 6230
LB/FT^2	90, 110, 130
ASPECT RATIO	7, 10, 13, 16
PROPELLER	
TIP SPEED, M/S	204, 229, 256
FT/S	670, 750, 840
NUMBER OF BLADES	6, 8, 10
NOMINAL DISK LOADING,	
KW/M^2	281, 402, 484, 640
HP/FT^2	35, 50, 60, 80
COST	
FUEL PRICE, ¢/L	13.2, 19.8, 26.4
¢/GAL	50, 75, 100

* Each container unit represents a payload weight of 6800 KG (15,000 lb)

mization. Such was the case in this study.

The variables in Table V fall into the four categories of mission, aircraft geometry, propeller, and cost. Of those in the mission category, a sufficient number of variable combinations was investigated to establish the desired sensitivities to variations in two main elements of productivity: payload and speed. The particular combinations investigated were not known a priori but were selected as the study progressed and trends became evident.

The parametric study was performed in two phases which are not indicative of a time sequence but of the subject addressed. The purpose of the first phase was to select values for initial cruise altitude, wing sweep angle, and wing loading for use in the second phase, which is more directly oriented toward addressing the overall study objective. In the second phase, the propeller parameters were varied to determine their effects on aircraft direct operating costs, fuel consumption, and noiseprint areas.

Phase I

Minimum ramp weight and minimum block fuel weight were jointly considered as criteria in Phase I for selecting values for the initial cruise altitude and wing sweep angle for the various payload-speed combinations that were investigated. In all cases, the wing loading values were established by one of four constraints: a maximum approach speed limit of 69 m/s (135 kt), technology limitations on cruise lift, a maximum takeoff distance of 2440 m (8000 ft), and a minimum fuel volume ratio (wing volume available to volume required to carry the mission fuel) of one.

Phase I was performed in three steps as indicated on the case schedule summary in Table VI. In the first step, attention was given to aircraft capable of carrying a 4-container payload at each of the three candidate cruise Mach numbers of 0.6, 0.7, and

Table VI. Case Schedule for Phase I of Turboprop Parametric

	STEP 1			STEP 2		STEP 3		
PAYLOAD CONTAINERS	4			2	6	9		
MACH NUMBER	0.6	0.7	0.8	0.8		0.8	0.75	0.7
ALTITUDE, 1000 M	7.6-10.1	9.2-11.0		10.1		10.1		
FT	25 - 33	30 - 36		33		33		
WING SWEEP, RAD	0.17	0.26 - 0.44		0.44		0.44	0.35	0.26
DEG	10	15 - 25		25		25	20	15
ASPECT RATIO	7 - 16							
WING LOADING, KN/M^2	4.3 - 6.2							
LB/FT^2	90 - 130							

PROPELLER CONSTANTS: 10 BLADES, TIP SPEED = 229 M/S, 750 FT/S, NOMINAL DISK LOADING = 484 KW/M^2, 60 HP/FT^2

0.8. For each payload-speed combination, a matrix of nine aircraft was developed for selecting the optimum values of wing sweep angle and cruise altitude. All nine aircraft in the matrix were previously identified as the optimum designs in separate matrices where aircraft wing loading and aspect ratio were varied.

Figure 11 contains a series of graphs which illustrate typical data for one such matrix of aircraft with varying wing loading and aspect ratio. Note that the constraints adopted as study guidelines are shown on the graphs of approach speed, takeoff field length, fuel volume ratio, engine-out climb gradient, and cruise lift. In

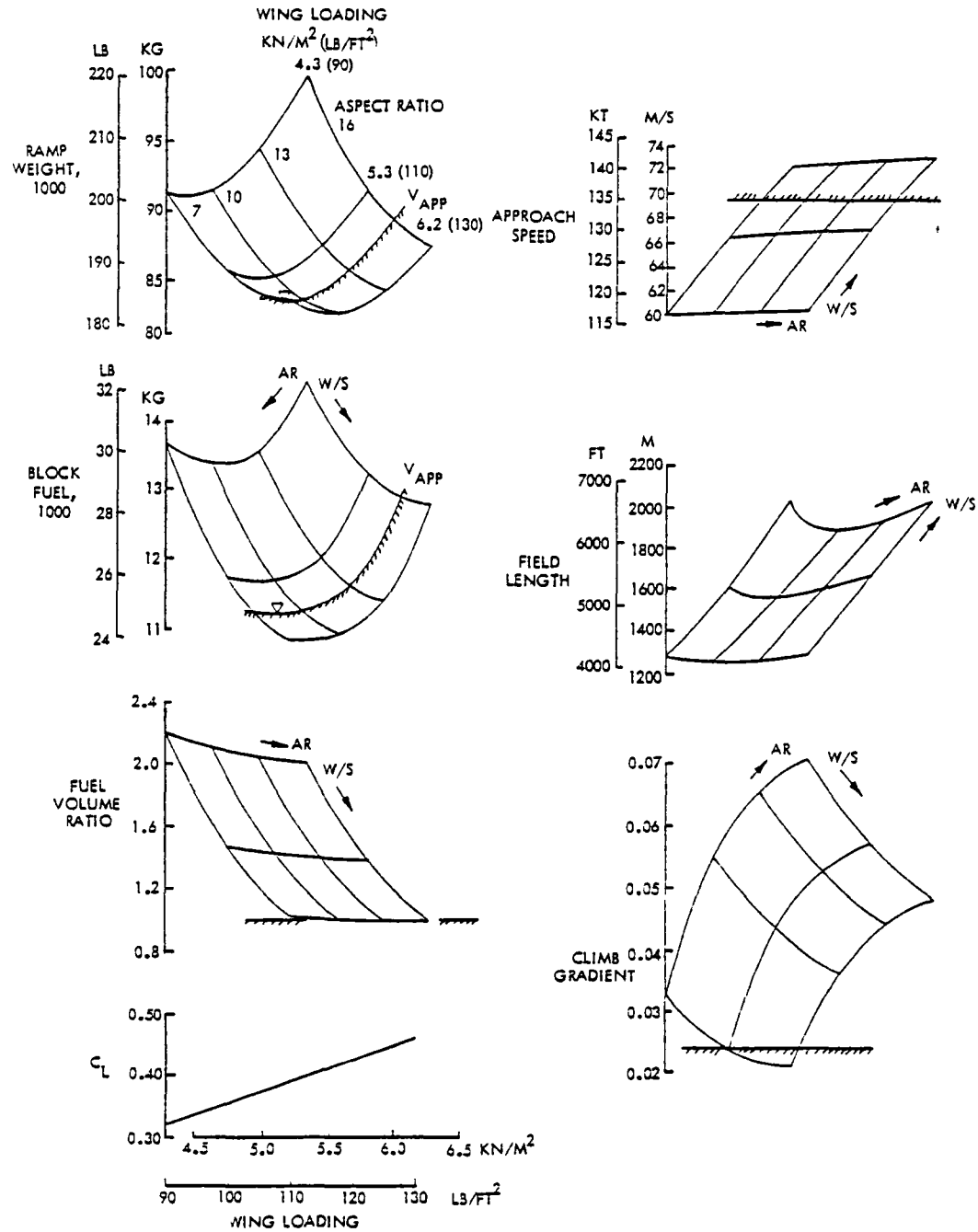

Figure 11. Typical Data for Parametric Matrix on Wing Loading and Aspect Ratio

this case it is evident that only the approach speed limit is critical in eliminating aircraft design points. Consequently, the approach speed limitation has been superimposed on the two weight graphs. By visual inspection, the minimum weight points can be pinpointed, as indicated by the triangles on the graphs, and the corresponding values of wing loading and aspect ratio may be read.

Similar exercises were performed for other combinations of wing sweep angle and cruise altitude. The minimum weight values for each combination were then plotted in Figure 12 so that sweep angle and altitude values could be selected for use in the Phase II portion of the study. Before proceeding with that selection, a few background comments are needed to explain the rationale used.

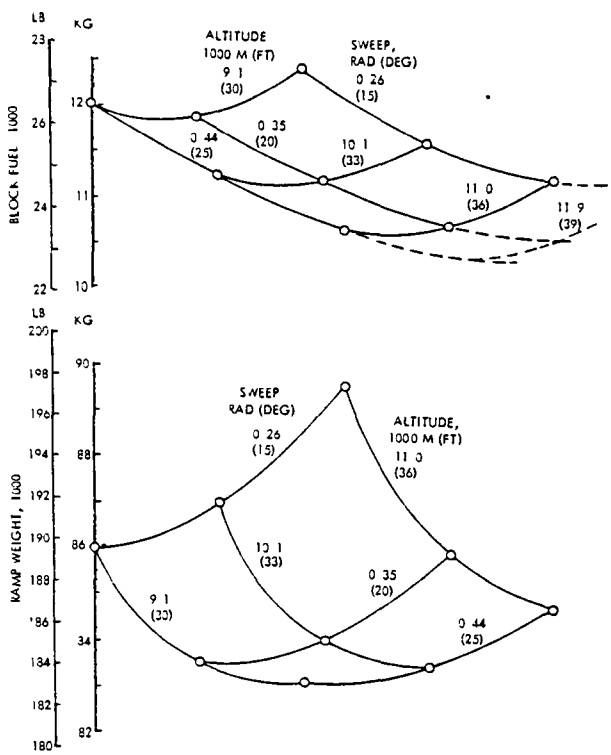

Figure 12. Sweep Angle and Altitude Effects for 4-Container Payload and 0.8 Mach Number Designs

One objective of this study is to show the sensitivity of aircraft noise to several parameters which typically serve as optimization criteria. Among these are ramp weight, fuel consumption, and direct operating cost (DOC). Experience has shown that aircraft designed to minimize DOC tend toward minimum ramp weight for relatively low fuel prices and toward minimum fuel consumption as fuel prices increase. Thus, through analysis of both ramp weight and fuel consumption for the designs of interest, certain parameters can be selected which, while minimizing neither ramp nor fuel weight, do provide a compromise between the two. This approach reduces to a manageable number the variables to be considered in further optimization efforts, such as Phase II.

As an example of this approach, consider the ramp weight and block fuel graphs in Figure 12 which are used to select a sweep angle and cruise altitude for the case of a 4-container payload and a Mach number of 0.8. Minimum ramp weight occurs at a sweep angle of 0.44 rad (25 deg) and an altitude of 9.5 km (31,000 ft). Alternately, minimum block fuel tends toward an altitude above 11 km (36,000 ft) and a sweep angle of 0.44 rad (25 deg). In this case, both criteria suggest the same sweep angle, but some compromise is required for the altitude. A value of 10.1 km (33,000 ft) was arbitrarily chosen.

Having selected a particular combination of wing sweep and cruise altitude values, attention is refocused on the effects of wing loading and aspect ratio variations. This means, in this case, a review of the graphs previously presented in Figure 11. A re-examination of the ramp weight and block fuel graphs reveals that the optimum designs are constrained by the approach speed limitation. Inspection of the approach speed graph shows that there is a strong correlation between approach speed and wing loading. In fact, for a specific approach speed, the wing loading change with aspect

ratio is so slight that it can be considered constant as a first approximation. Consequently, a value of 5.7 kN/m^2 (119.5 psf) was selected and assumed to be constant for all aircraft designed for 0.8 Mach number and a 4-container payload.

For those designs with a 4-container payload and a cruise Mach number of 0.7, a 0.26-rad (15-deg) sweep angle and a 10.1-km (33,000-ft) cruise altitude were selected based on the results shown in Figure 13. Following the same approach as for the 0.8 Mach number designs, a constant wing loading of 5.9 kN/m^2 (122.5 psf) was found to give optimum designs limited only by cruise lift technology.

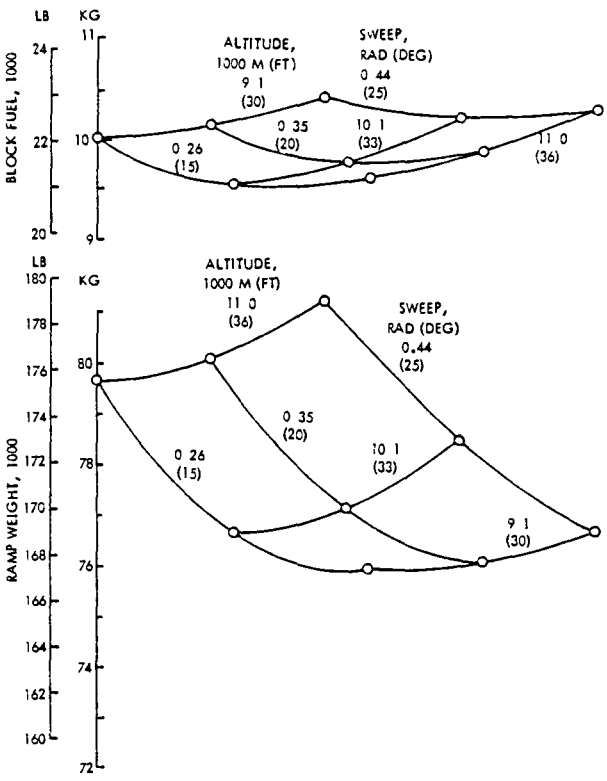

Figure 13. Sweep Angle and Altitude Effects for 4-Container Payload and 0.7 Mach Number Designs

A slightly different approach was taken for those designs intended to carry a 4-container payload at a cruise Mach number of 0.6. Typically at this low speed, there is no need for wing sweep based on aerodynamic considerations. However, a wing with a taper ratio of 40 percent, which is used in this study, and a zero sweep angle at the quarter chord gives a visual appearance of being swept forward. Rather than have this occur and risk the possibility of subverting attention from the intent of this study for all those who have become acclimated to straight or swept-back wings, the wing sweep was set at 0.17 rad (10 deg). This produces zero sweep for the wing trailing edge and a swept-back leading edge.

With the wing sweep angle set, the cruise altitude was selected based on the results shown in Figure 14. The curves on the figure show significant changes in slope at an altitude of 8.4 km (27,400 ft). Above this altitude, the designs are limited by cruise lift technology, while below it, takeoff field length limitations apply. So that a false sense of accuracy will not be implied, an altitude of 8.5 km (28,000 ft) was selected for aircraft designed to carry a 4-container payload at a cruise Mach number of 0.6. As for the 0.7 Mach number cases, the optimum designs are limited by cruise lift

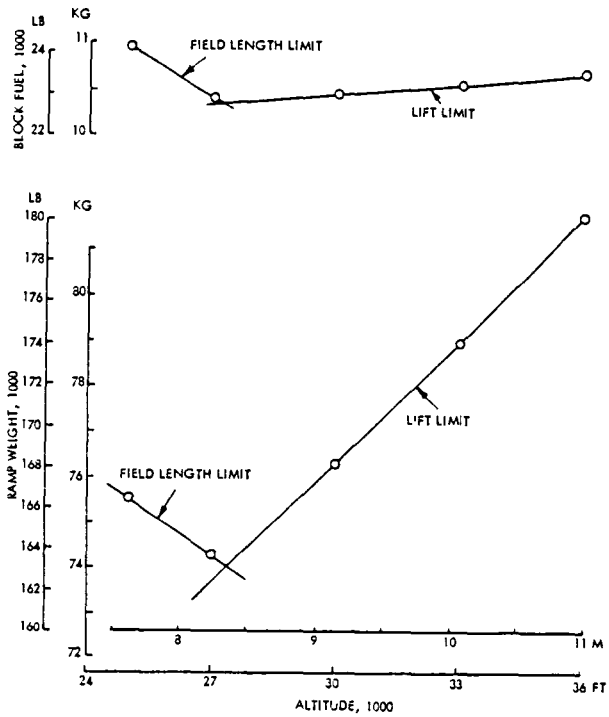

Figure 14. Altitude Effects for 4-Container Payload and 0.6 Mach Number Designs

technology. The corresponding wing loading value is 5.6 kN/m^2 (117.9 psf).

The first step of the Phase I study was concerned only with a 4-container payload. The second and third steps covered other payloads of 2, 6, and 9 containers. Our previous experience has shown that wing sweep angle and initial cruise altitude are much more dependent upon cruise speed than payload size. Consequently, the sweep angle and altitude values for these other payloads were assumed to be the same as for the 4-container payload at the same cruise speeds.

One 9-container payload case is for a cruise Mach number of 0.75, which was not investigated previously. However, both 0.7 and 0.8 Mach numbers were considered. For this 0.75 Mach number case, sweep angle and altitude values were selected as the average of those values obtained for the 0.7 and 0.8 cases.

Values for the altitude, sweep angle, and wing loading for each payload-speed combination are summarized on the top portion of Table VII, which also serves as a case schedule for the Phase II study.

Phase II

Attention during Phase II was directed toward identifying the effects of the propfan parameters on aircraft noiseprint areas and direct operating costs, and of producing graphs which illustrate the relationship between noiseprint area and direct operating cost. Table VII shows the sequential order in which the aircraft were investigated, in terms of payload and speed, and at the bottom, are the ranges of variations of the propfan parameters. To be more specific, 6, 8, and 10-blade propfans were considered with tip speeds of 204, 229, and 256 m/s (670, 750, and 840 ft/s) at sea-level-rated disk loadings of 281, 402, 484, and 640 kW/m^2 (35, 50, 60, and 80 hp/ft^2)*. Variations in wing aspect ratio were also included to gain an indication of two effects of the propeller diameter. One is the effect of different percentages of the wing being

*Cruise disk loadings are approximately one half of the value at sea level.

Table VII. Summary of Phase I Results and Case Schedule for Phase II of Turboprop Parametric

	STEP 1			STEP 2		STEP 3		
PAYLOAD CONTAINERS	2	4	6	4		9		
MACH NUMBER	0.8			0.6	0.7	0.7	0.75	0.8
ALTITUDE, 1000 M	10.1							
FT	33							
WING SWEEP, RAD	0.44			0.17	0.26	0.26	0.35	0.44
DEG	25			10	15	15	20	25
WING LOADING, KN/M^2	5.03	5.71	5.76	5.63	5.85	5.84	5.88	5.69
LB/FT^2	105.25	119.5	120.5	117.9	122.5	122.3	123.0	119.0
ASPECT RATIO	7 - 16							
PROPELLER BLADES	6 - 10							
TIP SPEED, M/S	204 - 256							
FT/S	670 - 840							
DISK LOAD, KW/M^2	281-640							
HP/FT^2	35 - 80							

subjected to the propeller slipstream. The second is how the propfan diameter affects engine spacing along the wing, which in turn becomes a factor in aircraft design through consideration of propeller tip-to-ground clearance, engine-out operation, and wing weight relief benefits.

STEP 1 - Aircraft designed to fly at a cruise Mach number of 0.8 and carry payloads of 2, 4, and 6 containers were studied in the first step to obtain results on the "cost of quietness" - that is, the impacts on block fuel and direct operating cost of reducing noiseprint areas. Figure 15 shows the cost of quietness for the 4-container payload case, as an example. The graphs in the figure provide optimum designs for minimum noiseprint areas for an 80-EPNdB noise level under full power and cutback* conditions for variations in the level of block fuel and direct operating costs** at three fuel prices. The number of propeller blades and the tip speed are listed with the designated points. Appendix F contains all of the parametric results and provides an explanation, with examples, of the process used to obtain the minimum values for each designated point on the figures. Consequently, only a few representative sets of data are presented here as needed to aid the discussion.

In each case, the minimum noiseprint area occurs when the propeller diameter reaches a limit of 6.1 m (20 ft). This limit was imposed based on geometric considerations, or more specifically, to assure that the propeller can be installed without having to change the aircraft by, for example, extending the length of the landing gear. For clarification, the engine centerline is 4.1 m (13.5) above the ground for the aircraft used in this study. With a 6.1 m (20 ft) diameter propeller, this leaves only 1.1 m (3.5 ft) of clearance between the ground and the tip of the propeller - a clearance that was judged to be minimal in the interest of avoiding propeller damage from ground debris. Although over-the-wing engine mounting and extended landing gear length will permit larger propeller diameters, they introduce additional problems that are beyond the scope of this study and might, therefore, warp the parametric study results by introducing additional variables.

In general, the trends of the results in Figure 15 are as expected with increasing fuel prices causing higher operating costs. The decreasing noiseprint areas and increasing operating costs that are experienced in moving from right to left along the curves are caused by reductions in the propeller tip speed. Also, lower noiseprint areas are obtained with cutback power than for full power. The only exception to this is for the case of a 6-container payload at the highest tip speed of the propeller. What has happened in this case is that the reduced rate of climb of the aircraft extends the length and area of the noiseprint by an amount that exceeds the benefits obtained by reducing the width and area of the noiseprint through the cutback in engine power and noise emission.

By comparing the results for a single fuel price, as shown in Figure 16, the effect of changes in payload size becomes apparent. Of the three payload sizes considered, aircraft designed for the 4-container payload have slightly lower operating costs than those with a 6-container payload and considerably lower costs than those with a 2-container payload for a constant noiseprint area. The initial tendency might be to disbelieve the

---

* Cutback power was assumed to consist of full power through takeoff and climb to 305 m (1000 ft) altitude, followed by a power reduction to the minimum levels permitted by FAR 36. This gives a flight profile that is consistent with the guidelines of FAR 36 for measuring takeoff noise. That is, the only change to the takeoff configuration permitted in climb is that the gear is retracted; the flaps remain at the takeoff setting.

** Direct operating costs presented throughout this report are based on a short ton of 910 kg (2000 lb).

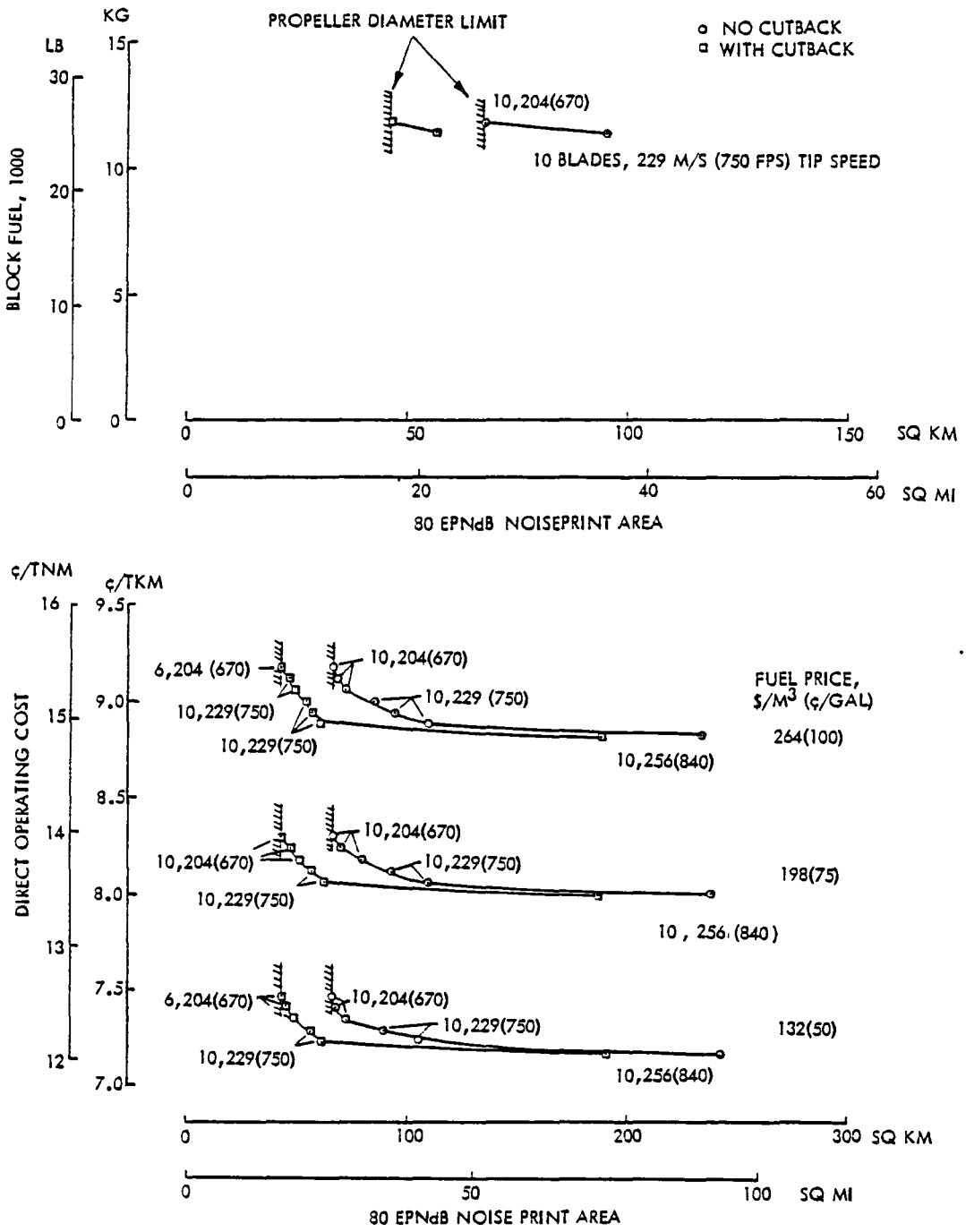

Figure 15. Cost of Quietness for 0.8 Mach Number and 4-Container Payload

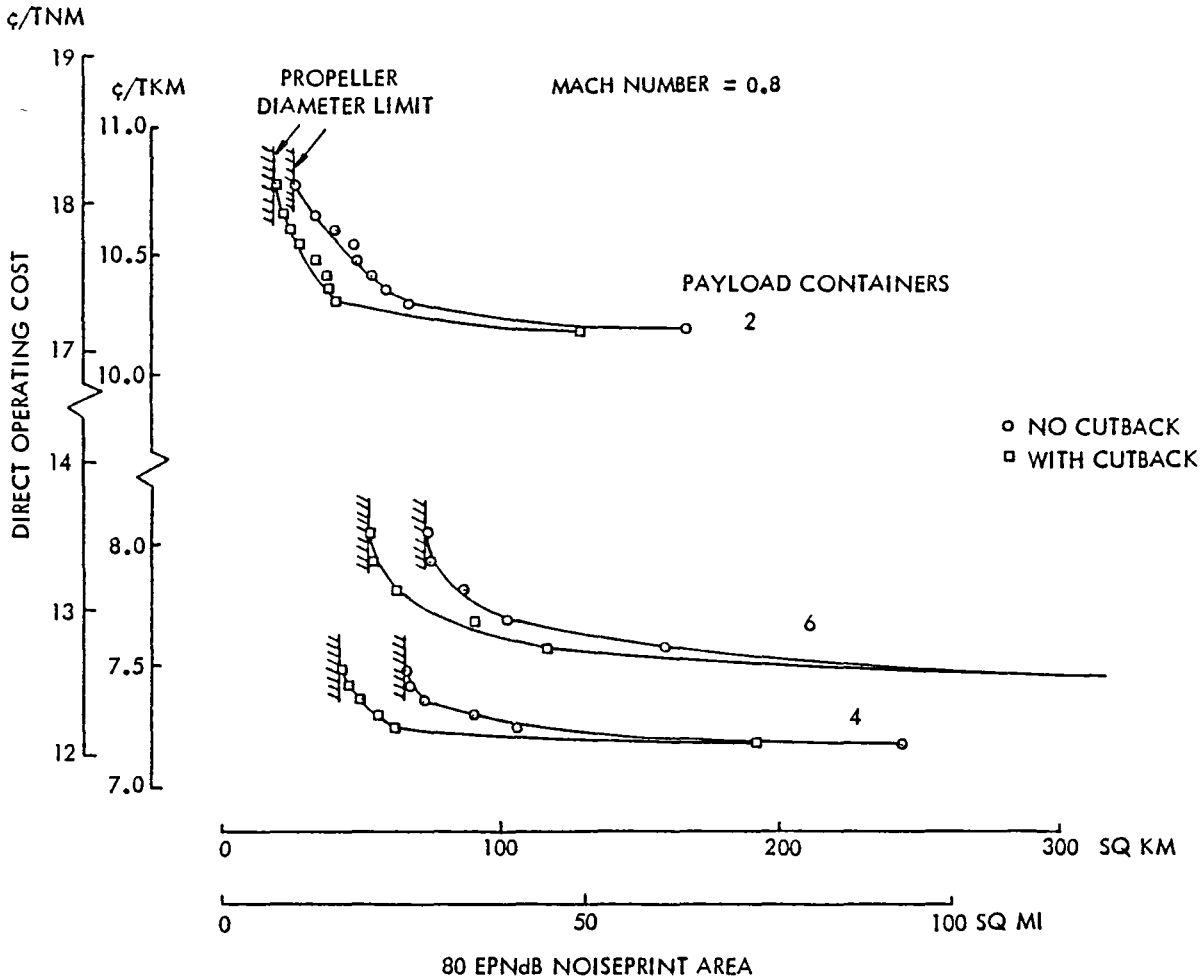

Figure 16. Effect of Payload on Cost of Quietness for 132 $/m^3 (50 ¢/gal) Fuel

results if one is engrained with the philosophy that "bigger is better" and has forgotten the discussion provided earlier on cargo compartment sizing. Recall, that the cargo compartment was designed to carry containers two abreast for part of its length to accommodate the 6-container payload in a fuselage of reasonable length, while the smaller payloads were carried in a single row of containers. Thus, the results in the figures merely reflect the inefficiency of trying to design for a 6-container payload, which is the size that requires a transition from one to two rows of containers.

STEP 2 - Based on the typical results in Figure 16, the 4-container payload was selected for use in the second step of this Phase II study, which was concerned with the effect of cruise speed. "Cost of quietness" data were then obtained for each of the three fuel prices for cruise Mach numbers of 0.6 and 0.7. These results were combined, as illustrated in Figure 17, with those for an 0.8 Mach number to illustrate the effects of speed.

Several features of the curves merit some comments and explanations. As in the first step, the 6.1 m (20 ft) propeller diameter limit defines the minimum noiseprint area for each case. The increase of these minimum areas with increasing Mach number is the result of larger engines required by the aircraft.

Increasing fuel price has the most dramatic effect on the result. At the lowest value of 132 $/m^3 (50 ¢/gal), the 0.8 and 0.7 Mach number designs are

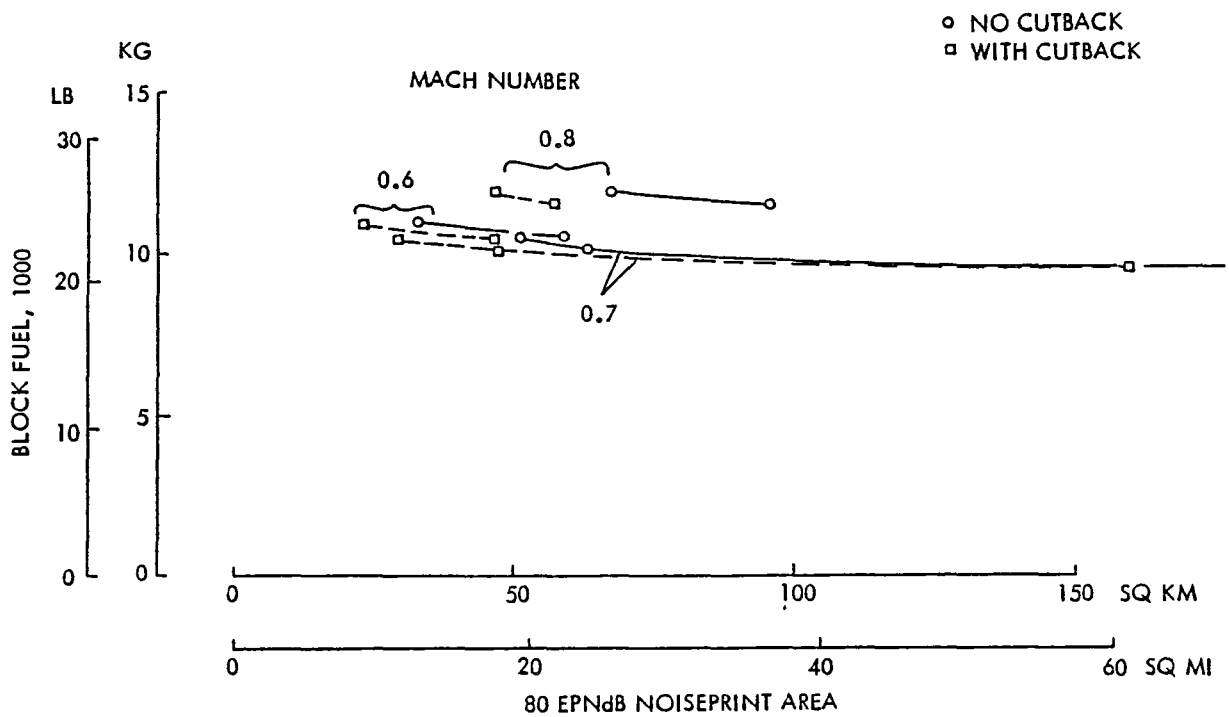

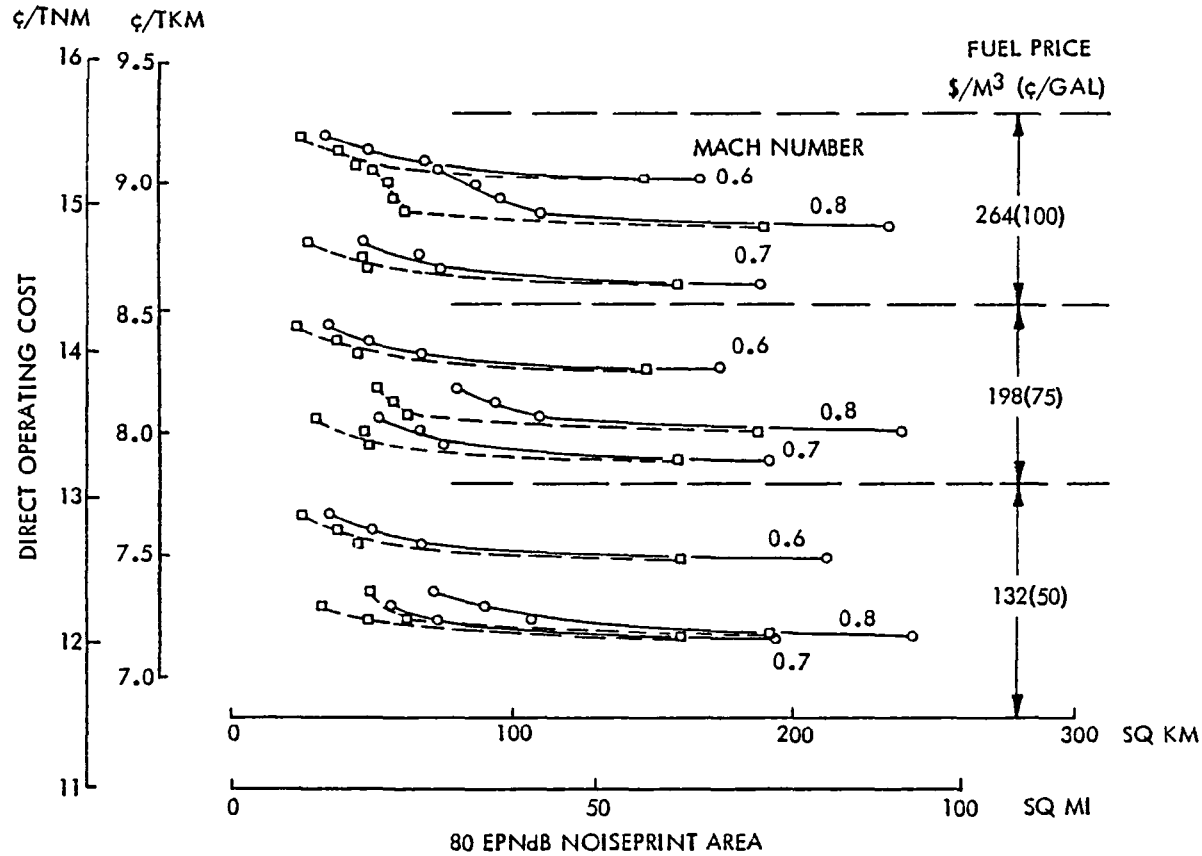

Figue 17. Speed and Fuel Price Effects on Cost of Quietness for 4-Container Payload Aircraft

close together for the different noiseprint areas, but as the fuel price increases, the 0.8 Mach number designs are driven toward those at 0.6 Mach number, which are the most expensive set by a substantial margin. It appears that the increasing fuel cost for the highest speed is tending to balance the poorer productivity penalties of the lowest speed. This is borne out by the block fuel portion of Figure 17, which shows that the 0.8 Mach number designs have the highest fuel requirements.

The indications from Figure 17 are that the best cruise Mach numbers for minimizing block fuel or direct operating costs are between 0.6 and 0.8, with the fuel price having a significant influence on the value which minimizes the direct operating cost. To find the best speed, the cost results of Figure 17 were replotted, as in Figure 18, for full power conditions. With the results in this carpet-plot format, optimum trends and values are more readily apparent. At the lowest fuel price, minimum costs occur at a Mach number of 0.75 for all of the noiseprint areas. As the fuel price increases to the middle value, the optimum Mach number decreases to 0.74, and eventually it reaches 0.73 for the highest fuel price. Further increases in fuel price could conceivably drive the optimum Mach number even lower, but based on the block fuel results, the minimum optimum value appears to be about 0.7.

One additional observation needs to be made about the results in Figure 18. The curves of constant noiseprint area are very shallow near the optimum Mach number values for all three fuel prices. In fact, for any particular noiseprint area, variations of the Mach number within 3 percent of the optimum value produce less than a 0.3 percent increase in the direct operating cost. Based on these trends and results, a Mach number of 0.75 is selected as preferable because of immeasureable benefits of higher speed.

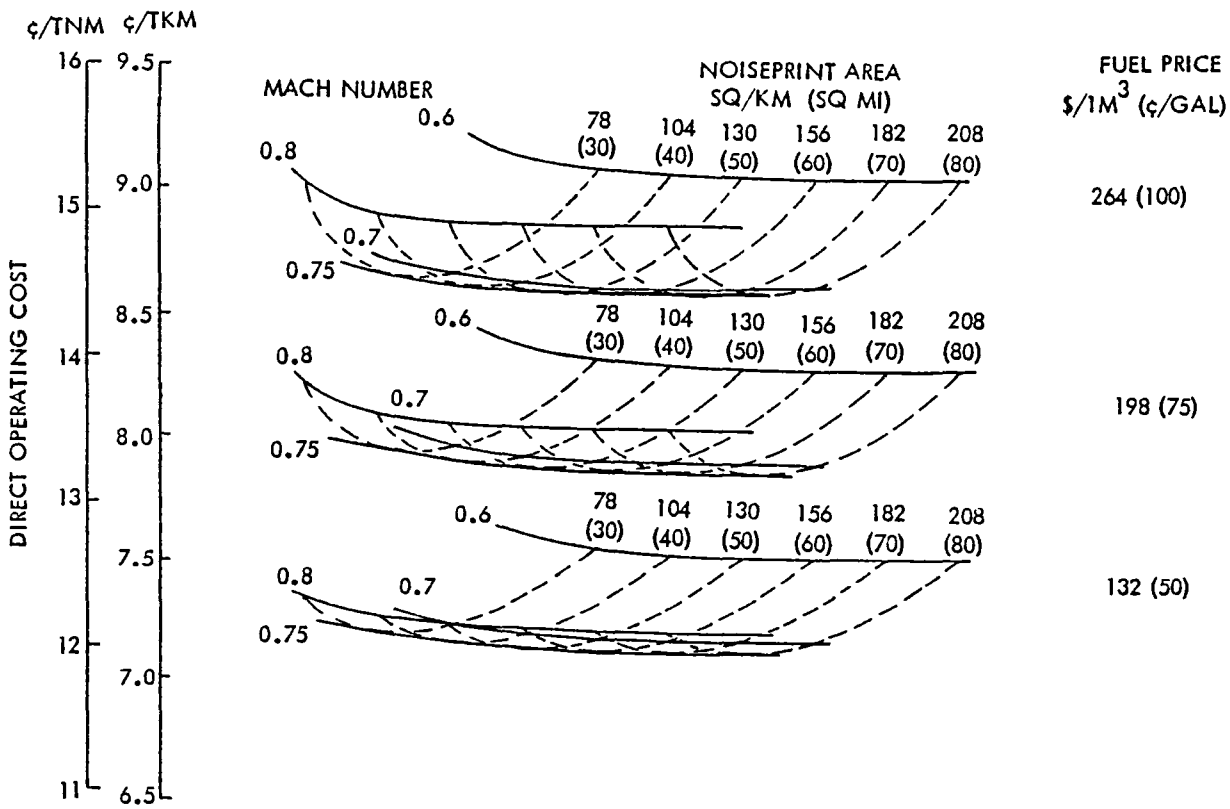

Figure 18. Comparison of Speed Effects for 4-Container Payload Aircraft at Full Power

STEP 3 - The investigation of payload size variation in the first step indicated that larger payloads are required to achieve efficient aircraft designed with two rows of containers. Consequently, a 9-container payload was selected for this third step because it does give an efficient cargo compartment arrangement with two adjacent rows of four containers each, followed by a single container in the center of the tapered portion of the aft fuselage. Also, if the aircraft is to be considered for joint civil and military applications, the corresponding payload weight of 30,600 kg (135,000 lb) is just adequate for carrying one fully equipped main battle tank - an item of prime military importance.

The range of Mach numbers considered in this step was reduced commensurate with the results in Step 2, which showed that the optimum Mach number is approximately 0.75. To concentrate attention close to the expected optimum value, cruise Mach numbers of 0.7, 0.75, and 0.8 were chosen for this third step.

Following the same approach as in the previous steps, noiseprint areas and direct operating costs were calculated for the matrix of aircraft designs indicated earlier in Table VII. The costs were calculated only for a fuel price of 264 $/m^3 (100 ¢/gal) because by this time in the study the other two prices had faded into historical oblivion. Subsequently, the data were compared, as shown by the example presented in Figure 19, to obtain the minimum values for each Mach number.

As in the previous cases, the trends of the results are those expected with both the direct operating cost and the block fuel decreasing toward an asymptotic minimum value as the noiseprint area becomes larger. The minimum noiseprint areas, which occur at the termination points on the left-hand side of each curve, are restricted by the 6.1 m (20 ft) propeller diameter limit. On the right-hand

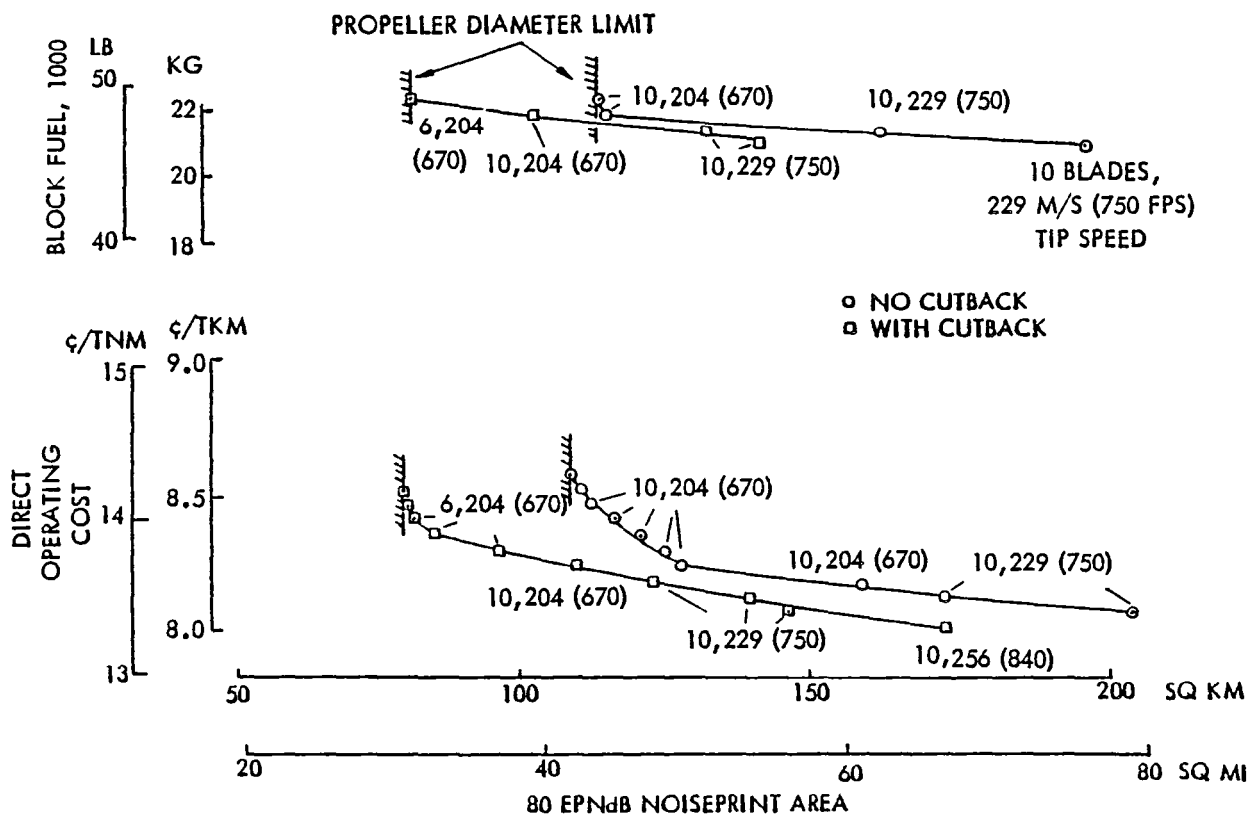

Figure 19. Cost of Quietness for 0.75 Mach Number and 9-Container Payload

side, the curves tend to become horizontal, which indicates that any further decreases in operating cost will be accompanied by very large increases in noiseprint area. This also suggests that additional increases in the number of blades or the tip speed of the propeller are not likely to prove beneficial.

To obtain a better insight into the effect of speed at this payload, the results were combined into a carpet plot format, as in Figure 20. The shape of the curves suggest that the minimum direct operating costs are achieved at 0.7 Mach number for the family of noiseprint areas, while minimum block fuel requires a Mach number at or slightly below 0.7. Before settling on a particular speed, however, some consideration of the vertical scales on the graph is in order. Inspection reveals that the direct operating cost increases by between 2 and 3 percent as the cruise Mach number rises from 0.7 to 0.75. In view of the small magnitude of the penalty for this speed increase, a Mach number of 0.75 was selected as preferable because it provides better compatibility with current aircraft flight operations. Also, by having the same speed as the other selected designs, a better indication can be obtained of the effect of payload variation than would be otherwise possible.

These parametric results show two trends on the cost of quietness curves (see Figures 15, 19, and in Appendix F, Figures F-19, F-21, F-26, and F-27), one of which is as expected, but the other is not. The expected trend is that increasing propeller tip speed reduces direct operating cost due to better efficiency, but increases noiseprint area because of helical Mach number effects, which are discussed further in Appendix C. Not expected is the result from varying the number of propeller blades. Ten blades always produced the aircraft with lowest direct operating costs, six blades

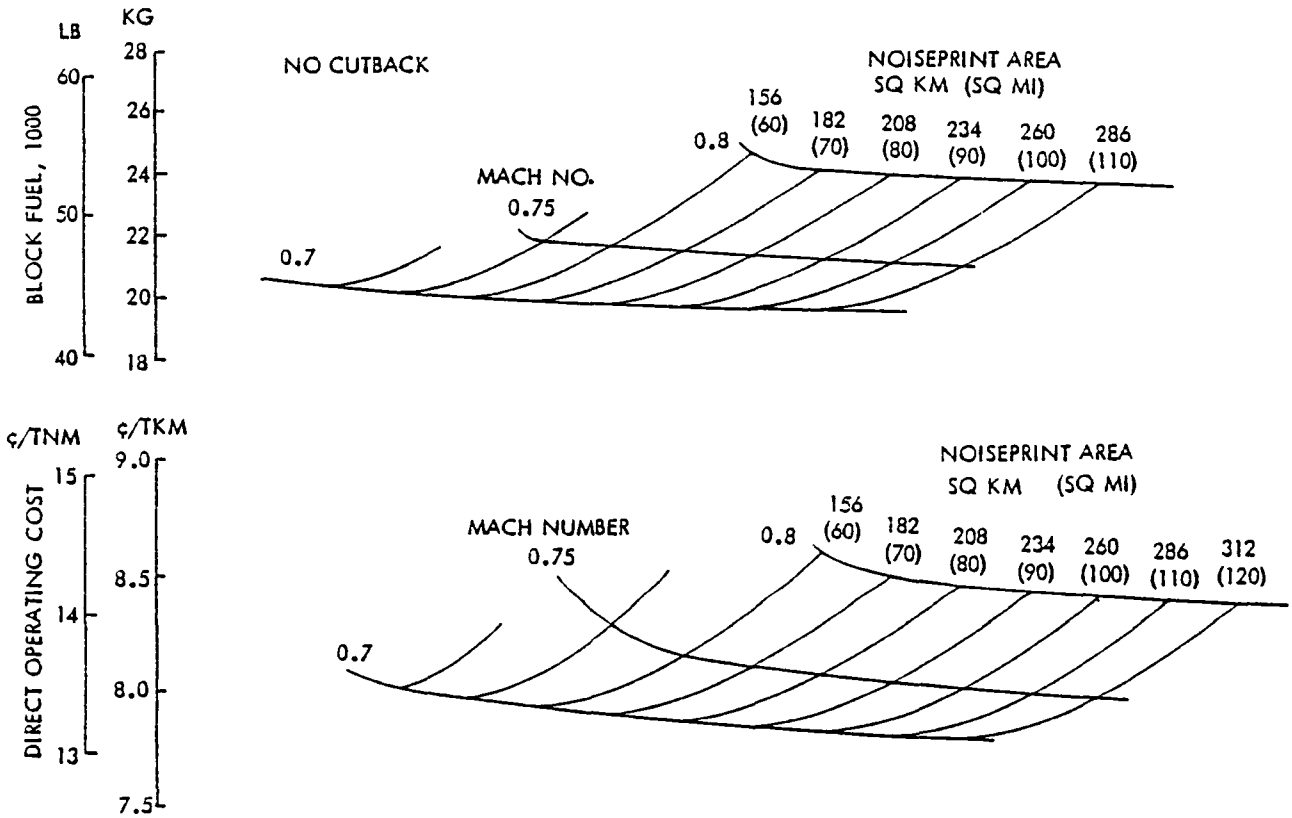

Figure 20. Comparison of Speed Effects for 9-Container Payload Aircraft

often gave the quietest aircraft, but aircraft with eight blades are conspicuously absent from all of the cost of quietness curves. The reason for this second trend is unknown; however, the differences in the cost and performance guidelines for the only data available on each number of blades may be responsible..

According to the propeller manufacturer and as noted in Appendix B, for a given diameter, both the 8 and 10-blade propellers will cost the same, but the 6-blade version will cost less. Differences in the total and per blade activity factors for each number of propeller blades may also contribute to the bias in the results. As noted in Appendix E, the data for the 6 and 8-blade propellers are for the same activity factor per blade of 230, but the 10-blade propeller has the same total activity factor as the 8-blade propeller, that is the activity factor per blade is 184 for the 10-blade propeller.

SELECTED DESIGNS

Three aircraft were selected from the parametric results for further study. They have been designated:

- o No. 1 Compromise Aircraft
- o No. 2 Quietest Aircraft
- o No. 3 Compromise Aircraft

and their major characteristics are summarized in Table VIII. As used here, the term "compromise" means a subjective attempt to minimize direct operating cost (DOC) and noiseprint area simultaneously. Thus, a compromise aircraft is selected from the "knee" of the DOC versus noiseprint area curve, and hence, is neither the quietest nor lowest DOC aircraft.

Necessarily, the compromise selection had to be subjective because no one has yet established the value of a unit reduction in noiseprint area. If the value of a unit reduction were known, then the graph could be drawn with the two axes labeled so that the length for an incremental change in one axis would correspond to that in the other. The compromise point would then be defined by the point where a line drawn at 0.785 rad (45 deg) to both axes is tangent to the curve. Until that value for a unit reduction is defined, however, changing the scale on the axes will produce different apparent compromise points.

Table VIII. Major Characteristics Selected for Turboprop Aircraft Designs

CHARACTERISTICS	AIRCRAFT SELECTION		
	1	2	3
GENERAL CLASSIFICATION	COMPROMISE	QUIETEST	COMPROMISE
MISSION FEATURES			
NUMBER OF CONTAINERS	4	4	9
CRUISE MACH NUMBER	0 75	0 75	0 75
CRUISE ALTITUDE, 1000M (FT)	10 1 (33)	10 1 (33)	10 1 (33)
WING GEOMETRY			
SWEEP, RAD (DEG)	0 35 (20)	0 35 (20)	0 35 (20)
LOADING, KN/M^2 (PSF)	5 89 (123 3)	5 85 (122 5)	5 88 (123 0)
ASPECT RATIO	12	15	12
PROPELLER			
NUMBER OF BLADES	10	6	10
TIP SPEED, M/S (FT/S)	229 (750)	204 (670)	229 (750)
DISK LOADING, $KW/M^2(HP/FT^2)$	402(50)	345(43)	402(50)

The first and third aircraft were selected to show the effects of increasing payload size. The first aircraft carries all of its 4-container payload in a single row, while the third aircraft, with a 9-container payload, uses a two-row arrangement. Both designs have the same cruise speed and their propulsion systems provide a compromise between lowest DOC and lowest noiseprint area. The second selection is the quietest aircraft possible for the same mission as the first. It will be used to illustrate the effects of changing a design to reduce noise.

TURBOPROP AIRCRAFT DESIGN REFINEMENTS AND SENSITIVITIES

Typically, parametric studies of aircraft preliminary designs include only the primary sizing variables of interest in order to isolate the optimum design with a reasonably limited effort. Many of the aircraft design details and performance characteristics are not addressed in the parametric study itself but are investigated afterwards, along with secondary sizing factors, only for the optimum design. In this study, the four secondary areas considered for design refinement on the three turboprop aircraft selected in the previous section were the landing gear, flight station, access to the cargo compartment, and engine mounting. Detailed weight estimates and distributions were then prepared for each aircraft along with estimates of the performance, noise, and economic characteristics. To benefit future efforts, a variety of sensitivity studies were performed to determine the most significant mission and cost parameters in terms of their effects on the aircraft designs.

This section contains detailed descriptions of the refined versions of the three selected turboprop aircraft, the results of the sensitivity analyses, and discussions of the various design refinements.

SELECTED TURBOPROP AIRCRAFT DESCRIPTIONS

Figures 21, 22, and 23 provide three-view drawings of the three aircraft, while the major characteristics of each are summarized in Table IX. Detailed descriptions of the various discipline-related characteristics are presented under the headings of Design, Weights and Balance, Propulsion, Performance, Noise, and Economics.

Design

Geometric dimensions of the three aircraft are compiled in Table X. Of

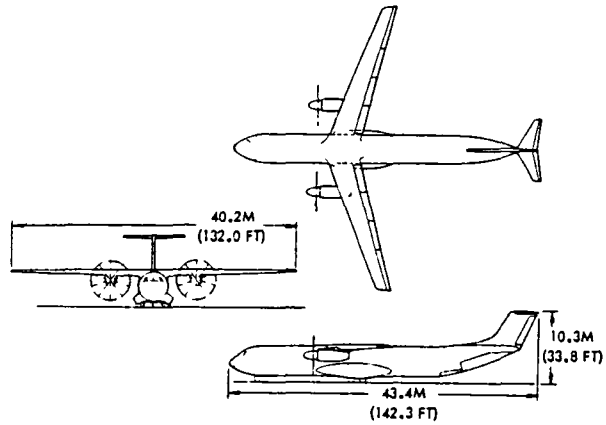

Figure 21. Layout of No. 1 Compromise Turboprop Aircraft

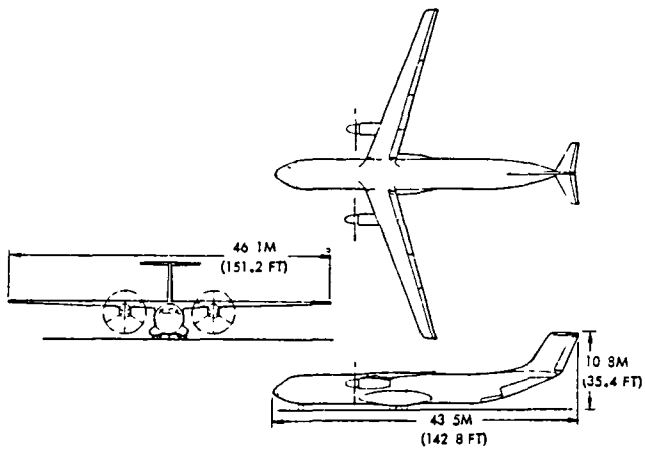

Figure 22. Layout of No. 2 Quietest Turboprop Aircraft

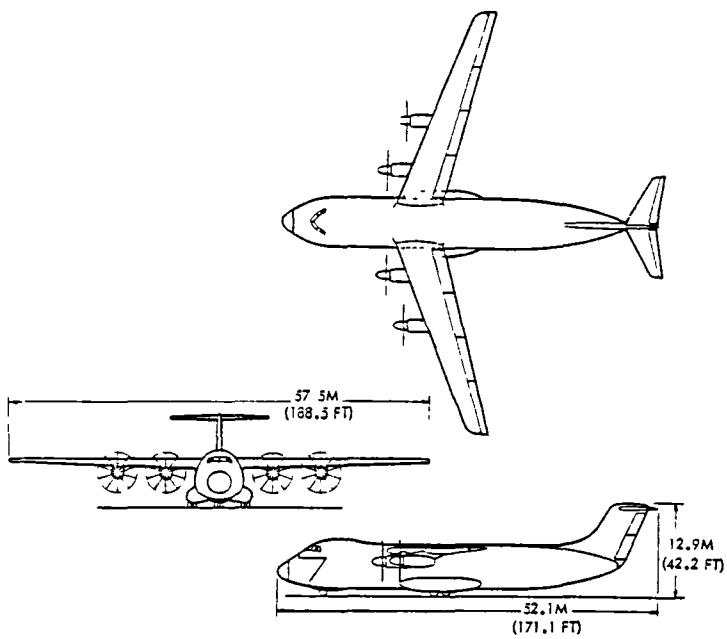

Figure 23. Layout of No. 3 Compromise Turboprop Aircraft

Table IX. Summary of Selected Turboprop Aircraft Characteristics

CHARACTERISTIC	TURBOPROP AIRCRAFT 1 COMPROMISE	2 QUIETEST	3 COMPROMISE
PAYLOAD CONTAINERS	4	4	9
CRUISE MACH NUMBER	0 75	0 75	0 75
CRUISE ALTITUDE, 1000 M (FT)	10 (33)	10 (33)	10 (33)
PROPELLER BLADES	10	6	10
TIP SPEED, M/S (FT S)	229 (750)	204 (670)	229 (750)
DISK LOAD, KW M^2 (HP/FT^2)	402 (50)	345 (43)	402 (50)
DIAMETER, M (FT)	5 6 (18 5)	6 1 (20)	5 6 (18 4)
WING ASPECT RATIO	12	15	12
LOADING, KN/M^2 (LB/FT^2)	5 9 (123 3)	5 9 (122 5)	5 9 (122 3)
WEIGHTS, 1000 KG (LB)			
OPERATING	40 3 (88 6)	44 1 (97 1)	78 1 (171 8)
FUEL	13 4 (29 6)	13 6 (30 0)	26 7 (58 9)
PAYLOAD	27 3 (60 0)	27 3 (60 0)	61 4 (135 0)
RAMP	81 0 (178 2)	85 0 (187 1)	166 2 (365 6)
FIELD LENGTH, M (FT)	1684 (5524)	1877 (6157)	1517 (4973)
80 EPNdB NOISEPRINT AREA KM^2 (MI^2)	82 8 (32 0)	57 7 (22 3)	164 9 (63 7)
DIRECT OPERATING COST * ¢/TKM (¢/TNM)	8 8 (14 7)	8 9 (15 0)	8 0 (13 3)

* FUEL AT 264 $/$M^3$ (100 ¢ GAL)

Table X. Geometry Summary for Selected Turboprop Aircraft

ITEM	TURBOPROP AIRCRAFT 1 COMPROMISE	2 QUIETEST	3 COMPROMISE
WING*			
ASPECT RATIO	12	15	12
SPAN M (FT)	39 6 (130)	45 7 (150)	57 0 (187)
AREA, M^2 (FT^2)	131 8 (1419)	139 3 (1499)	270 8 (2916)
THICKNESS RATIO	0 139	0 141	0 139
LOADING, KN/M^2 (PSF)	5 9 (123 3)	5 9 (122 5)	5 9 (122 8)
SWEEP, RAD (DEG)	0 35 (20)	0 35 (20)	0 35 (20)
FUSELAGE			
LENGTH, M (FT)	40 5 (133)	40 5 (133)	46 8 (154)
EQUIV DIA , M (FT)	4 2 (13 7)	4 2 (13 7)	6 3 (20 5)
HORIZONTAL TAIL**			
SPAN, M (FT)	8 6 (28 1)	8 4 (27 7)	13 2 (43 3)
AREA, M^2 (FT^2)	16 3 (175)	15 8 (170)	38 7 (416)
VERTICAL TAIL+			
SPAN, M (FT)	5 1 (16 8)	5 6 (18 5)	7 8 (25 5)
AREA, M^2 (FT^2)	21 7 (234)	26 4 (284)	40 2 (433)
CARGO COMPARTMENT			
ROWS OF CONTAINERS	1	1	2
LENGTH, M (FT)	24 7 (80 9)	24 7 (80 9)	31 1 (102 0)
WIDTH, M (FT)	2 7 (9 0)	2.7 (9 0)	5 6 (18 5)
HEIGHT, M (FT)	2 9 (9 5)	2 9 (9 5)	2 9 (9 5)

* TAPER RATIO = 0 40
** TAPER RATIO = 0 35 SWEEP = 0 44 RAD (25 DEG) ASPECT RATIO = 4 5, THICKNESS RATIO = 0 095
+ TAPER RATIO = 0 8 SWEEP = 0 52 RAD (30 DEG), ASPECT RATIO = 1 2, THICKNESS RATIO = 0 095

these, the cargo compartment size is fixed by the requirement to carry specified numbers of containers with reasonable allowances for tie-down and loading clearances. Similarly, the fuselage is constrained, being the minimum size that will encapsulate the cargo compartment.

Cargo is loaded into both the No. 1 and No. 2 aircraft through full-width doors located in the aft end of the fuselage. The doors are the clam-shell type that are used on the C-141 aircraft. Straight-in cargo loading is also standard on the No. 3 aircraft except that it is through a full-width nose visor door that allows simultaneous loading of two containers side-by-side.

On all three aircraft, the wings are attached to the top of the fuselage to accommodate the large propeller diameters without having to include extensions to the length of the landing gear. The engines are mounted beneath the wings, rather than above, to minimize both axi-symmetric thrust effects on the horizontal tail and adverse flow effects on the wing.

The landing gear is comprised of a single-strut nose gear and twin-tandem main gears mounted on each side of the fuselage. The nose gear consists of a single shock strut with two wheels mounted on a single axle. Each main landing gear has four wheels in a twin-tandem arrangement. Each pair of wheels is mounted on a common axle which, in turn, is attached to either the forward or the aft side of a trunnion-mounted support frame. Separate shock absorbers provide independennt suspension for the front and rear wheels on the main gear.

Weights and Balance

Table XI lists the weights for the major subsystems of the three aircraft. The propeller weight includes the weights of the blades, pitch change mechanism, and spinner. Under the Systems & Equipment heading have been combined the weights of the auxiliary

Table XI. Weight Summary for Selected Turboprop Aircraft, kg (lb)

ITEM	TURBOPROP AIRCRAFT		
	1 COMPROMISE	2 QUIETEST	3 COMPROMISE
STRUCTURE			
WING	9,135 (20,096)	11,672 (25,678)	22,050 (48,510)
FUSELAGE	9,791 (21,541)	9,837 (21,642)	18,277 (40,210)
HORIZONTAL TAIL	448 (986)	445 (980)	1,020 (2,243)
VERTICAL TAIL	525 (1,155)	607 (1,336)	931 (2,049)
NOSE GEAR	491 (1,081)	517 (1,138)	1,008 (2,218)
MAIN GEAR	3,287 (7,231)	3,462 (7,616)	6,748 (14,845)
NACELLE	825 (1,815)	819 (1,801)	1,628 (3,582)
PROPULSION			
ENGINES	2,216 (4,876)	2,549 (5,608)	4,365 (9,603)
PROPELLERS	2,395 (5,268)	2,599 (5,718)	4,700 (10,341)
GEARBOX	1,553 (3,416)	1,901 (4,183)	3,037 (6,681)
FUEL SYSTEM	903 (1,987)	909 (2,000)	1,270 (2,794)
MISCELLANEOUS	455 (1,000)	455 (1,000)	909 (2,000)
SYSTEMS & EQUIPMENT	8,246 (18,141)	7,430 (16,347)	10,070 (22,153)
OPERATING WEIGHT	40,270 (88,594)	44,132 (97,091)	77,796(171,152)
CARGO	27,273 (60,000)	27 273 (60 000)	61,364(135,000)
ZERO FUEL WEIGHT	67,543(148,594)	71,405(157,091)	139,160(306,152)
FUEL	13,463 (29,618)	13,638 (30,003)	26 626 (58,577)
RAMP WEIGHT	81 005(178,211)	85 043(187 094)	165,787(364,729)

power system, surface controls, instruments, hydraulics and pneumatics, electrical, avionics, furnishings, air conditioning, anti-ice system, auxiliary gear equipment, and operating equipment.

Figure 24 shows the loadability limits of the three aircraft along with the actual center of gravity envelopes. The zero fuel and gross weight values are based on an assumed uniform distribution of the payload throughout the cargo compartment. Similarly, a uniform distribution is assumed for the fuel in the wing at the ferry and gross weight conditions. The two loadability extremes are set by the horizontal tail size. The forward limit is imposed by trim constraints on the No. 1 and No. 2 aircraft and by nose wheel lift-off at 80 percent of stall speed for the No. 3 aircraft. Stability sets the aft limit for all three aircraft.

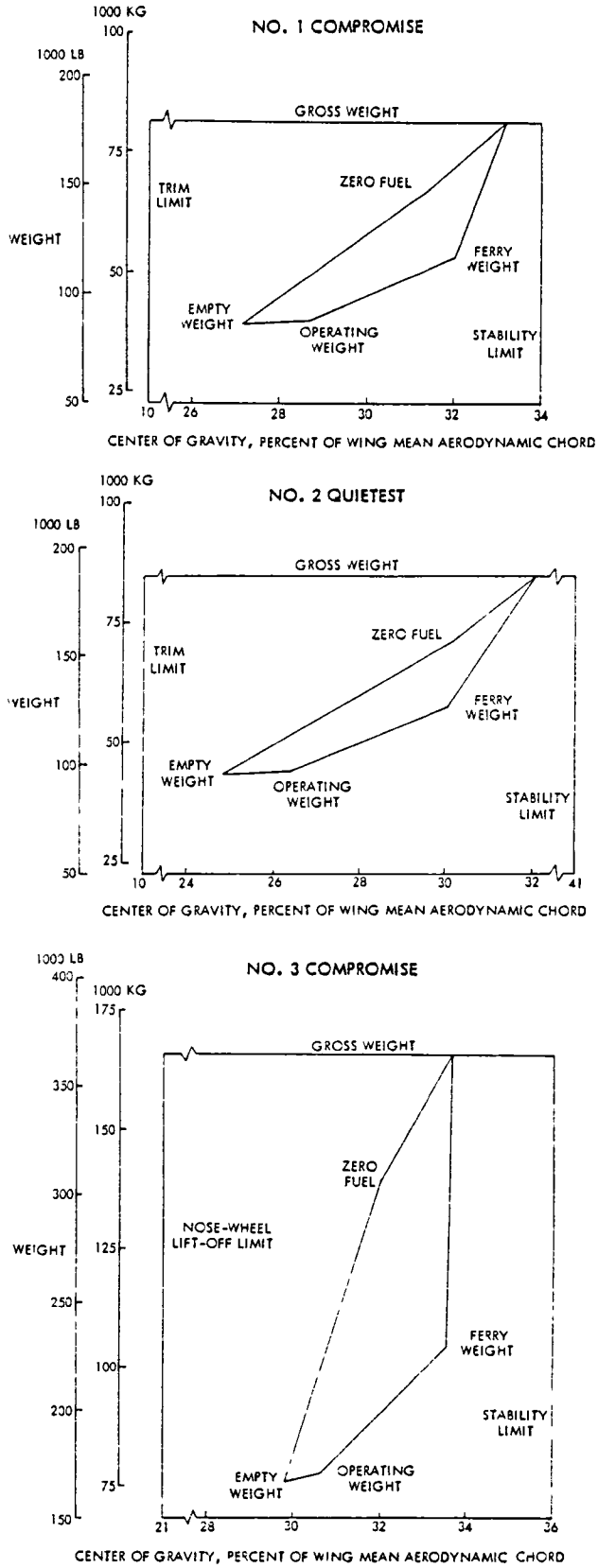

Figure 24. Loading Envelopes for Turboprop Aircraft

Performance

Some of the airport performance features of the three aircraft are presented in Table XII. Note that all three exhibit takeoff and landing field lengths that are considerably shorter than the 2440 m (8000 ft) maximum limitation of the study guidelines. Also, in every case there is sufficient thrust available to exceed the regulatory minimums of 2.4 percent and 3.0 percent for aircraft with two and four engines, respectively, for the engine-out condition during second segment climb. The maximum approach speed limit of 69 m/s (135 kt) is, however, a constraint on all three.

Table XII. Airport Performance Summary for Selected Turboprop Aircraft

	TURBOPROP AIRCRAFT		
	1 COMPROMISE	2 QUIETEST	3 COMPROMISE
TAKEOFF DISTANCES, M (FT)			
BALANCED FIELD	1684 (5524)	1877 (6157)	1440 (4726)
OVER 11 M (35 FT) OBSTACLE	1415 (4641)	1602 (5256)	1322 (4337)
OVER 15 M (50 FT) OBSTACLE	1473 (4837)	1656 (5432)	1379 (4523)
FAA FACTORED	1672 (5337)	1843 (6045)	1520 (4988)
TAKEOFF SPEEDS, M/S (KT)			
STALL	62 (121)	62 (121)	62 (121)
ROTATION	70 (137)	70 (137)	64 (125)
LIFT OFF	75 (146)	74 (144)	70 (136)
APPROACH SPEED, M/S (KT)	69 (135)	69 (135)	69 (135)
LANDING DISTANCE, M (FT)	1849 (6067)	1855 (6085)	1848 (6062)
FLAP DEFLECTION, RAD (DEG)			
TAKEOFF	0 35 (20)	0 35 (20)	0 35 (20)
LANDING	0 87 (50)	0 87 (50)	0 87 (50)
ENGINE-OUT GRADIENT	0 0498	0 0473	0 1142
LIFT COEFFICIENTS			
TAKEOFF	2 60	2 60	2 60
LANDING	3 14	3.14	3 14

Productivity capabilities of the three aircraft are indicated by the payload-range curves in Figure 25. The particular payload-range combination specified for each aircraft, as a basic design point, is specially designated on the graphs. As per the study guidelines, the aircraft have the capability to carry up to a 20 percent payload overload. For this overload, the range is reduced to the value indicated at the point of intersection of the con-

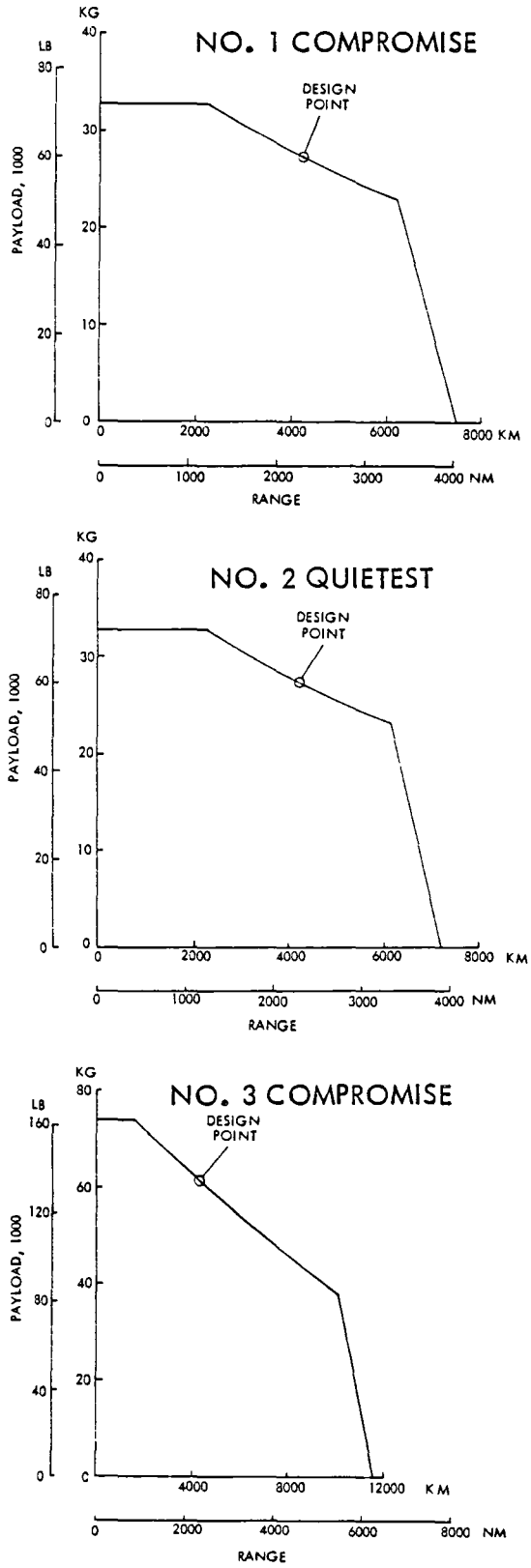

Figure 25. Productivity Capabilities of Turboprop Aircraft

stant gross weight line with the horizontal line which represents the 2.5-g structural limitations. Increased range is attainable by trading payload weight for fuel weight until the wing volume for carrying fuel becomes a limitation. Further increases in range are achieved only at a reduced gross weight with smaller payloads until the ferry range, or zero-payload range, is eventually reached.

The payload-range results were calculated based on the aircraft performance characteristics which are presented in Table XIII and Figures 26 to 28. Table XIII shows the various components that contribute to the total drag buildup and lists the values for the three aircraft. Note that there is no item labelled nacelle drag because it is accounted for in the net thrust of the propulsion system.

Table XIII. Drag Buildups for Selected Turboprop Aircraft

	TURBOPROP AIRCRAFT		
	1 COMPROMISE	2 QUIETEST	3 COMPROMISE
PROFILE DRAG			
WING	62 7 *	64 9	58 4
FUSELAGE	68 5	64.9	55 9
EMPENNAGE	17 6	18 2	17 0
INTERFERENCE	7 4	7 4	6 6
ROUGHNESS	4 5	4 4	3 9
SWIRL	17 6	16.6	24 4
SCRUBBING	1 8	1 4	2 2
TRIM	12 0	12 0	12.0
TOTAL PROFILE	192 1	189 8	180 4
INDUCED DRAG	94 4	74 6	93.7
TOTAL DRAG			
PROFILE	192.1	189 8	180 4
INDUCED	94.4	74 6	93.7
COMPRESSIBILITY	10 0	10 0	10 0
MISCELLANEOUS	5.2	5.2	5 2
TOTAL	301 7	279.6	289 3
CRUISE LIFT COEFFICIENT	0 57	0 57	0 57
LIFT/DRAG	18.97	20.34	19 71

* DRAG IN COUNTS, 1 COUNT = 0 0001

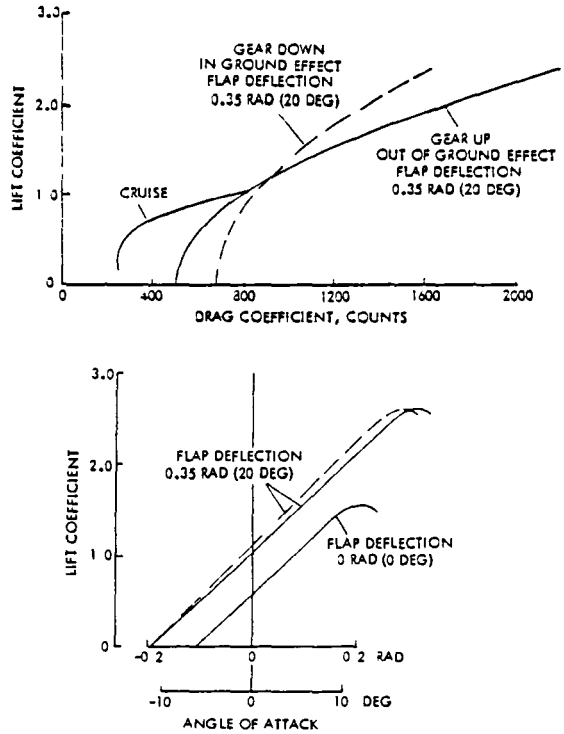

Figure 26. Drag Polars and Lift Curves for No. 1 Compromise Turboprop Aircraft

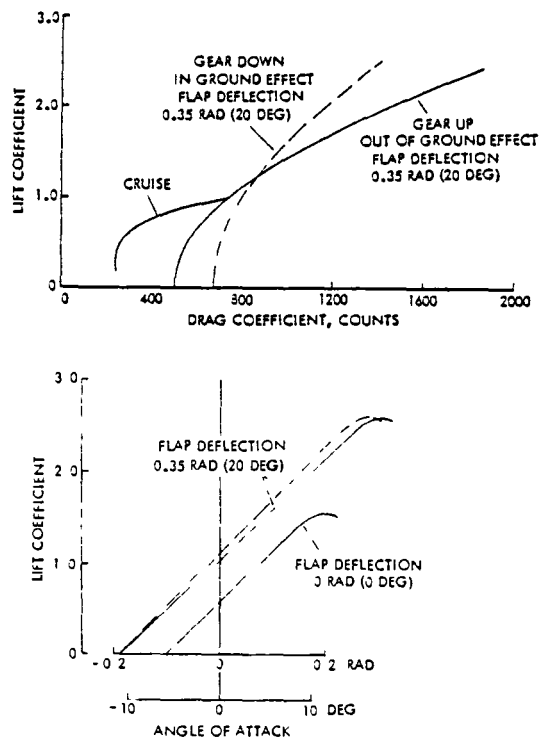

Figure 27. Drag Polars and Lift Curves for No. 2 Quietest Turboprop Aircraft

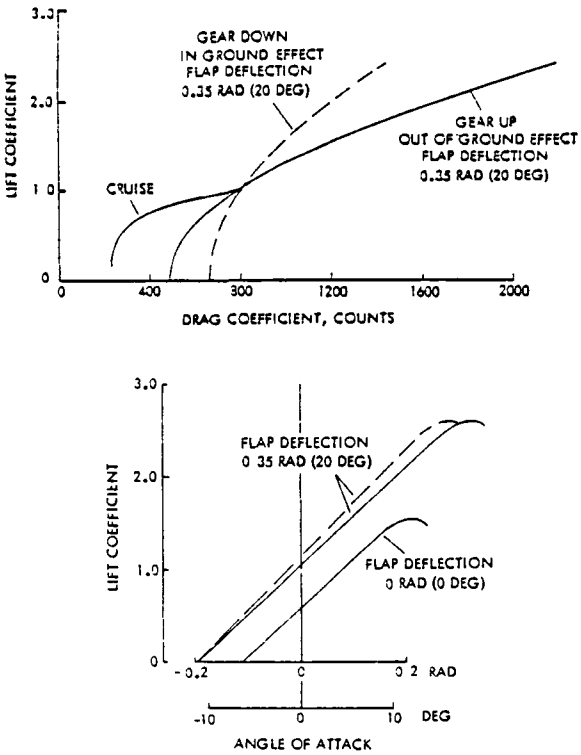

Figure 28. Drag Polars and Lift Curves for No. 3 Compromise Turboprop Aircraft

These drag buildup results were subsequently used to produce the drag polars shown in Figures 26 through 28. In each case, several polars are included. One is for cruise and the others are for various takeoff conditions of: flaps extended, in or out of ground effect, and gear retracted or extended. For completeness, the corresponding lift curves are also included in each figure.

Propulsion System

The main characteristics of the propulsion system for each aircraft are listed in Table XIV. For the propeller, disk loading values are given for both sea level and cruise conditions. In the area of performance, both the rated power and an equivalent thrust are shown.

Table XIV. Propulsion Summary for Turboprop Aircraft

ITEM	TURBOPROP AIRCRAFT 1 COMPROMISE	2 QUIETEST	3 COMPROMISE
PROPELLER			
BLADES	10	6	10
TIP SPEED, M/S (FT/S)	229 (750)	204 (670)	229 (750)
DISK LOAD, KW/M^2 (HP/FT^2)			
RATED	402 (50)	345 (43)	402 (50)
CRUISE	173 (21.5)	149 (18.5)	173 (21.5)
DIAMETER, M (FT)	5.6 (18.5)	6.1 (20)	5.6 (18.4)
ENGINE			
NUMBER	2	2	4
DIAMETER, M (FT)	0.8 (2.7)	0.9 (2.8)	0.8 (2.7)
LENGTH, M (FT)	2.1 (6.8)	2.1 (6.8)	2.1 (6.8)
NACELLE			
DIAMETER, M (FT)	1.6 (5.4)	1.6 (5.2)	1.6 (5.4)
LENGTH, M (FT)	4.3 (14.2)	4.4 (14.3)	4.3 (14.1)
PERFORMANCE			
RATED POWER, KW (HP)	12,779 (17,130)	12,895 (17,286)	12,589 (16,875)
RATED THRUST, 1000 N (LB)	124 (27.9)	102 (22.9)	122 (27.4)
CRUISE THRUST, 1000 N (LB)	22 (4.9)	21 (4.8)	21 (4.8)
THRUST/WEIGHT, N/KG (LB/LB)	3.0 (0.31)	2.3 (0.24)	2.9 (0.30)
CRUISE SFC, KG/HR-N (LB/HR-LB)	0.045 (0.46)	0.046 (0.47)	0.045 (0.46)

The dimensions and performance characteristics of both the propeller and engine are based on those for the Hamilton Standard Propfan and the Pratt & Whitney STS487 turboshaft engine, respectively. Descriptions and detailed data for the baseline versions of each are included in Appendix E along with an outline of the methods used to scale the baseline systems to other sizes.

Noise

For new aircraft, FAR 36 stage 3 noise limits specify maximum equivalent perceived noise levels (EPNL) in decibels (dB) at three measuring point conditions: takeoff flyover, takeoff sideline, and approach. Figure 29 shows the proximity of these measuring points relative to an airport and an aircraft flight profile. For illustration purposes, both takeoff and approach are shown slightly offset from the runway centerline which is used as a base for specifying distances to the measuring points. Two of the three measuring

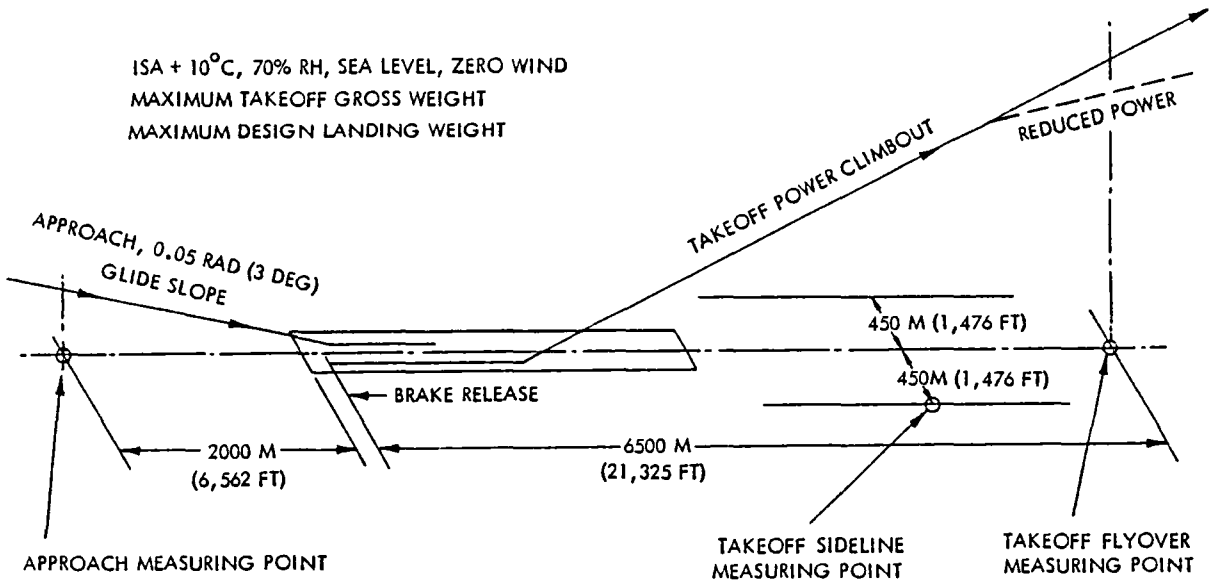

Figure 29. Location of Noise Measuring Points Relative to Runway and Aircraft Flight Profile

points, takeoff flyover and approach, are clearly fixed in space, but the third, takeoff sideline, varies for each aircraft. This occurs because, while the distance outward from the flight profile centerline to the measuring point is fixed, the position along the flight profile is defined in terms of a particular condition rather than a dimension. Specifically, the takeoff sideline noise is measured at that point along the flight profile where the sideline noise reaches the highest value.

Figure 30 shows the FAR 36 noise limits, which are a function of aircraft size, along with the noise levels predicted for the three aircraft at the three measuring points. For all cases, the three aircraft are quieter than the FAR 36 limitations.

Two noise-level values are shown for takeoff flyover for each aircraft. One is for a full-powered takeoff and climb, while the other is for a cutback power profile*. An interesting result is illustrated for the takeoff flyover cases: cutting back power during climb is not always beneficial in reducing noise at the measuring point. This occurs because the reduction in propulsion noise is more than compensated for by the reduced flyover altitude.

Further insight is gained into the noise levels at the measuring points by examining the contributions of the various noise sources, which are listed in Tables XV, for the three aircraft. Several observations are readily apparent:

- The propeller is the predominant contributor to full-power takeoff and sideline noise levels.
- By cutting power during climb, propeller noise is reduced to about the same level as airframe noise.
- During approach, airframe noise is either the predominant source or close to it.
- Engine noise is not a primary contributor on takeoff but it is much more significant during approach.

*FAR 36 defines a cutback power profile, relative to a full-powered profile, as follows. Takeoff is the same for both and during climb the flaps remain deployed at the takeoff position. After reaching 305 m (1000 ft) altitude, engine power is reduced in the cutback case to a level that will still satisfy the FAR 36 requirements.

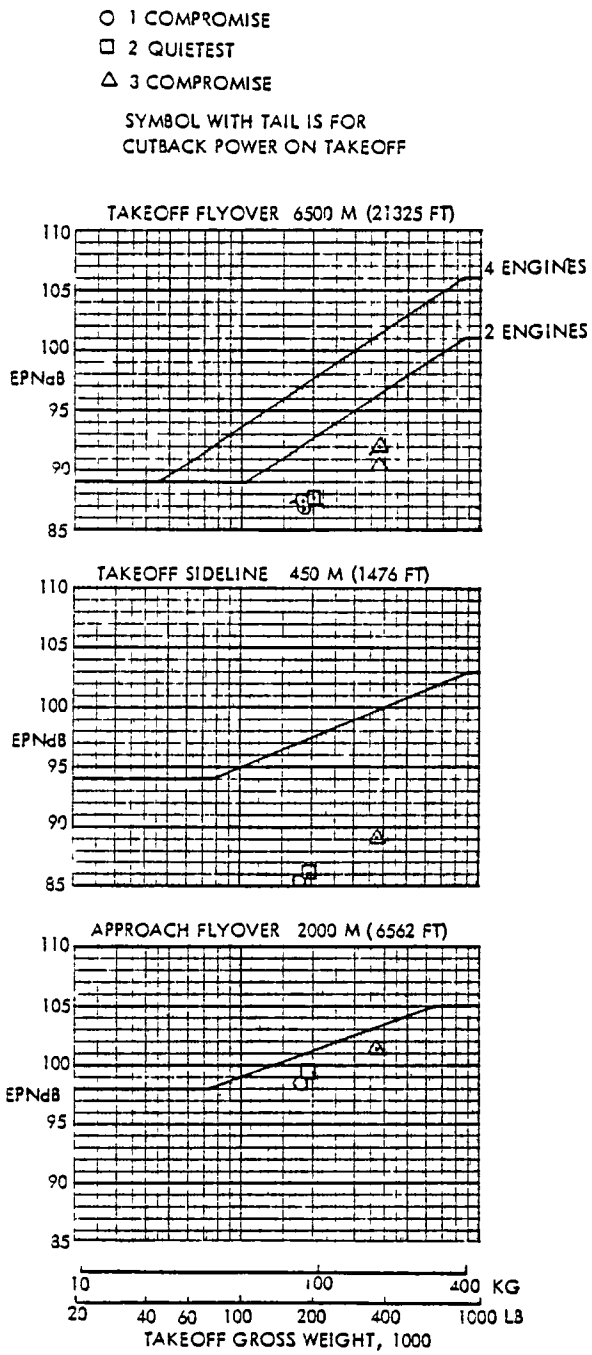

Figure 30. FAR 36 Stage 3 Noise Limits and Noise Levels of Selected Turboprop Aircraft

Table XV. Noise Source Distribution for Turboprop Aircraft

NO. 1 COMPROMISE

NOISE SOURCE	MEASURING POINT: TAKEOFF FULL POWER	TAKEOFF CUTBACK	APPROACH	SIDELINE
PROPELLER*	84.81	85.42	97.73	83.25
COMPRESSOR	55.70	68 05	96.53	52.45
TURBINE	71.62	76 62	96.19	69.54
CORE	74.49	73 13	81 58	73.00
JET	62.30	56.89	56.49	60.57
AIRFRAME	80.29	83.17	98.81	78.47
TOTAL	88 18	89 76	105 22	86.53
DURATION CORRECTION	-1.45	- 2 54	- 6 71	-0.97
EPNL	86.73	87 21	98 50	85.56

NO. 2 QUIETEST

NOISE SOURCE	MEASURING POINT: TAKEOFF FULL POWER	TAKEOFF CUTBACK	APPROACH	SIDELINE
PROPELLER*	86.74	84 86	92 95	84 88
COMPRESSOR	58 61	69 91	100.73	54 84
TURBINE	74 22	78 55	95 56	70.98
CORE	75 44	73 79	80.74	74 14
JET	63 73	56 55	53 89	61 88
AIRFRAME	81 00	84 19	98 93	78 66
TOTAL	88 45	89 01	105 51	86 46
DURATION CORRECTION	-0.87	- 1 69	- 5 99	-0 36
EPNL	87.58	87 32	99 51	86.11

NO. 3 COMPROMISE

NOISE SOURCE	MEASURING POINT: TAKEOFF FULL POWER	TAKEOFF CUTBACK	APPROACH	SIDELINE
PROPELLER*	88 28	90.33	100 70	86.74
COMPRESSOR	59.68	74.29	99 92	56.37
TURBINE	75.45	83.58	99 19	72.66
CORE	77.94	76 26	84 76	76.37
JET	67.05	57.86	60.83	65.25
AIRFRAME	84 32	89 44	100.76	82.59
TOTAL	91.72	95.37	108.11	90.05
DURATION CORRECTION	-1.46	- 3.43	- 6.60	-0.98
EPNL	90.27	91.95	101.52	89 07

*NOISE LEVEL OF SOURCES ARE IN PERCEIVED NOISE LEVEL TONE-CORRECTED MAXIMUMS (PNLTM)

Because the propeller is the predominant noise source, Hamilton Standard made a separate estimate of the propeller noise for the aircraft at the measuring points. As pointed out in Appendix G, there is good agreement between the propeller noise predictions that were derived based on the Hamilton Standard and Lockheed estimates of sound pressure level spectra.

Several additional observations are not quite as apparent but may be discerned with some reflection.

- For the takeoff and sideline cases, airframe noise is either the obvious second largest contributor or is in a group that ranks second. Assuming that the largest contributor, the propeller, can be reduced substantially, the airframe noise level represents somewhat of a plateau in possible noise reduction. Less flap deflection will reduce the airframe noise but will increase the takeoff distance and reduce the altitude over the measuring points. Other efforts to reduce the airframe noise will probably prove to be very expensive for very small improvements because the aircraft is otherwise in a clean configuration.

- There is a possibility that aircraft noise on approach can be reduced by decreasing the flap deflection from the 0.87-rad (50-deg) setting used. With a decreased flap deflection, there would be an increased approach speed for a given wing, or to maintain the same approach speed, the wing area would have to be increased. Both of these results tend to increase noise, but it is not known if the amount would be more or less than the reduction obtained from a smaller flap deflection. This is addressed later in a sensitivity study.

- Engine insulation will be, at best, a secondary consideration for noise reduction. In the takeoff and sideline cases, even if large reductions in propeller noise can be achieved so that it is no longer the primary noise source, the airframe, and not the engine, will be the main noise source. On approach, however, engine insulation offers more potential for noise reduction, but the extent of the reduction is still limited by propeller noise and the airframe noise plateau.

Thus far, attention has been focused solely on aircraft noise relative to the three standard measuring points. The shortcoming of this approach is that improvements in noise levels at the measuring points are usually accompanied by an increase in noise at other non-measuring points which are not taken into account. For example, although cutting the power may result in a lower noise over the measuring point, the adverse effect is that the aircraft is not able to climb at the same rate as with full power, thereby extending the length of the area under the flight path that is subjected to high noise levels.

When there is concern for minimizing the noise impact on the airport community, that is, if the objective is to minimize the number of people living around an airport who are exposed to high noise levels, then the size of the total area affected by aircraft noise is probably more meaningful than noise only at the measuring points. The boundary around such a noiseprint area is defined by the sequence of positions on the ground where a specified minimum noise level is reached. For this study, noiseprint areas have been calculated for three noise levels of 70, 80, and 90 EPNdB. The shapes of these areas are indicated by the contours in Figures 31 to 33 for the three selected aircraft. Due to the thin, long nature of the noiseprint areas, the takeoff and approach portions are shown separately, but the overlap of the two portions at the approach end of the runway is accounted for in determining the total noiseprint area.

Two sets of takeoff contours are presented: one for a normal full-powered condition and the other for a

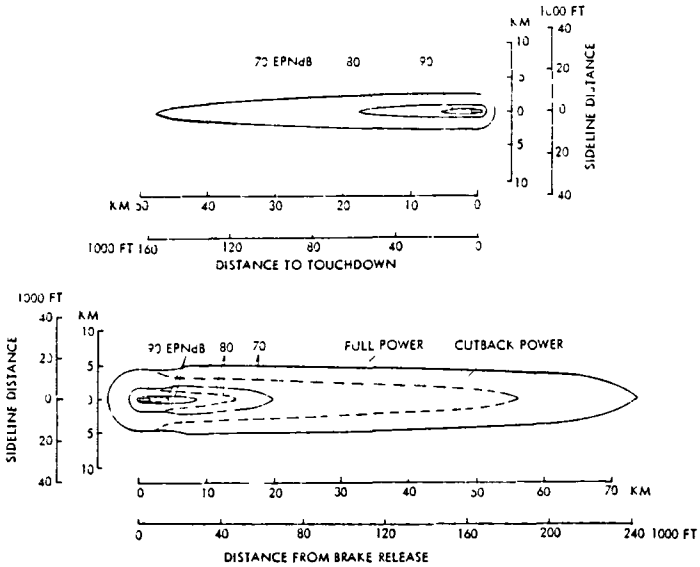

Figure 31. Noiseprints for No. 1 Compromise Turboprop Aircraft

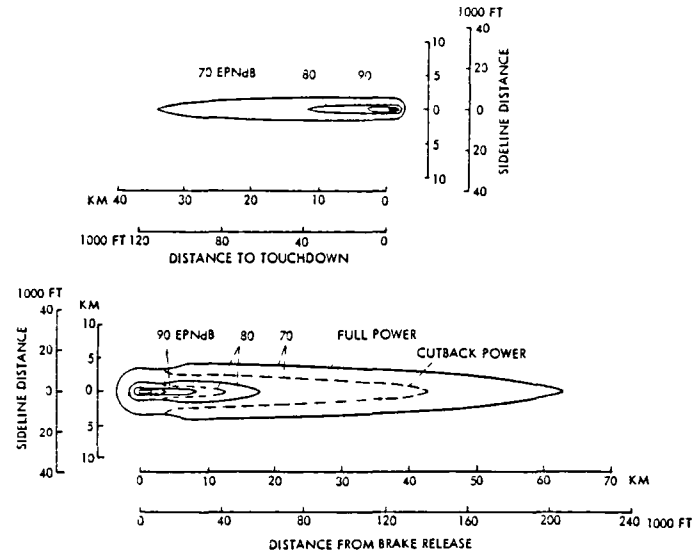

Figure 32. Noiseprints for No. 2 Quietest Turboprop Aircraft

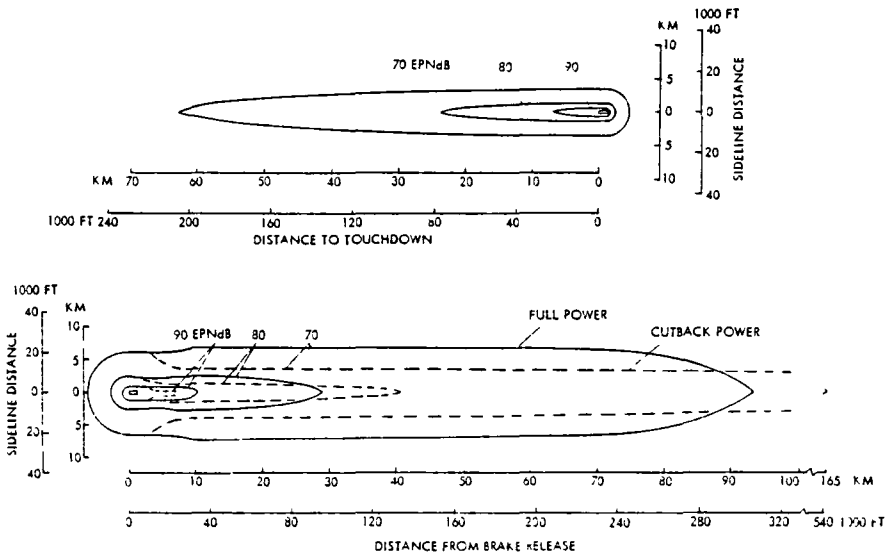

Figure 33. Noiseprints for No. 3 Compromise Turboprop Aircraft

cutback power case. In the cutback case, the engine power is reduced above a 305 m (1000 ft) altitude to the minimum permitted by regulation, and the aircraft continues to fly at that reduced power until after the noiseprint closes; i.e., the specified minimum noise level for the noiseprint is no longer perceived on the ground. Thereafter, power can be gradually increased to enhance climb performance, but care must be exercised to assure that the minimum noise level of the noiseprint is not subsequently experienced on the ground.

All of the full-power takeoff noiseprints show a slight inward dip of the sideline distance during takeoff and initial climb. The aircraft flight profile is responsible for this effect. Once the aircraft leaves the ground, it climbs at approximately constant speed while the gear and flaps are retracted, thereby decreasing the sideline distance slightly. The subsequent small increase in sideline distance occurs when the aircraft flies at nearly constant altitude while increasing its speed to that for the best rate of climb.

The noiseprints for the cutback power condition exhibit a substantial reduction in sideline distance shortly after takeoff. This reduction reflects the effect of cutting back the engine power and keeping the flaps deflected.

Both the No. 1 Compromise and the No. 2 Quietest aircraft have similar noiseprint characteristics in that the cutback power contour always closes before the one for full power and it has a smaller area. For the No. 3 Compromise aircraft, the cutback power contour still encompasses a smaller area than for full power; however, its closure distance becomes greater than that for full power as the minimum noise level is reduced. This difference in the behavior of the closure distance is the result of the number of engines on the three aircraft. The more engines there are on the aircraft the less severe the engine-out regulation. As a result, the greater the number of engines, the larger the amount of possible power cutback per engine, which means the quieter the propulsion system. Recall that the No. 3 aircraft has four engines, but the No. 1 and No. 2 aircraft have only two engines each.

Too much power reduction, however, may be counterproductive, because as power is reduced so is the aircraft capability to climb. To illustrate with an example, consider the No. 3 aircraft with the noiseprint contours in Figure 33. Cutback power reduces the 90-EPNdB noiseprint by 39 percent, the 80-EPNdB noiseprint by 16 percent, and the 70-EPNdB noiseprint by 11 percent. The trend here is that cutback power is less beneficial for reducing the areas at lower noise levels. Reference to Figure 33 indicates why this happens. Although the power cutback reduces the intensity of the noise source and the radial distance over which it is perceived, the inability of the aircraft to climb is keeping the aircraft in close proximity to the ground over much greater distances from brake release. In effect, for the 70-EPNdB noiseprint, the shorter sideline distance with cutback is nearly compensated for by the extended closure distance.

These results strongly indicate that further analyses are needed to optimize the climb profile for minimum noiseprint area for a particular noise level. Because of the limitations of this study, a representative profile was selected for use in sizing and evaluating all of the aircraft. The impact of this assumption will remain unknown pending identification of the optimum profile for one or more of the selected aircraft.

Because of the thin, elongated nature of the noiseprints and the varying curvilinear nature of the contours, the impact of cutback and different noise levels on the noiseprints is not easily visualized. To overcome this problem, the noiseprint areas are displayed in Figure 34 as squares of equivalent area. In this form, a correlation between the noise level and

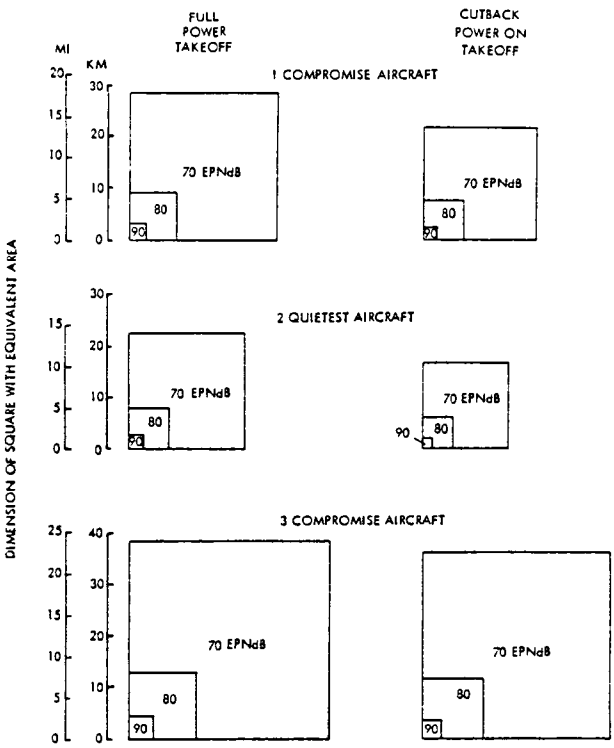

Figure 34. Squares of Equivalent Noiseprint Areas for Selected Turboprop Aircraft

area becomes apparent. It is: a 10 EPNdB reduction in the minimum noise level for the noiseprint produces approximately an order-of-magnitude increase in the noiseprint area.

Economics

Acquisition and direct operating costs for the selected turboprop aircraft were calculated using Lockheed's Aircraft Life-Cycle Cost Evaluation model, which is described in more detail in Appendix B. The acquisition cost portion of the model computes the cost of each structural and functional subsystem, that is, the wing, fuselage, engine, furnishings, etc., and then adds them all to obtain a total acquisition cost. Direct operating costs are determined based on the 1967 Air Transportation Association methodology with the coefficients updated to 1980 values.

Tables XVI and XVII contain the evaluation of the various elements that contribute to the acquisition and

Table XVI. Acquisition Cost Breakdown for Turboprop Aircraft

(COSTS IN $1000)

ELEMENTS	TURBOPROP AIRCRAFT 1 COMPROMISE	2 QUIETEST	3 COMPROMISE
WING	1877	2336	5289
TAIL	430	460	1021
FUSELAGE	2517	2528	5840
LANDING GEAR	361	377	716
FLIGHT CONTROLS	378	388	724
NACELLES	291	289	752
ENGINE INSTALLATION	51	55	103
FUEL SYSTEM	223	225	473
PROPULSION MISC	159	159	418
INSTRUMENTS	94	96	240
HYDRAULICS	215	222	490
ELECTRICAL	385	410	672
AVIONICS INSTALLATION	52	52	73
FURNISHINGS	383	383	678
AIR CONDITIONING	284	285	425
AUXILIARY POWER	52	54	74
SYSTEM INTEGRATION	334	368	984
TOTAL EMPTY MFG COST	8086	8687	18,972
SUSTAINING ENGINEERING	683	733	2,538
PROD TOOL MAINT	757	813	2,412
QUALITY ASSURANCE	519	557	1,297
AIRFRAME WARRANTY	502	539	1,261
AIRFRAME FEE	1582	1700	3,972
ENGINE	3951	3968	7 842
PROPELLER	498	387	994
AVIONICS	500	500	500
RESEARCH & DEVELOPMENT	2292	2379	8,601
TOTAL ACQUISITION COST	19,370	20,265	48,389

Table XVII. Direct Operating Cost Breakdown for Turboprop Aircraft

ELEMENTS	TURBOPROP AIRCRAFT 1 COMPROMISE	2 QUIETEST	3 COMPROMISE
CREW	1324*	1331	1440
FUEL & OIL**	3590	3635	7104
INSURANCE	750	785	1874
MAINTENANCE			
AIRFRAME LABOR	185	197	307
AIRFRAME MATERIAL	237	253	628
ENGINE LABOR	145	146	289
ENGINE MATERIAL	583	589	1157
BURDEN	660	686	1192
DEPRECIATION	2629	2743	6491
TOTAL TRIP COST	10,103	10,365	20,481
DOC, ¢/ATKM	8.73	8 93	7 91
¢/ATNM	14 65	15 03	13 31

* COSTS IN DOLLARS UNLESS NOTED OTHERWISE

** FUEL AT 264 $/M^3 (100 ¢/GAL)

direct operating costs, respectively, for the three selected aircraft. Inherent in the calculation of these costs are a number of guidelines and assumptions, which are summarily reiterated in Table XVII for continuity even though they have been presented

elsewhere in this report. To meet the specified productivity requires fleet sizes of 394 aircraft for the No. 1 and No. 2 designs and 175 of aircraft No. 3.

Direct operating costs are presented in this section for only the largest fuel price of 264 $/m^3 (100 ¢/gal). Although all three fuel prices are now historical, and are likely to remain so, the highest of the three is fairly close to current prices and, therefore, more meaningful. Direct operating costs based on the two lower fuel prices will be included with those derived for higher values as part of the sensitivity study results. Likewise, as part of the sensitivity studies, several of the items listed in Table XVIII will be subject to further scrutiny.

Table XVIII. Costing Guidelines and Assumptions

- JANUARY 1980 DOLLAR VALUES
- PRODUCTIVITY REQUIREMENT 26×10^{15} REVENUE KG-M, 15.4×10^{9} REVENUE T-NM
- LOAD FACTOR 100%
- AIRCRAFT ANNUAL UTILIZATION 3000 HR
- CREW SIZE 3
- DEPRECIATION 15 YR STRAIGHT LINE WITH 10% RESIDUAL
- HULL INSURANCE RATE OF 2%
- FUEL PRICES 132, 198, 264 $/M^3, 50, 75, 100 ¢/GAL

The relative importance of the various elements that make up the direct operating cost is more readily apparent when the data of Table XVII are presented pictorially, as in Figure 35. All three cost distribution layouts are drawn to the same scale so that the total area covered is an indication of the relative magnitude of the direct operating costs for each aircraft, with the No. 3 aircraft being the smallest and the No. 2 the largest. Because of the similarity between the No. 1 and No. 2 aircraft, their cost distributions are nearly identical, as expected. The No. 3 aircraft is somewhat different from the other two and, quite naturally, exhibits some variances in its cost distribution.

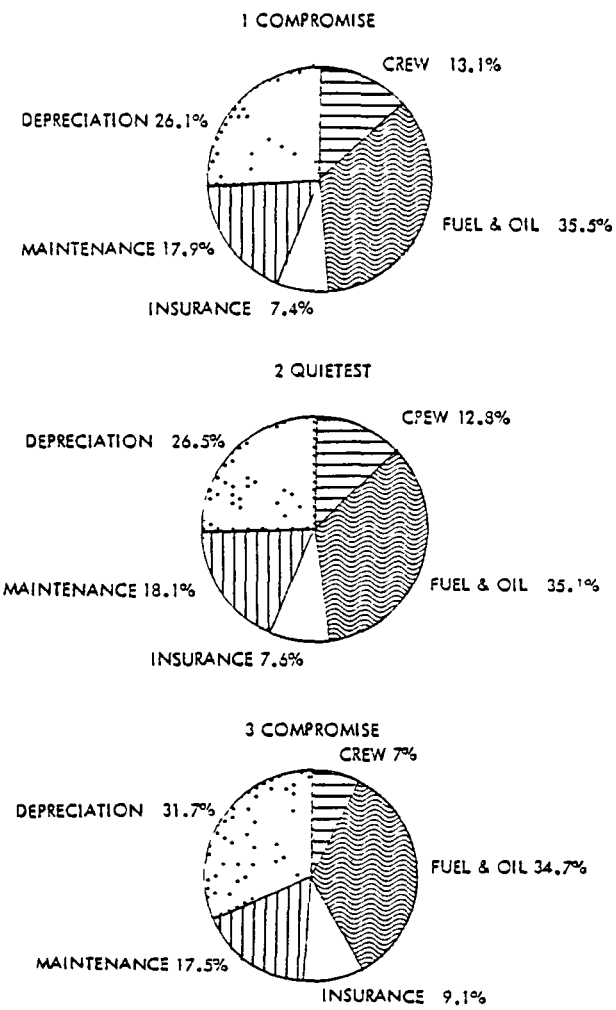

Figure 35. Direct Operating Cost Distributions for Turboprop Aircraft

In every case, the fuel and oil is the largest single element, and the two elements of maintenance and of fuel and oil remain essentially a constant percentage of the total. The changing features result from the increased payload. With more than twice the payload of the other two, aircraft No. 3 realizes a relative crew cost reduction of almost 50 percent that balances the increased depreciation and insurance for a larger aircraft.

SENSITIVITY STUDIES

Numerous sensitivity studies were performed for the three selected turboprop aircraft to isolate the effects of the parametric study variables, the study guidelines and constraints, and the design methodology. The particular sensitivity parameters investigated may be grouped under five general category headings of propulsion system, performance, wing geometry, weight, and economics. Results of these sensitivity studies on the three turboprop aircraft are summarized in Figure 36 while the details are contained in Appendix H.

The percent variations in DOC, block fuel, and noiseprint area were used as indicators, where applicable, of the effect of the various sensitivity parameters. To determine which factors have the greatest impact on these indicators, a measure of sensitivity (MOS) was devised. It is the ratio of the percent change realized in one of the indicators divided by the corresponding percent change in the sensitivity parameter. For evaluation purposes, the numerical MOS values are arbitrarily interpreted as follows:

Numerical Evaluation	Qualitative Interpretation
MOS < 1	Negligible
$1 \leq$ MOS < 2	Marginal
$2 \leq$ MOS < 5	Significant
MOS > 5	Critical

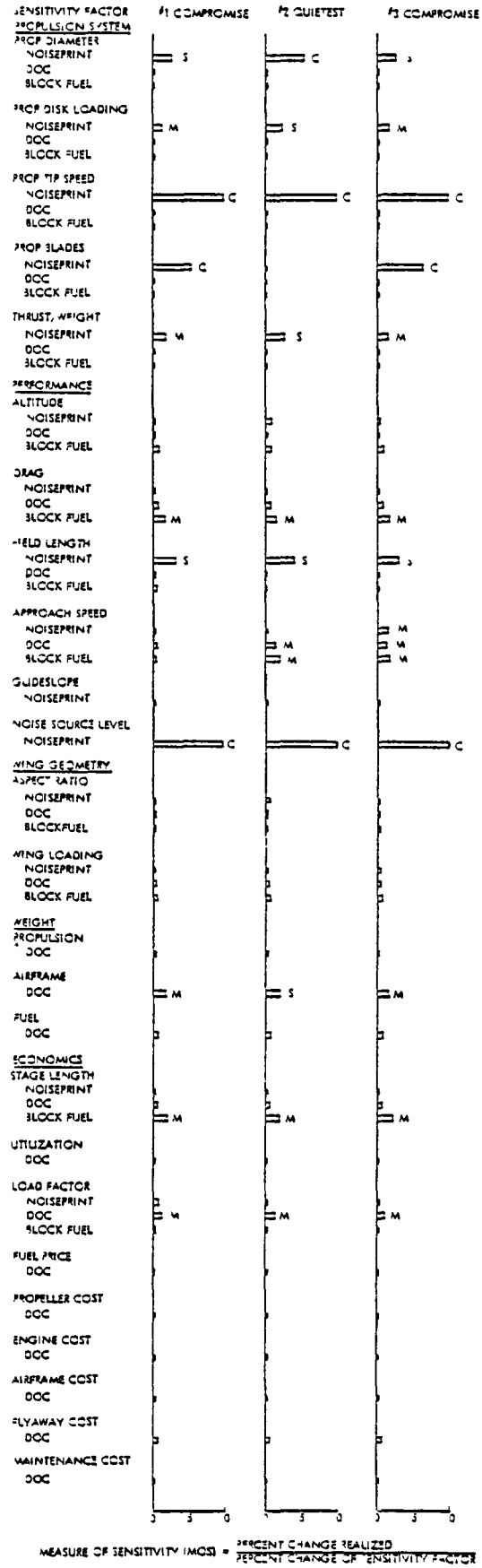

Figure 36. Summary of Turboprop Aircraft Sensitivity Study Results

A review of the sensitivity results shows that all of the propulsion related parameters (thrust/weight and propeller diameter, disk loading, tip speed, and number of blades) have a marginal-to-critical effect on the noiseprints for the three aircraft. In contrast, the DOC and block fuel are insensitive to the propulsion parameters.

Of the various performance related parameters, the only critical sensitivity is the result of noise source level variations. Likewise, there is only one significant sensitivity area - the effect of field length on noiseprint. Grouped in the marginally sensitive category are the effects of drag on block fuel, and approach speed on DOC, block fuel, and noiseprint. Negligible importance is attributed to both cruise altitude and the approach glideslope.

The two wing geometry parameters of wing loading and aspect ratio have only neglible effects on the three aircraft. In the weight category, variations in the airframe weight produce marginal to significant effects on the DOCs of the aircraft, but propulsion and fuel weight changes are of negligible concern.

In the area of economics, stage length and load factor have marginal effects on block fuel and DOC, respectively. All other effects are negligible.

Further details on each sensitivity study are provided in Appendix H. Unless otherwise noted, only one independent variable is allowed to change in each sensitivity study. In general throughout the sensitivity studies, the DOC variations are for a fuel price of \$264 \$/m^2 (100 ¢/gal), and the noiseprint variations are for an 80-EPNdB level.

DESIGN REFINEMENTS

Several features of the aircraft were examined in sufficient depth to assure that a feasible design would probably be achieved in a more detailed effort. In particular, four features were addressed: the flight station, landing gear, cargo compartment loading doors, and engine mounting.

Flight Station

Figure 37 shows a possible flight deck arrangement that is based on previous studies of numerous aircraft designs for a crew of three consisting of a pilot, copilot, and flight engineer. The flight station uses conventional wheel columns and rudder pedals for control of the aerodynamic surfaces. Nose wheel steering is achieved through a hand wheel on the side console by the pilot. The seating, instrumentation layout, equipment and system control location, work load distribution, center and side consoles, and avionics displays are intended to be readily accessible to the pilots to minimize fatigue.

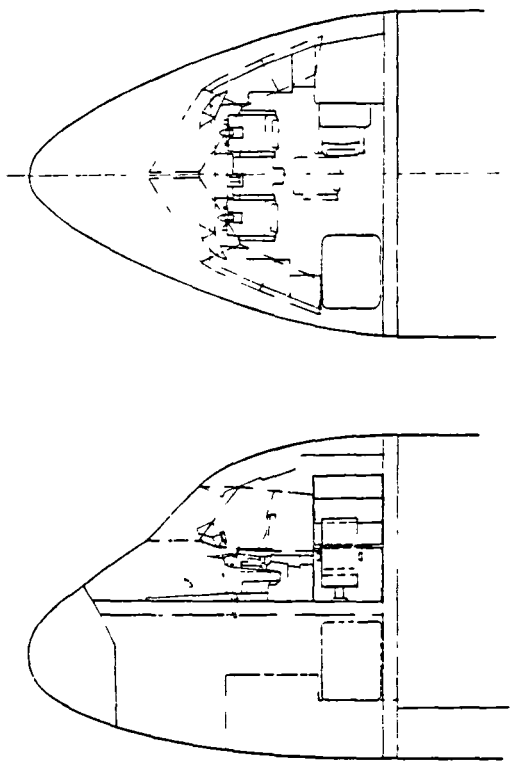

Figure 37. Flight Station Layout

A full crew station for the flight engineer is located directly behind the copilot, facing outward. The seat for this station is mounted on tracks so that it can be rolled to a position on the aircraft centerline (shown by the phantom lines) within easy reach of the overhead and center console panels. Besides assisting the pilots in subsystem management, the third crew member can serve as a scanner.

The No. 1 and No. 2 aircraft have a crew lavatory located below the flight deck on the right side under the flight engineer's station. Access to it is through the cargo compartment. The No. 3 aircraft, with its 747-type cockpit above the cargo compartment, has ample room aft of the flight station layout shown to accommodate a lavatory, bunks, and a galley.

The forward fuselage lines of the three selected aircraft are compatible with the basic geometry requirements of this flight station. External visibility is expected to be at least as good as on an L-1011 aircraft.

Landing Gear

The landing gear consists of a single strut nose gear and a twin-tandem main gear mounted on each side of the fuselage. Both the nose and main gears are based on the designs used in the L100 aircraft - a commercial version of the C-130 aircraft.

MAIN GEAR - Each main landing gear has a four-wheel, twin-tandem arrangement, as shown in Figure 38 for the No. 1 and No. 2 aircraft. Each pair of wheels is mounted on a common axle with lever arms that are attached to the fore and aft ends of a trunnion-mounted support frame. Individual shock absorbers between the axles and support frames provide independent suspension for the forward and aft sets of wheels. The No. 3 aircraft has a similar design with larger structural components and tires.

To retract the main gear, the wheels are first raised to the compressed position by the shock absorbers. The folding vertical brace

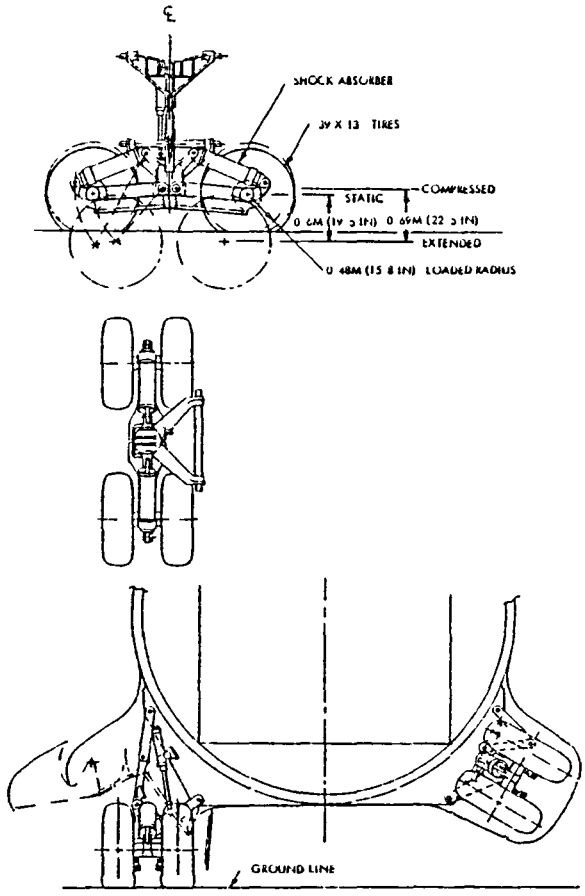

Figure 38. Typical Main Landing Gear Arrangement

is then folded outboard, and the main structural members together with the axle beams and wheels are rotated about the lower fuselage attach point so that the gear is enclosed in the wheel-well pod. One large outboard door and a smaller inboard door are automatically closed by the gear retraction motion.

During the gear extension cycle, the gear is rotated into the down position and the folding vertical brace is positioned on center. The shock absorbers are then extended to the normal gear-down configuration.

Separate up-locks and down-locks are provided for each gear. In case of a failure of the normal hydraulic system, an alternate hydraulic system is available for gear extension. A separate manual system is provided as backup to both the normal and alternate hydraulic systems. Also, in the event of a malfunction, there are panels in the cargo compartment through which

access to the main landing gear retraction mechanism is possible.

NOSE GEAR - The nose landing gear consists of a shock strut with two wheels mounted on a single axle. This gear is trunnion-mounted to the airframe, and it uses folding drag links to react any forward and aft loads that are encountered. Figure 39 shows the nose landing gear that is sized for the No. 1 and No. 2 aircraft. The No. 3 aircraft has a similar, but larger-sized, arrangement.

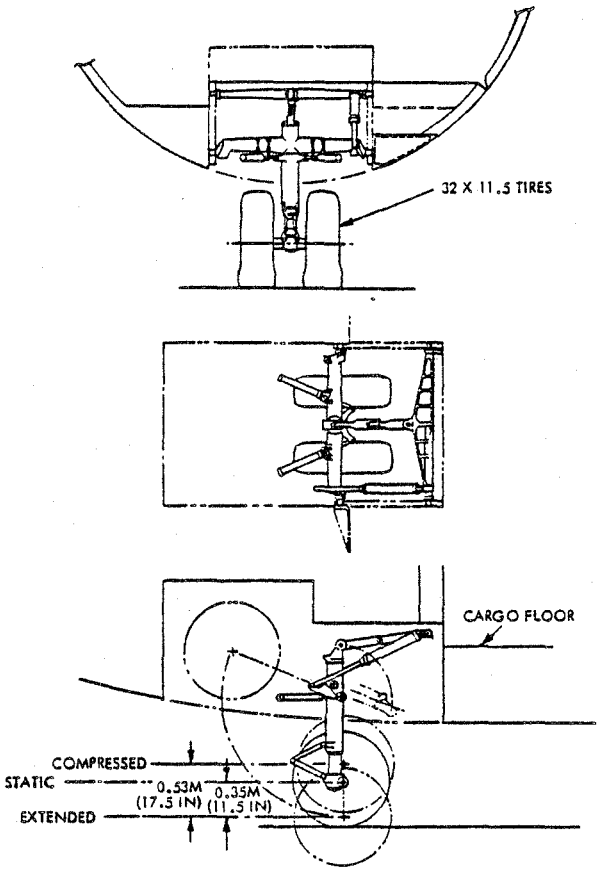

Figure 39. Typical Nose Landing Gear Arrangement

The nose gear is retracted and extended by means of a hydraulic drag strut with an actuating cylinder. An integral down-lock and an automatic up-lock are used to hold the gear in the desired position. In the retracted position, the nose gear is contained within the fuselage nose and enclosed by doors hinged to the fuselage. The aft door is opened mechanically by the first motion of the gear in the extending sequence and is closed by the last motion of the gear in the retracting sequence. The forward door is opened and closed during both extending and retracting sequences.

In case of failure on the normal hydraulic system, there is an alternate hydraulic system for extending the gear. A separate manual system serves as a backup to both the normal and alternate hydraulic systems.

Cargo Compartment Loading Doors

Several door arrangements from previous aircraft design studies were considered for the No. 1 and No. 2 aircraft which are aft loaded. Based on our engineering experience, the petal-type doors shown on the C-141 aircraft in Figure 40 were selected because they are simple, relatively inexpensive to design and maintain, and yield an aerodynamically clean afterbody in the closed position. For this application, the doors are hinged on the aft fuselage and hydraulically operated to provide a minimum opening of 1.4 rad (80 deg) to the sides to permit straight-in loading of the containerized payload.

Figure 40. C-141 Aircraft Being Loaded through Petal-Type Doors on Aft Fuselage

As noted previously, the requirement to simultaneously load two rows of containers is more efficiently satisfied with a nose-loaded aircraft having a full-width nose visor door. Based on experience with the nose visor door on the C-5 aircraft, as shown in Figure 41, such a door is judged to be eminently feasible for the No. 3 aircraft.

Figure 41. C-5 Aircraft Being Loaded through Nose-Visor Door on Forward Fuselage

Engine Mounting

Figure 42 shows a structural assembly for attaching a turboprop engine to the underside of the wing leading edge. This design consists of two longitudinally-directed, A-shaped, mounting brackets with bracing structure at the end which attaches to the wing.

Three quick-disconnect points are visible in the side views of the brackets. The foremost point is for attachment to the engine at the gearbox, the lower aft point provides attachment to the engine at the diffuser, and the upper point connects to structure from the wing front beam. Thrust, side, and vertical loads from the engine are transmitted through the aft attachment point, while vertical and side loads are carried through the forward point. The bracing structure between the brackets is intended to handle the torsional loads produced by propeller rotation.

Some localized strengthening along the wing span is provided inside the wing box near the engine mounting positions to distribute the loads. This added structure is indicated by the backward-K elements shown at the front of the wing box in the two section views.

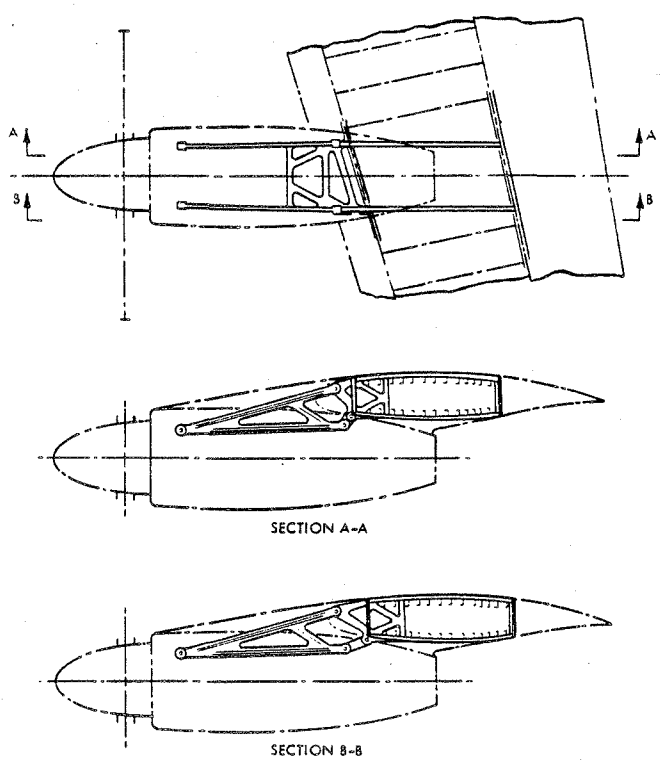

Figure 42. Typical Structure for Attaching Turboprop Engine to Aircraft Wing

REFERENCE TURBOFAN AIRCRAFT STUDIES

How well does an aircraft with an advanced turboprop propulsion system compare with one with advanced turbofan engines? Before a response can be made to this question, a reference aircraft with turbofan engines must be developed for the comparison. Three reference aircraft were developed in this study - one for comparison with each selected turboprop aircraft. To minimize the differences between the turboprop and turbofan-powered aircraft and allow attention to be concentrated on just the comparative effects of the two propulsion systems, each reference aircraft has the same delivery capabilities as its corresponding selected aircraft. That is, both aircraft to be compared have the same payload, cargo compartment, cruise speed and altitude. Furthermore, they are subject to the same operating constraints such as field length and approach speed.

PARAMETRIC ANALYSIS

The three reference turbofan aircraft were chosen from parametric study results that were obtained in two steps, as indicated on Table XIX. The first step provided the data for defining the two reference aircraft with 4-container payloads, while the third reference aircraft with a 9-container payload was selected based on the results of the second step.

Table XIX. Case Schedule for Turbofan Parametric

	STEP 1	STEP 2
PAYLOAD CONTAINERS	4	9
MACH NUMBER	0 75	0 75
CRUISE ALTITUDE, 1000 M FT	10 1 33	10 1 33
WING SWEEP, RAD DEG	0 35 20	0 35 20
WING LOADING, KN/M^2 LB/FT^2	3 3 - 6 2 70 - 130	4 3 - 6.2 90 - 130
WING ASPECT RATIO	8 - 16	8 - 16
ENGINE POWER SETTING, %	70 - 95	70 - 95
ENGINE BYPASS RATIO	5 8 - 18	5 8 - 18

Values for the cruise altitude and wing sweep angles are those of the selected turboprop aircraft. Although the designs of turbofan aircraft generally tend to optimize at higher altitudes than those for turboprop aircraft, the same altitude was used to minimize the number of variables to be considered when comparing the two aircraft. Later, as a sensitivity study, the effect of different altitudes was investigated.

Variations in engine bypass ratio were included in the parametric study by considering four design point engines with ratio values of 5.8, 8.4, 13, and 18. The weight and performance characteristics of each engine were developed in consultation with Pratt & Whitney from the basic STF477 turbofan engine [22] by using Lockheed's propulsion cycle analysis program. Appendix J contains a description of the basic engine and a discussion of the methodology used to derive these alternate versions along with detailed data on each.

The approach used in this parametric study parallels that followed for the turboprop aircraft. For each combination of engine bypass ratio and power setting values, aircraft designs were generated for the complete set of wing loading and aspect ratio values. The study constraints were then applied to the results to eliminate some of the candidates. For the remaining designs, the minimum noiseprint areas were determined for various levels of block fuel and direct operating cost. Subsequently, these areas were compared with those at the same block fuel or direct operating cost for other bypass ratio and power setting cases. The outcome of the comparison is graphs of direct operating cost and block fuel versus noiseprint area. Figure 43 presents such a set of results for a 4-container payload, and Figure 44 shows them for the 9-container payload case. Appendix K provides a fuller description of how the results in these figures were obtained by showing some of the initial data and by explaining the method of analysis step by step.

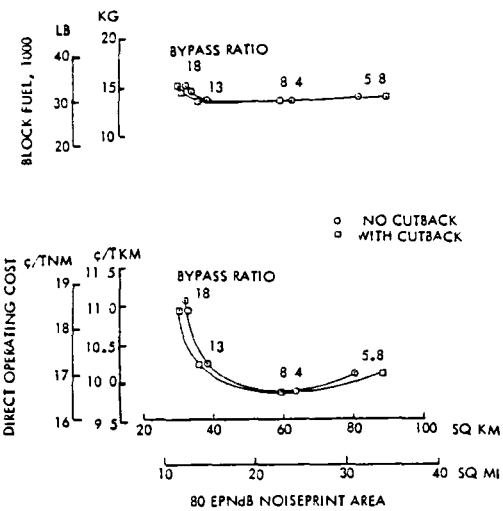

Figure 43. Cost of Quietness for 0.75 Mach Number and 4-Container Payload Turbofan Aircraft

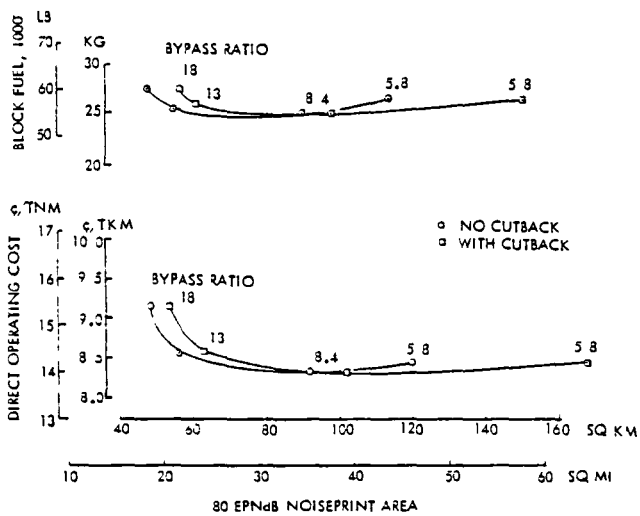

Figure 44. Cost of Quietness for 0.75 Mach Number and 9-Container Payload Turbofan Aircraft

These results merit a comment before we proceed to the selection of the reference aircraft. Of the four discrete bypass-ratio values that were considered, the three higher values give the expected option of being able to choose between reducing the operating cost by tolerating a larger noiseprint area or reducing the noiseprint area by paying a higher operating cost. In contrast, there are no apparent benefits from bypass ratios between 8.4 and 5.8 because both the cost and noiseprint areas are higher in this range than those at the 8.4 bypass ratio.

SELECTED DESIGNS

The major design parameters selected to define the three reference turbofan aircraft are listed in Table XX along with the major characteristics that were determined for each. The values for the mission features are the same as for the three selected turboprop aircraft for eventual comparative purposes.

Table XX. Major Characteristics for Selected Turbofan Aircraft Designs

	TURBOFAN AIRCRAFT		
CHARACTERISTIC	1 COMPROMISE	2 QUIETEST	3 COMPROMISE
MISSION FEATURES			
NUMBER OF CONTAINERS	4	4	9
CRUISE MACH NUMBER	0 75	0 75	0 75
CRUISE ALTITUDE, 1000 M (FT)	10 1 (33)	10 1 (33)	10 1 (33)
ENGINE			
BYPASS RATIO	10	13	10
POWER SETTING	0 773	0 80	0 85
WING GEOMETRY			
SWEEP, RAD (DEG)	0 35 (20)	0 35 (20)	0 35 (20)
ASPECT RATIO	13 45	16	12
LOADING, KN/M^2 (PSF)	6 0 (125)	6 0 (125)	6 0 (125)
WEIGHTS, 1000 KG (LB)			
OPERATING	41 2 (90 7)	45 3 (99 7)	75 6 (166 3)
FUEL	17 0 (37 3)	17 1 (37 7)	32 4 (71 3)
PAYLOAD	27 3 (60 0)	27 3 (60 0)	61 4 (135 0)
RAMP	85 5 (188 0)	89 7 (197 4)	169 4 (372 6)
FIELD LENGTH, M (FT)	2444 (8018)	2354 (7722)	2468 (8074)
80 EPNdB NOISEPRINT AREA KM^2 (MI^2)	52 8 (20 4)	37 0 (14 3)	79 5 (30 7)
DIRECT OPERATING COST*, c ATKM (¢/ATNM)	10 0 (16 9)	10 4 (17 5)	8 6 (14 5)

* Fuel at 264 $ M^3 (100 ¢ GAL)

For the two compromise aircraft, an engine bypass ratio of 10 was chosen because it represents the probable upper limit on bypass ratio for a direct-drive engine. Engines with higher bypass ratios will necessitate going to a geared-fan arrangement with its attendant weight and technology problems. The noise reduction offered by a geared fan is such an attractive feature, however, that one was selected for the No. 2 Quietest aircraft. Technology problems are expected to increase in direct proportion with the

level of the bypass ratio for geared fans. To minimize these problems while still gaining an indication of the potential benefits, a bypass ratio of 13 was chosen for the third aircraft.

Of the remaining selected items in the table, the wing loading is set by the maximum approach speed limit, and the engine power setting is established by the maximum field length limitation. The aspect ratio values are intended to minimize the cost and the noiseprint areas.

Using the design parameter values listed in the table down through the heading of wing geometry, three reference turbofan aircraft designs were developed. Figures 45, 46, and 47 provide three-view drawings of these aircraft, while the major derived characteristics for each are summarized at the bottom of Table XX. Further details on each aircraft are described in the following sections.

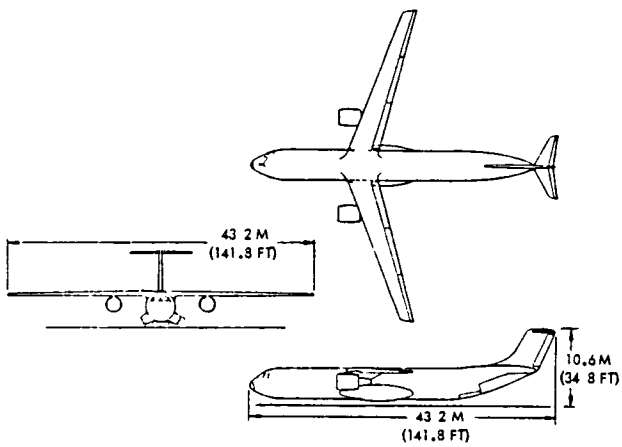

Figure 45. Layout of No. 1 Compromise Turbofan Aircraft

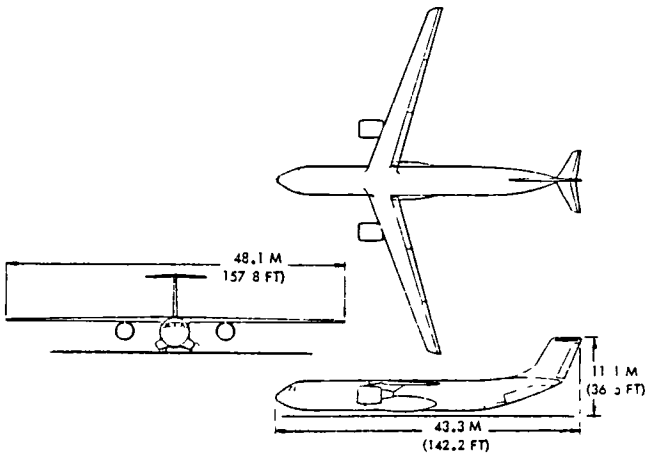

Figure 46. Layout of No. 2 Quietest Turbofan Aircraft

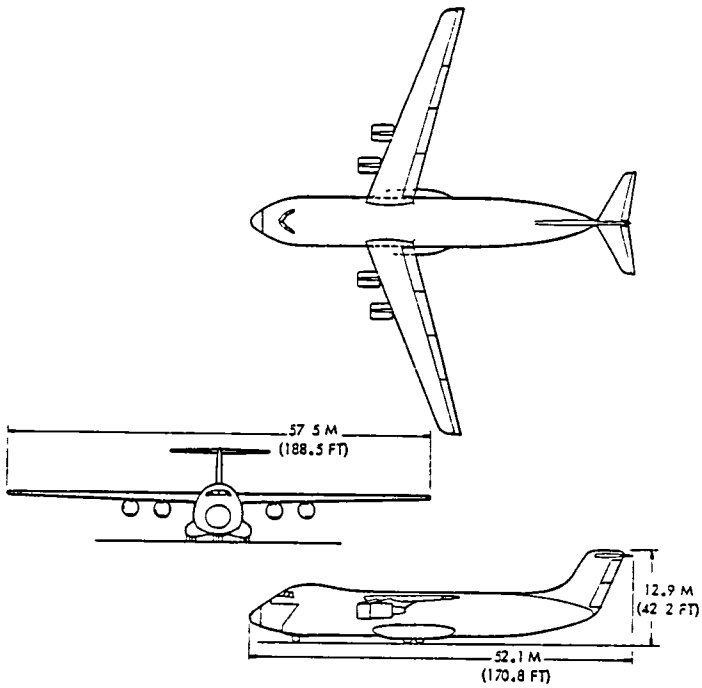

Figure 47. Layout of No. 3 Compromise Turbofan Aircraft

Design

Geometric dimensions of the three aircraft are compiled in Table XXI. The cargo compartment and fuselage are the same size as for the turboprop aircraft because both types have identical payload requirements. Also, both types of aircraft exhibit other common design features to simplify the comparison of the effects of the propulsion systems. The most prominent of these common features will be mentioned only briefly. For a fuller description of design features, reference should be made to the corresponding section on the turboprop aircraft.

The No. 1 and No. 2 aircraft are loaded through a full-width aft door, while the No. 3 aircraft achieves straight-in loading through a full-width nose visor door. All of the aircraft have a high wing, engines mounted on pylons beneath the wing, and a T-tail empennage. The landing gear is comprised of a single-strut nose gear and twin-tandem main gears mounted on each side of the fuselage.

Table XXI. Geometry Summary for Selected Turbofan Aircraft

ITEM	TURBOFAN AIRCRAFT		
	1 COMPROMISE	2 QUIETEST	3 COMPROMISE
WING*			
ASPECT RATIO	13 5	16	12
SPAN, M (FT)	43 0 (141)	47 9 (157)	56 4 (185)
AREA, M^2 (FT^2)	137 (1475)	144 (1548)	271 (2921)
THICKNESS RATIO	0 139	0 139	0 138
LOADING, KN/M^2 (PSF)	6 0 (125)	6 0 (125)	6 0 (125)
SWEEP, RAD (DEG)	0 35 (20)	0 35 (20)	0 35 (20)
FUSELAGE			
LENGTH, M (FT)	40 5 (133)	40 5 (133)	46 8 (154)
EQUIV DIA , M (FT)	4 2 (13 7)	4 2 (13 7)	6 3 (20 5)
HORIZONTAL TAIL**			
SPAN, M (FT)	8 6 (28 1)	8 5 (27 9)	13 2 (43 3)
AREA, M^2 (FT^2)	16 3 (175)	16 1 (173)	38 7 (417)
VERTICAL TAIL+			
SPAN, M (FT)	5 4 (17 8)	5 9 (19 2)	7 0 (23 0)
AREA, M^2 (FT^2)	24 4 (263)	28 6 (308)	40 8 (439)
CARGO COMPARTMENT			
ROWS OF CONTAINERS	1	1	2
LENGTH, M (FT)	24 7 (80 9)	24 7 (80 9)	31 1 (102 0)
WIDTH, M (FT)	2 7 (9 0)	2 7 (9 0)	5 6 (18 5)
HEIGHT, M (FT)	2 9 (9 5)	2 9 (9 5)	2 9 (9 5)

* TAPER RATIO = 0 40
** TAPER RATIO = 0 35 SWEEP = 0 44 RAD (25 DEG), ASPECT RATIO = 4 5 THICKNESS RATIO = 0 095
+ TAPER RATIO = 0 3 SWEEP = 0 52 RAD (30 DEG), ASPECT RATIO = 1 2 THICKNESS RATIO = 0 095

Weights and Balance

Table XXII lists the weights for the major subsystems of the three turbofan aircraft. Based on the distribution of these weights, the actual center-of-gravity positions of the aircraft were calculated as fuel and payload weights change. The resulting center-of-gravity envelopes for the three aircraft, as shown in Figure 48, are for an assumed uniform distribution of fuel and payload. Some variation from this uniform distribution assumption is permitted as long as the aircraft center of gravity does not move outside the two loadability limits on the figures. These limits are established by the horizontal tail size. The forward limit is fixed by nose wheel lift-off at 80 percent of the stall speed for the No. 1 and No. 2 aircraft and by trim constraints for the No. 3 aircraft. Stability sets the aft limit for all three aircraft.

Table XXII. Weight Summary for Selected Turbofan Aircraft, kg (lb)

ITEM	TURBOFAN AIRCRAFT		
	1 COMPROMISE	2 QUIETEST	3 COMPROMISE
STRUCTURE			
WING	10,523 (23,150)	12,948 (28,486)	22,553 (49,616)
FUSELAGE	9 823 (21 610)	9,871 (21,717)	18 285 (40,227)
HORIZONTAL TAIL	456 (1,003)	458 (1,008)	1,028 (2,261)
VERTICAL TAIL	576 (1,267)	650 (1,430)	945 (2 080)
NOSE GEAR	509 (1,120)	537 (1,181)	1,013 (2,228)
MAIN GEAR	3,406 (7,493)	3,592 (7,903)	6,777 (14,910)
NACELLE	612 (1,346)	686 (1,509)	1,111 (2,445)
PYLON	716 (1,575)	812 (1,786)	1,256 (2,764)
PROPULSION			
ENGINES	4,325 (9,514)	5,240 (11,529)	7,525 (16 555)
THRUST REVERSERS	726 (1,598)	880 (1,937)	1,264 (2,781)
FUEL SYSTEM	751 (1,652)	755 (1,661)	1,038 (2,283)
MISCELLANEOUS	455 (1,000)	455 (1,000)	909 (2,000)
SYSTEMS & EQUIPMENT	8,332 (18,330)	8,438 (18,563)	11,880 (26,137)
OPERATING WEIGHT	41,210 (90,658)	45,322 (99,709)	75,584 (166,287)
CARGO	27,273 (60,000)	27,273 (60,000)	61,364 (135,000)
ZERO FUEL WEIGHT	68,483 (150,658)	72,595 (159,709)	136,948 (301 287)
FUEL	16,966 (37,325)	17,150 (37,730)	32,397 (71,273)
RAMP WEIGHT	85,449 (187,983)	89,745 (197,438)	169,345 (372 560)

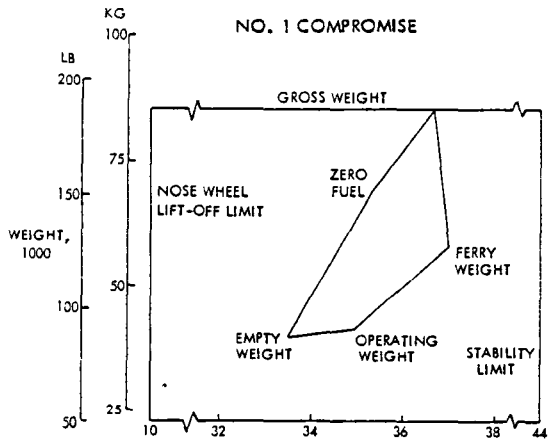

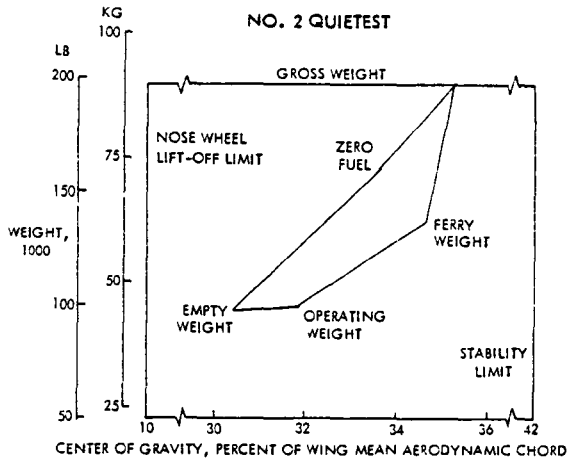

Figure 48. Loading Envelopes for Turbofan Aircraft

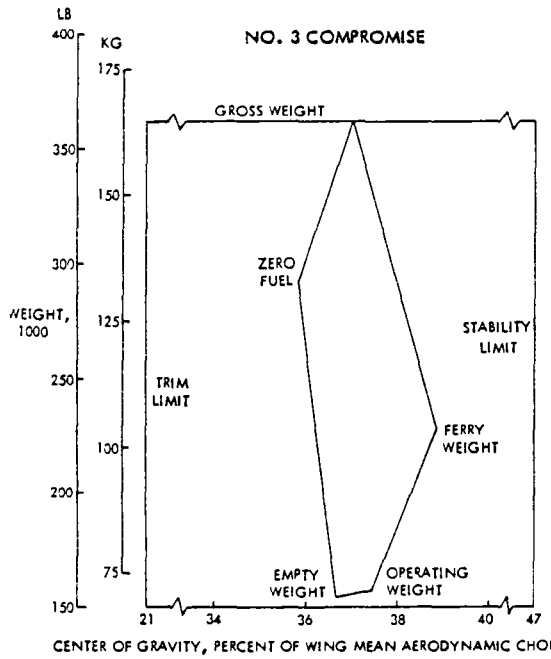

Figure 48. (Cont'd) Loading Envelopes for Turbofan Aircraft

volume available for carrying fuel becomes a limitation. Additional range may be achieved only at a reduced gross weight with smaller payloads until the zero-payload, or ferry, range is eventually reached.

These payload-range data were calculated based on the aircraft performance characteristics which are presented in Table XXIV and Figures 50 to 52. Table XXIV shows the various components that contribute to the total drag buildup along with the particular values for each aircraft. Nacelle drag is not listed on the table because it is accounted for in the net thrust of the propulsion system.

The drag polars shown in Figures 50 to 52 were derived based on the drag buildups in the table. In each case, several polars are included for cruise and for takeoff conditions of gear down in ground effect and gear up out of ground effect. The corresponding lift curves are also included for completeness.

Performance

Table XXIII summarizes the major airport performance features of the three aircraft. In contrast to the turboprop aircraft, which take off in distances considerably under the 2440 m (8000 ft) field length limit, the turbofan aircraft require the full field length permitted.

Productivity capabilities of the aircraft are shown by the payload-range curves in Figure 49. In each case, the payload-range combination that corresponds to the basic design point is specially designated. All of the aircraft have the required capability to carry up to 20 percent more payload than the design value for some reduced range. The range for the maximum overload is defined by the intersection of the constant gross weight line and the horizontal line which represents the 2.5-g structural limitation. Some increase in range is attainable at constant gross weight by trading payload weight for fuel weight until the wing

Table XXIII. Airport Performance Summary for Selected Turbofan Aircraft

ITEM	TURBOFAN AIRCRAFT		
	1 COMPROMISE	2 QUIETEST	3 COMPROMISE
TAKEOFF DISTANCES, M (FT)			
BALANCED FIELD	2444 (8018)	2354 (7722)	2294 (7527)
OVER 11 M (35 FT) OBSTACLE	2061 (6762)	2058 (6751)	2140 (7021)
OVER 15 M (50 FT) OBSTACLE	2119 (6951)	2117 (6947)	2215 (7268)
FAA FACTORED	2370 (7776)	2366 (7764)	2461 (8074)
TAKEOFF SPEEDS, M/S (KT)			
STALL	63 (123)	63 (122)	63 (122)
ROTATION	74 (143)	73 (142)	70 (136)
LIFT OFF	76 (148)	76 (147)	73 (141)
APPROACH SPEED, M/S (KT)	69 (135)	69 (135)	69 (135)
LANDING DISTANCE, M (FT)	1853 (6078)	1862 (6110)	1852 (6075)
FLAP DEFLECTION, RAD (DEG)			
TAKEOFF	0 34 (19)	0 35 (20)	0.35 (20)
LANDING	0 87 (50)	0 87 (50)	0 87 (50)
ENGINE-OUT GRADIENT	0 024	0 029	0 055
LIFT COEFFICIENTS			
TAKEOFF	2 60	2 60	2 60
LANDING	3 14	3 14	3 14

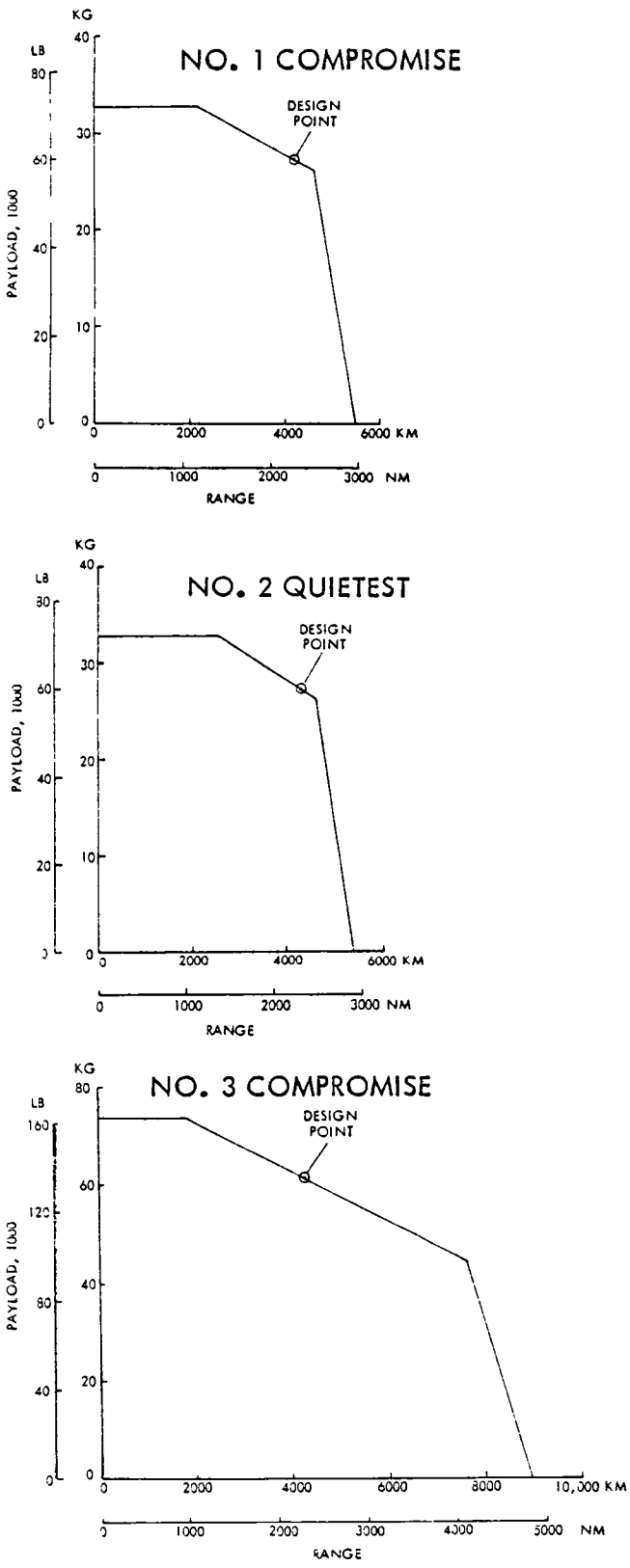

Figure 49. Productivity Capabilities of Turbofan Aircraft

Table XXIV. Drag Buildups for Selected Turbofan Aircraft

	TURBOFAN AIRCRAFT		
	1 COMPROMISE	2 QUIETEST	3 COMPROMISE
PROFILE DRAG			
WING	63 7*	65 4	58 3
FUSELAGE	65 9	62 7	55 7
EMPENNAGE	17 9	18 6	17 0
INTERFERENCE	7 4	7 4	6 6
ROUGHNESS	4 5	4 4	4 0
TRIM	12 0	12 0	12 0
PYLON	1 2	1 2	1 1
TOTAL PROFILE	172 6	171 7	154 7
INDUCED DRAG	83.9	70 5	97 1
TOTAL DRAG			
PROFILE	172 6	171 7	154 7
INDUCED	83 9	70 5	97 1
COMPRESSIBILITY	10 0	10 0	10 0
MISCELLANEOUS	5 2	5 2	5 2
TOTAL	271 7	257 4	267 0
CRUISE LIFT COEFFICIENT	0 58	0 58	0.58
LIFT/DRAG	21 35	22 54	21 73

*DRAG IN COUNTS 1 COUNT = 0 0001

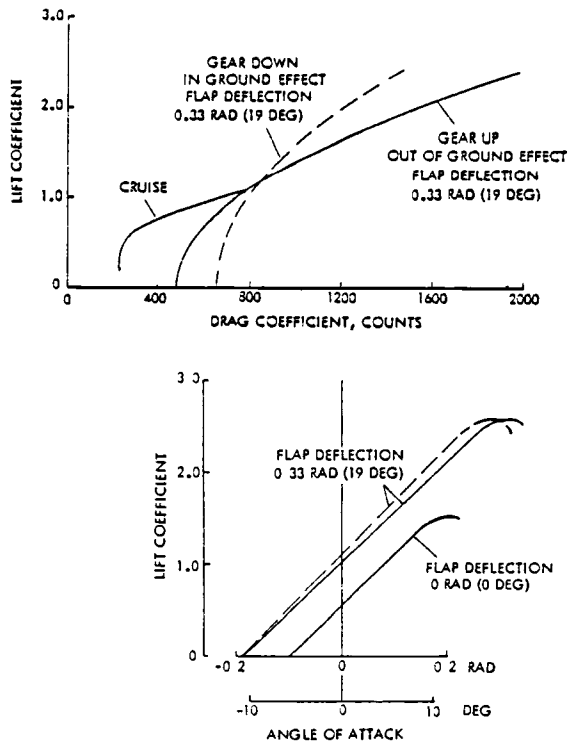

Figure 50. Drag Polars and Lift Curves for No. 1 Compromise Turbofan Aircraft

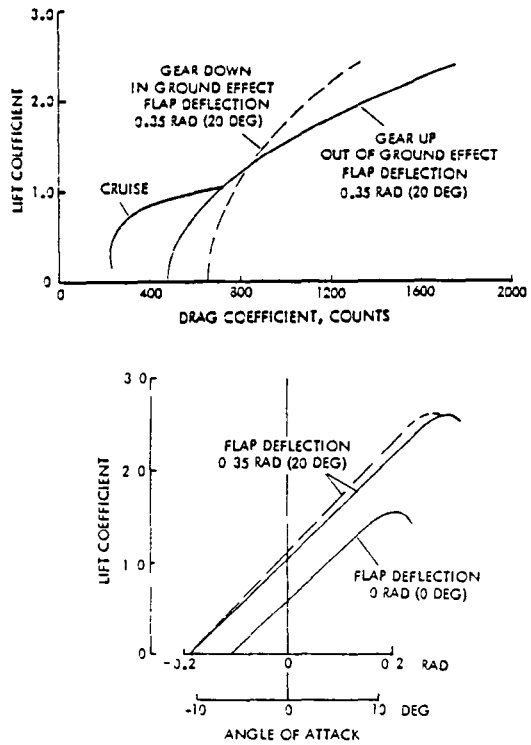

Figure 51. Drag Polars and Lift Curves for No. 2 Quietest Turbofan Aircraft

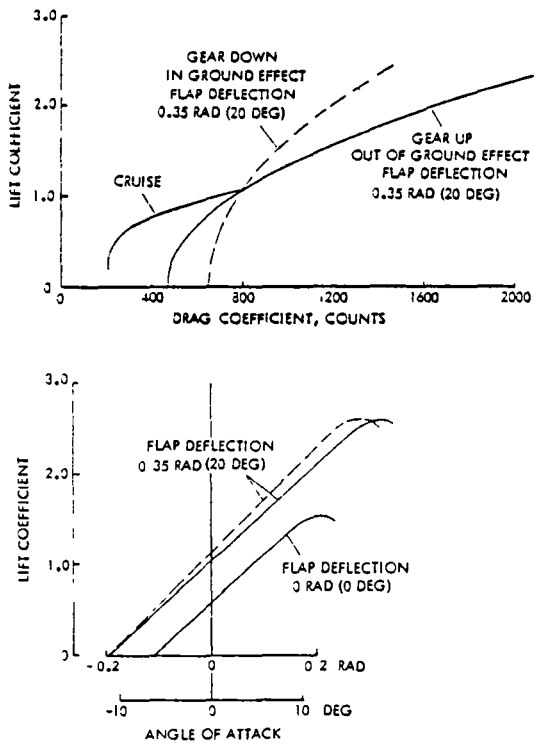

Figure 52. Drag Polars and Lift Curves for No. 3 Compromise Turbofan Aircraft

Propulsion System

The main characteristics of the propulsion system are listed in Table XXV for the three aircraft. The bypass ratio 10 engines on the No. 1 and No. 3 aircraft are direct-drive engines, while the bypass ratio 13 engine uses a geared fan.

The dimensions and performance characteristics of the engines are based on those for the Pratt & Whitney STF477 turbofan engine. Descriptions and detailed data for the baseline versions of this engine are included in Appendix J along with an outline of the methods used to scale the baseline systems to other sizes.

Table XXV. Propulsion Summary for Turbofan Aircraft

	TURBOFAN AIRCRAFT		
ITEM	1 COMPROMISE	2 QUIETEST	3 COMPROMISE
ENGINE			
NUMBER	2	2	4
BYPASS RATIO	10	13	10
DIAMETER, M (FT)	2 0 (6 5)	2 2 (7 1)	1 9 (6 2)
LENGTH, M (FT)	3 1 (10 3)	3 4 (11 2)	3 0 (9 9)
NACELLE			
DIAMETER, M (FT)	2 3 (7 6)	2 5 (8 3)	2 2 (7 1)
LENGTH, M (FT)	3 1 (10 3)	3 4 (11 2)	3 0 (9 9)
PERFORMANCE			
RATED THRUST, 1000 N (LB)	118 3 (26 a)	125 4 (28 2)	104 5 (23 a)
CRUISE THRUST, 1000 N (LB)	24 9 (5 6)	24 0 (5 4)	21 8 (4 9)
THRUST WEIGHT, N/KG (LB/LB)	2 74 (0 28)	2 84 (0 29)	2 45 (0 25)
CRUISE SFC, KG HR-N (LB HR-LB)	0 06 (0 60)	0 062 (0 61)	0 061 (0 60)

Noise

Figure 53 shows the predicted noise levels of the three turbofan aircraft at the standard measuring points of takeoff, sideline, and approach. Also included on the figure are the FAR 36 stage 3 noise limits applicable to new aircraft. It is immediately obvious from comparing the predictions and limits that the turbofan aircraft selected from the parametric study are unable to meet the noise regulations in most cases. This was not completely unexpected, nor is it necessarily disastrous!

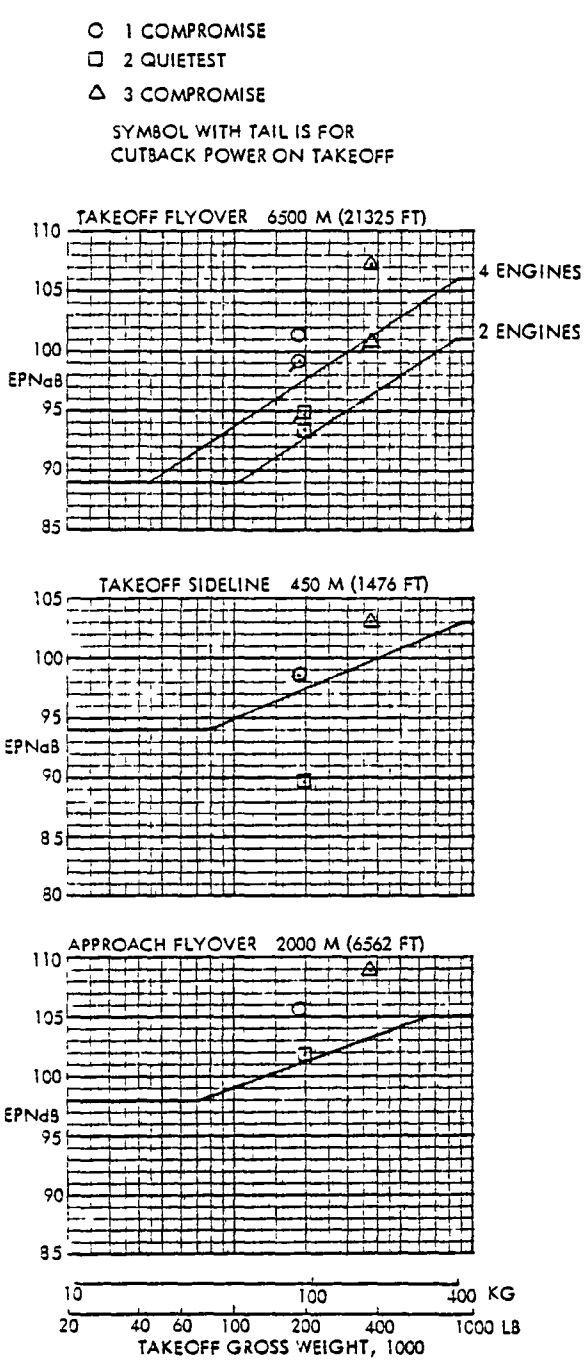

Figure 53. FAR 36 Stage 3 Noise Limits and Noise Levels of Selected Turbofan Aircraft Without Treatment

All of the turboprop and turbofan aircraft were originally designed with hardwall nacelles around the engines; that is, no attempt was made to suppress engine noise. This approach has little effect on the turboprop aircraft because the propeller is the predominant noise source, not the engine. For the turbofan aircraft, however, the converse is true because the engine fan and turbine are the major noise sources, and these can be quieted through proper design of the nacelle for noise suppression.

At the beginning of the turbofan aircraft parametric study, there was no way of knowing how much noise treatment would be required for each aircraft to meet the FAR 36 limits. Rather than penalize some aircraft by adding too much treatment while possibly not adding enough treatment to others, the approach was adopted of using hardwall (untreated) nacelles for all of the parametric aircraft and then modifying only the selected designs as required.

Pratt & Whitney has investigated a modified nacelle for the STF477 engine using an approach that was previously applied to a JT9D engine. In concept, the STF477 nacelle could be modified as indicated schematically in Figure 54 to achieve the noise reductions shown at the bottom of the figure. This figure presents noise reductions for only the two predominate engine sources - the fan and the turbine - and for the total engine. Essentially no reductions are realized by the engine core and jet.

By designing a nacelle with noise suppression included from the beginning, rather than as a modification or add-on, the weight penalty for the suppression has been estimated to be approximately 15.9 kg (35 lb) per nacelle for the engine thrust levels in this study. This weight is so small, relative to the aircraft ramp weight (about 0.04 percent), that the aircraft need not be resized to take advantage of the amount of noise reduction. With this treatment, the three turbofan aircraft are considerably quieter, and as

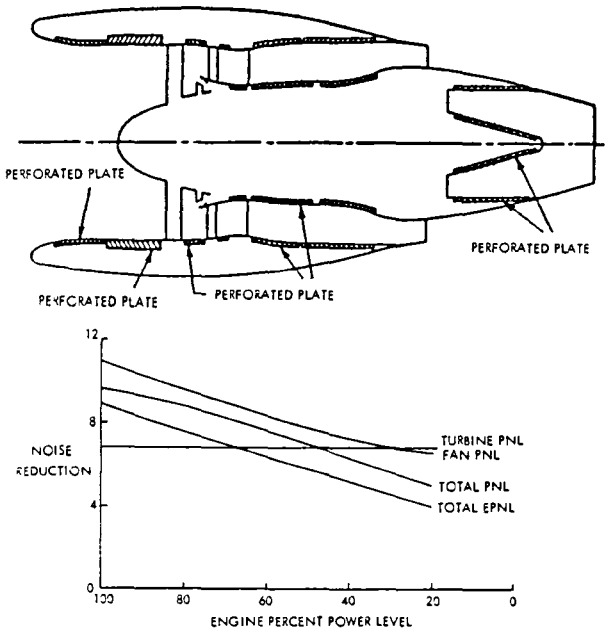

Figure 54. Modifications to Turbofan Engine Nacelle for Noise Suppression and Predicted Level of Noise Reduction

shown in Figure 55, their predicted noise levels over the measuring points easily comply with the FAR 36 regulations.

Two noise-level values are shown in Figure 55 for takeoff flyover for each aircraft. One is for full-powered takeoff and climb, while the other is for a cutback power profile*. Note that the same result is achieved as for the turboprop aircraft; cutting back the power during climb is not always beneficial in reducing the noise at the measuring point. This occurs because the reduction in propulsion noise is more than compensated for by the reduced flyover altitude.

* The only difference between the two profiles occurs after the aircraft reaches an altitude of 305 m (1000 ft). In the cutback case, the engine power is reduced to the minimum level that will satisfy the FAR 36 regulations. No power reduction occurs for the full-power case.

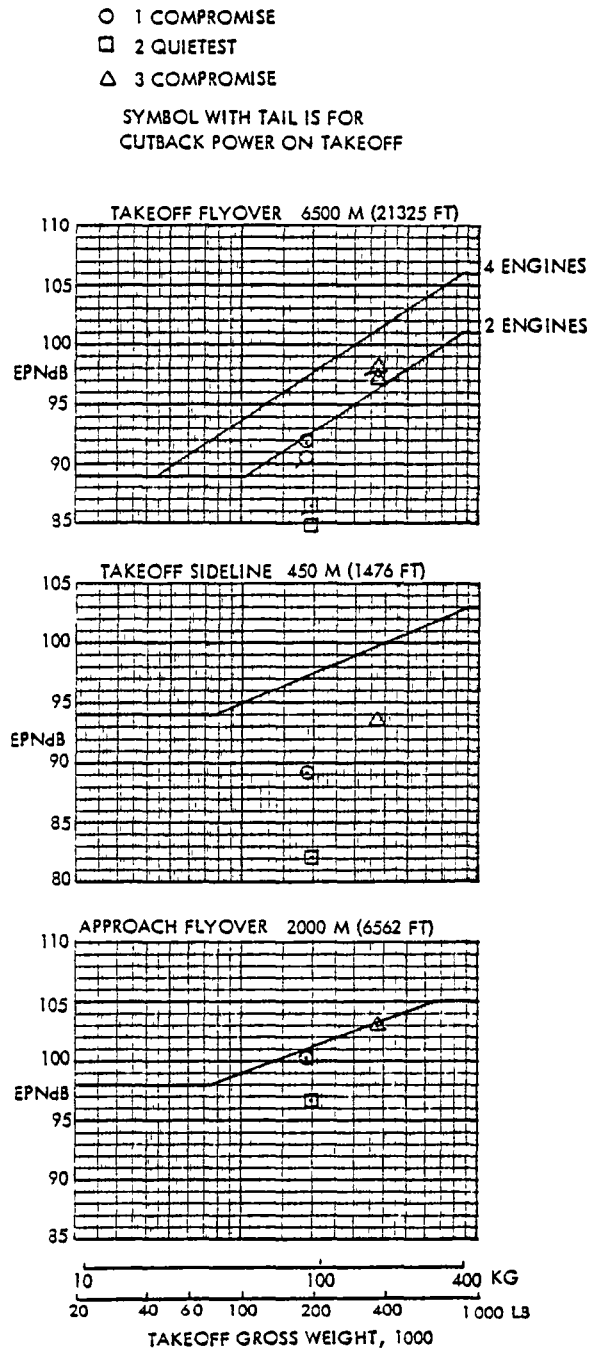

Figure 55. FAR 36 Stage 3 Noise Limits and Noise Levels of Selected Turbofan Aircraft with Treatment

Further insight into the aircraft noise at the measuring points is gained by examining the contributions from the various noise sources, which are listed in Table XXVI, for the three turbofan aircraft with their nacelles treated. Based on these tables, the following observations are made.

- There is no clear pattern of any one noise source being predominant for all or most cases. The fan and turbine noise sources, however, are generally the largest, or close to the largest, contributors.

- During approach, turbine noise is the predominant source for all three aircraft. Fan and airframe noise are the next largest contributors.

- For the No. 1 Compromise aircraft, fan noise is the major source for sideline and takeoff cases. Fan noise, along with airframe noise, ranks second to turbine noise during approach.

- For the No. 2 Quietest aircraft, there is no predominant noise source. The three or four loudest contributors for each condition are all within 3 dB of each other. Airframe and fan noise are always members of this group.

- For the No. 3 Compromise aircraft, fan noise is by far the loudest contributor to the full-powered takeoff and sideline cases. Airframe noise is predominent during cutback takeoff, and turbine noise holds this distinction for approach.

- In general, the two compromise aircraft could benefit substantially from additional noise treatment in the nacelles before airframe noise becomes the limit to further noise reduction. Conversely, additional treatment on the quietest aircraft would not be beneficial because airframe noise is, or is nearly, the major noise source.

Table XXVI. Noise Source Distributions for Turbofan Aircraft

NO. 1 COMPROMISE

	MEASURING POINT			
	TAKEOFF		APPROACH	SIDELINE
NOISE SOURCE	FULL POWER	CUTBACK		
FAN*	92.97	92 86	97 22	89 31
TURBINE	82.18	84 65	102 14	77.16
CORE	80 61	79 51	85 81	77 48
JET	77 56	76 37	81 57	74 13
AIRFRAME	80 12	82 35	95.90	76.25
TOTAL	94 55	93 50	104 76	90 78
DURATION CORRECTION	-2.69	-2 85	-4.44	-1 69
EPNL	91 86	90.65	100.32	89 09

NO. 2 QUIETEST

	MEASURING POINT			
	TAKEOFF		APPROACH	SIDELINE
NOISE SOURCE	FULL POWER	CUTBACK		
FAN*	79 85	81 23	95.16	74 82
TURBINE	77 23	80 18	98 50	72.01
CORE	80 56	79 51	86 81	77 43
JET	75 00	74 30	79 35	71 87
AIRFRAME	80 69	83 19	96 48	76 81
TOTAL	83 80	86.06	102.31	80 03
DURATION CORRECTION	0 96	-0 43	-5 60	2 09
EPNL	84 76	86 49	96 71	82.12

NO. 3 COMPROMISE

	MEASURING POINT			
	TAKEOFF		APPROACH	SIDELINE
NOISE SOURCE	FULL POWER	CUTBACK		
FAN*	99 51	90 68	101.07	93.95
TURBINE	90 03	91 16	105.45	83.05
CORE	86 85	84 07	89 60	82.04
JET	83 78	80 43	92 38	78 66
AIRFRAME	84 86	86.34	97.15	79 66
TOTAL	101.13	98 20	107.82	95 49
DURATION CORRECTION	-3 71	-0 34	-4.69	-2 07
EPNL	97 42	97 86	103.13	93.42

*NOISE LEVELS OF SOURCES ARE IN PERCEIVED NOISE LEVEL TONE-CORRECTED MAXIMUMS (PNLTM)

- Cutting back on engine power during climb is as likely to be a detriment as a benefit. This points out the need for optimizing the takeoff and climb profile for each aircraft to minimize noise.

As discussed previously for the turboprop aircraft, noise at the measuring point conditions is inadequate when the impact of aircraft noise on the airport community is the major concern. Noiseprints, which indicate the total area affected by particular noise levels of the aircraft, are more meaningful. For this study, noiseprint areas have been calculated for the three turbofan aircraft at 70, 80, and 90 EPNdB noise levels. The shapes of these noiseprints, as shown in Figures 56 to 58 are separated into two portions of takeoff and approach for ease of presentation. The apparent overlap of the two contours at the approach end of the runway is accounted for in determining the total noiseprint area.

Note that the scale for the No. 3 aircraft is half that for the other two aircraft and that these noiseprints are for the three aircraft with hardwall nacelles. Noiseprints for these aircraft with the treated nacelles will be between one-fourth and one-third the size of those shown without the treatment, based on the sensitivity results which are presented later.

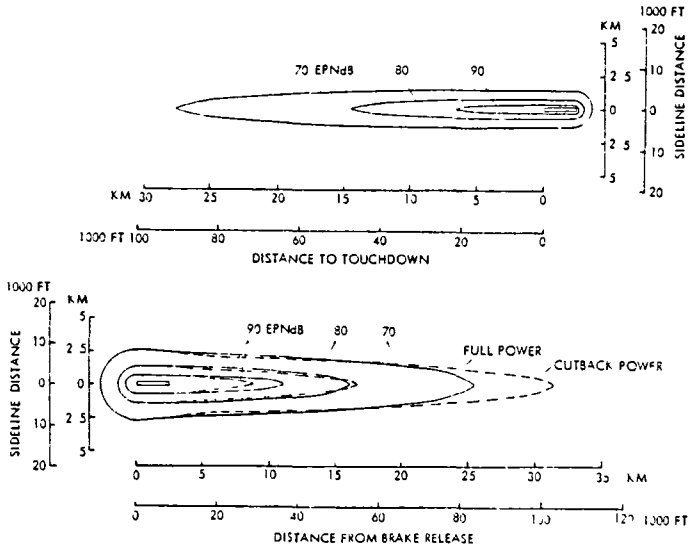

Figure 56. Noiseprints for No. 1 Compromise Turbofan Aircraft

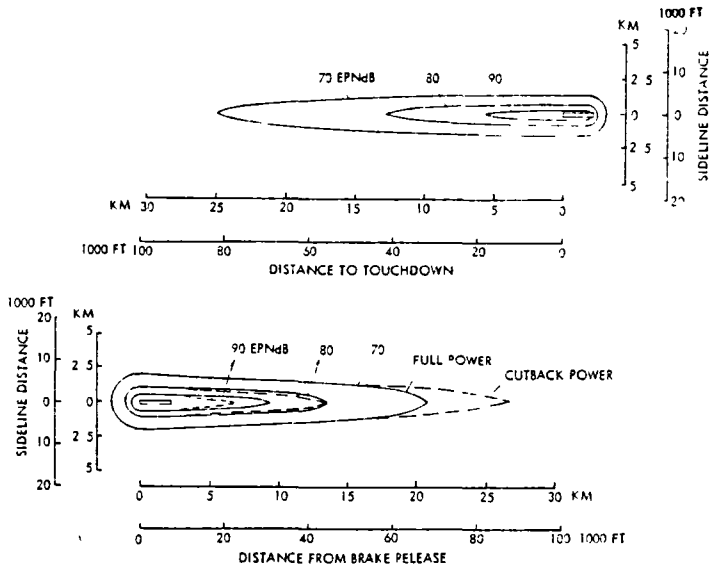

Figure 57. Noiseprints for No. 2 Quietest Turbofan Aircraft

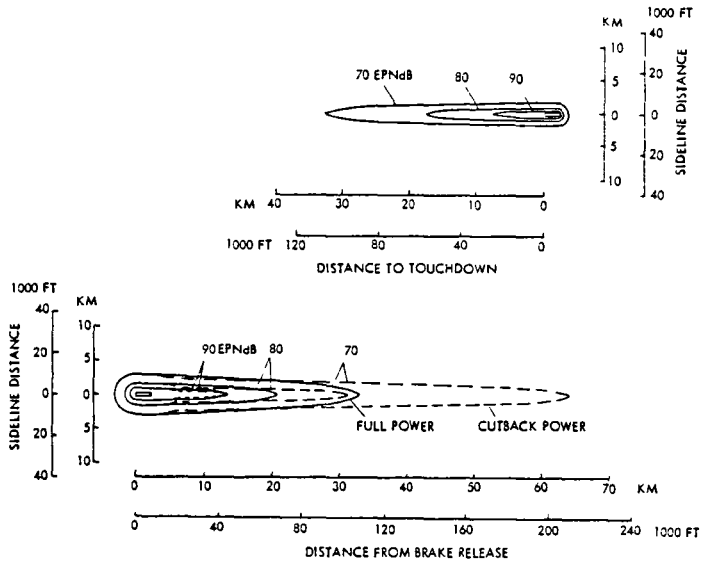

Figure 58. Noiseprints for No. 3 Compromise Turbofan Aircraft

Aircraft altitude changes are largely responsible for the gradual reductions in sideline distance on the noiseprints after takeoff and for the increasing sideline distance on approach. A further reduction in sideline distance is evident shortly after takeoff for the cutback case when the engine power is reduced. However, cutback is not always beneficial because it tends to lengthen the noiseprint, particularly at low noise levels, as a result of less climb capability.

Because of the tapered and elongated nature of the noiseprints which necessitated presenting them in two parts, the impacts of cutback and different noise levels are not easily visualized. To overcome this, the noiseprints have been converted into squares of equivalent area, which are shown in Figure 59. In this form, correlation between the noise level and area becomes apparent. It is: a 10 EPNdB reduction in the minimum noise level for the noiseprint produces a three to fourfold increase in the noiseprint area.

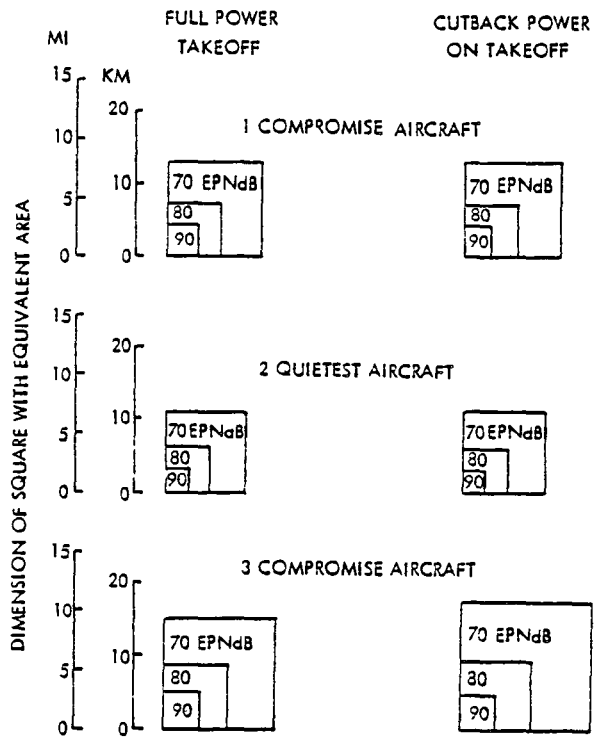

Figure 59. Squares of Equivalent Noiseprint Areas for Selected Turbofan Aircraft

Economics

Acquisition and direct operating costs for the three turbofan aircraft were calculated using Lockheed's Aircraft Life-Cycle Cost Evaluation model, which is described in more detail in Appendix B. The acquisition cost portion of the model computes the cost of each structural and functional subsystem, and then adds them to obtain a total acquisition, or unit flyaway, cost. Direct operating costs were determined based on the 1967 Air Transportation Association methodology with the coefficients updated to 1980 values.

Tables XXVII and XXVIII list the values for the various elements that contribute to the acquisition and direct operating costs, respectively, for the three turbofan aircraft. These costs are based on the same guidelines and assumptions as for the corresponding turboprop aircraft. For a refresher, the reader may wish to refer to Table XVIII, which was presented earlier, for a summary of the costing basis. Required for the costing, but not listed in that table, are the fleet sizes to meet the specified productivity. The fleet consists of 394 aircraft for the No. 1 or No. 2 design, and 175 for aircraft No. 3.

The direct operating cost breakdown in Table XXVIII uses a fuel price of 264 $/m^3 (100 ¢/gal). Admittedly, this price is lower than the current market value, but of the three values specified for this study, the one used is closest to reality. Direct operating costs based on the two lower fuel prices, as well as some higher values, will be included in some sensitivity study results that will be presented later.

The relative importance of the various elements that make up the direct operating cost is easier to perceive when the data of Table XXVIII are presented as in Figure 60. All three cost distribution layouts are drawn to the same scale so that the total area covered is indicative of the relative magnitude of the costs for each aircraft. Thus, the No. 2 aircraft has the largest area while the No. 3 aircraft has the smallest.

Aircraft No. 1 and No. 2 are very similar in design, and as expected, their cost distributions are nearly identical. In contrast, the No. 3 aircraft is considerably larger than the other two and it possesses a different cost distribution. In every case, the fuel and oil item is the

Table XXVII. Acquisition Cost Breakdown for Turbofan Aircraft
(COSTS IN $1000)

ELEMENT	TURBOFAN AIRCRAFT		
	1 COMPROMISE	2 QUIETEST	3 COMPROMISE
WING	2,130	2,565	5,395
TAIL	452	492	1,031
FUSELAGE	2,525	2,536	5,842
LANDING GEAR	372	390	719
FLIGHT CONTROLS	388	399	730
NACELLES	485	553	1,123
ENGINE INSTALLATION	42	46	79
FUEL SYSTEM	169	170	344
THRUST REVERSER	341	375	586
PROPULSION MISC	159	159	417
INSTRUMENTS	95	97	240
HYDRAULICS	222	229	496
ELECTRICAL	399	420	673
AVIONICS INSTALLATION	52	52	73
FURNISHINGS	383	383	679
AIR CONDITIONING	284	285	425
AUXILIARY POWER	54	55	75
SYSTEM INTEGRATION	342	379	951
TOTAL EMPTY MFG COST	8,894	9,575	19,878
SUSTAINING ENGINEERING	717	770	2,564
PROD TOOL MAINT	796	854	2,437
QUALITY ASSURANCE	545	585	1,310
AIRFRAME WARRANTY	548	589	1,310
AIRFRAME FEE	1,725	1,856	4,125
ENGINE	4,181	4,589	7,849
AVIONICS	500	500	500
RESEARCH & DEVELOPMENT	2,382	2,476	8,723
TOTAL ACQUISITION COST	20,288	21,794	48,696

Table XXVIII. Direct Operating Cost Breakdown for Turbofan Aircraft

ELEMENTS	TURBOFAN AIRCRAFT		
	1 COMPROMISE	2 QUIETEST	3 COMPROMISE
CREW	1786*	1793	1902
FUEL & OIL**	4516	4566	8646
INSURANCE	734	843	1885
MAINTENANCE			
AIRFRAME LABOR	196	210	316
AIRFRAME MATERIAL	256	273	649
ENGINE LABOR	128	130	247
ENGINE MATERIAL	574	630	1078
BURDEN	648	680	1125
DEPRECIATION	2734	2941	6492
TOTAL TRIP COST	11,622	12,066	22,340
DOC, ¢/AT KM	10 0	10 4	8 6
¢/AT NM	16 87	17 51	14 52

* Costs in dollars unless noted otherwise
** Fuel at 264 $/M^3 (100 ¢/GAL)

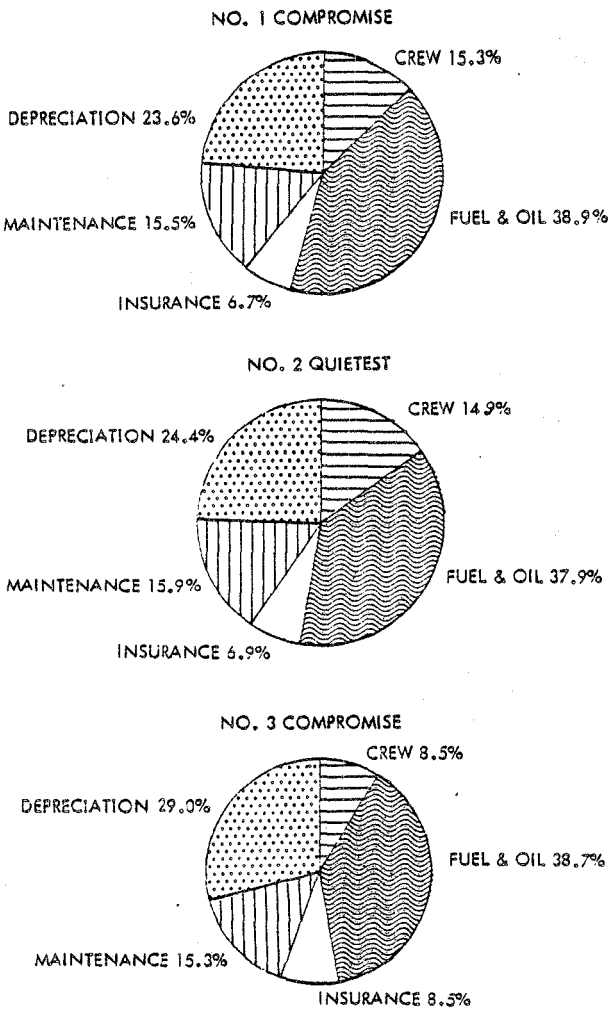

Figure 60. Direct Operating Cost Distributions for Turbofan Aircraft

largest single entity, and it, like the maintenance category, remains essentially a constant percentage of the total. The changing features are mostly a result of the increased payload. With more than double the payload of the other two, aircraft No. 3 has a crew cost that is approximately one-half that of the two smaller aircraft. This balances the increased depreciation and insurance costs incurred by being larger.

SENSITIVITY STUDIES

The three turbofan aircraft served as baseline values in a series of sensitivity studies in which the objective was to isolate the effects of the parametric study variables, the study guidelines and constraints, and the design methodology.

Using the same approach as for the turboprop aircraft sensitivity studies, percent variations in noiseprint, DOC, and block fuel were used as indicators, where applicable, of the effect of the various sensitivity parameters. To determine which factors have the greatest impact on these indicators, the previously defined measure of sensitivity (MOS) was used. As a refresher, the MOS is the ratio of the percent change that occurred in one of the indicators to the percent change in the sensitivity parameter. For qualitative evaluation, the numerical MOS values are arbitrarily interpreted as follows:

Numerical Evaluation	Qualitative Interpretation
$MOS < 1$	Negligible
$1 \leq MOS < 2$	Marginal
$2 \leq MOS \leq 5$	Significant
$MOS > 5$	Critical

The MOS values and qualitative assessments for all of the sensitivity studies on the turbofan aircraft are summarized in Figure 61.

Noise source level is the only parameter in all of the turbofan aircraft sensitivity studies that critically affects the results, and it does so for all three aircraft. Likewise, there is only one significant sensitivity area; it is the effect of airframe weight on DOC, but only for the No. 2 Quietest aircraft. Marginally sensitive ratings are given to the effects of: drag on block fuel for all three aircraft, approach speed on block fuel for the No. 2 aircraft, airframe weight on DOC for the No. 1 and No. 3 aircraft, and load factor on DOC for aircraft No. 1 and No. 2. All other sensitivity parameters have negligible effects. Further details on the individual sensitivity studies are provided in Appendix L.

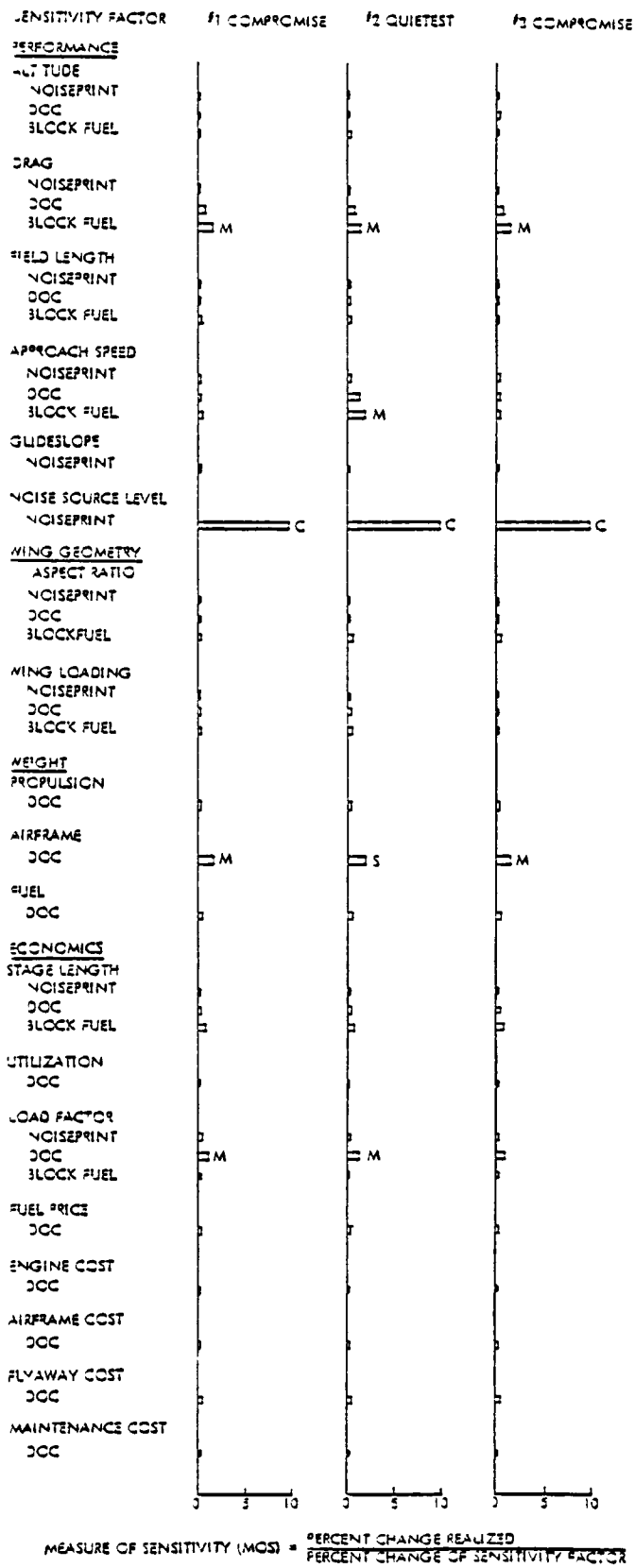

Figure 61. Summary of Turbofan Aircraft Sensitivity Study Results

AIRCRAFT COMPARISON

One of the main objectives of this study is to compare the effects of turboprop and turbofan propulsion systems installed on similar aircraft. The six aircraft - three with turboprops and three with turbofans - that were described in the preceding sections provide the basis for fulfilling this objective. Because each pair of competitive aircraft is similar in external appearance, geometrical differences are negligible and can be ignored. Instead, the comparison can be focused on the difference in the areas of performance including cost, noise, and sensitivities.

PERFORMANCE

Numerical values are listed in Table XXIX for five parameters which provide an indication of the performance capabilities of the six aircraft. A comparison of the three turboprop or three turbofan aircraft revels that two purported axiomatic trends are met: "quietness costs" and "bigger is better." The quietness axiom is supported by comparing aircraft No. 1 and No. 2 for both propulsion systems. Aircraft No. 2, a quiet version of aircraft No. 1, pays for its quietness by being relatively heavier, less fuel efficient, and more expensive to operate. Consistent with the size axiom, aircraft No. 3 achieves better fuel efficiency and lower DOC than aircraft No. 1 by carrying a larger payload.

A companion illustration, Figure 62, graphically highlights the percent benefits that each turboprop aircraft enjoys relative to its counterpart turbofan aircraft. In every case, the turboprop wins with lower ramp weights and less block fuel used, resulting in higher fuel efficiencies*, lower DOCs, and shorter field lengths. The magnitude of some of the benefits is particularly noteworthy with fuel savings of 17 to 21 percent, 21 to 26 percent improvement in fuel efficiency, and

Table XXIX. Numerical Comparison of Aircraft Performance

		AIRCRAFT					
		1 COMPROMISE		2 QUIETEST		3 COMPROMISE	
PAYLOAD 1000	KG	27 2		27 2		61 4	
	LB	60		60		135	
PROPULSION TYPE		PROP	FAN	PROP	FAN	PROP	FAN
RAMP WEIGHT 1000	KG	81	85	85	90	166	169
	LB	178	188	187	197	365	373
BLOCK FUEL 1000	KG	10 7	13 5	10 8	13 6	21 2	25 8
	LB	23 5	29 6	23 8	29 9	46 6	56 7
FUEL EFFICIENCY,	TKM KG	12 38	9 60	11 91	9 47	13 69	11 23
	TNM/LB	2 93	2 33	2 89	2 30	3 32	2 73
DOC	c TKM	8 9	10 0	8 9	10 4	8 0	8 6
	c TNM	14 7	16 9	15 0	17 5	13 3	14 5
FIELD LENGTH	M	1349	2444	1877	2366	1848	2438
	FT	5067	8018	6157	7764	6062	8000

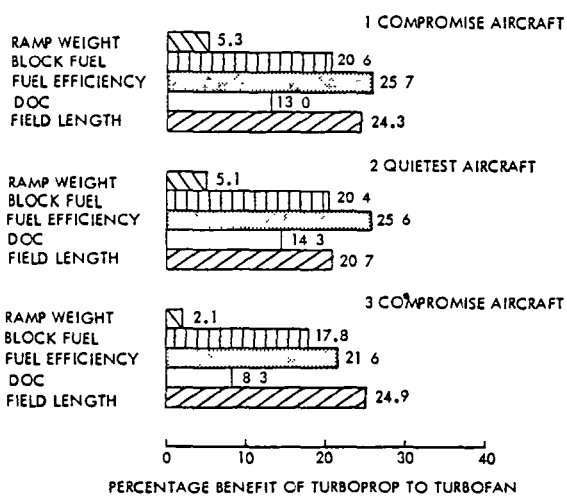

Figure 62. Turboprop Aircraft Performance Benefits Relative to Turbofan Aircraft

* Fuel efficiency, as used here, is the product of the payload and range divided by the block fuel. Thus, fuel efficiency indicates the amount of payload that may be carried a unit distance per unit of fuel, or alternately, the total distance a unit payload will be carried for a unit of fuel.

DOCs down by 8 to 15 percent. The 20 to 25 percent shorter field lengths are also significant because this means that the turboprop aircraft can operate into small airports that may not be accessible to turbofan aircraft.

Although not shown on the figure, both the turboprop and turbofan aircraft have about 20 percent lower fuel consumption than today's commercial aircraft. Thus, the turboprop offers a total potential fuel saving of 40 percent in comparison with current aircraft.

NOISE

There are two types of noise measurements of concern. One, measuring point noise, is set by federal regulations, and hence, demands compliance. The second, the noiseprint concept, is intended to provide an indication of the effect of an aircraft on the airport community. In this report, noiseprint areas are presented for several noise levels without attempting to judge what is an acceptable level or area for any community.* Such a judgment must take into account the community's proximity to the airport and the background of its constituency, both of which are considerably outside the scope of this study.

Measuring Point Noise

Because of the regulatory requirements concerning it, measuring point noise is addressed first in comparing the two types of propulsion systems. Figure 63 illustrates the FAR 36 stage

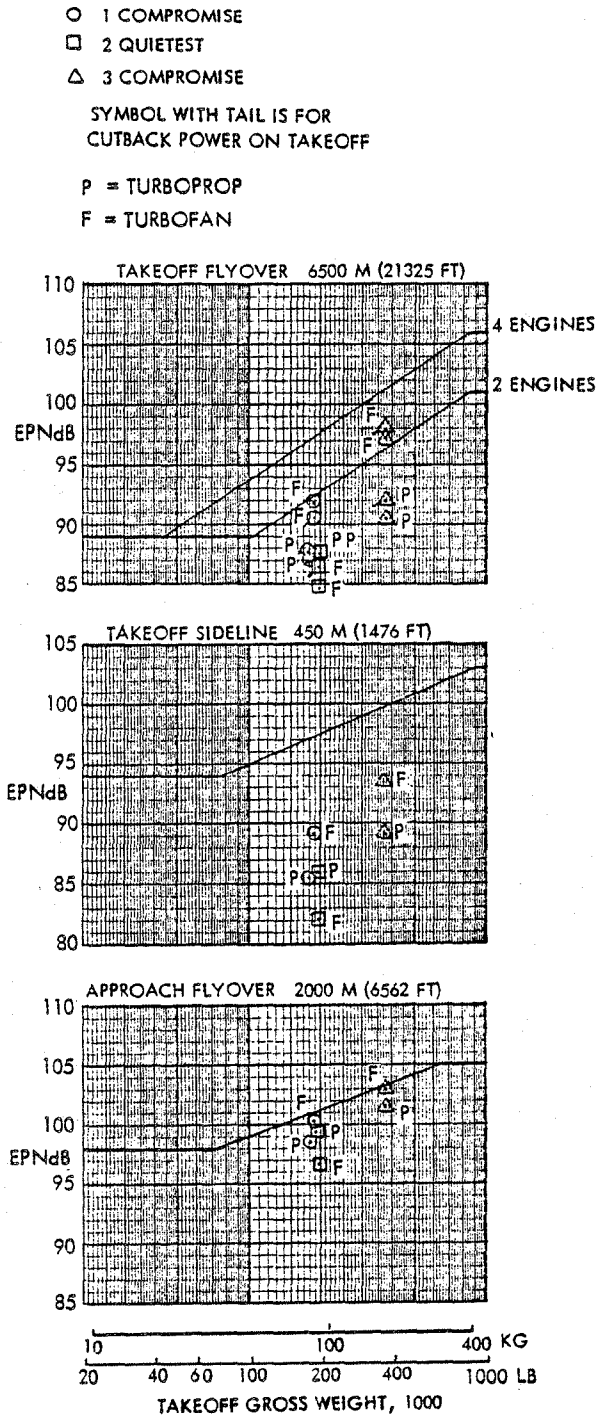

Figure 63. Comparison of Aircraft Noise Levels with FAR 36 Stage 3 Limits

* Even though an 80 EPNdB noise level is used for presenting much of the sensitivity data in this report, this level simply served as a convenient base and is not intended to imply a preferred or suggested level.

3 noise limits as a function of gross weight at the three standard measuring points of takeoff flyover, sideline, and approach. All six aircraft necessarily comply with the regulations, as indicated by all of the predicted noise level points being below the limit. That some aircraft points are further below the limits than others is not the result of any concerted design effort on that particular aircraft. As discussed in previous sections, the six aircraft were selected based on their impact on noiseprint areas. The noise levels of the turboprop aircraft at the measuring points are simply a fall-out; those for the turbofans are the result of applying equal noise suppression treatment to the nacelles after it was observed that the original selections with hardwall nacelles could not satisfy the regulations - an expected result.

Although the propeller or fan is the predominant noise source in the respective aircraft for most cases, generally, only small reductions in these noise sources will prove beneficial before airframe noise becomes the major source. In fact, airframe noise predominates on approach for all three turboprop aircraft.

Airframe noise is higher for a turboprop aircraft than for a turbofan aircraft because of propeller slipstream effects on the wing and flaps, all other things being equal. The influence of these effects on airframe noise may be observed by comparing corresponding aircraft (see Tables XV and XXVI) at the approach measuring point where all conditions are essentially equal. In these cases, the slipstream is responsible for about a 3 dB increase in airframe noise. Further details on this slipstream effect are presented in Appendix M.

In regard to the aircraft noise levels at the measuring points, the only significant point is that all comply with the regulations. No significance is attached to the noise level of one aircraft relative to another because no attempt was made to minimize noise at the measuring points. The reason for the apparent contradiction in several cases of louder noise with cutback power than for full power will be explained later.

Noiseprints

Noiseprint areas previously calculated are listed in Table XXX for the six aircraft at three noise levels for both full and cutback power conditions.* Although such a tabulation is beneficial if absolute magnitudes are of interest, a relative comparison is much easier to illustrate in the format of Figure 64. The lengths of the bars on the figure indicate the percentage by which the noiseprint area for the louder propulsion system exceeds the area for the quieter system. Thus, when the bars project to the left, the turbofan is louder, has a larger area, and is less desirable. Projections of the bars to the right occur for unfavorable turboprop results.

Two results occur which require an explanation. First, the turboprops have smaller noiseprints than the turbofans at the 90 EPNdB level, but the reverse is true at the lower levels. In fact, the lower the level, the greater the difference between the two. Second, cutback power may be counterproductive and increase, rather than decrease, the noiseprint.

Before we can explain what is happening in these particular cases we need to review some details on the basic noise characteristics of the two propulsion systems. Consider Figures 65 and 66 which combine the results of several figures from Appendix C. Figure 65 shows that turbofan noise

* The noiseprint areas for the turbofan aircraft are based on the original hardwall nacelles around the engines. The effects of the insulation required to reduce the noise to meet the measuring point requirements have not been accounted for here.

Table XXX. Numerical Comparison of Aircraft Noiseprints

	AIRCRAFT					
	1 COMPROMISE		2 QUIETEST		3 COMPROMISE	
PROPULSION TYPE	PROP	FAN	PROP	FAN	PROP	FAN
NOISE LEVEL, EPNdB	FULL POWER AREAS IN SQ KM					
90	10.6	17.1	7.8	11.1	20.5	25.4
80	84.5	54.1	59.3	37.5	165.0	77.6
70	816.0	161.3	496.0	115.6	1472.0	229.2
	CUTBACK POWER AREAS IN SQ KM					
90	6.2	13.7	4.1	8.8	12.7	22.6
80	54.1	51.3	34.4	36.0	138.0	89.0
70	470.0	173.2	274.5	126.6	1306.0	311.0
	FULL POWER AREAS IN SQ MI					
90	4.1	6.6	3.0	4.3	7.9	9.8
80	32.6	20.9	22.9	14.5	63.7	30.0
70	315.3	62.3	191.7	44.6	568.5	88.5
	CUTBACK POWER AREAS IN SQ MI					
90	2.4	5.3	1.6	3.4	4.9	8.7
80	20.9	19.8	13.3	13.9	53.2	34.4
70	181.9	66.9	106.0	48.9	504.6	120.2

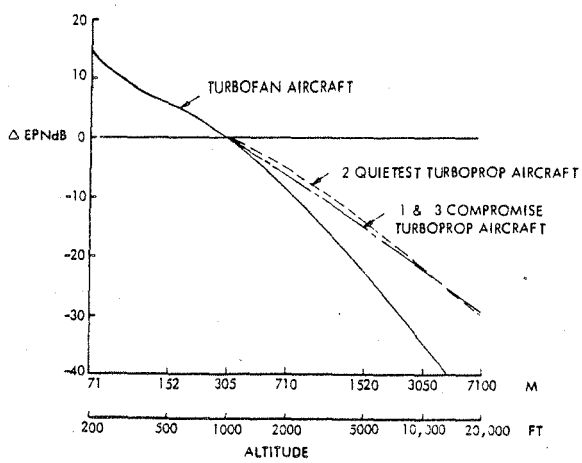

Figure 65. Comparison of Altitude Effects on Noise Predictions

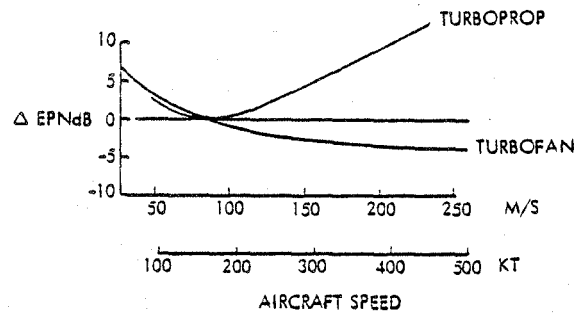

Figure 66. Comparison of Forward Speed Effects on Noise Predictions

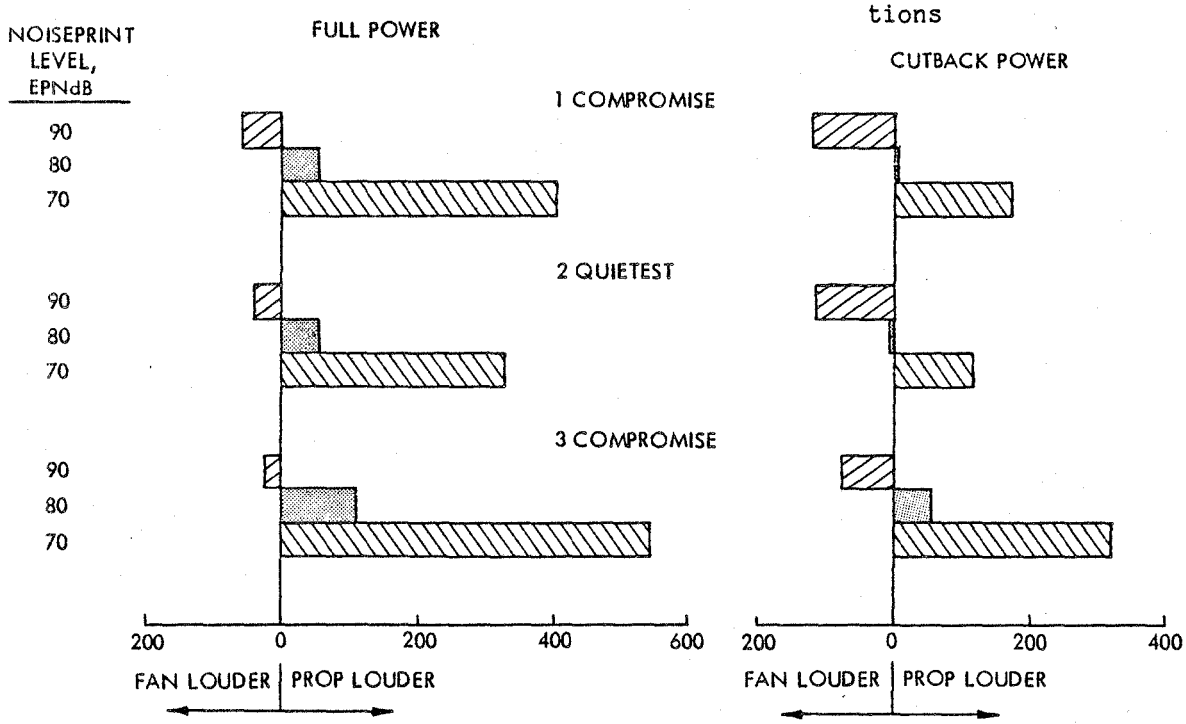

Figure 64. Comparison of Propulsion Effects on Noiseprint Areas

attentuates much quicker with distance than turboprop noise. For example, turbofan noise will be 13 EPNdB quieter over a 3280 m (10,000 ft) distance than a turboprop of equal noise level. This is directly related to the attenuation characteristics of the two systems. Turbofans characteristically have high-frequency noise which dissipates rapidly, while turboprops emit low-frequency noise which is not so readily suppressed with distance.

Another basic difference between the two systems is the radically divergent speed corrections, as indicated in Figure 66. Turbofan perceived noise levels are basically independent of aircraft forward speed, but the EPNdB benefits because of the duration correction which becomes more negative with higher speed. The turboprop experiences the same duration correction benefit, but it is severely overridden by the propeller tip speed effect. Although the propeller rotates at constant speed, its noise level varies in proportion to its total velocity, which is the resultant of the rotational speed and the aircraft forward speed. Thus, at 138 m/s (250 kt) a turbofan aircraft is 5 EPNdB quieter than an otherwise identical turboprop aircraft because of the forward speed effect.

With that background, the noiseprint area variations can now be explained in conjunction with the initial flight path profiles in Figures 67 for the six aircraft. Each section of the figure compares the flight paths for two competitive aircraft at both normal and cutback power during climb. The profiles at full power are those that would typically be flown in normal commercial operation consistent with FAR 25, while those at cutback power are in accord with the FAR 36 measuring point requirements. Points are noted on the profiles to indicate aircraft positions when the noiseprint for a particular level closes. The position of the FAR 36 takeoff flyover measuring point, relative to brake release, is also designated.

The following explanations are based on the flight profiles for the No. 1 Compromise aircraft but apply equally to the others. At the 90-EPNdB level, the noiseprints close when both aircraft are at altitudes of approximately 650 m (2000 ft). Because of their greater climb capabilities, the turboprops reach this altitude at shorter distances from brake release, which results in smaller noiseprints. For this noiseprint, the distance and speed correction effects are not a consideration.

At the 80-EPNdB level, the distance and speed corrections begin to have an effect on the noiseprint size. Under full power, the noiseprint for the turboprop does not close until it is about 4000 m (12,000 ft) further down range than the turbofan, even though the turboprop is about 1000 m (3000 ft) higher. This substantially increases the noiseprint area. Under cutback power, the noiseprint for the turboprop closes about 2500 m (7500 ft) sooner than that for the turbofan, with both at about the same closure altitude. However, the smaller amount of noise attenuation with distance for the turboprop gives a wider sideline distance to more than balance the reduced closure length. Consequently, the noiseprint for the turboprop is slightly larger than for the turbofan at cutback.

At the 70-EPNdB level, the speed and distance correction effects are so pronounced that the closure locations of the turboprops will not fit on the graph. Rather, they can only be hinted at by listing the distance from brake release to closure on the right side of the graph. With the closure distance for the turboprop at three times that for the turbofan at full power, it is quite evident that the noiseprint for the turboprop will exceed that for the turbofan by a substantial margin. The same phenomena occur under cutback power.

Next, attention will be focused on the relative merits of cutting back power during climb. As a result of re-

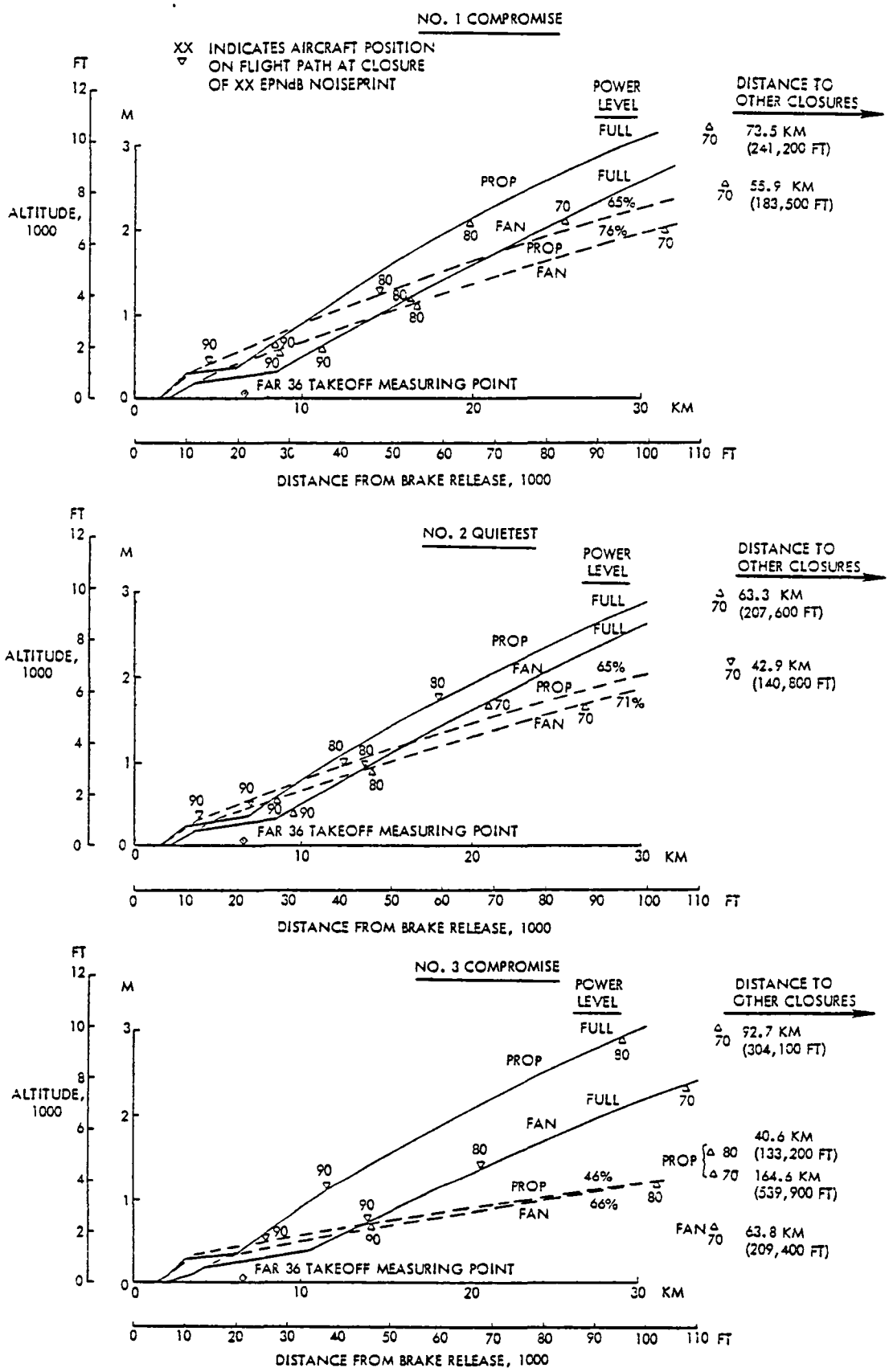

Figure 67. Initial Flight Path Comparison for Turboprop and Turbofan Aircraft

ducing power, two things happen which tend to be counterproductive. The positive aspect is that the noise source level goes down in proportion to the amount of power reduction. A consequence of less power, however, is that the aircraft climbs at a slower rate, thereby increasing the length of the noiseprint. For the flight profiles shown, this effect is experienced by the turbofan aircraft as the noiseprint level becomes lower. This effect is also responsible for the apparent anomaly in several measuring point noise cases where the aircraft is louder under cutback power than full power.

As mentioned earlier, the flight profiles in Figure 67 for cutback power are in accordance with FAR 36 for recording noise at the measuring points. The profiles for full power are not according to FAR 36 but are for normal operation which gives noiseprints that will typically be borne by the airport community - the type of noiseprints that must be minimized to gain community acceptance.

For the FAR 36 regulations, the flaps must remain in the takeoff position regardless of power level. As a result, the aircraft reaches a higher altitude over the measuring point than in normal operation. In relation to the flight profiles in Figure 67, the aircraft will be at a higher altitude over the measuring point than indicated by the solid lines for normal full-power operation. Sometimes this higher altitude is more beneficial than the reduced level of the noise source. Such is the case, as may be seen in Figure 63, for all three turbofan aircraft and for the No. 3 turboprop aircraft. Consequently, FAR 36 noise levels are not indicative of actual aircraft noise during normal operation. Figure 68 shows how much the FAR 36 noise levels are below the levels that would actually be perceived for the six aircraft in this study. In reviewing the differences, remember that each 3 dB noise change represents a doubling in noise intensity.

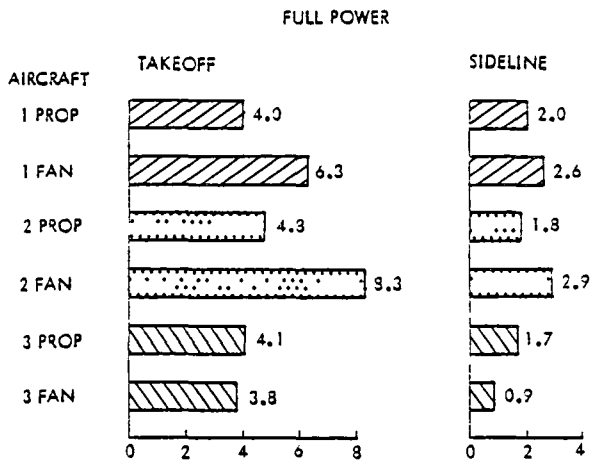

Figure 68. Effect on Noise Levels at the Measuring Points from Varying the Takeoff Operating Procedure

One other point must be made concerning the noiseprints. In the previous discussion, we noted that the noiseprints for the turbofan aircraft are based on the original hardwall nacelles around the engines and do not reflect the effects of the insulation that was added to meet the measuring point regulations. Obviously, this treatment will reduce the noiseprints of the turbofan aircraft. No attempt was made, however, to calculate the noiseprints for the treated turbofan aircraft for the following reason.

One objective of this study is to evaluate turboprops relative to turbofans. Figure 64 shows that the noiseprints for the untreated turbofans are smaller than those for the turboprops at the two lower noise levels, which must be the noise levels of interest to meet the goal of unrestricted airport operations. Having established that the noiseprints for the turbofans are smaller than for the turboprops, there is no need to determine how much smaller the turbofan noiseprints can be made. For those to whom this is vitally important, though, an indication of the possible reduction can be

made based on the sensitivity results. They showed that a 3-dB reduction in the noise source produces a one-third to one-fourth smaller noiseprint. Typically, the turbofan treatment provided a 9-EPNdB reduction in the noise source. Correspondingly, the noiseprint area should drop to about three-eighths of the previous size.

SENSITIVITY RESULTS

Of all the sensitivity studies that were performed, only a few parameters were found to have a critical or significant impact on the results. For the purposes of this comparison, those sensitivity results are summarized in Table XXXI. To review, the ratings are as follows. A critical assessment means that a one percent change in the sensitivity factor produces more than a five percent change in the particular measure of sensitivity, be it noiseprint area, DOC, or block fuel. Significant ratings are for two to five percent changes in the measure of sensitivity per unit change in the sensitivity factor. Marginal ratings apply when only one to two percent changes are realized for each one percent change in the sensitivity factor, and negligible ratings are given for changes of less than one percent.

Table XXXI. Comparison of Sensitivity Results

PROPULSION SYSTEM	SENSITIVITY RATINGS: TURBOPROP			TURBOFAN		
MEASURE OF SENSITIVITY	NOISE PRINT	DOC	B F	NOISE PRINT	DOC	B F
PROP DIAMETER	C, S	N	N			
DISK LOADING	S, M	N	N			
TIP SPEED	C	N	N			
BLADES	C, N	N	N			
THRUST/WEIGHT	S, M	N	N			
ALTITUDE	N	N	N	N	N	N
DRAG	N	N	M	N	N	M
FIELD LENGTH	S	N	N	N	N	N
APPROACH SPEED	M	M	M	N	N	M
GLIDESLOPE	N	N	N	N	N	N
NOISE SOURCE LEVEL	C			C		
WING LOADING	N	N	N	N	N	N
ASPECT RATIO	N	N	N	N	N	N
WEIGHT - PROPULSION		N			N	
AIRFRAME		S, M			S, M	
FUEL		N			N	
STAGE LENGTH	N	N	M	N	N	N
UTILIZATION		N			N	
LOAD FACTOR	N	M	N	N	M	N
FUEL PRICE		N			N	
PROP COST		N				
ENGINE COST		N			N	
AIRFRAME COST		N			N	
FLYAWAY COST		N			N	
MAINTENANCE COST		N			N	

RATINGS C - CRITICAL, S - SIGNIFICANT, M - MARGINAL, N - NEGLIGIBLE
BLANK SPACES INDICATE NOT APPLICABLE OR ASSESSED

The propeller parameters have major impacts on the noiseprints, but negligible effects on the DOC and block fuel. The particular propeller parameters have the following effects on the noiseprints of each aircraft. Tip speed is a critical factor for all three aircraft. Propeller diameter is critical for the No. 2 aircraft which has the maximum size allowed, but only a significant factor for the No. 1 and No. 3 aircraft which have propellers smaller than the maximum. The number of blades is critical for the 10-bladed No. 1 and No. 3 aircraft but is negligible for the 6-bladed No. 2 aircraft. Disk loading has a significant effect on the No. 2 aircraft, which has the lowest disk loading of the three, but only a marginal effect is experienced by the No. 1 and No. 3 aircraft.

Thrust/weight variations have a significant effect on the noiseprint of the No. 2 turboprop aircraft which has the lowest thrust/weight ratio of the three. This parameter has only a marginal effect on the noiseprints of the other two aircraft, and has a negligible effect on the block fuel and DOC for all three aircraft.

Initial cruise altitude and approach glideslope along with wing geometry factors of wing loading and aspect ratio have negligible effects on all six aircraft. Drag variations have marginal effects on only the block fuel for the six aircraft; the other measures are negligibly affected.

Field length has a significant effect on the noiseprints of the three turboprop aircraft, but only negligible effects on those for the turbofan aircraft. Negligible changes in DOC and block fuel occur with field length changes for all six aircraft.

Approach speed variations have a marginal effect on the block fuel of the No. 3 turboprop aircraft and the No. 2 turboprop and turbofan aircraft. The DOC of the No. 2 turboprop and the

noiseprint of the No. 3 turboprop are also marginally affected by changing approach speed. These effects occur in some of the cases where wing loading is constrained by the approach speed. Thus, changing the approach speed means going to another wing loading, thereby changing the whole design.

Variations in the noise source level produce critical changes in the noiseprints of all six aircraft. Of all the parameters considered, this one is judged to be most in need of further attention and analysis.

Possible errors in estimated weights of the airframe have marginal to significant effects on aircraft DOC. Similar variations in propulsion and fuel weights have only negligible effects because of the relatively smaller importance of these parameters to DOC.

Stage length has a marginal effect on the block fuel of the turboprop aircraft and a negligible effect on the turbofan aircraft. This difference arises because of the much lower specific fuel consumption of the turboprops.

Load factor has a marginal impact on DOCs for the aircraft. All other factors considered have negligible effects.

SPECIAL STUDIES

Several areas were identified during the study as meriting further investigation. Of these, the five that were undertaken as part of this program, and are reported next, covered the following topics:

- o Alternate Takeoff and Climb Profiles
- o Variable Tip Speed Propeller
- o Alternate Point Design Aircraft
- o C-X Mission Application
- o Effect of Nearer-Term Engines

ALTERNATE TAKEOFF AND CLIMB PROFILES

In the preceding studies, the mission performance and noiseprints were calculated for only one fixed takeoff and climb procedure that is consistent with current commercial practice. This resulted in aircraft designed to minimize the 80-EPNdB noiseprints for that flight profile, but without any guarantee that the flight profile itself is the best one for minimizing the noiseprint. What effect variations to the flight profile will have on the aircraft noiseprints is the subject of the studies in this section.

Several operational parameters that define takeoff and climb were varied to determine their effects on the noiseprint areas for the No. 1 and No. 2 turboprop and turbofan aircraft. In this study, each parameter was analyzed separately while all other parameters were held constant. From the results, a parameter value was selected which minimized the 80-EPNdB noiseprint in each case, and it was then held constant in the subsequent analyses of the other parameters. This approach was followed until all of the parameters were investigated and the best takeoff and climb procedures for minimizing the 80-EPNdB noiseprints

were defined for each of the four selected aircraft.

Originally, all of the aircraft took off with the flaps deflected at 0.35 rad (20 deg) and achieved an obstacle speed 5.1 m/s (10 kt) above the minimum safe speed. Upon reaching an altitude of 122 m (400 ft), the flaps were retracted and the aircraft continued on to cruise altitude at their maximum rate of climb. The changes to this procedure that were investigated for reducing the noiseprint areas were: different flap angles, different altitudes for retracting the flaps, increased obstacle speeds, climbing at maximum gradient (altitude gained per unit of horizontal distance travelled) instead of maximum rate of climb (altitude gained per unit of time in flight), and cutback power. Of these, keeping the flaps deployed to higher altitudes was consistently most beneficial in reducing the noiseprints.

Figure 69 summarizes the results of this study to reduce the noiseprints of the four selected aircraft, while further details are contained in Appendix N. As before, the noiseprints have been expressed as equivalent squares for the three noise levels. The original size of the noiseprint, as previously noted in Table XXX, is shown for each case along with the extent of the noiseprint reduction, which is indicated by the shaded area.

Of greatest significance is the impact on the relative comparison of the turboprop and turbofan propulsion systems from changing the takeoff and climb procedures. Before, the turboprops were quieter (that is they affected a smaller area) only at the 90-EPNdB noise level. Now, with the changed profiles, the turboprop noiseprints are smaller than or equal to those of the turbofans for both the 90 and 80 EPNdB levels, and the advantage enjoyed by the turbofans at 70 EPNdB is reduced significantly.

Improvements to the turbofan aircraft noiseprints are considerably

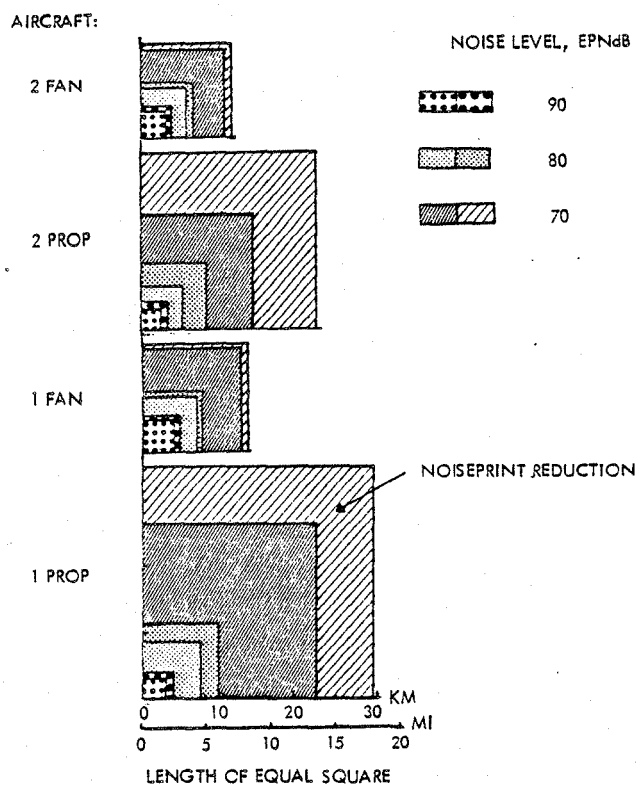

Figure 69. Effects of Alternate Profiles on Noiseprint Areas

smaller than those for the turboprop aircraft because of the characteristics of the two propulsion systems. Typically, turboprop aircraft have much better takeoff power features which produce shorter field lengths and greater climb capabilities than for turbofan aircraft. As a result, when both turboprop and turbofan aircraft are designed for the same mission conditions, the turbofan aircraft design is often constrained by these conditions and has minimal to no latitude in changing its operational procedure, while the turboprop is not so restricted. Such was the case in this study where the turbofan aircraft could not vary the takeoff flap setting, for example, by more than a couple of degrees. With less than 0.35 rad (20 deg) flaps, the aircraft could

not take off within the 2440 m (8000 ft) field length limitation, and with a greater flap deflection the aircraft could not satisfy the FAR 25 minimum requirements for the engine-out gradient during second segment climb.

In this study, the optimizations were directed toward the 80-EPNdB noiseprints only. The benefits achieved at the 70 and 90 EPNdB levels are merely a fallout and probably are not representative of the minimum attainable noiseprints. Additional study would probably identify other takeoff and climb procedures that would further reduce the noiseprint areas of one or both propulsion systems at other levels, and might even change the relative comparisons.

Before leaving this section, we feel impelled to reiterate a disclaimer noted earlier: Even though an 80-EPNdB noise level has been used here for the optimization, this level simply served as a convenient base and is not intended to imply a preferred or suggested level.

VARIABLE TIP SPEED PROPELLER

Our results have shown that the propeller is the primary noise source on these turboprop aircraft, and furthermore, that tip speed is the characteristic most responsible for the propeller noise. While reducing the tip speed does tend to produce a quieter propeller and aircraft, the lower speed means less performance, which must be compensated for by going to a larger, and somewhat noisier, propeller and engine.

An alternative for reducing the noiseprint is to operate the propeller at its design tip speed during cruise but at a lower tip speed when the aircraft is close to the ground. This approach is ideal for a propeller powered aircraft because its propulsion system is usually sized to provide the required cruise performance and, as a fallout, has a surplus of power available for satisfying airport-related performance requirements.

This method of operation was investigated for the No. 1 Compromise Turboprop aircraft. In the analysis, the aircraft was assumed to retain all of its cruise characteristics and performance, which are based on a propeller tip speed of 229 m/s (750 ft/s). For operations around the airport, the aircraft, engine, and propeller remain unchanged but the propeller tip speed was reduced to 204 m/s (670 ft/s) with an accompanying drop in propulsion thrust. New takeoff, climb, and landing flight paths were determined with the reduced thrusts and were used to recalculate the noiseprints at 70, 80, and 90-EPNdB noise levels.

Figure 70 shows the relative effects on the baseline aircraft noiseprints of reducing the propeller tip speed. Also provided on the figure are the effects of cutting back engine power at 305 m (1000 ft) altitude to the minimum level permitted by FAR 36, and of leaving the flaps deployed to altitudes greater than the 122 m (400 ft) normal retraction altitude. This latter effect was investigated based on the results of the study on alternate takeoff and climb profiles.

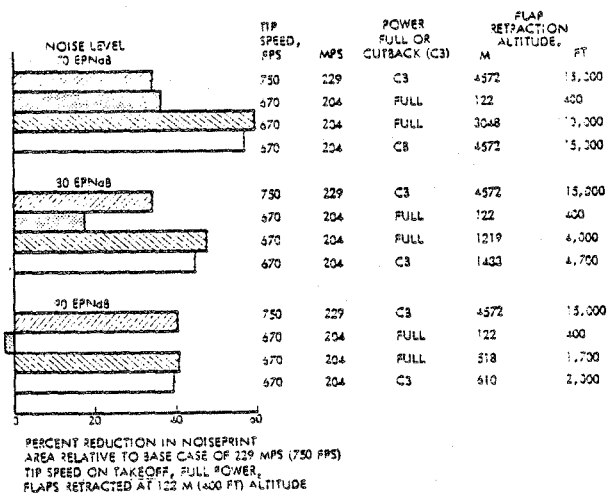

Figure 70. Effects of Variable Tip Speed Propeller on Noiseprints

As shown on the figure, just reducing the tip speed has mixed effects in that the 90 EPNdB noiseprint is increased by 2.4 percent, but 17.5 and 36.7 percent reductions are realized for the 80 and 70 EPNdB noiseprints, respectively. These results occur because of two counterproductive effects which are caused by changing the tip speed. Beneficially, the propulsion system noise is reduced. Adversely, the rated takeoff thrust is lower by 21 percent which, in turn, increases the takeoff distance by 9 percent and restricts the aircraft's ability to climb.

The influence of each of these effects is more clearly evident in Figure 71 which compares the FAR 36 measuring point noise for the aircraft at the two tip speeds. Note first the comparison at the approach measuring point. Here, for both tip speeds, the aircraft is at the same flight speed, at the same distance from the microphone, and at the same attitude. Thus, the difference in the perceived noise levels is due solely to the reduction in the noise of the propulsion system as a result of the lower tip speed. In contrast, the measuring point noise is greater at the lower tip speed for the other two conditions of takeoff flyover and sideline. This is the direct result of the lower engine thrust and

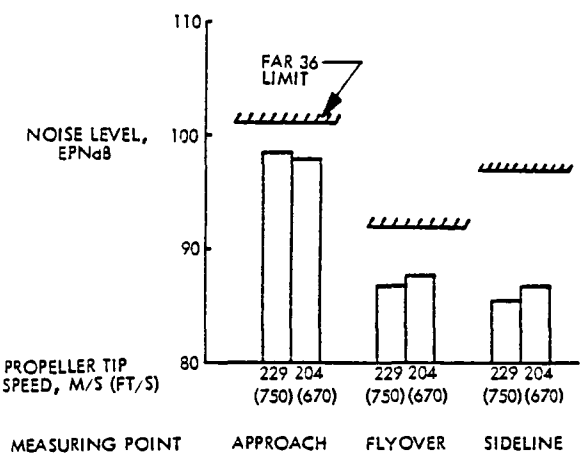

Figure 71. Effects of Variable Tip Speed Propeller on FAR 36 Measuring Point Noise

reduced climb capability which causes the aircraft to be closer to the measuring point. In these two cases, the benefits of the quieter propulsion system are more than offset by the lower altitude and shorter noise attenuation distance at the measuring point.

Returning now to the results shown in Figure 70, the changes in the noiseprints for the three noise levels are as expected with the noiseprints at the lower levels realizing greater reductions in area. This occurs because noise attenuates logarithmically with distance, that is, for a given distance there is greater attenuation over that half of the distance which is closer to the noise source than over the half that is closer to the receiver. As the difference between the noise source and receiver levels becomes greater, reducing the source noise is much more effective in decreasing the noiseprint than a similar percentage increase in the attenuation distance.

As was found in the study of alternate climb profiles, keeping the flaps deployed to higher altitudes is effective in reducing the noiseprint areas and further enhances the benefits of lower tip speeds. Interestingly, the most effective approach for reducing the noiseprints at all three noise levels, in conjunction with the reduced tip speed, is to remain at full power with the flaps down rather than following a FAR 36 cutback procedure.

ALTERNATE POINT DESIGN AIRCRAFT

NASA wind tunnel tests of propfan scale models have been for a set of conditions that are somewhat different from those suggested by our aircraft design optimization studies. As an aid to visualizing the effects of these differences, our No. 1 Turboprop Aircraft was used as a base to derive an alternate point design aircraft subject to the NASA test conditions, which are listed in Table XXXII.

The alternate design has the same fuselage geometry and carries the same 27,273 kg (60,000 lb) payload as the base aircraft. All of the other mission requirements and study constraints

Table XXXII. NASA - Model Test Conditions

CRUISE MACH NUMBER	0.8
CRUISE ALTITUDE	10,668 M (35,000 FT)
WING SWEEP	0.44 RAD (25 DEG)
PROPELLER BLADES	10
TIP SPEED	244 MPS (800 FPS)
CRUISE DISK LOADING	300 KW/M^2 (37.5 HP/FT^2)
RATED DISK LOADING	750 KW/M^2 (93.75 HP/FT^2)

applicable to the base aircraft have also been imposed on the alternate design.

In developing the alternate aircraft, a parameteric matrix of wing loading and aspect ratio values were investigated to determine the optimum designs for minimum noiseprint, minimum DOC, and a compromise between the two. Figure 72 provides a graphical comparison of the major characteristics of the 12 aircraft point designs that were generated. Imposed on the figures are the study constraints on field length, engine-out gradient, fuel volume, and approach speed, which eliminate some of the designs. As in our previous work, the maximum approach speed limit typically defines wing loading values for the optimum designs.

While the wing loading and aspect ratio values can be readily read from the graphs for the minimum noiseprint and DOC designs, selection of the best compromise design point is not as easily accomplished with the existing graphs. The selection process is simplified considerably, however, if the values along the limiting lines of the pertinent characteristics are replotted as in Figure 73. The triangles on the figure denote the wing aspect ratio values which minimize each characteristic parameter, such as noiseprint and DOC. To select the compromise aircraft, the most straightforward approach is to choose the aspect ratio value midway between those for the other two point designs, which was done.

Due to the flatness of the DOC and noiseprint curves, there is very little difference in the major characteristics of the three selected point designs, which is apparent from the comparisons in Table XXXIII. Because of the similarity of the three designs, subsequent efforts were concentrated on only the compromise aircraft, which will be referred to as the alternate design.

Subsequently, the design was checked for compliance with the FAR 36 requirements and, as indicated by the results in the top part of Table XXXIV, was found to be unsatisfactory during takeoff flyover. To solve this problem, the aircraft was resized with successively higher thrust-to-weight values, thereby shortening the takeoff distance and increasing the altitude over the measuring point, until the compliance noted in the bottom of the table was obtained. Figure 74 shows the resized version of the alternate design.

As a result of the resizing, the aircraft weights and DOCs increased while the noiseprints became smaller. The extent of these changes are summarized in Table XXXV. In every comparison of likely measures of effectiveness, as shown in Table XXXVI, the baseline aircraft is superior. This result is to be expected because the baseline aircraft is a fully optimized design, while the alternate design is not.

Table XXXIII. Comparison of Alternate Designs

CHARACTERISTIC	SELECTION CRITERIA		
	MINIMUM NOISEPRINT	COMPROMISE	MINIMUM DOC
WING			
LOADING, KN/M^2 (PSF)	5.61 (119.3)	5.40 (118.3)	5.39 (118.5)
ASPECT RATIO	10.0	10.6	11.2
WEIGHTS, 1000 KG (LB)			
OPERATING	40.6 (89.5)	41.1 (90.5)	41.6 (91.6)
BLOCK FUEL	11.3 (24.8)	11.1 (24.5)	11.3 (24.8)
RAMP	52.1 (180.9)	52.4 (131.5)	52.8 (182.4)
DOC, ¢/TKM (¢/TNM)	3.33 (14.37)	3.31 (14.34)	3.30 (14.33)
30 EPNdB NOISEPRINT AREA, KM^2 (MI^2)	275.5 (105.3)	276.3 (106.1)	277.6 (106.6)

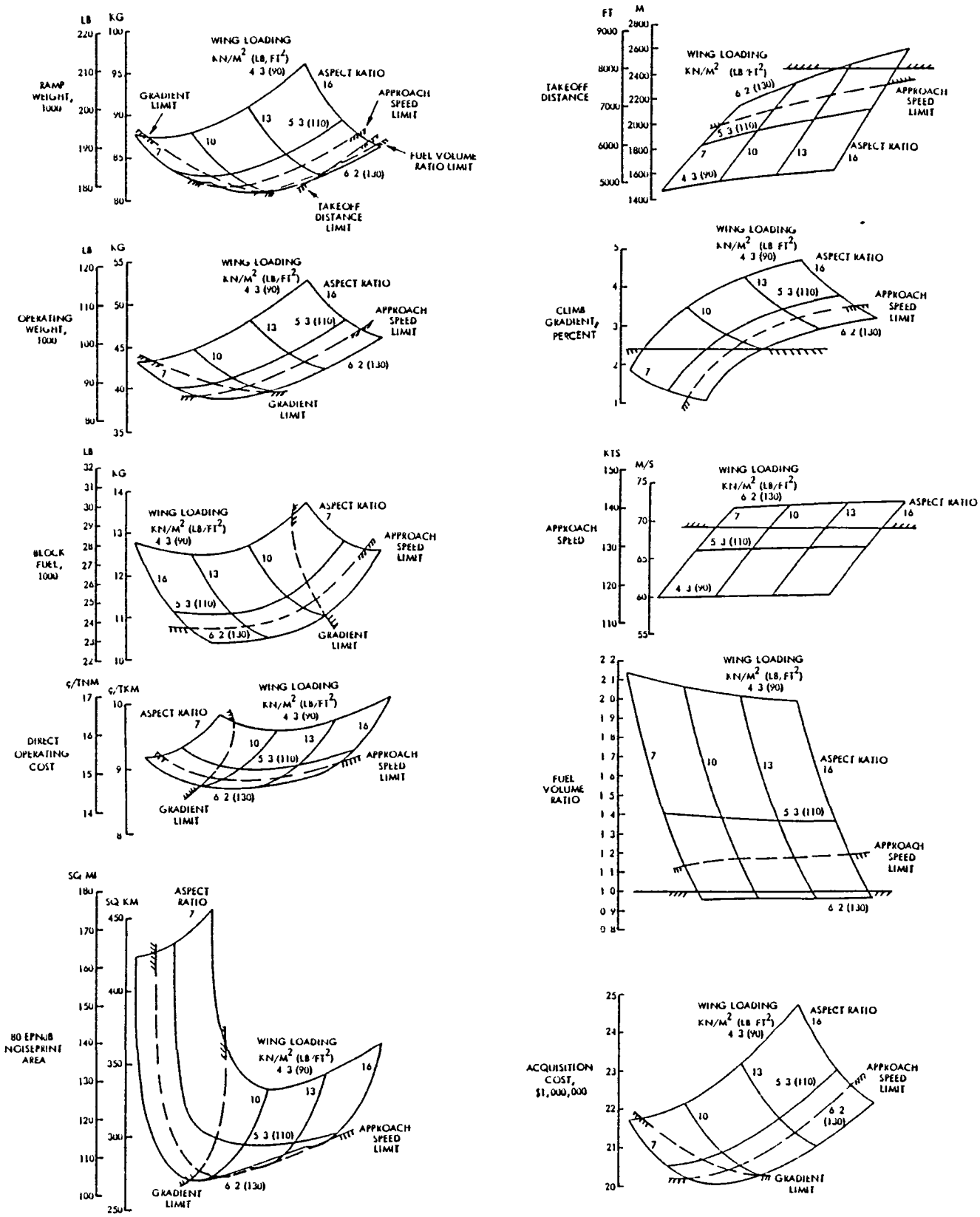

Figure 72. Characteristics of Candidates for Alternate Point Design Aircraft

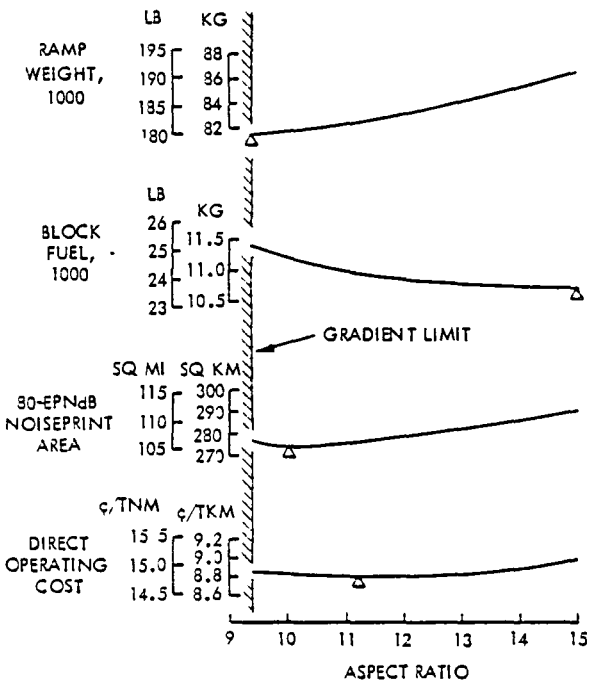

Figure 73. Alternate Point Design Aircraft Selection Curves

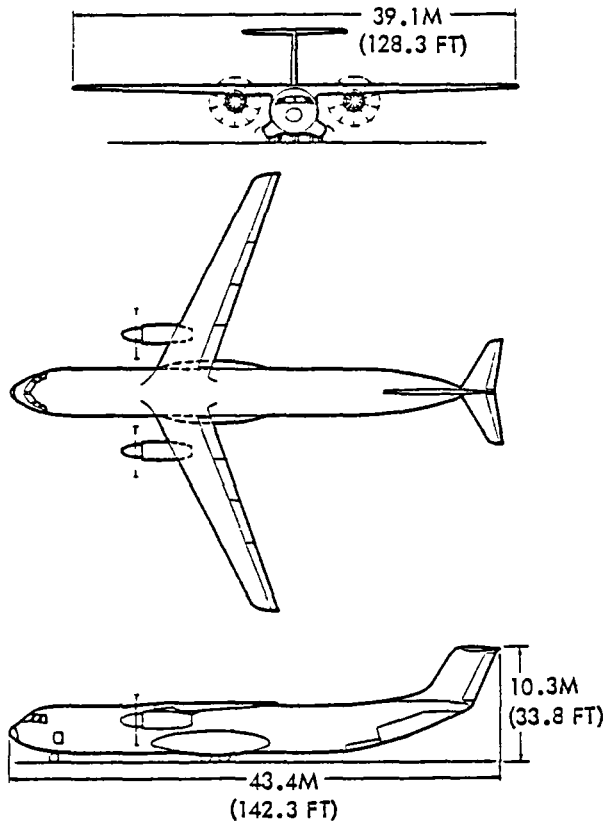

Figure 74. Alternate Point Design Aircraft

Table XXXIV. FAR 36 Noise Compliance Results for Alternate Design

ALTERNATE AIRCRAFT	FAR 36 CONDITIONS		
	TAKEOFF FLYOVER	TAKEOFF SIDELINE	APPROACH
INITIAL DESIGN*			
NOISE LIMITS	92.3	97.3	101.3
PREDICTED NOISE	94.8	92.3	98.2
COMPLIANCE?	NO	YES	YES
RESIZED DESIGN**			
NOISE LIMITS	92.2	97.1	101.1
PREDICTED NOISE	92.0	89.5	98.1
COMPLIANCE?	YES	YES	YES

*RAMP WEIGHT - 82,500 KG (181,932 LB)
**RAMP WEIGHT - 84,350 KG (186,073 LB)

Table XXXV. Effect of Resizing Alternate Aircraft for FAR 36 Compliance

CHARACTERISTIC	ALTERNATE AIRCRAFT		
	INITIAL	RESIZED	PERCENT CHANGE
PROPULSION			
THRUST/WEIGHT, N/KG (LB/LB)	1.37 (0.19)	2.13 (0.22)	+13.9
RATED THRUST, 1000 N (LB)	77.3 (17.5)	91.6 (20.6)	+17.7
WEIGHTS, 1000 KG (LB)			
RAMP	82.5 (181.5)	84.9 (186.7)	+2.3
OPERATING	41.1 (90.5)	42.9 (94.4)	+4.4
BLOCK FUEL	11.1 (24.5)	11.5 (25.4)	+3.7
FIELD LENGTH, M (FT)	2150 (7051)	1861 (6106)	-13.4
DOC, ¢/TKM (¢/TNM)*	8.9 (14.8)	9.2 (15.3)	+3.1
NOISEPRINTS, KM^2 (MI^2)			
AT 70 EPNdB	2820 (1090.0)	2332 (901.1)	-17.3
80 EPNdB	400 (154.7)	225 (90.7)	-41.4
90 EPNdB	40 (15.5)	22 (8.7)	-43.9

*FUEL AT 266 $/M^3$ (100 ¢/GAL)

Table XXXVI. Comparison of Alternate and Baseline Aircraft Characteristics

AIRCRAFT	BASELINE	ALTERNATE
MISSION		
CRUISE MACH NUMBER	0.75	0 80
CRUISE ALTITUDE, 1000 M (FT)	33	35
PROPULSION		
PROPELLER BLADES	10	10
TIP SPEED, MPS (FPS)	229 (750)	244 (800)
CRUISE DISK LOAD, KW/M^2 (HP/FT^2)	173 (21 5)	300 (37 3)
RATED DISK LOAD, KW/M^2 (HP/FT^2)	402 (50 0)	750 (93 8)
THRUST/WEIGHT, N/KG (LB/LB)	3 0 (0 31)	2.13 (0 22)
WING GEOMETRY		
SWEEP, QAD (DEG)	0 35 (20)	0 44 (25)
ASPECT RATIO	12	10 6
LOADING, KN/M^2 (PSF)	5.9 (123.3)	5.6 (118 8)
WEIGHTS 1000 KG (LB)		
RAMP	91 0 (178 2)	84 9 (186 7)
OPERATING	40 3 (88 6)	42 9 (94 4)
BLOCK FUEL	10 7 (23 5)	11 5 (25 4)
FIELD LENGTH, M (FT)	1861 (6106)	1684 (5524)
DOC ¢/TKM (¢/TNM)		
FUEL, $/M^3 ($/GAL) - 264 (1)	8 8 (14 7)	9 2 (15 3)
528 (2)	11 9 (19 9)	12 6 (20 9)
792 (3)	15 0 (25 0)	15.9 (26 5)
NOISEPRINTS, KM^2 (MI^2)		
NOISE LEVEL, EPNdB - 70	316 (315 3)	2332 (901 1)
80	84 (32.6)	235 (90.7)
90	11 (4 1)	23 (8 7)

C-X MISSION APPLICATION

Considerable interest has been expressed in recent years in the concept of a common aircraft for dual civil and military use because of the potential reduction in unit price afforded by a larger production run. The obvious disadvantage in the concept is that both the civil and military users must compromise their requirements to achieve a common design.

Thus far in this study, all of the aircraft have been designed strictly for civil use. The benefits obtainable with the advanced turboprop propulsion system are so substantial, however, that application to military use merits consideration. Even more importantly, the idea of a joint civil/military turboprop aircraft bears investigation.

In pursuit of this dual-role aircraft concept, the No. 3 Aircraft from this study was analyzed for applicability to the Air Force's C-X mission because of the apparent compatibility between the aircraft capabilities and the mission requirements. The C-X specifications were reviewed to determine those most pertinent to this analysis; they are summarized in Appendix O. As a result of this review, several physical modifications to the aircraft were found to be necessary so that it could comply with the performance requirements. Because of the need to maintain the payload, range and speed capability of the No. 3 aircraft, it was resized but not reoptimized as the various modifications were added.

Aircraft Modifications

The following six changes were made to the aircraft:

1) Cargo floor strength increased to handle concentrated loads, such as the M1 main battle tank

2) Aft ramp and door added for enhanced loadability and aerial delivery

3) Forward ramp added for loading and unloading at austere fields

4) Landing gear modified for soft field operations

5) Aerial refueling system added

6) Wing span shortened to permit independent operation of two aircraft on the ramp of a small austere airfield

The individual and collective effects of these changes on the ramp weight, fuel consumption, 80-EPNdB noiseprint, and costs of the aircraft are indicated in Figures 75 to 79. As expected, modifying the aircraft to enhance its capabilities enlarges its size; and, consequently, each measure of its performance is degraded, but not

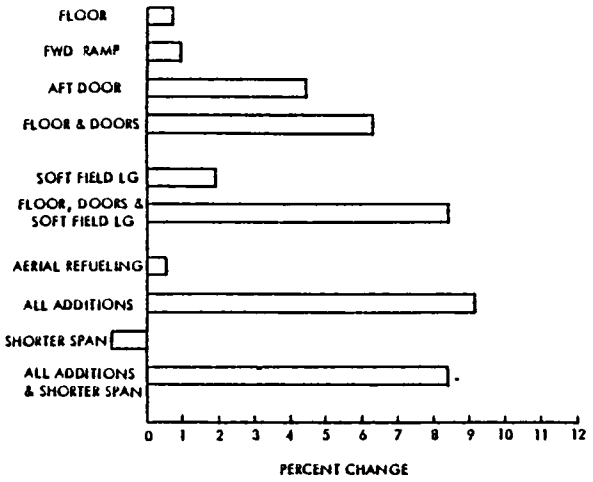

Figure 75. Effects of C-X Modifications on Ramp Weight

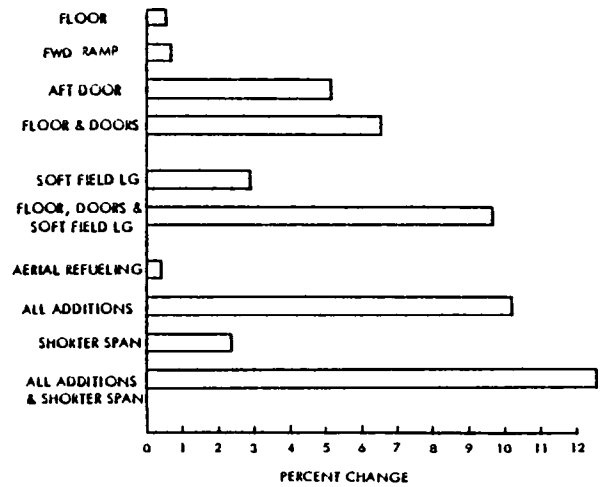

Figure 76. Effects of C-X Modifications on Fuel Consumption

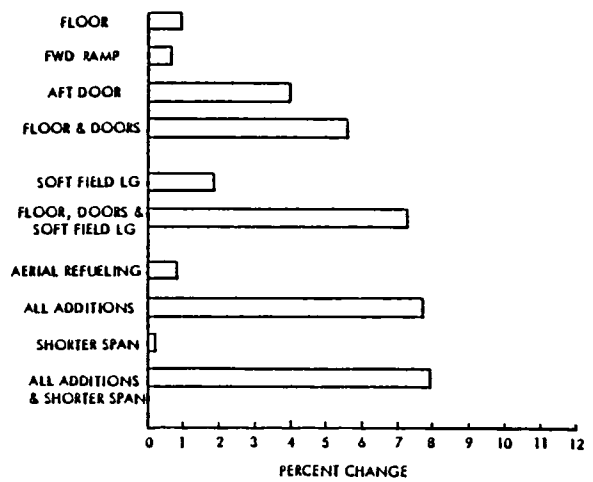

Figure 77. Effects of C-X Modifications on 80-EPNdB Noiseprint

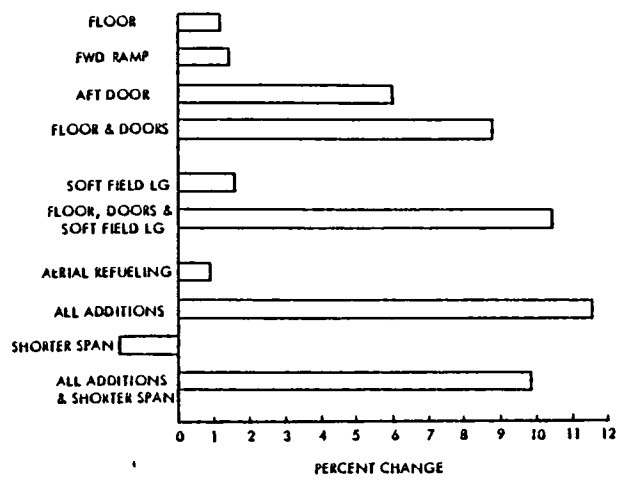

Figure 78. Effects of C-X Modifications on Acquisition Cost

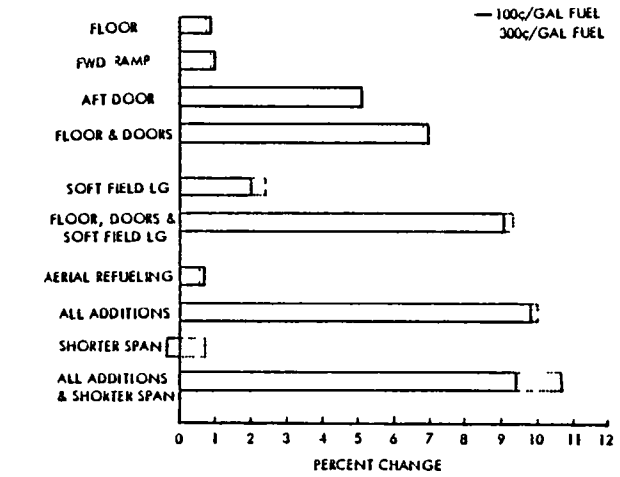

Figure 79. Effects of C-X Modifications on Direct Operating Costs

by large amounts. For example, the block fuel increases by 12.6 percent, which is the greatest penalty, while all others change by less than 10 percent. An important point to note is that these changes were, in essence, added on to a point design without any reoptimization. Had they been incorporated at the start of the optimization process, the resulting penalties would have been smaller.

Figure 80 contains a three-view drawing of the modified aircraft. Unfortunately, with just this drawing one cannot readily appreciate how the aircraft was modified to serve in a dual civil/military role. Figure 81, however, overcomes this shortcoming by comparing the "before" and "after" versions. As a further aid to understanding the growth in size, the geometric characteristics, weights, and propulsion systems of the two versions are compared in Tables XXXVII, XXXVIII, and XXXIX, respectively.

Superficial effects of some of the modifications are evident in the comparative layouts in Figure 81. For example, as a result of adding aerial delivery capability, the fuselage is longer and both the wing and main landing gear locations have changed. Likewise, evidence of soft field operational capability is suggested by the greater number of wheels and the bigger landing gear fairing. Deeper

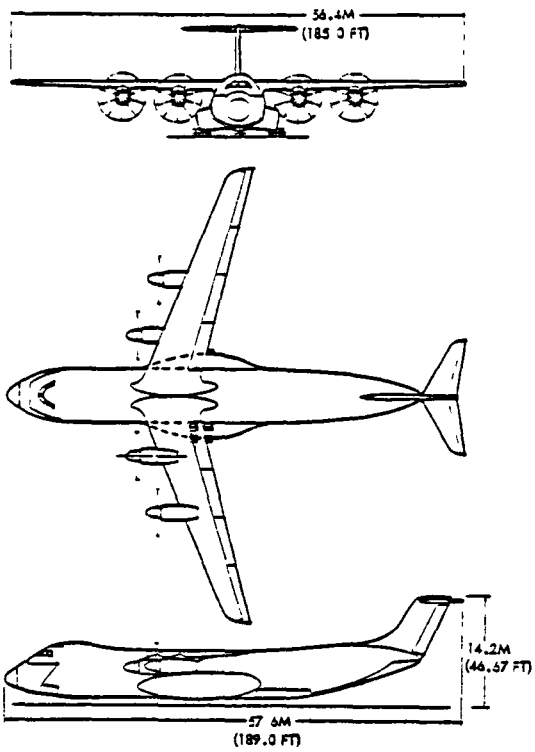

Figure 80. No. 3 Turboprop Aircraft Modified for C-X Application

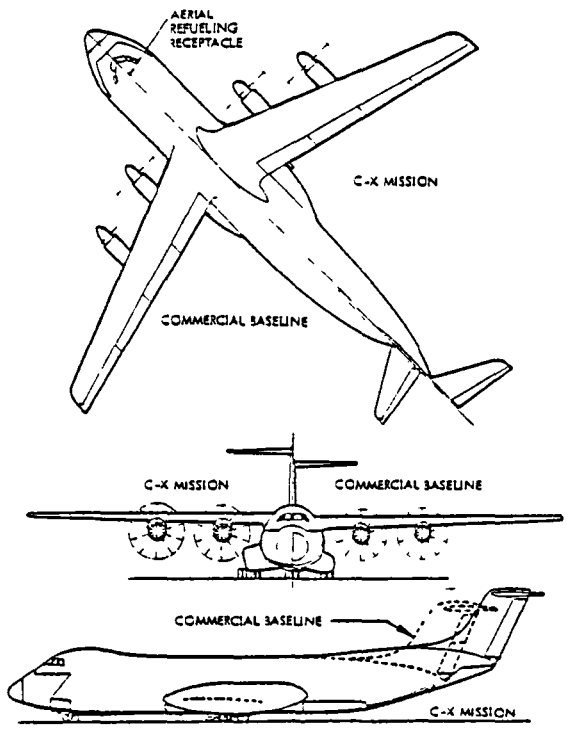

Figure 81. Effects of C-X Modifications on External Appearance of No. 3 Turboprop Aircraft

Table XXXVII. Geometry Comparison for No. 3 Turboprop Aircraft in C-X Application

MODEL	CIVIL BASELINE	CIVIL/MILITARY VERSION
WING		
ASPECT RATIO	12.0	10.8
SPAN, M (FT)	57.0 (187)	56.4 (185)
AREA, M^2 (FT^2)	270.8 (2916)	293.7 (3161)
THICKNESS RATIO	0.139	0.139
SWEEP, RAD (DEG)	0.35 (20)	0.35 (20)
FUSELAGE, M (FT)		
LENGTH	46.8 (154)	52.2 (171)
EQUIVALENT DIAMETER	6.3 (20.5)	6.3 (20.5)
HORIZONTAL TAIL		
SPAN, M (FT)	13.2 (43.3)	13.7 (44.9)
AREA, M^2 (FT^2)	38.7 (416)	41.6 (448)
VERTICAL TAIL		
SPAN, M (FT)	7.8 (25.5)	7.6 (24.9)
AREA, M^2 (FT^2)	40.2 (433)	38.5 (414)

Table XXXVIII. Weight Comparison for No. 3 Turboprop Aircraft in C-X Application, KG(LB)

MODEL	CIVIL BASELINE	CIVIL MILITARY VERSION
STRUCTURE		
WING	22,050 (48,510)	22,130 (48,686)
FUSELAGE	18,277 (40,210)	23,937 (52,661)
HORIZONTAL TAIL	1,020 (2,243)	1,100 (2,420)
VERTICAL TAIL	931 (2,049)	918 (2,019)
NOSE GEAR	1,008 (2,218)	1,242 (2,733)
MAIN GEAR	6,748 (14,845)	9,313 (18,288)
NACELLE	1,628 (3,582)	1,850 (4,070)
PROPULSION		
ENGINES	4,365 (9,603)	5,067 (11,148)
PROPELLERS	4,700 (10,341)	5,610 (12,342)
GEARBOX	3,037 (6,681)	3,753 (8,257)
FUEL SYSTEM	1,270 (2,794)	1,348 (2,965)
MISCELLANEOUS	909 (2,000)	909 (2,000)
SYSTEMS & EQUIPMENT	10,070 (22,153)	12,185 (26,808)
OPERATING WEIGHT	77,796 (171,152)	88,362 (194,395)
CARGO	61,364 (135,000)	61,364 (135,000)
ZERO FUEL WEIGHT	139,160 (306,152)	149,726 (329,395)
FUEL	26,626 (58,577)	29,990 (65,978)
RAMP WEIGHT	165,787 (364,729)	179,716 (395,373)

Table XXXIX. Propulsion System Comparison for No. 3 Turboprop Aircraft in C-X Application

MODEL	CIVIL BASELINE	CIVIL/MILITARY VERSION
PROPELLER		
BLADES	10	10
TIP SPEED, M/S (FT/S)	229 (750)	229 (750)
DISK LOAD, KW/M^2 (HP/FT^2)		
RATED	402 (50)	402 (50)
CRUISE	173 (21 5)	173 (21 5)
DIAMETER, M (FT)	5.6 (18.4)	6 0 (19 7)
ENGINE		
NUMBER	4	4
DIAMETER, M (FT)	0 8 (2.7)	0.9 (2.9)
LENGTH, M (FT)	2.1 (6.8)	2.2 (7 2)
NACELLE		
DIAMETER, M (FT)	1 6 (5.4)	1 8 (5 8)
LENGTH, M (FT)	4.3 (14 1)	4 6 (15.0)
PERFORMANCE		
RATED POWER, KW (HP)	12,539 (16,875)	14,507 (19,446)
RATED THRUST, 1000 N (LB)	122 (27 4)	141 (31 6)
CRUISE THRUST, 1000 N (LB)	21 (4.8)	24 (5 5)
THRUST/WEIGHT, N/KG (LB/LB)	2.9 (0.30)	3.1 (0 32)
CRUISE SFC, KG/HR-N (LB/HR-LB)	0 045 (0 44)	0 045 (0.44)

insights are gained, however, by examining the modifications in more detail.

Cargo Floor Strengthened - Originally, the cargo floor was designed for a uniform loading of 979 kg/m^2 (200 lb/ft^2) to accommodate containerized or palletized cargo. For the C-X mission, however, the vehicular equipment axial load of 10,000 kg (22,000 lb) sets the design criteria for the floor. As a result, the cargo floor weight increased by 702 kg (1544 lb), for almost a 4 percent rise in fuselage weight.

Aerial Delivery Capability Added and Loadability Enhanced - The baseline aircraft has no aft opening for cargo movement, and its aft fuselage is configured to minimize upsweep drag while providing sufficient ground clearance during takeoff rotation. To permit aerial delivery, an aft door and ramp were added which produced the following changes that are reflected in Figure 81:

- Fuselage lengthened by 5.3 m (17.4 ft) with a corresponding weight increase of 1404 kg (3089 lb), or 7.7 percent
- Aft-fuselage upper contour raised to permit straight-in loading and delivery. This also increased the height of the tail relative to the ground.
- Upsweep of the aft-fuselage lower contour increased to maintain the same minimal level of ground clearance during rotation. Changing the upsweep angle from 0.05 rad (3 deg) to 0.11 rad (6.5 deg), added 5.4 counts of drag.
- Aft movement of wing and main landing gear required to maintain mass balance and aid in ground clearance during takeoff rotation.

Figure 82 provides side views of the aft door open with the ramp in position for aerial and ground delivery. Also

included is a view of the end of the fuselage which shows the 3.2 m (10.5 ft) width of the opening. This width is less than that of the full cargo compartment, but it is consistent with the overall dimensions of the largest item in inventory that was specified for aerial delivery. Similarly, the total height of the aft door opening of 3.6 m (11.7 ft) is dictated by the tallest item that was specified for aerial delivery.

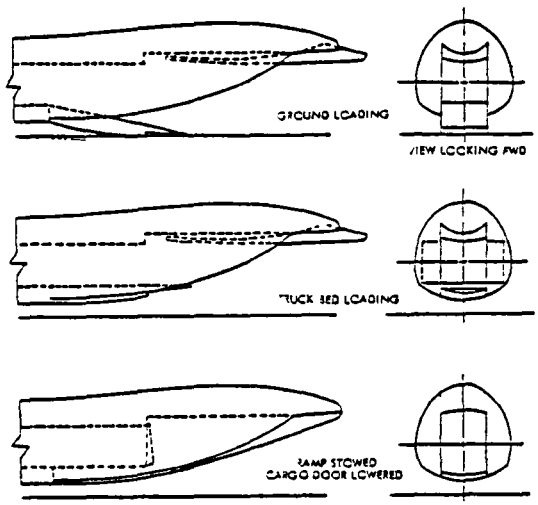

Figure 82. Aft Door and Ramp Required for C-X Application

This height of the aft opening is 0.66 m (26 in) greater than the cargo height of the baseline aircraft. To provide the additional space, the cargo compartment height was increased, as noted in Figure 83, and the wing carry-through structure was raised to avoid interference with the cargo compartment. As a result of elevating the wing, the shape of the wing-fuselage intersection has changed, as indicated on Figure 81. Raising the wing does provide a side benefit of more clearance between the ground and the propeller tips.

Forward Ramp Added - For commercial loading and unloading operations, the aircraft would taxi up to a cargo dock with an adjustable mating section,

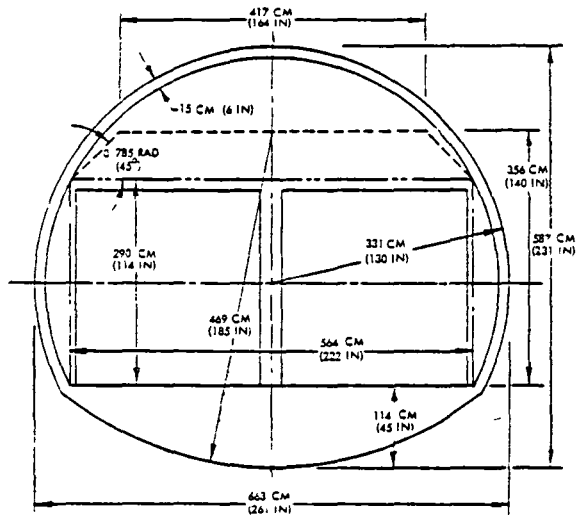

Figure 83. Cargo Compartment Cross-Section Change for C-X Application

similar to the moveable walkway used for passenger movement. Thus, for maximum efficiency no special provisions would be carried onboard the aircraft for cargo movement; rather, they would be ground based. During military operations at austere fields, however, such ground-based equipment would probably not be available, and some provisions for cargo transfer would have to be included in the aircraft.

A foldable ramp, which is stored in the fuselage, has been added to the aircraft for rapid cargo deployment once the visor door has been opened. Figure 84 shows this ramp in its three standard positions - stowed, level for cargo transfer to a commercial loading dock, and fully down for roll-on, roll-off ground delivery of vehicles and bulk cargo. This ramp, which is as wide as the cargo compartment, consists of two major sections plus a toe plate, the latter of which is deployed only for ground deliveries.

Installing this forward ramp added 842 kg (1853 lb) to the fuselage, a fuselage weight increase of 4.6 percent. It also required moving the nose gear aft 3 m (10 ft).

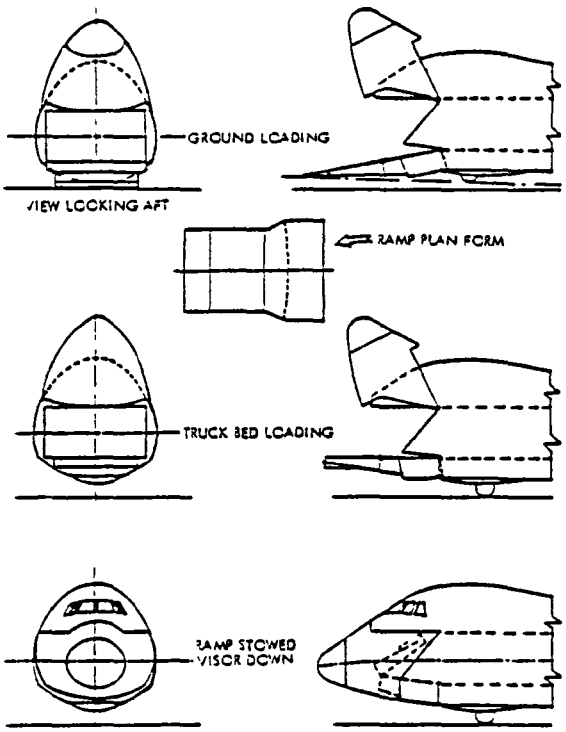

Figure 84. Forward Ramp for C-X Application

Landing Gear Modified - The baseline aircraft has four wheels on each main gear, which permits it to operate on paved commercial runways with a load classification group (LCG) III rating. For application to the C-X mission, the number of main wheels was doubled to eight to insure compliance with the specified requirements to be able to operate on LCG IV paved runways and on designated unpaved, semi-prepared, compacted surface (sand, gravel, etc.) runways. With these additional wheels, the landing gear fairing had to be enlarged considerably, as indicated in Figure 81, which added five counts of drag. The other penalty resulting from these changes was a 15.5 percent increase in main gear weight of 1045 kg (2299 lb).

Aerial Refueling System Added - The Universal Aerial Refueling Receptacle Slipway Installation (UARRSI) was installed on top of the fuselage, just behind the cockpit, as indicated by the dashed line portion of the drawing in Figure 81. Adequate space exists for running the fuel lines inside the top of the fuselage from the UARRSI to the fuel tanks in the wing. Adding this aerial refueling capability increased the fuel system weight by 457 kg (1005 lb), or 36 percent. No drag penalties were incurred because the receptacle was installed flush-mounted.

Wing Span Shortened - The C-X specifications on ground maneuvering dictate that: the aircraft must maintain at least a 7.6-m (25-ft) horizontal clearance between itself and other aircraft or ramp obstructions; when parked, will not prevent another aircraft from taxiing to or from its parking space; and once parked for loading or unloading, will not be moved until it has completed that operation. This specification imposes the severest constraint on the smallest ramp, which is the 76-m (250-ft) by 91-m (300-ft) ramp at austere airfields.

Figure 85 contains a sequence of simulated movements of the aircraft as it enters the ramp area, moves to a parking area for loading or unloading, and then returns to the runway. Of critical importance is the dashed line that traces the position of the wing tip throughout this movement. For the wing tip to keep at least 7.6 m (25 ft) from the parked aircraft, which is as far from the access taxiway as possible, the wing span cannot exceed 56.4 m (185 ft). Thus, the wing span must be shortened because on the baseline aircraft it is 57 m (187 ft), while on the modified version it has grown to 60 m (197 ft). Shortening the span offers benefits of reduced aircraft structural weight and acquisition cost, but inflicts penalties of higher induced drag and operating cost.

In addition to the requirement for a 7.6-m (25-ft) lateral clearance from all obstacles, the following criteria were specified for vertical obstacles that must be cleared. For runways, no obstacle will extend above a line starting at the runway edge and extending 12.2 m (40 ft) at an upward gradient of 5 percent, then changing to a

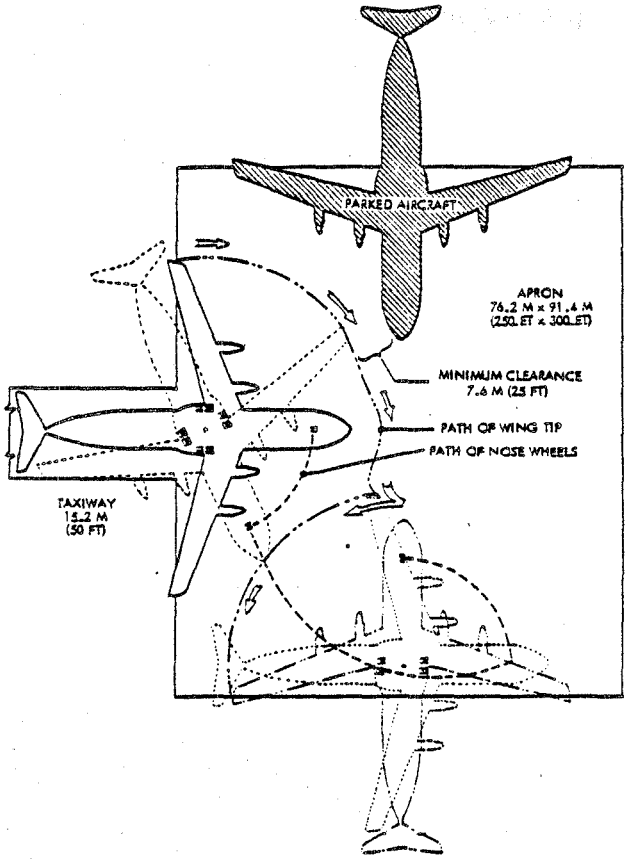

Figure 85. Ramp Maneuvers on C-X Mission and Wing Span Limit

safety zone extending indefinitely at a gradient of 14.2 percent. For taxiways, no obstacle will extend above a line starting at the taxiway edge and extending for 21.3 m (70 ft) at a gradient of 10 percent, then changing to a safety zone extending indefinitely at a gradient of 14.2 percent. No part of the aircraft shall overhang these areas with less than 1.2 m (4-ft) vertical clearance with all landing gear on the runway or taxiway.

Figure 86 graphically illustrates these obstacle height limits in relationship to our modified aircraft. The point on the aircraft that comes closest to the 1.2-m (4-ft) minimum vertical distance limit is at the outboard propeller tip. Here, the distance from the obstacle height limit to the tip is 1.7 m (5.6 ft), which is

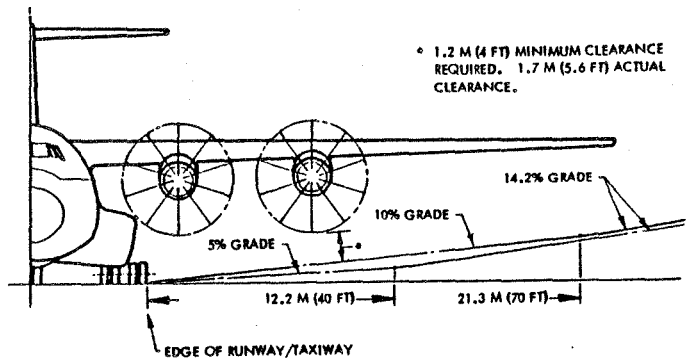

Figure 86. C-X Obstacle Height Limits Relative to Aircraft

40 percent more clearance than the minimum.

Aircraft Performance

The C-X performance specifications, as summarized in Appendix O, fall into three broad categories of mission, field, and noise. These headings will be used to report the performance capabilities of our modified aircraft.

Mission Performance - Payload-range characteristics of the aircraft are shown in Figure 87 for three structural limits. Points that represent the minimum C-X specifications for the five missions discussed in Appendix O are marked on the graph for comparative purposes. In every case, the aircraft provides more than the minimum required capabilities. For reference, the aircraft point design is at 2.5 g's and is designated by the triangle.

With a design cruise speed of 0.75 Mach number at an initial cruise altitude of 10 km (33,000 ft), the modified aircraft exceeds the C-X minimums of 0.7 Mach number at 7.9 km (26,000 ft). It is also compliant with the requirements on airdrop and low altitude speeds.

Field Performance - The aircraft's takeoff and landing performance capabilities are compared in Figure 88 with the C-X requirements. In every case, it takes off or lands in a distance below the limit.

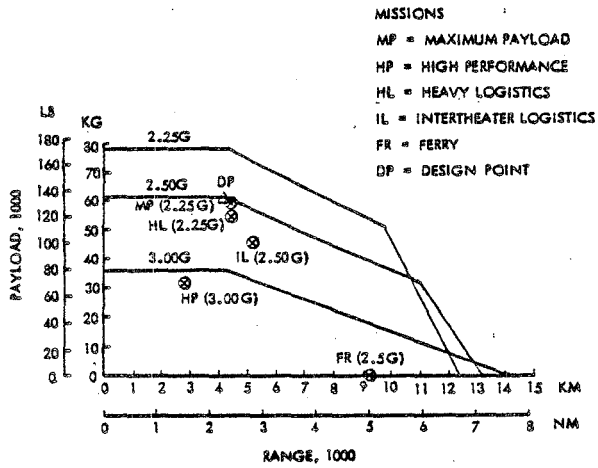

Figure 87. Mission Performance for C-X Application

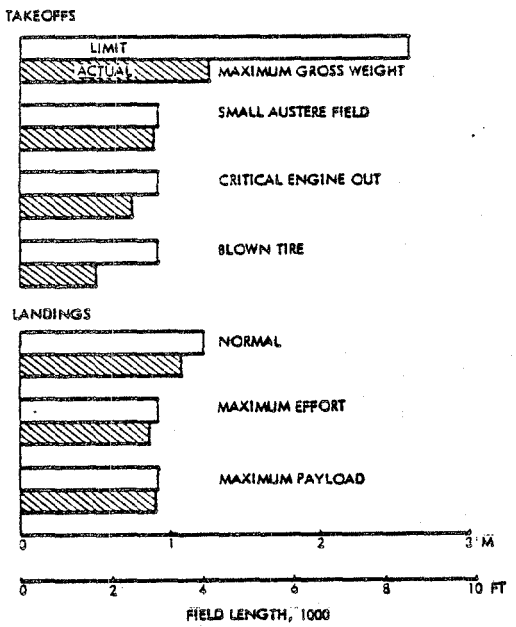

Figure 88. Field Performance for C-X Application

These distances were calculated following the prescribed military procedures. This includes the assumption of zero slope runways and no wind.

All of the takeoff distances are critical field lengths* except for the cases of critical engine-out and blown tire takeoffs. These two takeoff distances are defined as the distance to accelerate from brake release to liftoff speed with the most critical engine failed and one main landing gear tire deflated, respectively.

The normal landing distance is the horizontal distance from a 15-m (50-ft) height to a complete stop. The maximum effort and maximum payload landing distances are the distances from touchdown to a complete stop plus 150 m (500 ft). Both the normal and maximum effort landings are with the critical engine inoperative and idle reverse thrust. For the maximum payload landing, however, all engines are operative and maximum reverse thrust is permitted.

The ground maneuvering capability of the aircraft was partially covered in a prior discussion that addressed limiting the wing span to permit movement within the prescribed guidelines on the ramp of a small austere airfield. Another aspect of this type of capability is being able to make a 3.1-rad (180-deg) turn on a 27-m (90-ft) wide runway without external assistance. Figure 89 shows the sequential positions of the aircraft as it accomplishes such a maneuver.

With its 11.2-m (37-ft) wide main landing gear tread, the aircraft is able to operate from relatively narrow runways. Also, by changing the pitch angle of the propeller blades to achieve reverse thrust, the aircraft can back up the prescribed 1.5 percent grade on a paved runway without external assistance.

FAR 36 Noise - Even though the No. 3 Turboprop aircraft must grow larger if modified to perform the C-X mission, it is still able to comply with current FAR 36 stage 3 regulations on noise. This conclusion is based on the comparative results in Table XL, which show that the aircraft predicted noise for all three measuring points is several decibels below the regulatory limit.

*Critical field length is the distance required to accelerate with all engines operating, experience a failure of the most critical engine and either continue to accelerate with the critical engine inoperative to liftoff velocity or decelerate to a stop in the same distance.

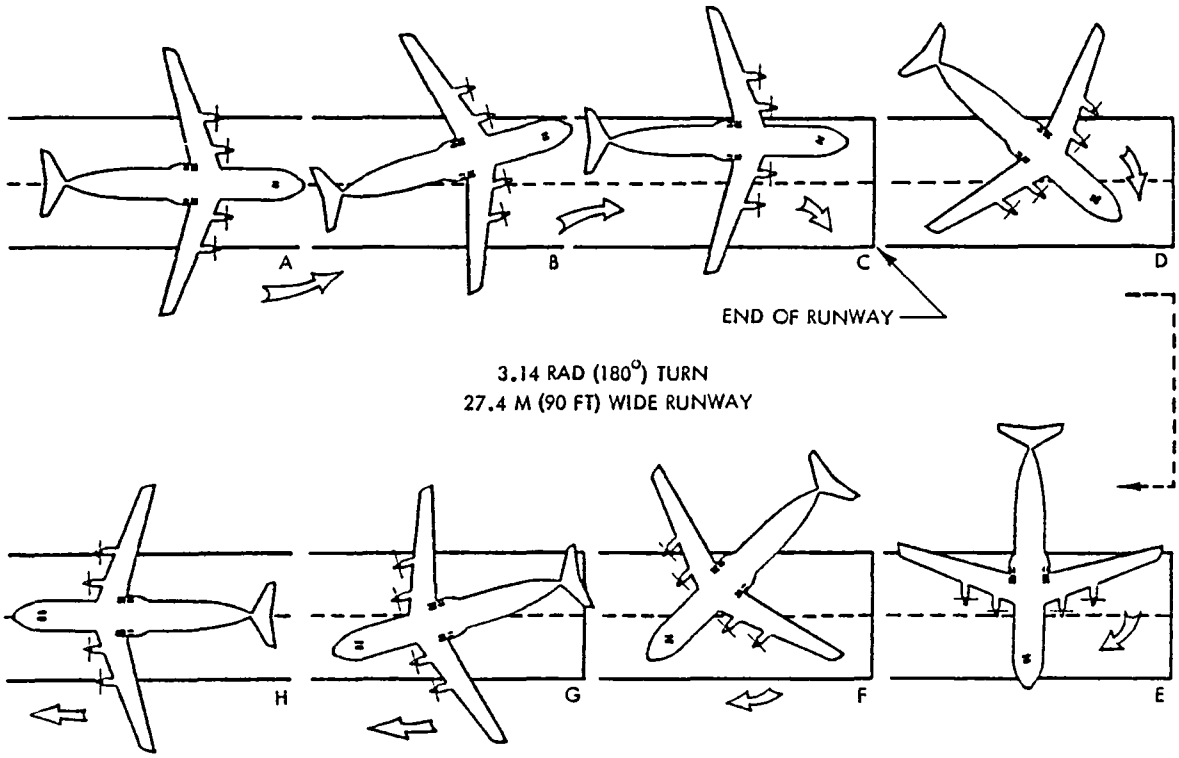

Figure 89. Turn-around Maneuver on Runway for C-X Application

Table XL. FAR 36 Noise Check for C-X Application

MEASURING CONDITION	FAR 36 LIMIT	PREDICTED NOISE
TAKEOFF FLYOVER	101 7	91 5
TAKEOFF SIDELINE	100 0	90 6
APPROACH	103.4	99 6

Aircraft Costing

The cost results, previously shown in Figures 78 and 79, are based on the original civil fleet size requirements. Had the production run been increased to include the required number of C-X aircraft, the learning curve benefits and the smaller research and development allotment per aircraft might have produced a net reduction in both the acquisition and operating costs, even with the modifications.

NEARER-TERM ENGINES

All of the results presented so far are based on the use of the Pratt & Whitney STS487 turboshaft and STF477 turbofan study engines in the propulsion system. These engines were chosen because, when the study began, they were the only two advanced engines from one family with equivalent technology. With normal planning and development, these engines could achieve an initial operational capability in 1998. Earlier availability is possible but would be accompanied by some degradation in performance, by heavier weights, and by louder noise levels.

Recently, Pratt & Whitney released data on two similar, but nearer-term, engines that could be available in the late 1980s. These two study engines - designated the STS589 turboshaft and STF592 turbofan - rely extensively on the technology base developed as part of the NASA Energy Efficient Engine Program. Using these engines for competitive turboprop and turbofan-powered

cargo aircraft permits a comparison to be made of the two types of propulsion that may be more attractive because the engines are nearer-term, require considerable less scaling, and involve substantially less risk as a result of their broader technology base.

To gain some insight into the possible effects of these nearer-term engines, they were put on the No. 1 Turboprop and Turbofan Aircraft in place of their original engines. For this change, the aircraft were resized, but not reoptimized, with all of the mission requirements, study guidelines, and geometric ratios that define the aircraft held constant. Tables XLI and XLII summarize the major effects of these changes for the turboprop and turbofan aircraft, respectively.

As noted in Table XLI, installing the STS589 engine increased the turboprop aircraft ramp weight by 6.3 percent with most of this increase coming from higher fuel consumption, which rose by 18.6 percent. Further examination of the trends in the table reveals a consistent pattern of similar increases. Overall, these results merely reflect the benefits of advanced engine technology with the more advanced STS487 engine using less fuel and, consequently, producing a lighter weight aircraft with lower operating costs.

Similar effects of a larger aircraft, higher fuel consumption, and greater operating cost are obtained by introducing a nearer-term engine on the No. 1 Turbofan Aircraft. As indicated in Table XLII, the ramp weight grows by 5.3 percent with fuel consumption and the propulsion system being the major contributors. In this case, fuel consumption is up by 14.2 percent and the propulsion system is 18.6 percent heavier.

Much of the additional fuel consumption with the STF592 engine could be eliminated by increasing its 5.3 bypass ratio toward the value of 10 which was used for the STF477 engine. Such a change, however, would require considerable effort to revise the engine performance estimates to determine how much.

Table XLI. Effect of Nearer-Term Engine on No. 1 Turboprop Aircraft

ENGINE	ORIGINAL STS 487	NEARER-TERM STS 589
PROPULSION		
RATED DISK LOADING, KW/M^2(HP/FT^2)	402 (50)	402 (50)
RATED POWER, 1000 KW (HP)	12.8 (17 1)	13.7 (18.3)
RATED THRUST, 1000 N (LB)	124 (27 9)	129 (29 1)
CRUISE THRUST, 1000 N (LB)	22 0 (4 9)	22.9 (5.1)
CRUISE SFC, KG/N-HR (LB/LB-HR)	0 045 (0 46)	0.052 (0 53)
PROP DIAMETER, M (FT)	5 6 (18 5)	5 8 (19 2)
WEIGHTS, 1000 KG (LB)		
RAMP	81.0 (178.2)	86.1 (189 4)
OPERATING	40.3 (88.6)	42 8 (94.3)
FUEL	13.5 (29 6)	16.0 (35.1)
ENGINE	2.2 (4 9)	3.2 (7 0)
PROP	2 4 (5.2)	2 6 (5 8)
GEARBOX	1.5 (3 4)	1.9 (4 1)
NACELLE	0 8 (1 8)	1 0 (2.1)
PERFORMANCE		
FIELD LENGTH, M (FT)	1,684 (5,524)	1,415 (4,640)
ENGINE-OUT GRADIENT, %	4 98	7 71
CRUISE L/D	18 97	19.21
DOC, c/TKM (c/TNM)		
FUEL AT 264 $/M^3 (1 $/GAL)	8 7 (14 7)	9 4 (15.3)
FAR 36 NOISE EPNdB		
FLYOVER	86.7	88.4
SIDELINE	85.6	87 4
APPROACH	98 5	98 6

Table XLII. Effect of Nearer-Term Engine on No. 1 Turbofan Aircraft

ENGINE	ORIGINAL STF477	NEARER-TERM STF592
PROPULSION		
BYPASS RATIO	10 0	5 3
RATED THRUST, 1000 N (LB)	118 3 (26.6)	132.1 (29.7)
CRUISE THRUST, 1000 N (LB)	24 9 (5.6)	26.7 (6 0)
CRUISE SFC, KG/N-HR (LB/LB-HR)	0 06 (0.60)	0.066 (0.66)
WEIGHTS, 1000 KG (LB)		
RAMP	35.4 (188 0)	89 9 (197 3)
OPERATING	41 2 (90 7)	43 3 (95 2)
FUEL	17 0 (37 3)	19 4 (42.6)
ENGINE	4 3 (9 5)	5.2 (11.4)
NACELLE	0 6 (1 3)	0 7 (1.5)
PYLON	0 7 (1 6)	0.8 (1 8)
THRUST REVERSER	0 7 (1 6)	0.9 (1 9)
PERFORMANCE		
FIELD LENGTH, M (FT)	2,446 (8,018)	2,440 (8,308)
ENGINE-OUT GRADIENT, %	2 4	2.4
CRUISE L/D	21 35	21.68
DOC, c/TKM (c/TNM)		
FUEL AT 264 $/M^3 (1 $/GAL)	10 0 (16 9)	10 4 (17 6)
FAR 36 NOISE, EPNdB		
FLYOVER	91 9	39 6
SIDELINE	89 1	86 9
APPROACH	100.3	99 2

The FAR 36 measuring point noise values are the exception to the previously noted trend that poorer results accrue with the nearer-term engines. Even though the absolute values of the noise for the nearer-term turboprop engines in Table XLI are higher, the real concern is with the noise values relative to the FAR 36 regulations, which change with aircraft weight. To permit a proper relative assessment, the noise predictions are compared with the regulatory limitations in Figure 90. Relative to the limits, the takeoff flyover and sideline noise of the nearer-term turboprop increase slightly, but the approach noise remains essentially constant. In contrast, the nearer-term turbofan has lower noise in both absolute and relative comparisons. This improvement is a direct result of the lower bypass ratio, which typically means better field performance. That is, the aircraft takes off in a shorter distance and gains altitude, initially, at a greater rate. In fact, with the STF592 engines the aircraft is about 91 m (300 ft) higher in altitude at the takeoff measuring points, than with the STF477 engines.

Fan and turbine noise are predominant on the turbofan-powered aircraft and can be partially suppressed through nacelle treatment. The noise predictions shown for both turbofan engines are based on using the treated nacelle depicted earlier in Figure 54 and include the level of noise suppression suggested in the figure.

Propeller noise, not engine noise, is predominant on the turboprop-powered aircraft. While noise treatment added to the nacelle would suppress the engine noise, it would not attack the major noise source. Therefore, nacelle treatment was not added to the turboprop aircraft.

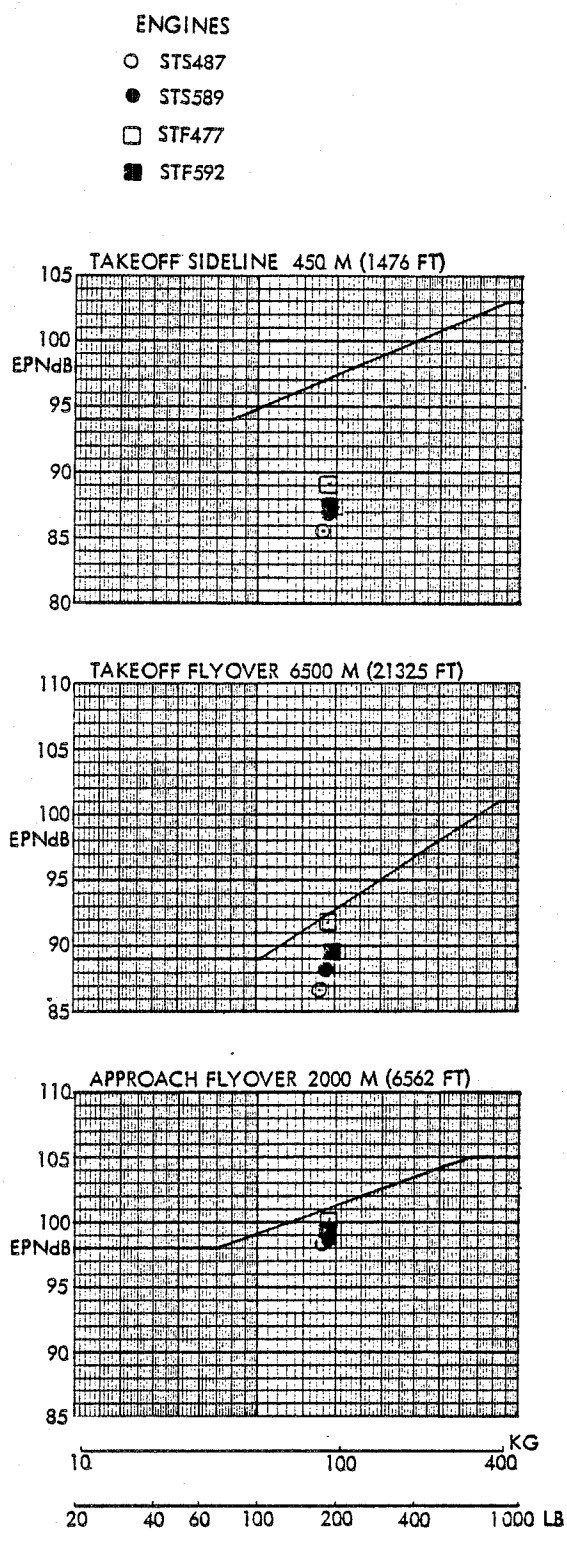

Figure 90. Comparison of FAR 36 Noise for Original and Nearer-Term Engines

CONCLUSIONS

Several conclusions have been reached based on the results of this study. Each one is presented in a highlighted single summary sentence and is followed by a brief discussion that explains and justifies the conclusion.

- o Advanced turboprop (propfan) propulsion systems offer potentially significant benefits over a turbofan propulsion system and merit further development efforts.

A comparison of competitive aircraft with the two types of propulsion shows that an advanced turboprop offers advantages relative to an advanced turbofan that may be as large as:

- o Fuel savings of 21 percent
- o Fuel efficiency 26 percent higher
- o DOCs 14 percent lower
- o Field lengths 25 percent shorter

These fuel savings for the turboprop nearly double to 40 percent in comparison with current commercial turbofan aircraft. The magnitude of these potential fuel savings provide tremendous incentive for considering further development of the turboprop in view of rising fuel prices and limited fuel availability in the future.

The lower DOCs are an attractive feature for both the airlines and the paying public. The substantially shorter field lengths are another plus for the turboprop. They permit turboprop aircraft to service small airports that are inaccessible to turbofan aircraft.

- o Operation at cruise Mach numbers below 0.8 becomes increasingly attractive as fuel price increases and becomes a greater percentage of aircraft direct operating cost.

Aircraft designs were produced for cruise Mach numbers of 0.6, 0.7, and 0.8 in the parametric study, and aircraft operating costs were estimated for fuel prices of 132 to 264 \$/m (50 to 100 ¢/gal). At the time of the selection of the first aircraft design points, the lowest fuel price was representative of then-current prices. For that price, the parametric data showed that a cruise Mach number of 0.75 gave the minimum operating cost. The data also showed that a 0.72 cruise Mach number minimizes operating cost for the highest fuel price considered, a historical price by the end of this study. With higher fuel prices, even lower cruise speeds may be best for minimizing the aircraft operating costs.

- o A propeller tip speed of about 229 m/s (750 fps) provides a compromise for minimizing cost and noiseprint.

Parametric study results showed that increasing the propeller tip speed above 229 m/s (750 fps) offered only minimal reductions in operating costs while substantially increasing the noiseprint area. Conversely, at lower speeds, only minimal decreases were obtained in the noiseprint areas and these were accompanied by disproportionately large increases in operating costs.

- o An installed sea-level disk loading of about 402 kW/m(50 hp/ft^2) for the propeller gives aircraft designs that effectively compromise conflicting design goals to minimize noiseprint area and direct operating cost.

Sea-level-installed disk loadings between 281 and 640 kW/m^2 (35 and 80 hp/ft^2) were considered in the parametric study. At the lower disk loadings, problems were encountered with excessively large diameter propellers and high operating costs. Conversely, with higher disk loadings, the aircraft noiseprints become exceedingly large.

o Changing the takeoff climb procedure reduced the noiseprint areas for turboprop aircraft by significantly greater amounts than for competitive turbofan aircraft.

By changing the takeoff climb procedure, the noiseprint areas for the No. 1 and 2 Turboprop Aircraft were reduced by 40 to 60 percent, while those for the No. 1 and 2 Turbofan Aircraft decreased by less than 20 percent. These reductions represent the maximum obtainable for each of the four aircraft based on independent analyses of varying the takeoff flap angle, flap retraction altitude, obstacle speed, power level, and type of climb - maximum gradient versus maximum rate. The reason for the differences is that turboprop aircraft typically have much better takeoff power features than turbofan aircraft. This produces shorter field lengths and greater climb capabilitties, both of which are extremely helpful in reducing noiseprint areas.

o Reducing the propeller tip speed on takeoff may or may not reduce the noiseprint area depending upon the noise level defining the noiseprint.

The propeller tip speed of the No. 1 Turboprop Aircraft was reduced from 229 m/s (750 ft/s) to 204 m/s (670 ft/s) for takeoff climb, and the flight profile and noiseprints were recalculated. The effect was that the 90-EPNdB noiseprint increased 2.4 percent, but the 80 and 70-EPNdB noiseprints decreased 17.5 and 36.7 percent, respectively. These results occur because of two counterproductive effects from the reduced propeller tip speed. Beneficially, the propulsion system noise is lower; but adversely, less thrust is available which means a longer takeoff distance and a slower rate of climb.

o Based on the only available noise and cost data, aircraft with ten-blade, high-speed propellers are least costly to operate; aircraft with ten-blade, moderate-speed propellers provide a compromise in minimizing cost and noise; and aircraft with six-blade, low-speed propellers are quietest.

Six, eight, and ten-blade propellers were considered for operation at tip speeds of 204 m/s (670 fps), 229 m/s (750 fps), and 256 m/s (840 fps). The parametric study results show that the six-blade propeller at the lowest tip speed gives the quietest aircraft, and that a ten-blade propeller at the highest tip speed produces the least expensive aircraft to operate. A ten-blade propeller at the middle speed provided the best compromise for attempting to simultaneously minimize both noise and cost.

o Eight-blade propeller is not a good candidate because of probable bias in available data.

An eight-blade propeller rarely offered any advantages. This may have occurred because the only available data on this advanced propeller are based on guidelines which naturally tend to preclude an eight-blade propeller from being a good candidate. To be more specific, the eight and ten-blade propeller data are for the same total propeller activity factor, while the six and eight-blade propellers have the same activity factor per blade. The bias is believed to be in the potential manufacturer's cost estimate (see Appendix B) which shows that propellers with eight blades cost more than those with six blades for a given diameter, but that eight and ten-blade propellers cost the same.

- Accuracy of predicted noise source levels is critical to study results.

Sensitivity study results suggest that a 3 dB increase in aircraft noise level produces 100 and 40 percent increases in the noiseprint areas for turboprop and turbofan aircraft, respectively. Thus, small changes in the noise sources mean large variations in the noiseprints. Because both propulsion systems used in this study are of the paper variety, that is they are design concepts and not hardware items, the actual noise characteristics of both systems may change considerably from the predicted values by the time these systems are built. This could drastically alter the results of this study.

- FAR 36 noise levels are probably not a valid indication of the impact of aircraft noise on the community.

Because of the artificial conditions imposed by the FAR 36 regulations, the noise levels recorded at the takeoff and sideline measuring points are lower than the levels perceived when the aircraft operate in a normal manner. Even though the FAR 36 noise levels are a poor indication of normal operating noise for an aircraft at two of the three measuring points, they are an even poorer indicator of the effect of aircraft noise on the total airport community, as is evident from the study results. The only measure that gives the total noise impact on the community is the size of the aircraft noiseprint area for several noise levels.

- High bypass ratios are preferred in turbofan engines.

Lower fuel consumption and quieter aircraft were obtained by using high bypass ratio (above 8) engines. Based on consultations with engine manufacturers, the turbofan engines were assumed to have direct-drive fans for bypass ratios up to 10 and geared fans above 10. The geared fans merit further consideration because of their quietness.

- An advanced turboprop aircraft can serve as a joint civil/military airlifter with minimal modifications and penalties.

The No. 3 Turboprop Aircraft, when modified so that it can also meet the C-X aircraft requirements, experiences a 12.6 percent penalty in block fuel and less than a 10 percent penalty in such measures as ramp weight, operating weight, acquisition cost, and operating cost. These penalties for the modifications were calculated for a resized, but not reoptimized, aircraft with the same payload, range, and speed capabilities. Smaller penalties would occur with a reoptimized aircraft. Also, the costs would be more attractive if credit had been taken for a larger production run to supply both the civil and military fleet sizes.

RECOMMENDATIONS

Considerable research and development will be required before an advanced turboprop (propfan) propulsion system can be flown on a new aircraft in the forseeable future. New propulsion systems have typically taken a minimum of five to seven years to develop and demonstrate the readiness of a new-technology level. Currently, plans are just being formulated for a program to develop a large turboshaft engine and gearbox.

One of the guidelines for this study was that the aircraft be designed consistent with 1985 technology readiness levels to permit an initial operational capability in 1990. Strict adherence to this guideline was impossible because the main item of interest, the propfan propulsion system, will require a miracle to achieve technology readiness status by 1985 because there is now less than the previously mentioned minimum of five years required for technology development and readiness demonstration. In many other related areas, too, the current level of effort, or lack of effort, will have to change drastically to meet the 1985 date.

In general, all efforts related to the development of propfan propulsion systems need to be accelerated so that the technology is available for application to the next generation of commercial aircraft, which should appear in the early 1990s. With its potential fuel savings, rapid development of the propfan propulsion system is in our national interest. Some specific tasks to be taken as part of that development are recommended, with no priority implied by the order of presentation.

- o Have engine manufacturer check performance and noise characteristics of the point design aircraft in this study.

Typically, the point design aircraft have engines that are not the baseline turboshaft or turbofan study engines supplied by the manufacturer. Instead, they represent engines that are scaled in thrust and size from the baseline engines. Even though the scaling programs use accepted thermodynamic and engine cycle theory, they are not always able to account for material and manufacturing constraints. Because of the critical impact of engine noise and fuel consumption on the results of this study, confirmation by an engine manufacturer of the engine characteristics for the point design aircraft is recommended.

- o Determine propeller/wing interference effects.

Limited wind tunnel tests are planned on this subject as part of the NASA Advanced Turboprop Program. Additional tests are needed not only for the base conditions of the planned tests but also for the propeller-related characteristics identified as best in this study, that is, lower tip speeds, disk loadings, and cruise speeds. There is also a need to correlate the wind tunnel results with the predictions of existing analytical programs such as that developed by Lockheed. Programs whose predictions have been shown to correlate well with actual results permit excellent design latitude at minimal expense compared to repeated wind tunnel tests.

- o Initiate design studies of large-size turboshaft engines and gearboxes.

Existing turboshaft engines and gearboxes are less than half the size of those needed by the selected aircraft in this study. Historically, it has taken longer to develop a new engine than a new aircraft, even when the technology for both is essentially in hand. Recognizing that the technology for about a 15,000 kW (20,000 hp) engine and its gearbox is definitely not state of the art, we recommend that design studies be initiated immediately if the propulsion system is to be available for an air-

craft that will begin initial operation in the early 1990s.

- o Establish what effect the propeller will have on the aerodynamic performance of a supercritical airfoil.

Wind tunnel tests are recommended to determine if the propeller effect on the airflow will cause the benefits of the supercritical airfoil to be lost or degraded. If this occurs, then a structural weight penalty will be incurred by having to go to a thinner airfoil to maintain the same drag level as for the supercritical airfoil. Or alternately, if the supercritical airfoil is to be retained to prevent a structural weight increase, then a drag penalty must be absorbed.

- o Analyze the effect of the propeller on the wing structure.

The large diameter and/or high disk loading of the propfan will impart torsional loads into the engine attachment structure and wing structure that are higher than those of current turboprop aircraft. Simultaneously, the propfan is likely to introduce acoustic fatigue and different flutter effects. Theoretical analysis of the engine mounting structure and the wing are recommended to determine the amount of the additional structural weight that is required to accommodate the torsional loads, to account for the acoustic fatigue, and to suppress any flutter. No attempt was made in the current study to address these subjects. Consequently, the effects of the recommended studies need to be applied to the selected aircraft to determine any performance degradation.

- o Determine desired noise levels and estimate airport noiseprint area limits.

Currently, there are no data to suggest what represents a minimum or acceptable noiseprint area for any noise level at any airport. Assuming that continuous operation from airports is desired without curtailment due to excessive noise, studies will be required to determine what constitutes acceptable noise levels and areas. There are two parts to this recommended effort. One is to determine what minimum noise level will disturb people asleep. The second part will require an analysis of existing airports to determine the size and shape of the area around each airport that will not be affected by continuous aircraft operation.

- o Investigate applicability of selected aircraft to military usage.

Dual civil and military use of an aircraft is usually beneficial because it decreases the unit cost by increasing the size of the production run. More importantly in this case, military interest in a propfan propulsion system should accelerate progress on its development. This study has shown that the No. 3 Turboprop Aircraft can also perform the C-X mission by taking advantage of the fuel savings and short field length afforded by the propfan system.

The merits of applying the selected aircraft to Navy missions of patrol, anti-submarine warfare, and carrier on-board delivery also warrant attention.

APPENDIX A. SYMBOLS AND ABBREVIATIONS

SYMBOLS

A	Area
AR	Aspect Ratio
b	Wing Span
C_D	Coefficient of Drag
$C_{D_{A/C}}$	Airframe Drag Coefficient
C_{D_p}	Scrubbing Drag Coefficient
$C_{D_{\pi}}$	Coefficient of Drag Based on Nacelle Frontal Area
$C_{D_{Swirl}}$	Swirl Drag Coefficient
C_{D_W}	Wave Drag Coefficient
$C_{D_{WP}}$	Wing Profile Drag Coefficient
CGF	Cost Factor for Geared-Fan Engine
C_L	Lift Coefficient
CP	Power Coefficient, $CP = \frac{(ESHP/1000)}{2\sigma(N/1000)^3 (D/10)^5}$
CSF	Cost Scale Factor for Engine
CT	Thrust Coefficient, $CT = \frac{0.1518 (T/1000)}{\sigma(N/1000)^2 (D/10)^4}$
D	Propeller Diameter
d	Nacelle Maximum Diameter
DENG	Engine Diameter

SYMBOLS

DL	Propeller Static Disk Loading
DNAC	Nacelle Diameter
ENGD	Engine Diameter
ENGL	Engine Length
ENGW	Engine Weight
ESHP	Equivalent Shaft Horsepower of Turboshaft Engine
e	Span Efficiency Factor
F	Propeller Tip-to-Fuselage Minimum Spacing
F/L	Field Length Limit
GR	Gear Ratio
g	Acceleration of Gravity
H	Altitude
HPYL	Pylon Height
J	Blade Advance Ratio, $J = \frac{V}{ND}$
K	Constant in Propeller Weight Equation
KI	Constant in Gearbox Weight Equation
LCLEAR	Clearance Length Between Propeller and Wing Quarter Chord Station
LENG	Engine Length
LNAC	Nacelle Length
LPYL	Pylon Length
LSP	Propeller Spinner Length
M	Mach Number
M_{EFF}	Effective Mach Number
M_0	Free-Stream Mach Number

SYMBOLS

ΔM	Mach Number Increment
N	Propeller Rotation Speed
OB	Octave Band
P_{amb}	Ambient Pressure
P_{std}	Standard Day Pressure
Q	Dynamic Pressure
Q_o	Free-Stream Dynamic Pressure
Q_1	Dynamic Pressure Behind Propeller
R_{REF}	Reference Radius for Noise Measurement
S_{IMM}	Wing Area Immersed in Prop Slipstream
S_{π}	Nacelle Frontal Area
S_{WING}	Wing Area
T	Tip Spacing Between Adjacent Propellers
T	Engine Rated Thrust
T_c	Thrust Coefficient
TS	Propeller Tip Speed
V	Aircraft Velocity
V_{APP}	Approach Velocity
V_{ref}	Reference Velocity for Drag
V_o	Free-Stream Velocity
V_1	Local Velocity
V_2	Aircraft Velocity over Takeoff Obstacle
ΔV	Safety Margin Applied to V_2

SYMBOLS

W_{ENG}	Engine Weight
W/S	Wing Loading
WT	Weight
WT_{GB}	Gearbox Weight
WT_{PROP}	Propeller Weight
γ	Flight Path Angle
δ_{amb}	Pressure Ratio, P_{amb}/P_{STD}
η_p	Propeller Efficiency
θ	Noise Emission Angle
Λ	Wing Sweep Angle
ρ	Density
σ	Density Ratio

SUBSCRIPTS

B, b	Baseline
s	Scaled

ABBREVIATIONS

AIP	Aircraft Interference Program
ALICE	Aircraft Life-Cycle Cost Evaluation Program
ANOPP	NASA Aircraft Noise Prediction Program
ATA	Air Transport Associatioon
BF	Block Fuel
BPR	Bypass Ratio
DOC	Direct Operating Cost

ABBREVIATIONS

E^3	Energy Efficient Engine
EPNdB	Equivalent Perceived Noise In Decibels
EPNL	Equivalent Perceived Noise Level
FAA	Federal Aviation Administration
FAR	Federal Aviation Regulations
FPR	Fan Pressure Ratio
FVR	Fuel Volume Ratio
ISA	International Standard Atmosphere
MOS	Measure of Sensitivity
NASA	National Aeronautics and Space Administration
PNL	Perceived Noise Level
PNLT	Perceived Noise Level, Tone-corrected
PNLTM	Perceived Noise Level, Tone-corrected Maximum
R&D	Research and Development
RH	Relative Humidity
SF	Scale Factor
SFC	Specific Fuel Consumption
SHP	Power Level
STOD	Source To Observer Distance
TF	Turbofan
TP	Turboprop

APPENDIX B. COSTING METHODOLOGY RELATIONSHIPS FOR PROPULSION SYSTEMS

Lockheed's Aircraft Life-Cycle Cost Evaluation (ALICE) Model* was used to estimate the costs of the candidate aircraft in this study. The model generates both acquisition cost and direct operating cost (DOC). For the acquisition cost, the model uses a level of detail that provides design sensitivity effects that can not be realized through the use of typical parametric cost methods which use only aircraft physical and performance data as their cost base. In the ALICE model, each structural and functional subsystem is individually costed, and then all are added to obtain the aircraft acquisition cost.

The methodology for determining the DOC uses the 1967 Air Transportation Association equations with the coefficients updated to the 1980 year level for this study. The only exception is in the area of maintenance where alternate methods, derived from experience, are used.

Typical results from the model are included on Figures B-1 and B-2. The level of detail used to determine the acquisition cost is illustrated by Figure B-1 which lists the various subsystem costs and research and development items that contribute to aircraft flyaway cost. Elements that contribute to DOC are listed on Figure B-2.

One of the objectives of this study is to compare the economics of aircraft with turboprop (TP) and turbofan (TF) propulsion systems for various noise levels. The validity of this comparison is dependent upon the relative similarity of the ground rules for the performance and costs of the main independent variable - the propulsion system. In regard to performance, both systems reflect equivalent technologies, design expertise, and goals of minimum fuel consumption. In the area of costs, the following relationships have been derived to be relatively compatible for the two systems. These equations assume that the typical initial production and operational problems have been corrected and that mature program levels have been reached.

* S. G. Thompson, "Aircraft Life-Cycle Cost Evaluation (ALICE) Model," LG77-ER0084, Lockheed-Georgia, April 1977, Revised March 1980 (Ref. 37)

ENGINE ACQUISITION COST

Engine prices are based on an assumed purchase in the commercial market, that is, the price is set by the engine manufacturer to cover both the production and development cost and does not include the use of a learning curve benefit as a function of production quantity.

Turboprop Engine Cost

The STS487 baseline TP engine is rated at 15.2 megawatts (20,424 shaft horsepower), and its 1980 cost is estimated to be 2.16 million dollars. This cost includes the gearbox. For other sizes, the cost is adjusted as a function of the scaled engine power according to the relationship:

$$CSF = 0.4\,SF + 0.6 \quad \text{if } SF \geq 1.0$$
$$= 0.533\,SF + 0.467 \quad \text{if } SF < 1.0$$

where CSF is the cost scale factor and SF is the ratio of the scaled power level to that of the base size.

Turbofan Engine Cost

The STF477 baseline TF engine is rated at 117.87 kilonewtons (26,500 pounds) of thrust, and its 1980 cost is estimated to be 2.03 million dollars. For other sizes, the cost is adjusted according to the same relationship as for the TP engine except that the ratio of scaled engine thrust to base size is used as the independent variable. A

CIVIL ACQUISITION COST SUMMARY

WING		5352708.94			
TAIL		1254534.05			
BODY		5846947.62			
NOSE LANDING GEAR		124058.84			
MAIN LANDING GEAR		599720.87			
FLIGHT CONTROLS		731894.47			
NACELLES		776766.95			
PROPULSION					
ENGINE	105426.33				
AIR INDUCTION	.00				
FUEL SYSTEM	483875.16				
PROPULSION MISC	417507.25				
ENGINE CONTROLS	.00				
FIRE EXTINGUSHING	.00				
EXH/THRUST REV.	.00				
LUBE SYSTEM	.00				
PROPELLERS	.00				
TOTAL PROPULSION		1006808.74			
INSTRUMENTS		240506.34			
HYDRAULICS		497130.82			
ELECTRICAL		674449.89			
AVIONICS (INSTL & RACKS)		73099.50			
FURNISHINGS		678465.11			
AIR CONDITIONING		426919.07			
ANTI ICING		.00			
APU		74391.39			
FINAL ASSEMBLY		.00			
PROD FLIGHT		.00			
LFC SURFACES		.00			
LFC DUCTS		.00			
SYSTEM INTEGRATION		1007898.28			
TOTAL EMPTY MFG. COST			19366299.75		
SUSTAINING ENGINEERI	2586739.62				
LFC SUCTION SYSTEM	.00				
TECHNICAL DATA	.00				
PROD. TOOLING MAINT.	2458106.94				
MISC.	.00				
ENG CHANGE ORDER	.00				
QUALITY ASSURANCE	1321813.48				
AIRFRAME WARRANTY		1286647.95			
AIRFRAME FEE		4052941.03			
AIRFRAME COST			31072548.00		
ENGINE WARRANTY		.00			
ENGINE FEE		.00			
ENGINE COST			8976616.75		
AVIONICS COST			500000.00		
REACTOR ASSEMBLY			.00		
NUCLEAR DUCTS			.00		
HEAT EXCHANGERS			.00		
RESEARCH & DEVELOPMENT			8696841.37		
TOTAL FLY AWAY COST				49246005.50	

R AND D	
DEVELOP TECH DATA	37383212.50
DESIGN ENGINEER.	830738064.00
DEVELOP TOOLING	422026452.00
DEVELOP TEST ARTICLE	129130687.00
FLIGHT TEST	30950038.00
SPECIAL SUPT EQUIP	9968856.75
DEVELOPMENT SPARES	61749994.00
ENGINE DEVELOPMENT	.00
AVIONICS DEVELOPMENT	.00
REACT DEVELOPMENT	.00
TOTAL R&D	1521947232.00
LFC R & D	.00

Figure B-1. Typical Output from ALICE Program for Aircraft Production Cost

NASA LANGLEY TURBOPROP,975-07550,04-29-80 MACOAT/SIPFC9

ROUTE	CREW	FUEL*OIL	INS	A/C LAB	A/C MAT	E LAB	E MATL	REA LAB	REA MAT	M BUR	DEPREC	TOTAL	CPINH	LC CST M$
2643.	1443.	3656.	1906.	311.	640.	292.	1178.	0.	0.	1206.	6604.	17235.72	11.20	133.65
2643.	1443.	7312.	1906.	311.	640.	292.	1178.	0.	0.	1206.	6604.	20891.77	13.58	162.01
2643.	1443.	14624.	1906.	311.	640.	292.	1178.	0.	0.	1206.	6604.	28203.88	18.33	218.71
2643.	1443.	21936.	1906.	311.	640.	292.	1178.	0.	0.	1206.	6604.	35515.98	23.08	275.41

Figure B-2. Typical Output from ALICE Program for Aircraft Direct Operating Cost Elements

bypass ratio of 10.0 is close to the limit for an engine with a direct drive for the fan. For higher bypass ratios, a geared fan arrangement is required to limit engine noise. An additional cost has been included for this gearing, and it is calculated from the equation:

$$CGF = 1.03 + 0.015\ (BPR - 10)^{1.246}$$

where CGF is the gear factor cost which is applied to the base price, and BPR is the engine bypass ratio.

ENGINE MAINTENANCE COST

Maintenance costs are typically divided into two categories of material and labor. The projected 1980 labor rate used in this study is $13 per maintenance manhour and the overhead burden factor is 2. Other specific maintenance rates and costing approaches that were derived for the baseline engines following consultations with Pratt & Whitney are:

Item	Turbofan	Turboprop
Material Cost, $/engine flt hr	40.93	43.49
Material Cost Scaling	Proportional to engine cost scaling	
Labor Rate, hr/engine flt hr	0.8	1.0
Labor Rate Scaling	$SF^{0.31}$	$SF^{0.31}$

where SF is the engine power scale factor. These material costs are in 1980 dollars. The labor rate on the turboprop includes the gearbox.

PROPFAN COST

The propfan cost data are based on those in Reference 12 and supplemented by Hamilton Standard. For parametric studies, these data can be represented in equation form as a function of number of blades and propeller diameter. Specifically, the equations for the costs in 1980 dollars are:

6 Blades -
  Cost = $123,864 + $2,382 D
8 and 10 Blades -
  Cost = $123,864 + $5,240 D

where D is the propeller diameter in feet. These are the commercial prices and, as such, include the development costs.

PROPFAN MAINTENANCE COSTS

Equations for the propfan material and labor maintenance were derived based on the data in Reference 12 and supplemented by Hamilton Standard.

Material Cost

Equations for the material costs in 1980 dollars are a function of propeller diameter, D, in feet and the number of blades:

6 Blades -
 Cost ($/flt hr) = (0.31 + 0.020 D)
8 and 10 Blades -
 Cost ($/flt hr) = (0.37 + 0.020 D)

Labor Rate

Similar equations were derived as a function of propeller diameter, D, in feet and the number of blades for the labor rates in terms of manhours per engine flight hour:

6 Blades	Labor Rate = 0.000735 D
8 Blades	Labor Rate = 0.000755 D
10 Blades	Labor Rate = 0.000785 D

APPENDIX C. PARAMETRIC NOISE PREDICTION METHODOLOGY

Lockheed's EPNL (Equivalent Perceived Noise Level) Prediction Program* is intended for detailed aircraft point designs, and as such, it requires extensive input to fully describe the aircraft. Because of the amount of input data and the actual run time of the program, it becomes impractical and too expensive to exercise the program to predict noise levels for the large number of aircraft that are usually considered in a parametric study. To alleviate these problems, Lockheed,** as part of its independent research and development studies, used the EPNL Prediction Program to develop simplified parametric methods for predicting the noise and footprint areas for turboprop and turbofan powered aircraft.

Prior experience with aircraft noise prediction has shown which parameters have the greatest influence on noise levels. Those parameters most pertinent to this study are listed in Table C-I along with ranges of values that are commensurate with the aircraft

---

* A. P. Pennock, "EPNL Prediction Program," LG78ER0211, Lockheed-Georgia, September 1978 (Ref. 28)

** N. Searle, "A Parametric Method for Predicting the Far-Field Noise and Footprint Area for Propfan-Powered Aircraft," LG79ER0163, Lockheed-Georgia, October 1979 (Ref. 29)

N. Searle, "A Parametric Method for Predicting the Far-Field Noise and Footprint Area for Turbofan-Powered Aircraft," LG80ER0023, Lockheed-Georgia, January 1980 (Ref. 30)

Table C-I. Parameters and Ranges of Values for Simplified Noise Prediction Methods

TURBOSHAFT ENGINE RATED POWER	3730 - 22,380 KW	(5000 - 30,000 HP)
TURBOFAN ENGINE RATED THRUST	26,689 - 333,615 N	(6,000 - 75,000 LB)
PERCENT POWER SETTING	40 - 100	
AIRCRAFT FORWARD SPEED	51 - 206 M/S	(100 - 400 KT)
SOURCE-TO-OBSERVER DISTANCE	305 - 9144 M	(1000 - 30,000 FT)
NUMBER OF ENGINES	2, 4	
PROPELLER FOR TURBOSHAFT ENGINES		
NUMBER OF BLADES	6, 8, 10	
TIP SPEED	204 - 256 M/S	(670-840 FPS)
NOMINAL DISK LOADING	281 - 640 KW M^2	(35 - 80 HP FT^2)
FOR TURBOFAN ENGINES		
BYPASS RATIO	5 8, 8 4, 13 0, 18 0	

sizes. Noise levels of aircraft with various combinations of these parameters were predicted with our EPNL program, and then, regression analyses were applied to the results to form algorithms that are suitable for predicting aircraft noise in a parametric study. Recognizing that the value of the resulting simplified method is dependent upon the level of sophistication of the program on which it is based, the following review of the EPNL Prediction Program is provided for the reader's benefit.

EPNL PREDICTION PROGRAM

Aircraft noise is a combination of the noise levels emitted by various propulsion system elements and by the aircraft aerodynamic features. The most significant propulsion system noise sources are the propeller or fan and the engine compressor, turbine, core (combustor), and jet turbulent mixing. These components give rise to discrete-frequency and broadband noise sources, each of which has a unique directionality and parameter dependence. Each source, therefore, requires its own prediction methodology.

The methods used in the EPNL Prediction Program for each engine source have been used in previous studies[Δ], and are very similar to those used in the NASA ANOPP (Aircraft Noise Prediction Program) code. These methods and the way the predictions are combined to predict EPNL are described briefly in the following sections.

Fan Noise

The method for predicting fan noise is based on that presented by Heidmann* and recommended for use by the NASA ANOPP office. It explicitly predicts radiated noise in terms of the broadband, discrete-tone, and multiple-pure-tone components. Based on comparisons of predictions with measured CFM56 data from General Electric and STF477 engine predictions by Pratt & Whitney, the method was modified slightly to correct over-predictions on the contribution of the multiple-pure-tone components.

Propeller or Propfan Noise

The method used to predict this noise source was developed by Hamilton Standard**. It predicts the propeller noise components, which include loading noise from steady and non-steady blade forces, thickness noise, and broadband noise. Inputs for running this method are propeller diameter, power and/or thrust, tip speed, number of blades,

---

Δ G. Swift and P. Magnur, "A Study of the Prediction of Cruise Noise and Laminar Flow Control Noise Criteria for Subsonic Air Transports," NASA CR-159104, -159105, Lockheed-Georgia, November 1979 (Ref. 31)

* M. F. Heidemann, "Interim Prediction Method for Fan and Compressor Source Noise," NASA TMX 71763, June 1975 (Ref. 32)

** "V/STOL Rotary Propulsion System Noise Prediction and Reduction," FAA-RD-76-49, Hamilton Standard Division of United Technologies, May 1976 (Ref. 33)

and forward speed. Output is in the form of one-third octave-band spectra at 0.17-rad (10-deg) increments from 0.35 to 2.79-rad (20 to 160-deg) azimuth.

Hamilton Standard also has a more advanced proprietary method for predicting far-field noise. This advanced method (frequency domain program) evaluates propeller noise sources in the form of monopole, dipole, and quadrupole (non-linear) distributions which make the influence readily discernible of such blade design features as sweep, camber, twist, and thickness. Hamilton Standard used this advanced method to produce data for developing corrections to the method currently used in the Lockheed program.

Compressor Noise

A NASA method [32] is used to predict compressor noise. The procedure is adaptable to both compressor and fan noise, and explicitly predicts radiated noise in terms of the broadband, discrete-tone, and (where applicable) combination-tone components. Results of the method have been correlated with the types of engines expected to be developed for the 1985-1990 time period.

Turbine Noise

Turbine noise predictions are included although this noise does not present a serious problem due to its relatively high frequency. The method is that developed by General Electric** under FAA contract. This method requires only limited description of the engine internal design, and it has been shown to correlate well with turbines of current engines and those envisioned for the near future.

Combustor Noise

Combustor noise is a broadband, low-frequency source which is radiated out of the exhaust duct and is usually centered around 400 Hertz. In the case of propeller-powered aircraft, this source is likely to be buried by the low-frequency propeller noise, in which the blade fundamental and harmonics usually cover the range from 100 to 500 Hertz, and by the broadband noise which is usually centered around 400 to 500 Hertz. However, this component is included because the relative levels of propeller and combustor noise were not known at the beginning of this study.

The method used for predicting combustor noise was developed by General Electric [34]. It has been shown to give results that are in good agreement with measured data for several current engines.

Exhaust Jet Turbulent Mixing Noise

The magnitude of turbulent mixing noise from the exhaust jet is dependent primarily upon the aircraft forward speed, the effluent velocity and temperature, and the jet diameter. These and other parameters are input to a NASA developed method* which is used to predict jet noise. The method is based on jet noise theory, test data, and existing prediction methods. Experimental data over a wide range of test conditions have been shown to verify the method, which is very versatile in that conical, plug coaxial, and slot nozzles can all be accommodated.

Airframe Aerodynamic Noise

The method for predicting airframe noise was developed based on a United

** R. K. Matta, G. T. Sanduski, and V. L. Doyle, "GE Core Engine Noise Investigation - Low Emission Engines," FAA-RD-77-4, General Electric, 1977 (Ref. 34)

* J. R. Stone, "Interim Prediction Method for Jet Noise," NASA TMX 71618, 1975 (Ref. 35)

Technologies Research Center study** and includes separate routines for wing, empennage, flap, and landing-gear noise. The method uses empirical equations to predict the spectra and directivity of the various aerodynamic sources. Propeller slipstream and flap interaction noise, which is suspected to have considerable influence on large propeller-powered aircraft, is addressed by applying slipstream velocity effects to the flap noise prediction routine.

EPNL Calculation

The EPNL Prediction Program combines the noise spectra for the various noise sources along the aircraft flight profile to obtain the EPNL at points on the ground below the aircraft. The procedure followed involves a number of steps.

For a specified set of aircraft parameters, each of the noise prediction routines is exercised to predict airframe, propeller or fan, and engine components (jet, core, turbine, and compressor) sound pressure levels. These levels are predicted as one-third octave band (1/3 OB) spectra over a range of angles, measured relative to the engine axis, at some reference radius. As the aircraft is flown along the input flight profile, positions are reached such that if the lines defined by each angle are extended radially they will impinge on the observer, as indicated in Figure C-1. At the instant when impingement occurs for a particular angle, the noise spectrum for that angle is projected out the appropriate source-to-observer distance (STOD) between the aircraft and the observer on the ground, taking into account spherical divergence and atmospheric absorption. This step is repeated for each angle so that a 1/3 OB time history is obtained for each noise source (airframe, propeller or fan, and engine components) as the aircraft overflies the observer. These 1/3 OBs are then added to obtain the total noise time history from all sources. Subsequently, perceived noise levels (PNLs) and tone-corrected PNLs (PNLTs) are computed as a function of time, similar to that shown in Figure C-2. Next, the EPNLs are calculated from the total aircraft PNLT-time history, consistent with the FAR 36 guidelines.

SIMPLIFIED METHODOLOGY FOR TURBOPROP AIRCRAFT NOISE PREDICTION

The EPNL Prediction Program was used to generate EPNLs for a given aircraft with a matrix of the propeller parameters: tip speed, disk loading, and number of blades. Subsequently, a least squares regression analysis of the EPNL values provided the basic algorithms for calculating EPNLs in para-

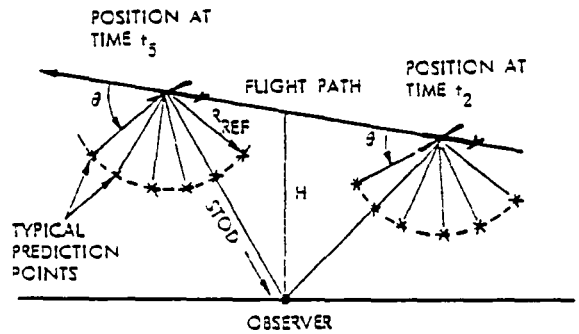

Figure C-1. Noise Spectrum Angularity Relationship to Noise Level Measurement at the Observer

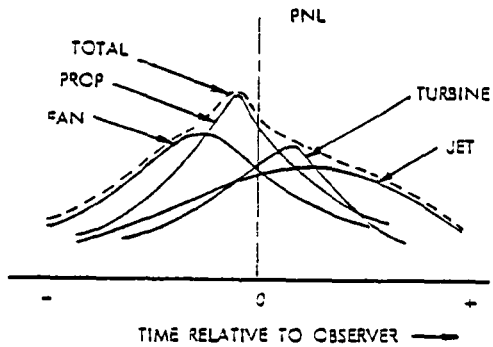

Figure C-2. Typical PNL - Time History

** M. R. Fink, "Airframe Noise Prediction," FAA-RD-77-29, United Technologies Research Center, March 1977 (Ref. 36)

metric aircraft sizing studies. These basic equations predict EPNL as a function of tip speed and sea-level-rated disk loading for 6, 8, and 10 propeller blades. Secondary equations were then developed to account for variations from the baseline conditions of 100 percent power, 9142 kW (12,255 hp), 82 m/s (160 kt) forward speed, a source-to-observer distance (or altitude) of 305 m (1000 ft), and 2 engines. Figures C-3 through C-8 illustrate the basic EPNL predictions and the adjustments required for variations from the base codes.

Figure C-4, which shows noise attenuation with distance, contains an apparent anomaly for which there is an explanation. Typically, the high-frequency noise associated with high tip speeds is attenuated more rapidly with distance than the low-frequency noise from low tip speeds. Just the opposite trend is evident in Figure C-4, which shows greater reductions for the lower tip speeds. This apparent anomaly is the result of two effects. First, the sound pressure level of the blade passing frequency is substantially lower for the lower tip speed noise sources, thereby causing the high-frequency broadband component to be a proportionately greater contributor to the overall sound pressure level spectrum. This high-frequency broadband component is attenuated more rapidly with distance than the low-frequency component with the result that the low tip speed noise source is attenuated faster than the high tip speed noise source. Second, the Noy tables, which are used in computing the PNLs from the 1/3 OB spectra, are formulated in such a way that the Noy value associated with the blade passing frequency of the low tip speed noise sources decreases quicker with distance, even though the sound pressure level itself does not decrease as fast. This causes the PNL and the EPNL to decay faster with distance because the Noy value associated with the blade passing frequency is the major contributor to PNL.

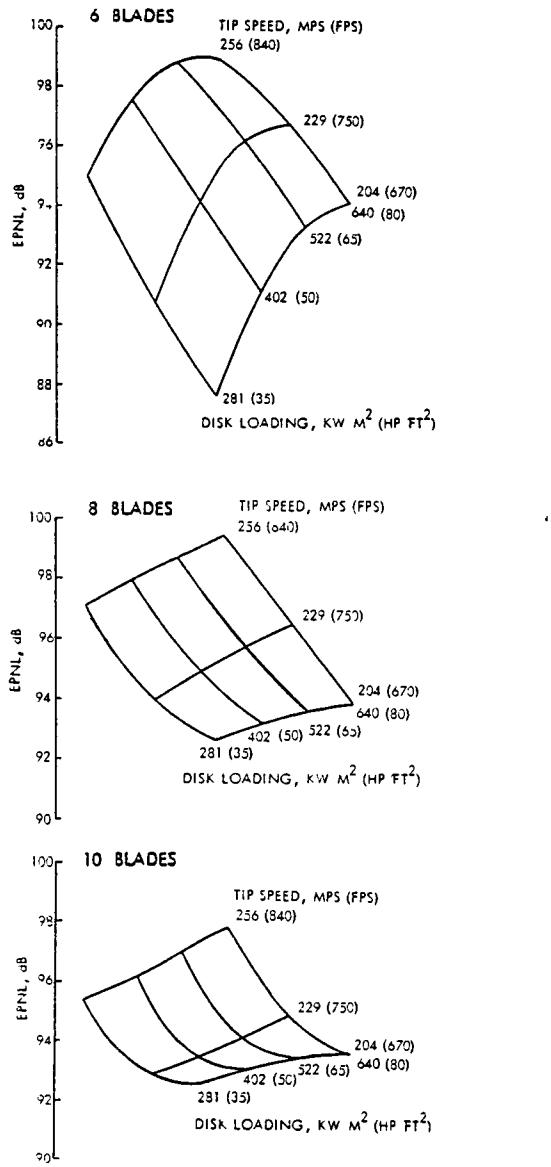

Figure C-3. Baseline EPNL Predictions for Turboprops

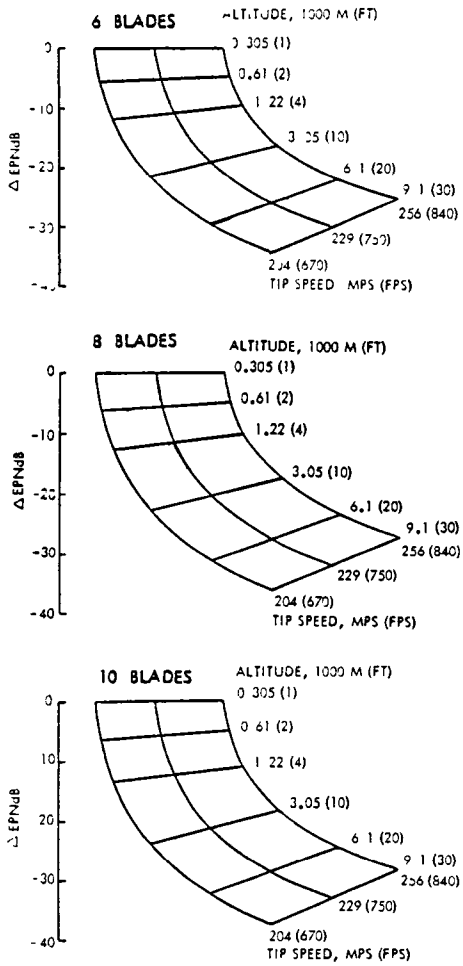

Figure C-4. Altitude Corrections for Turboprops

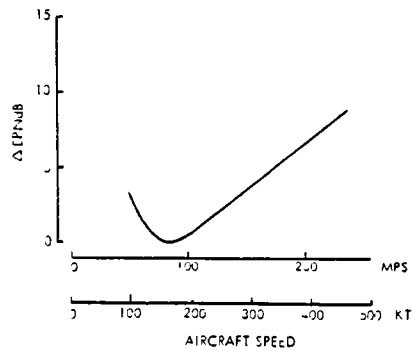

Figure C-6. Forward Speed Corrections for Turboprops

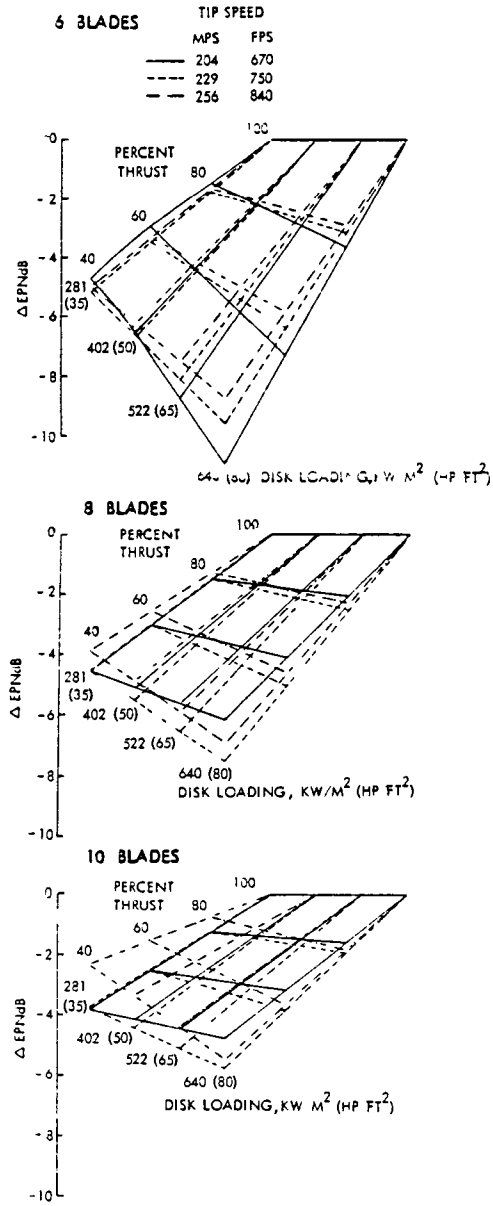

Figure C-5. Power Corrections for Turboprops

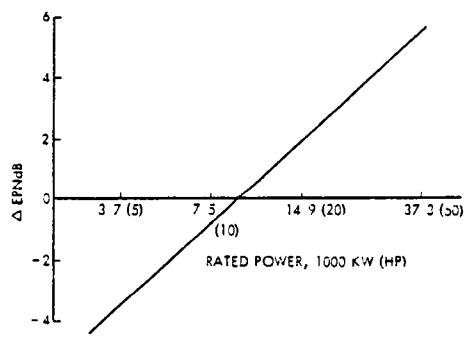

Figure C-7. Correction for Turboprop Engine Power Level Scaling

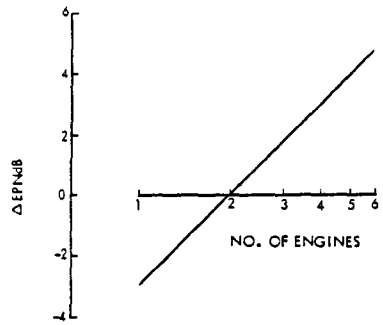

Figure C-8. Correction for Number of Turboprop Engines

The propfan noise prediction routine used by Lockheed is designed for use in cases with relative propeller tip Mach numbers below 0.9. However, the combination of a cruise Mach number of 0.8 and rotational tip speeds as high as 256 m/s (840 fps), exceeds the program limits for accurate prediction. To provide valid predictions at relative tip Mach numbers above 0.9, a correction was derived with the assistance of Hamilton Standard. This involved inputting a matrix of points to both the Lockheed and Hamilton Standard propfan prediction programs, of which the latter is unencumbered by speed limits. The two sets of predicted propfan spectra obtained from these programs were then exercised through the EPNL Prediction Program along with the other noise component predictions. Based on a comparison of the results, equations were devised for correcting the EPNL predictions at relative tip Mach numbers exceeding 0.9. This correction is presented graphically in Figure C-9.

Aircraft flight path angle has a negligible effect on the predicted EPNL and is not included in the routine. This conclusion is drawn from experience and from an examination of several cases representative of the range of study parametric variables. The results for one of these cases (a 2-container payload and a cruise Mach number of 0.6) are included in Figure C-10. As shown, variations in the flight path angle up to 0.12 rad (7 deg) produce less than a 0.1 decibel change in the predicted EPNL. Note that while flight path angle is not included in the predicted EPNL at a given point on the ground, the angle is accounted for in calculating the noise footprint area for a given noise level.

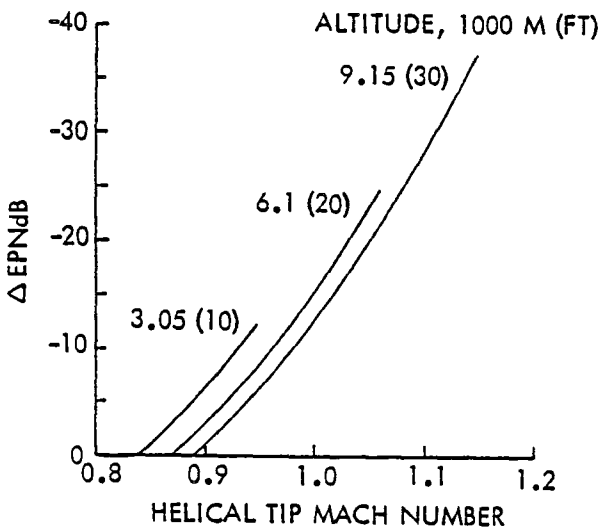

Figure C-9. Correction for Helical Tip Mach Number

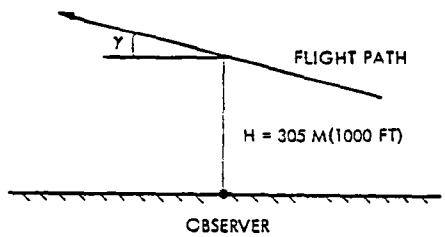

FLIGHT PATH ANGLE, γ, RAD (DEG)	0.017 (1)	0.052 (3)	0.087 (5)	0.122 (7)
	EPNL PREDICTIONS, EPNdB			
ANALYTICAL METHOD	94.77	94.78	94.80	94.84
VARIATION FROM BASELINE, Δ EPNL	0	-0.01	-0.03	-0.07

Figure C-10. Effect of Flight Path Angle on Noise

An indication of the accuracy of the simplified noise prediction method is presented in Table C-II. Noise levels predicted by the simplified method and by the EPNL Prediction Program are listed for two aircraft point designs at the ends of the parametric study spectrum. Cases 1 and 2 are for takeoff and approach of a 4-engine aircraft carrying a 6-container payload at a cruise Mach number of 0.8. Cases 3 and 4 are similar for a 2-engine aircraft carrying a 2-container payload at a cruise Mach number of 0.6. Note that there is less than a 1.0 EPNdB difference between the predictions of the two methods.

Table C-II. Comparison of Noise Prediction Methods

CASE	1	2	3	4
NUMBER OF CONTAINERS	6		2	
CRUISE MACH NUMBER	0 8		0 6	
PROPELLER				
NUMBER OF BLADES	10		6	
TIP SPEED, MPS (FPS)	256 (840)		204 (670)	
NOMINAL DISK LOAD, KW/M^2 (HP/FT^2)	640 (80)		281 (35)	
RATED ENGINE POWER, KW (HP)	9554 (12 807)		6426 (8614)	
NUMBER OF ENGINES	4		2	
OPERATIONAL MODE	TAKEOFF	APPROACH	TAKEOFF	APPROACH
PERCENT POWER	100	11 3	100	12 3
ALTITUDE OVER OBSERVER, M(FT)	462 (1515)	122 (400)	467 (1533)	122 (400)
EPNL PREDICTIONS, EPNdB				
SIMPLE METHOD	100 25	100 78	90 68	93 75
EPNL PREDICTION METHOD	100 04	101 35	91 04	92 79
Δ EPNL	0 21	-0 57	-0 36	0 96

SIMPLIFIED METHODOLOGY FOR TURBOFAN AIRCRAFT NOISE PREDICTION

A simple method for predicting the noise of turbofan-powered aircraft was developed following the same approach as that described in the preceding section for turboprop-powered aircraft. The EPNL Prediction program was used to generate EPNLs for a given aircraft with variable engine parameters of bypass ratio and percent power setting. A least squares regression analysis was applied to those EPNL values to obtain the basic algorithm for predicting the noise of turbofan-powered aircraft. Secondary equations were subsequently derived to account for variations from the baseline conditions of 82 m/s (160 kt) forward speed, a source-to-observer distance (or altitude) of 305 m (1000 ft), and 2 engines. Equations were also developed for scaling the engine from its base size. This required a separate equation for each bypass ratio because, with a common engine core, there are different thrust levels for the baseline engine at each bypass ratio. These baseline thrusts are listed in Table C-III. The basic noise prediction algorithm and those for providing corrections are presented graphically in Figures C-11 to C-15.

Table C-III. Rated Thrust of Baseline Turbofan Engines

BYPASS RATIO	BASELINE RATED THRUST NEWTONS	POUNDS
5.8	103,376	23,240
8.4	118,100	26,550
13.0	144,010	32,375
18.0	167,786	37,720

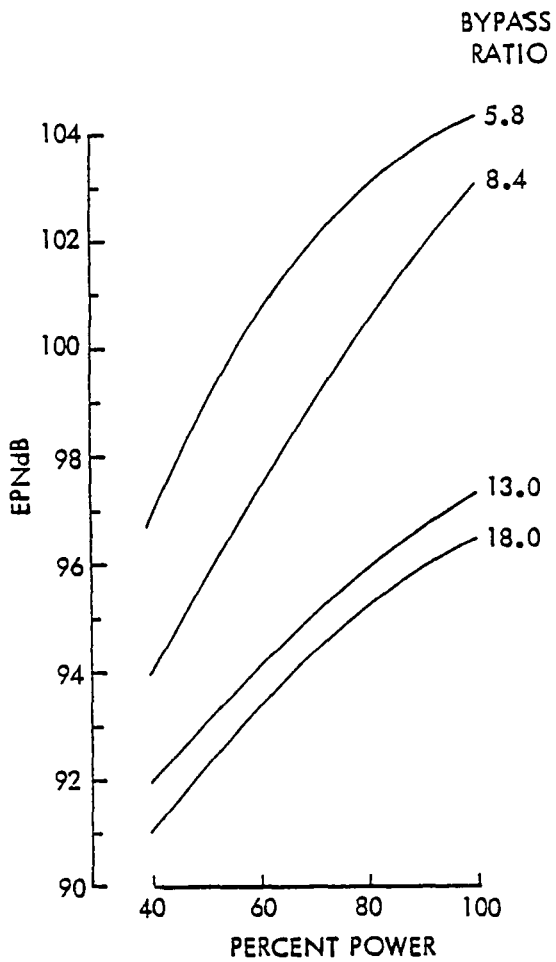

Figure C-11. Baseline EPNL Predictions for Turbofans

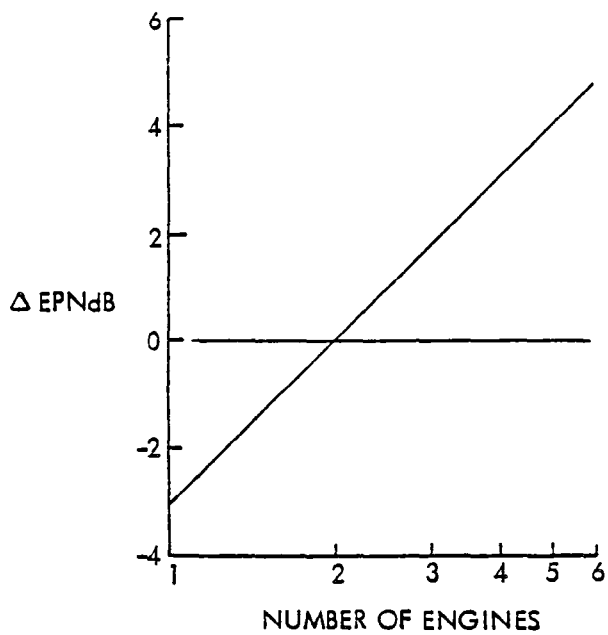

Figure C-12. Correction for Number of Turbofan Engines

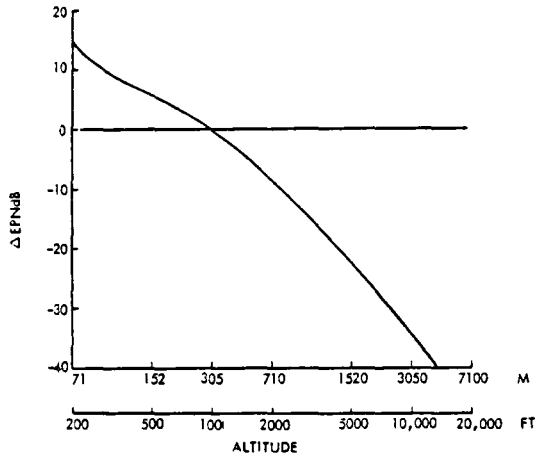

Figure C-13. Altitude Corrections for Turbofans

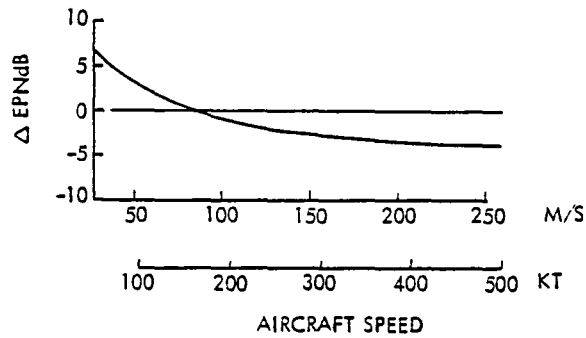

Figure C-14. Forward Speed Corrections for Turbofans

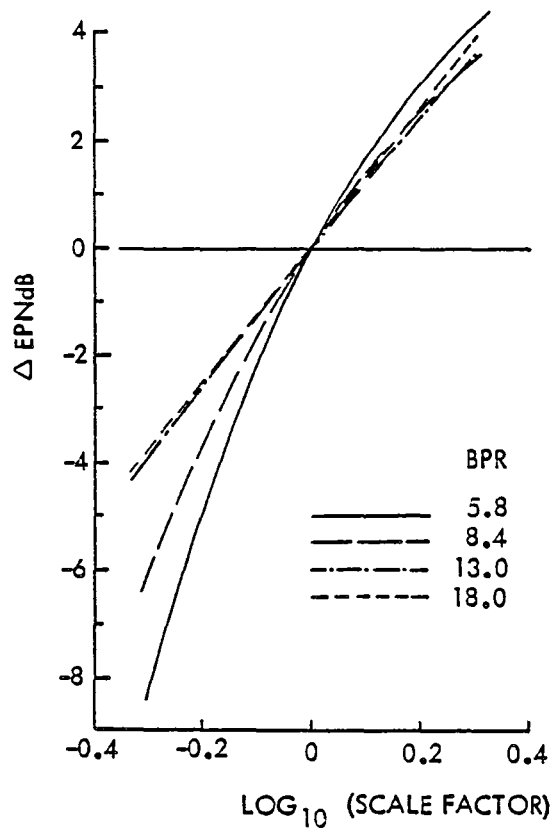

Figure C-15. Correction for Turbofan Engine Thrust Scaling

APPENDIX D. PROPFAN AERODYNAMIC INSTALLATION EFFECTS

Aerodynamic installation effects that can be directly attributed to the propfan propulsion system include the following:

- o engine nacelle/wing installation
- o induced drag
- o scrubbing drag on cruise and takeoff
- o swirl drag
- o drag divergence

There is very little test data available on propeller/propfan and wing interactions for the operating and design conditions of this study. Hence, it will be necessary to rely upon theoretically derived influences or use judgement to assess the effects of the interactions. The validity of these theoretical answers will remain in abeyance until sufficient test data are amassed to confirm the theory.

ENGINE NACELLES/WING INSTALLATION

The installation of a propfan nacelle on a wing causes an increase in drag and a loss in lift at constant angle of attack. The drag increase in the subsonic speed regime is comprised of a nacelle form drag and a drag penalty due to alteration of the span-load distribution, or induced drag. In the transonic regime, an additional drag penalty is incurred due to an increase in the wave or shock drag associated with recovering the lift loss. Form drag penalties due to aerodynamically-shaped nacelles can be reliably estimated using classical methods; however, the effects of the lift loss and an attendent change in the spanload distribution which affects the induced drag are more difficult to assess. Consequently, a combination of experimental and theoretical data are used. For example, Figure D-1 is a summary of the nacelle lift and drag increments from two separate experimental tests on a C-130 aircraft. Data are shown under two speed conditions. Note that the nominal drag penalty is 20 counts for the four C-130 nacelles, which results in a drag coefficient, based on frontal area, of 0.067 for a frontal area of 1.2 m^2 (12.98 ft^2) per nacelle full-scale. The nominal lift loss is 0.08 for four nacelles or 0.02 per nacelle.

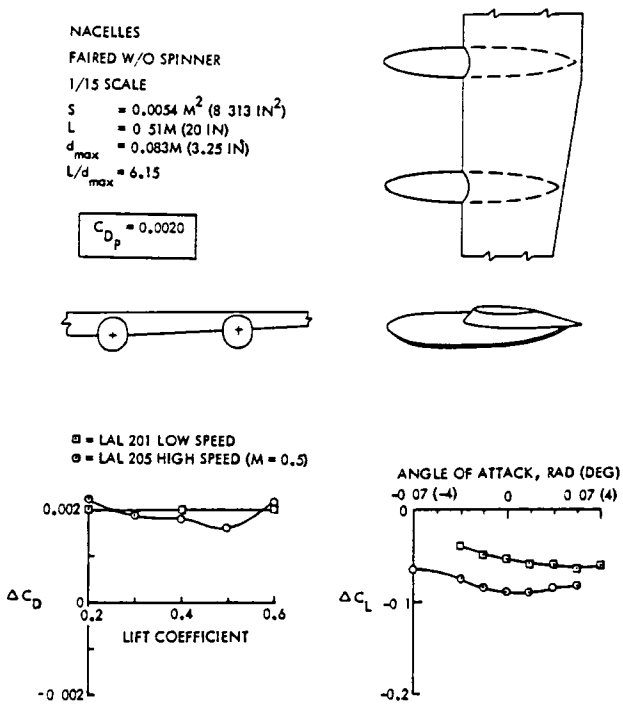

Figure D-1. C-130 Nacelle Drag and Lift Effects

In this study, the nacelle installation drag is estimated using a drag coefficient of 0.067, based on the nacelle frontal area. The effect of the nacelle installation on a swept-wing configuration for the higher cruise speeds is not defined with experimental data, but it is assumed that the same installation drag can be achieved as for the straight-wing C-130. The engine performance package (thrust and fuel flow) includes the nacelle drag; consequently, it is not included in the airplane drag buildup.

INDUCED DRAG

The presence of the engine nacelles on the wing affects the spanload distribution, causing an increase in induced drag. Based upon data from Lockheed's C-130 Aircraft Interference Program (AIP), the addition of the nacelles causes an increase in induced drag of three percent. The effect of the nacelles on the lift and spanload distribution is shown in Figure D-2. Both experimental and theoretical data are included.

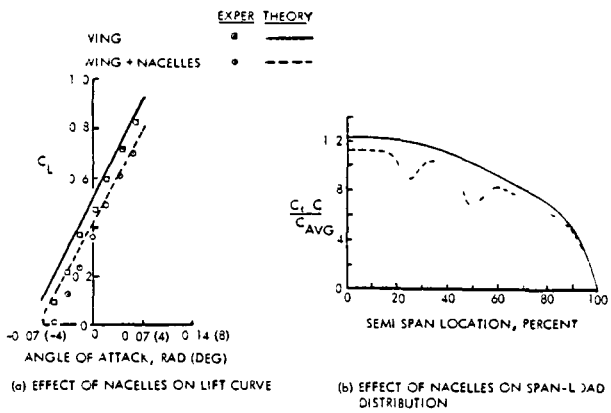

(a) EFFECT OF NACELLES ON LIFT CURVE

(b) EFFECT OF NACELLES ON SPAN-LOAD DISTRIBUTION

Figure D-2. Effect of Nacelles on C-130 Wing

For the design condition of this study, the span efficiency factor is decreased three percent for the propfan aircraft relative to the turbofan aircraft. The resulting span efficiency factor, e, for the propfan aircraft is then 0.92. This value is derived based on the 0.95 efficiency factor for the turbofan-powered C-5 and C-141 aircraft.

SCRUBBING DRAG

The scrubbing drag on the wing, caused by the increased velocity through the propfan, is calculated using classical momentum methods and is assumed to affect only that part of the wing immersed in the slipstream. Scrubbing drag penalties are included for both takeoff and cruise conditions with the latter being nominally two to three drag counts. Derivations of the equations applicable for these two conditions follow.

Cruise

The drag due to scrubbing during cruise (C_{DP}) is computed in the following manner:

$$C_{DP} = C_{D_{WP}} 2 S_{IMM} Q/(Q_o S_{WING})$$

where

$C_{D_{WP}}$ = Wing profile drag

S_{IMM} = Wing planform area immersed in prop slipstream

Q_o = Free-stream dynamic pressure

Q_1 = Dynamic pressure behind prop at wing quarter chord

$Q = Q_1 - Q_o$

To find Q_1,

T_c = Thrust/(2 Q_o D^2)

$a = 0.5 \left[(1 + 8 T_c/\pi)^{1/2} - 1\right]$

$b = a \left[1 + X/(D^2/4 + X^2)^{1/2}\right]$

X = Distance from prop plane to wing quarter chord

$V_1 = V_o (1 + b)$

$Q_1 = V_1^2/295$

D = prop diameter

Takeoff

The drag due to scrubbing during takeoff and initial climb is calculated in the following manner. Using the methodology of Smelt and Davies*, a drag equation may be developed of the form:

$$D_s = \text{Drag } (V^2_1 - V^2_0)/V_{ref}{}^2$$

where

D_s = Additional drag due to prop slipstream

Drag = Profile drag on wing area affected by prop slipstream at $T_c = 0$ and V_{ref}

V_0 = Free-stream velocity

V_1 = Local velocity at wing quarter chord

V_{ref} = Reference velocity at which Drag is computed

This can be rewritten as

$$D_s = 4 \text{ Drag } V^2_0 \; a \; (1 + a)/V_{ref}{}^2$$

where

$V^2_1 = V^2_o \; (1 + 2a)^2$ from momentum theory.

Also, from momentum theory:

$$\text{Thrust} = T = 2 \; A \; V^2_0 \; a \; (1 + a)$$

where

$A = D^2/4$

ρ = density

Assuming that the central third of the prop is ineffective for slipstream drag effects, then

$$A_{eff} = \pi/4 \; [D^2 - (D/3)^2] = 2\pi D^2/9$$

Thus,

$$a \; (1 + a) = T/(4 \pi \rho V^2_0 \; D^2/9)$$

Substituting this expression into the equation for drag gives,

$$D_s = \text{Drag } T/(V_{ref}{}^2 \pi \; \rho \; D^2/9)$$

For wing-mounted engines,

$$\text{Drag} = C_D{}^* \; Q \; S_{wing}$$

where

$C_D{}^*$ = Drag coefficient of immersed components

or $C_D{}^* = C_D \; S_{IMM}/S_{wing}$

Thus,

$$D_s = 4.0856 \; T \; C_D \; S_{IMM}/(\sigma D^2)$$

where σ is the density ratio.

This method produces thrust losses of approximately 10 to 12 percent for the propfan configurations, the primary driving function being the profile drag. Previous Boeing studies[7] assume losses as high as 13 percent for takeoff, while C-130 performance studies assume losses of approximately eight percent.

SWIRL DRAG

The only recent quantitative data on swirl effects on supercritical wings in the transonic speed regime are in the NASA-Douglas Wind Tunnel Test Report[13]. The drag increments extracted from this test are strongly a function of both the magnitude and direction of the swirl. From the Hamilton Standard

---

* Smelt and Davies, "Estimation of Increase in Lift Due to Slipstream," RAE R&M No. 1788, British A.R.C., 3 February 1937 (Ref. 38)

propfan data[12], the swirl angle is approximately 0.12 rad (7 deg) at the cruise disk loading and Mach number for best performance, compared to a swirl angle of 0.017 - 0.052 rad (1-3 deg) for the C-130. Even though the data in Reference 13 is highly inconsistent, the drag identified with the 0.12 rad (7 deg) swirl angle is used until the transonic modeling of swirl effects can be completed. At this angle, the test data of Reference 13 show a drag increment of 5 counts for positive swirl angles (up inboard rotation) and 9.5 counts for negative angles (up outboard rotation). Therefore, a 2-engine configuration will have values of 10 counts and 19 counts for positive and negative swirl angles. Because counter-rotating propellers require separate gearboxes and adversely affect acquisition costs and spares, only one rotational direction is used in the study. The resulting drag penalty for a 2-engine configuration, then, is 14.5 counts. Normalizing the value for use in the parametric sizing program and assuming that swirl drag is a function of propeller diameter and wing span (b), the following equation applies for a 2-engine configuration:

$$C_{D_{Swirl}} = \frac{0.00145 \times (D/b)}{(D/b)_{Ref}}$$

With $(D/b)_{Ref} = 0.1167$ for the Reference 13 model, the swirl drag equation reduces to

$$C_{D_{Swirl}} = 0.01243\ (D/b)$$

DRAG DIVERGENCE

The increase in local effective free-stream Mach number caused by the introduction of a velocity increment through the propeller produces a slight decrease in drag divergence. At the present time, no suitable experimental data base exists for the quantification of the drag divergence penalty. As a result, a theoretical/empirical approach is required to define the effect. Subsonically, this effect results in an increase in drag determined primarily through a scrubbing drag penalty; however, transonically, the shock strength and location can be expected to change. An approach for assessing the drag divergence penalty is:

(1) Determine the incremental Mach number through the propeller. The effective Mach number that the portion of the wing immersed in the slipstream feels is: $M_{EFF} = M_0 + \Delta M$.

(2) Having determined the effective Mach number, compute the incremental wave drag, using 2-dimensional transonic codes, between M_0 and $(M_0 + \Delta M)$. Call this C_{D_W}.

(3) Area weight the wave drag increment to the complete wing at the design Mach number.

$$\Delta C_D = C_{DW}\ S_{IMM}/S_{WING}$$

(4) In the event that the actual drag divergence Mach number increment is required, several Mach numbers can be considered using Steps 1 - 3 to define C_D vs Mach number, with and without the propeller.

The NASA-Douglas test data[13] effectively include a drag divergence penalty at the design Mach number. Therefore, no separate item is included.

SUMMARY OF EFFECTS ON TYPICAL AIRCRAFT

The magnitude of propeller installation effects are illustrated for the No. 1 Compromise aircraft, as an example.

Design Condition:

Mach Number	=	0.75
Range	=	4250 km (2295 n. mi.)
Payload	=	13,600 kg (60,000 lb)
Altitude	=	10.1 km (33,000 ft)
Engines	=	2

Aircraft:

Wing area	=	131.8 m^2 (1419 ft^2)
Wing span	=	39.6 m (130 ft)
Prop diameter	=	5.6 m (18.5 ft)
Takeoff disk loading	=	402 kW/m^2 (50 hp/ft^2)

Drag Coefficient Summary:

Aircraft without propulsion	=	0.02796
Scrubbing	=	0.00018
Induced	=	0.00030
Swirl	=	0.00176
(Nacelle	=	0.00216 Recorded as thrust reduction)
Total for Propulsion:		0.00224
Aircraft Total:		0.0302

Installation Effects:

$$\text{Without nacelle} = \frac{0.00224}{0.0302} \times 100 = 7.4\%$$

$$\text{With nacelle} = \frac{0.00224 + 0.00216}{0.0302 + 0.00216}$$

$$= 13.6\%$$

APPENDIX E. TURBOPROP PROPULSION SYSTEM DATA AND ANALYSIS

Performance data for the turboprop propulsion system were developed based on the Hamilton Standard propfan[12] and the Pratt & Whitney STS487 turboshaft engine[23]. To cover the wide range of performance design variables of this study, Hamilton Standard produced additional propfan data that are included in the propulsion system performance. Both Pratt & Whitney and Hamilton Standard are commended for their assistance in providing data and guidance during the development of the data base for the turboprop propulsion system.

PROPFAN DATA BASE

The use of 6, 8, and 10-blade propfans is investigated in the parametric sizing study for a variety of tip speeds, blade diameters, and engine power levels. These propfans have advanced thin airfoils with a design lift coefficient of 0.21. The 6 and 8-blade versions have an activity factor per blade of 230, while the 10-blade model has the same total activity as the 8-blade propeller; thus, the 10-blade model has an activity factor per blade of 184.

Performance data for these propfans are tabulated in Reference 12 in terms of power coefficient (CP) and thrust coefficient (CT) for series of values of advance ratio (J) and Mach number. These data have been combined graphically by Stone[26] with additional values that were calculated by Hamilton Standard for this study. The resulting performance characteristics for a 10-blade propfan are shown in Figures E-1 to E-7 as a typical set from the data base. Note on Figures E-1 and E-2 that the thrust coefficient reaches a maximum and then decreases with further increases in power coefficient for several low values of the advance ratio. This decrease in thrust coefficient is due to propeller blade stall. As power is increased, the

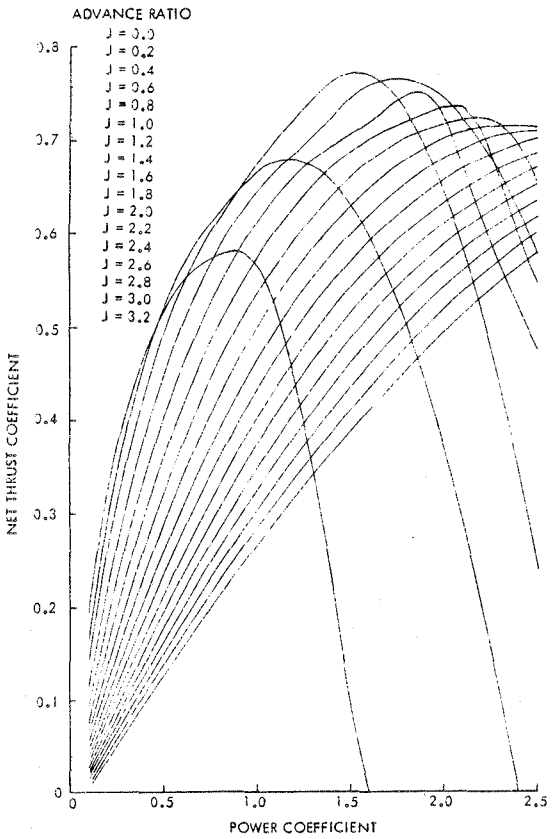

Figure E-1. Propfan Performance - 10 Blades, Mach = 0.30

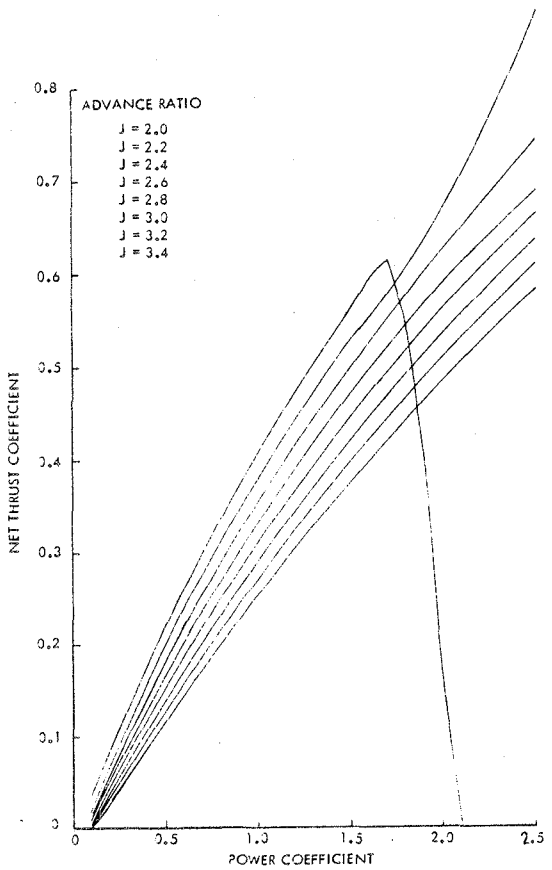

Figure E-2. Propfan Performance - 10 Blades, Mach = 0.55

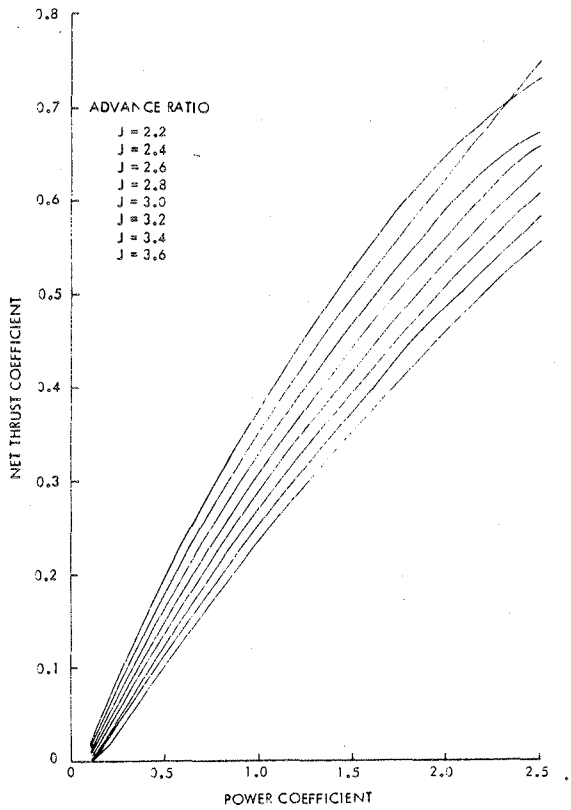

Figure E-3. Propfan Performance - 10 Blades, Mach = 0.60

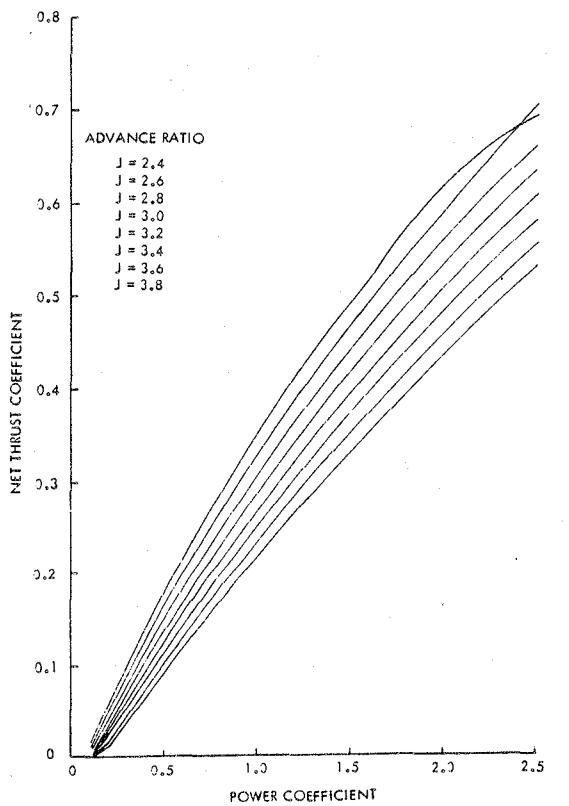

Figure E-4. Propfan Performance - 10 Blades, Mach = 0.65

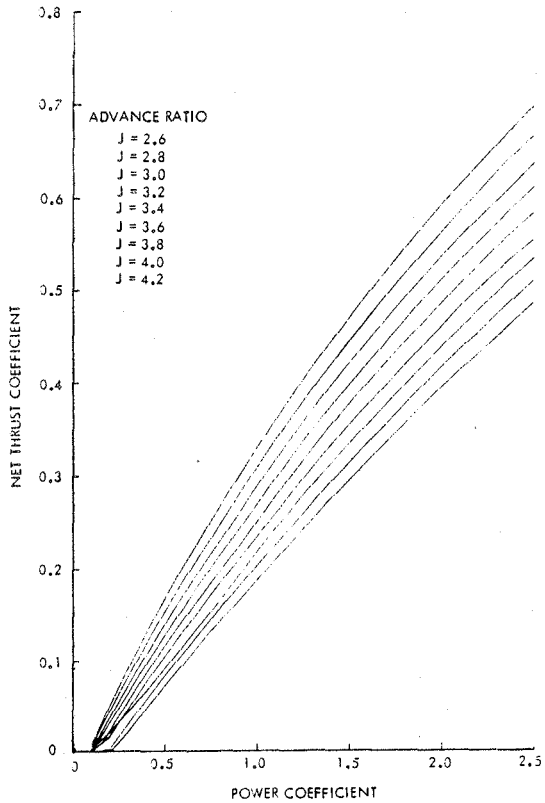

Figure E-5. Propfan Performance - 10 Blades, Mach = 0.70

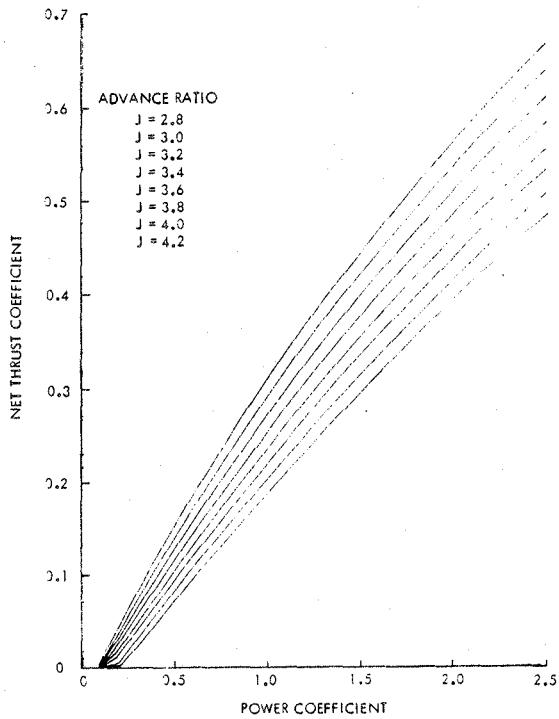

Figure E-7. Propfan Performance - 10 Blades, Mach = 0.80

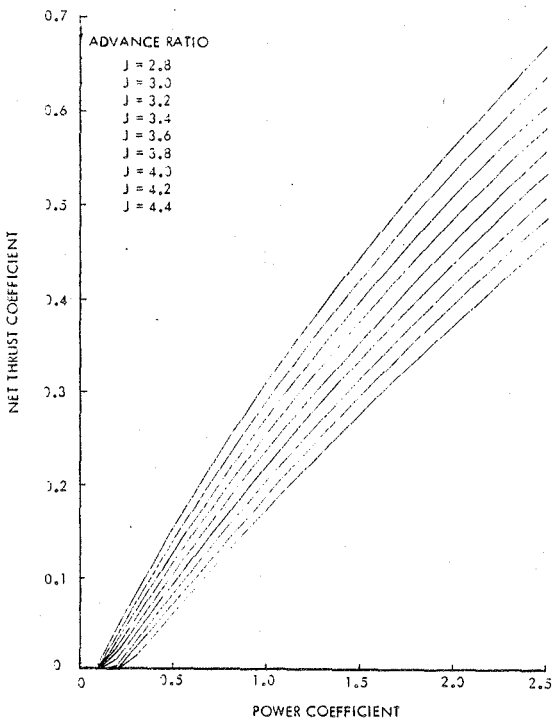

Figure E-6. Propfan Performance - 10 Blades, Mach = 0.75

speed control increases blade pitch to maintain a constant tip speed. For continued power increases, blade pitch is increased past its stall angle, resulting in decreasing thrust coefficients. The thrust coefficients would normally go negative for the range of power coefficients shown, except that they were arbitrarily restricted to remain non-negative.

The propeller weight information, which is presented graphically in Reference 12, includes the weight of the blades, the pitch change mechanism, and the spinner. To use this information in the computer program, equation (E1) was derived to fit the predicted propeller weight curves.

$$WT_{PROP} = K\,(D/D_B)^{2.5}\,(DL/DL_B)^{0.3}\,(TS/TS_B)^{0.3} \qquad \text{(E1)}$$

where:
D is the propeller diameter, m(ft),

D_B is a baseline propeller diameter of 4.57 m (15 ft),

DL is the propeller static disk loading, power/area,

DL_B is a baseline disk loading of 401.5 kW/m^2 (50 hp/ft^2),

TS is the propeller tip speed, m/s (ft/s),

TS_B is a baseline tip speed of 244 m/s (800 ft/s),

K is a constant with values of:

K = 720.88 kg (1589.27 lb) for 10 blades

K = 833.37 kg (1837.28 lb) for 8 blades

K = 692.76 kg (1527.28 lb) for 6 blades

Reference 12 also contains estimated gearbox weights, which may be calculated from equation (E2).

$$WT_{GB} = K1(D/D_B)^3 (DL/DL_B) (GR/GR_B)^{0.5} (TS_B/TS) \quad \text{(E2)}$$

where the symbols defined in equation (E1) apply and GR is the gear ratio, GR_B is a base ratio of 8, and K1 is a constant, 386.83 kg (852.82 lb)

BASELINE ENGINE

The baseline turboprop powerplant is the Pratt & Whitney STS487 turboshaft study engine, which was derived under NASA's program on advanced engines for low energy consumption. Reference 23 presents performance and installation characteristics for this engine with a caution that they should be regarded as maximum target levels because the engine incorporates very aggressive, energy-efficient, advanced-technology concepts with 1990+ operational capabilities. Some of the engine features are: an overall pressure ratio of 40:1, a maximum combustor exit temperature of 1811°K (2800°F), an uninstalled sea-level rating of 15.2 MW (20,424 hp) up to 302°K (84°F), and a mass of 970 kg (2134 lb).

INSTALLATION CONSIDERATIONS

A propeller operating alone in a uniform flow field creates a force which may be referred to as an "apparent thrust." When a nacelle (or other body) is placed behind the propeller, the pressure field generated by this body diffuses the incoming streamtube to produce a buoyancy effect which delays the drag rise of the propeller by retarding root choking. The resulting thrust is defined by Hamilton Standard as propeller net thrust, and it is dependent upon the propeller-to-nacelle diameter ratio which is a function of propeller disk loading. Values given in Reference 12 for this ratio are illustrated in Figure E-8.

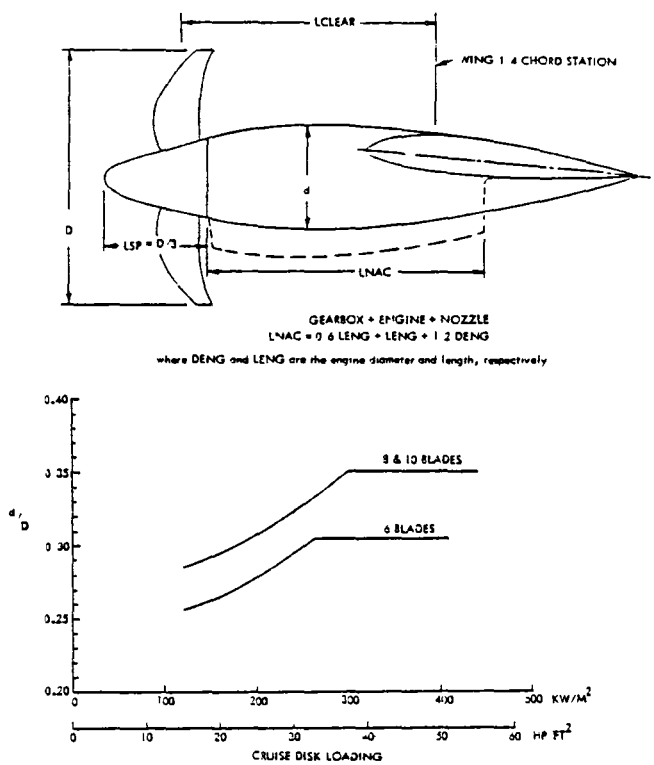

Figure E-8. Nacelle Installation Parameters

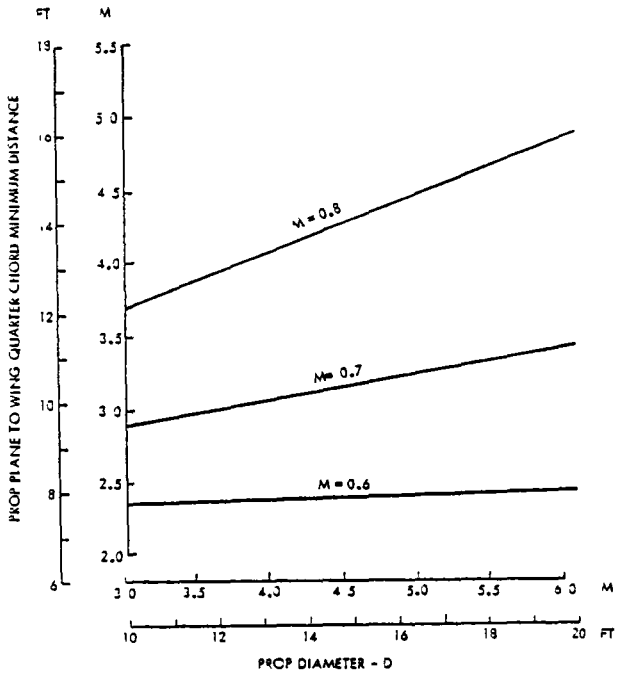

Figure E-8. (Cont'd) Nacelle Installation Parameters

Two of the dimensions shown on the figure are spinner length (LSP) and nacelle length (LNAC). A spinner length equal to one-third the propeller diameter was assumed based on the size of the scale model propfan to be tested on the JetStar aircraft for NASA. The nacelle length is equal to the sum of the gearbox, engine, and nozzle lengths. The length of the nozzle was defined to be 1.2 times the diameter of the engine power turbine case, and the length of the gearbox plus extension shaft was set equal to 60 percent of the engine length.

An under-the-wing engine location was selected to provide good engine accessibility without interrupting the wing box structure. The engine is installed as high as possible without interferring with the wing front beam to minimize the twisting moment on the wing due to the offset of the thrust centerline relative to the wing box. The jet nozzle is deflected downward to reduce impingement of the exhaust on the flaps.

The chordwise placement of the engine on the wing is the result of a compromise between aerodynamic, propulsive, and structural penalties. Typical pressure distributions from the lower surface of supercritical wings indicate that, if the nozzle exit is placed further aft than the 40-percent chord position on the wing, there will be adverse pressure gradients. Engine placement with the plane of the propeller about one diameter length forward of the wing quarter chord is desirable for propulsive efficiency based on the requirements shown in Figure E-8 from Reference 12, but the further forward the engine, the greater the structural weight penalties. Alternately, as the engine is moved aft to minimize structural weight, aerodynamic penalties are incurred and the propulsive efficiency may be jeopardized.

Because of these conflicts, the rear flange on the engine turbine casing is located under the front beam of the wing. This permits a relatively straight-forward structural attachment, and it keeps the exit of the nozzle forward of the 40-percent wing chord position.

Guidelines provided by Reference 12 for the spanwise distribution of propellers on a wing are shown in Figure E-9. The smaller value for F is desired for minimizing engine-out problems, while the larger value is preferred for reduced near-field cabin noise.

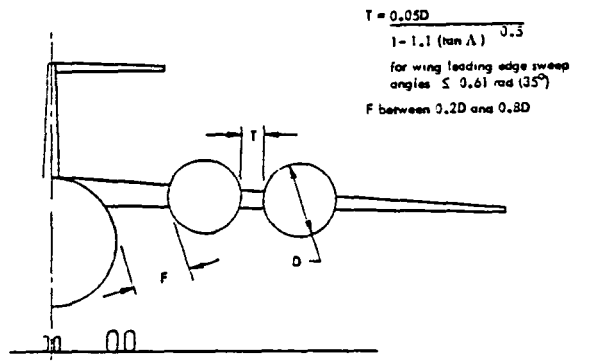

Figure E-9. Propeller Spanwise Spacing Requirements

PERFORMANCE

The performance of the total propulsion system, i.e., engine with propeller, has been compiled as specific fuel consumption and net pylon thrust for three rating conditions of maximum takeoff, climb, and cruise power. Net pylon thrust is defined as the algebraic sum of propeller net thrust, axial residual net jet thrust, and nacelle drag. Nacelle drag, as discussed in Appendix D, is calculated using a constant nacelle drag coefficient of 0.0671 based on nacelle maximum cross-sectional area. This drag coefficient includes the effect of the propeller slipstream on the nacelle; slipstream effects on the wing are included in the aircraft drag polar. Residual net jet thrust is the sum of nozzle gross thrust minus inlet ram drag.

During the definition of the takeoff thrust levels, some combinations of low tip speed and high disk loading (small propeller diameter) resulted in propeller power levels greater than could be absorbed efficiently at low advance ratios for low flight speeds. For these cases, takeoff thrust was defined as the maximum thrust obtainable at the given propeller diameter, tip speed, and advance ratio.

Installed engine performance was derived based on the assumption of 149 kW (200 hp) accessory power extraction, 100 percent inlet ram recovery, and a gearbox efficiency of 99 percent.

Figures E-10 through E-14 show, as an example, the net pylon thrust and specific fuel consumption at full power during takeoff, climb, and cruise for a particular combination of 10 blades, 229 m/s (750 ft/s) tip speed, and a nominal disk loading of 402 kW/m^2 (50 hp/ft^2). (Specific fuel consumption during takeoff remains essentially constant at 0.1865 kg/hr-kW (0.306 lb/hr-hp) and, therefore, is not shown as a separate figure). To cover the ranges of the three flight conditions, performance data were generated for altitudes from sea level up to 13.7 km (45,000 ft) and for Mach numbers up to 0.8. The effect of operating at part power is illustrated in Figure E-15. Similar performance data for this and other combinations of propeller characteristics for both full and part power are contained in Reference [26].

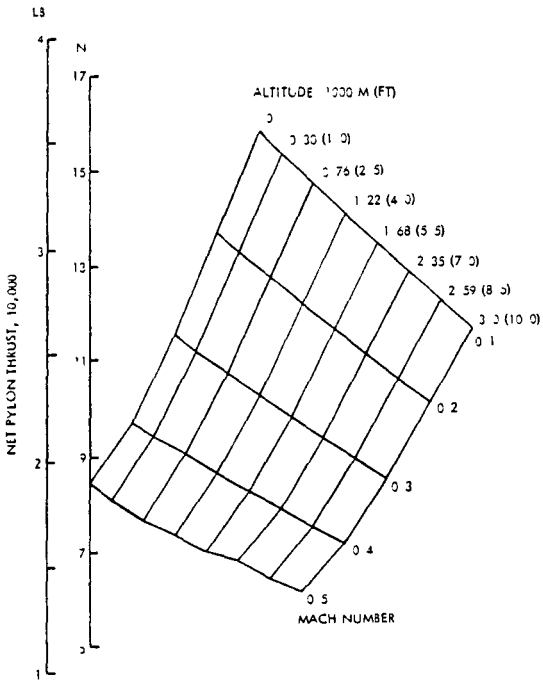

Figure E-10. Example of Maximum Takeoff Performance

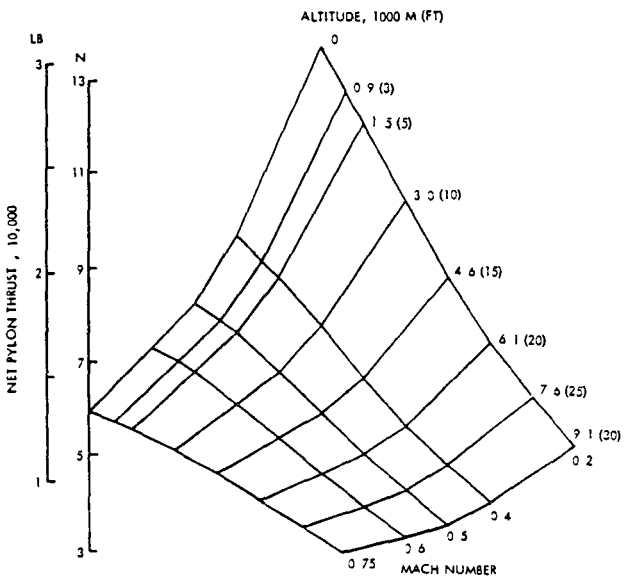

Figure E-11. Example of Maximum Climb Performance

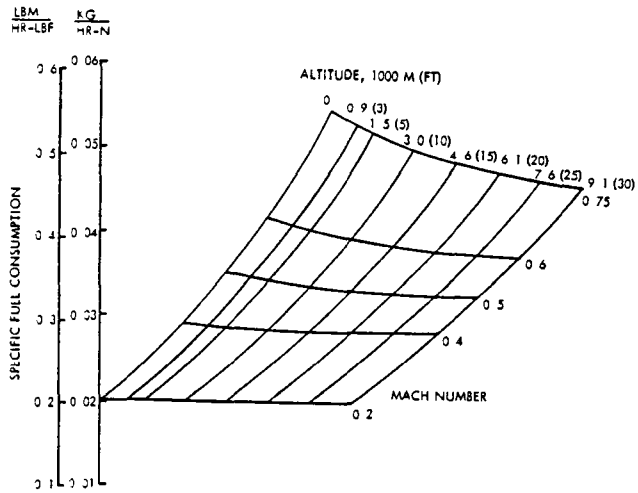

Figure E-12. Example of Fuel Consumption for Maximum Climb

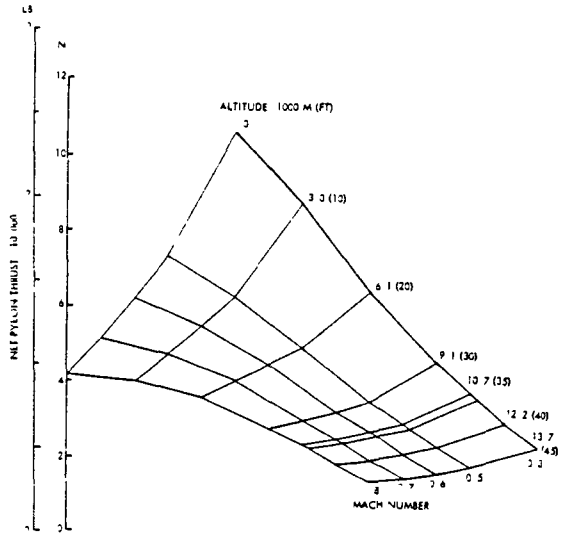

Figure E-13. Example of Maximum Cruise Performance

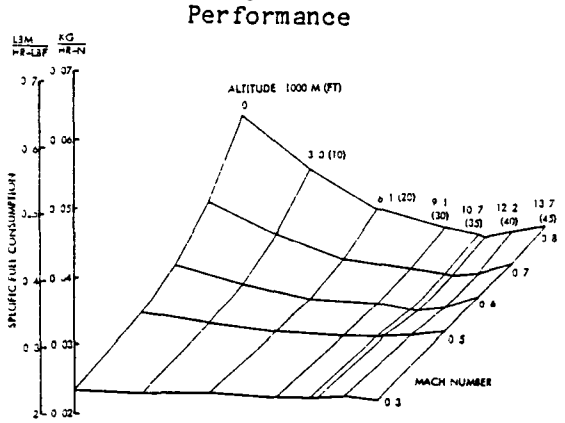

Figure E-14. Example of Fuel Consumption for Maximum Cruise

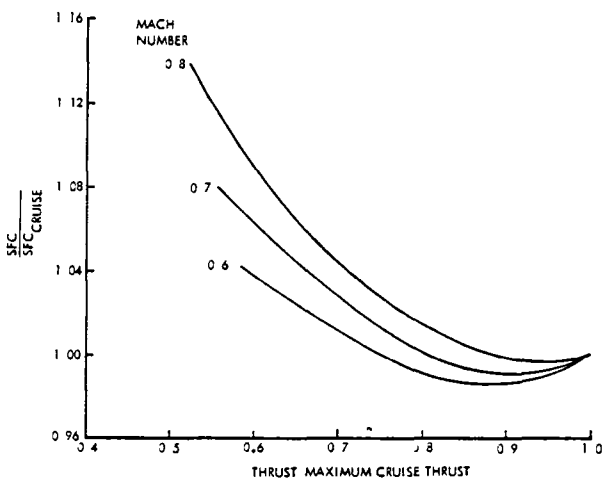

Figure E-15. Example of Part-Power Performance. Altitude - 9144m (30,000 ft)

SCALING PROCEDURE

All of the performance data presented thus far have been for the baseline engine power of 15.2 MW (20,424 hp). In the parametric study and for the selected design points, the aircraft require engine power levels other than those of the basepoint engine. To scale the basepoint engine to the power level required in each particular case, a procedure was devised which depends only on an assumption of constant propeller efficiency. The basic relationship between engine thrust and power is shown in equation (E3).

$$T/SHP = \eta_p \, 326/V \qquad (E3)$$

where:

T is the rated thrust, N (lb)
SHP is the power level, kW (hp)
V is the aircraft speed, m/s (ft/s)
η_p is the propeller efficiency

For a particular value of the aircraft speed (V), the ratio of engine thrust to power is constant if the propeller efficiency does not change with power, over the range of pitch change. This, then, yields the basic relationship that is needed to scale

the engine to any desired size. Mathematically, the basic relationship is

$$\frac{T_s}{SHP_s} = \frac{T_b}{SHP_b} \quad \text{(E4)}$$

where the subscripts s and b indicate the scaled and base engines, respectively.

Performance Scaling

The performance of the engine is scaled while maintaining a constant disk loading (SHP/D^2) and a constant tip speed (TS). When expressed mathematically, this statement takes the form of two equations:

$$\frac{SHP_s}{D^2_s} = \frac{SHP_b}{D^2_b} = \text{constant} \quad \text{(E5)}$$

$$TS_s = TS_b \quad \text{(E6)}$$

The scaling procedure uses a thrust scale factor (SF) which is the ratio of required thrust to available thrust at a given power setting, altitude, and flight Mach number, i.e.,

$$SF = T_{required}/T_{available}$$

or, in terms of the scaled and base engine subscripts,

$$SF = T_s/T_b \quad \text{(E7)}$$

Thus, the scaled thrust is given by

$$T_s = SF\ T_b \quad \text{(E8)}$$

and, from equation (E4), the scaled power is given by

$$SHP_s = T_s(SHP_b/T_b) = SF\ SHP_b \quad \text{(E9)}$$

An equation for the scaled propeller diameter may be derived by starting with equation (E5), substituting the definition of the scale factor of equation (E7), and rearranging to obtain

$$D_s = SF^{0.5} \times D_b \quad \text{(E10)}$$

Reference 23 shows the effect of engine scaling on specific fuel consumption. There is no effect when the engine is scaled to larger sizes, but there is a penalty in scaling to smaller sizes. The magnitude of the penalty is given by

$$\text{SFC Factor} = 0.143\ SF^2 - 0.379\ SF + 1.236 \quad \text{(E11)}$$

if SF is less than one.

Engine/Nacelle Dimension Scaling

Equations for scaling the engine dimensions were supplied in Reference 23. They are:

$$ENGD_s = ENGD_b \times SF^{0.5} \quad \text{(E12)}$$

$$ENGL_s = ENGL_b \times SF^{0.43} \quad \text{(E13)}$$

The maximum diameter (ENGD) of the baseline engine is 0.915 m (3 ft) at the rear turbine, and the overall length (ENGL) is 2.24 m (7.35 ft).

The nacelle length and diameter are functions of the engine length, engine diameter, and propeller diameter. Once the engine and propeller are scaled to the desired size, the nacelle dimensions are calculated to fit the engine. Hence, no relationships are needed to scale the nacelles.

Weight Scaling

Reference 23 gives a graphical relationship for scaling engine weight as the engine size varies between 50 and 200 percent of the baseline design. In equation form, the engine weight scaling relationship is:

$$ENGW_s = ENGW_b(0.098798SF^2 + 0.78176SF + 0.1199) \quad \text{(E14)}$$

where the weight of the baseline engine ($ENGW_b$) is 970 kg (2134 lb).

As discussed in a previous section, propeller and gearbox weights are defined as a function of propeller diameter. By using the scaled propeller diameter, the weights for the propeller and gearbox are automatically adjusted to the scaled size. Hence, no special scaling equations are needed for these two weight items.

Technology Scaling

The STS487 engine has technology levels that are predicted to be consistent with a 1998 commercial engine certification. An earlier introduction of the engine would be accompanied by weight and specific fuel consumption penalties that reflect lower levels of advanced technology. These penalties have been quantified in Reference 23 and are illustrated in Figure E-16. Early introduction of this engine is also likely to be accompanied by louder noise levels, which are not incorporated directly, but are recognized and partially accounted for indirectly through the larger power requirement resulting from less technology advancement.

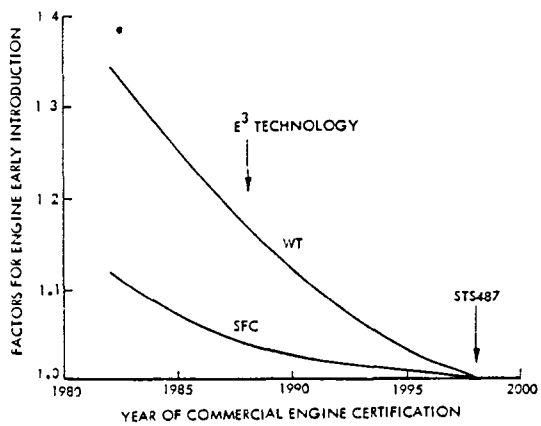

Figure E-16. Estimated Adverse Effects of STS487 Engine Early Introduction

APPENDIX F. TURBOPROP PARAMETRIC DATA ANALYSIS

This appendix provides a step-by-step description of the analytical process that was used to reduce the parametric data to a form that could be used for selecting aircraft for further study. In addition, all of the reduced parametric data are presented, which were instrumental in assessing the cost of quietness.

METHOD OF ANALYSIS

In the Phase II portion of the parametric study, four variables were considered: number of propeller blades, propeller tip speed, propeller disk loading, and wing aspect ratio. For these variables, three values were selected for the first two, and four for the last two. Then, for each combination of values, an aircraft design was produced by Lockheed's Generalized Aircraft Sizing and Performance program. Estimates were made of the noiseprint area at an 80-EPNdB noise level, and of the direct operating cost for each of the three fuel prices. To illustrate the data reduction process, a set of aircraft designs with varying wing aspect ratio and propeller disk loading was arbitrarily selected, which has these conditions:

- Cruise Mach Number - 0.8
- Payload - 4 Containers
- Cruise Altitude - 10.1 km (33,000 ft)
- Wing Sweep Angle - 0.44 rad (25 deg)
- Wing Loading - 5.71 kN/m^2 (119.5 lb/ft^2)
- Number of Propeller Blades - 10
- Propeller Tip Speed - 229 m/s (750 ft/s)

Obviously, when generating so many aircraft designs, there is a tremendous amount of data that can be graphed and analyzed. Consistent with the intent

of this study, we chose to graphically portray only the ramp weight, block fuel, takeoff distance, engine thrust-to-weight ratio, propeller diameter, fuel volume ratio, direct operating cost (DOC) for each of three fuel prices, and 80-EPNdB noiseprint areas for full power and cutback power conditions. These are presented in Figures F-1 through F-11.

Although a number of limitations have been imposed on this study, those that could impact the analysis for this set of designs are:

- Takeoff Distance $\leq$ 2440 m (8000 ft)
- Propeller Diameter $\leq$ 6.1 m (20 ft)
- Fuel Volume Ratio $\geq$ 1

A check of the data shows that only the propeller diameter limitation is a constraint for this case. As the first step in the analysis, this limiting value is indicated by the heavy line on Figure F-12, a reproduction of Figure F-5. It is then duly noted on the other figures by identifying combinations of aspect ratio and disk loading that are on the propeller diameter limit line and by locating these combinations on the various figures so that a limit line can be drawn on each. For this example, only Figures F-13 and F-14 (reproductions of Figures F-7 and F-10) are included with the limit illustrated.

The next step is to superimpose a regular pattern of constant cost lines on the DOC plot, as shown in Figure F-15. These lines are then transferred to the graph of noiseprint area in Figure F-16, and the minimum values are read for each cost line. This procedure is repeated for the eight other combinations of values of propeller tip speed and number of blades to complete a table similar to Table F-I. For each subset in the table, that is for the nine area values for each cost, a minimum value can be identified by either a visual or graphical comparison. The latter approach is depicted in Figure F-17 for a constant DOC of 7.40 ¢/t-km (12.4 ¢/T-n.mi.).

The minimum area from Figure F-17 is then combined with similarly defined values for the other DOC levels to obtain the desired end result, Figure F-18. By repeating the process three more times, similar figures can be obtained for the DOCs at the other two fuel prices and for block fuel.

PARAMETRIC DATA

All of the parametric data that were used to assess the cost of quietness and its relationship to payload size, cruise Mach number, and fuel price are presented here. Figures F-19 to F-21 show the cost of quietness for an 0.8 Mach number for the three fuel prices, and for 2, 4, and 6-container payloads. Figures F-22 through F-25 isolate the effects of payload on the cost of quietness for each fuel price.

Cost of quietness results for a 4-container payload and cruise Mach numbers of 0.6 and 0.7 are presented in Figures F-26 and F-27, respectively. Figures F-28 and F-29 compare the effects of speed and fuel price on the cost of quietness at full and cutback power conditions.

Figures F-30 to F-32 present cost of quietness data for a 9-container payload at three cruise Mach numbers of 0.7, 0.75, and 0.8. The effects of speed on the cost of quietness are included in Figures F-33 and F-34 for full power and cutback conditions, respectively.

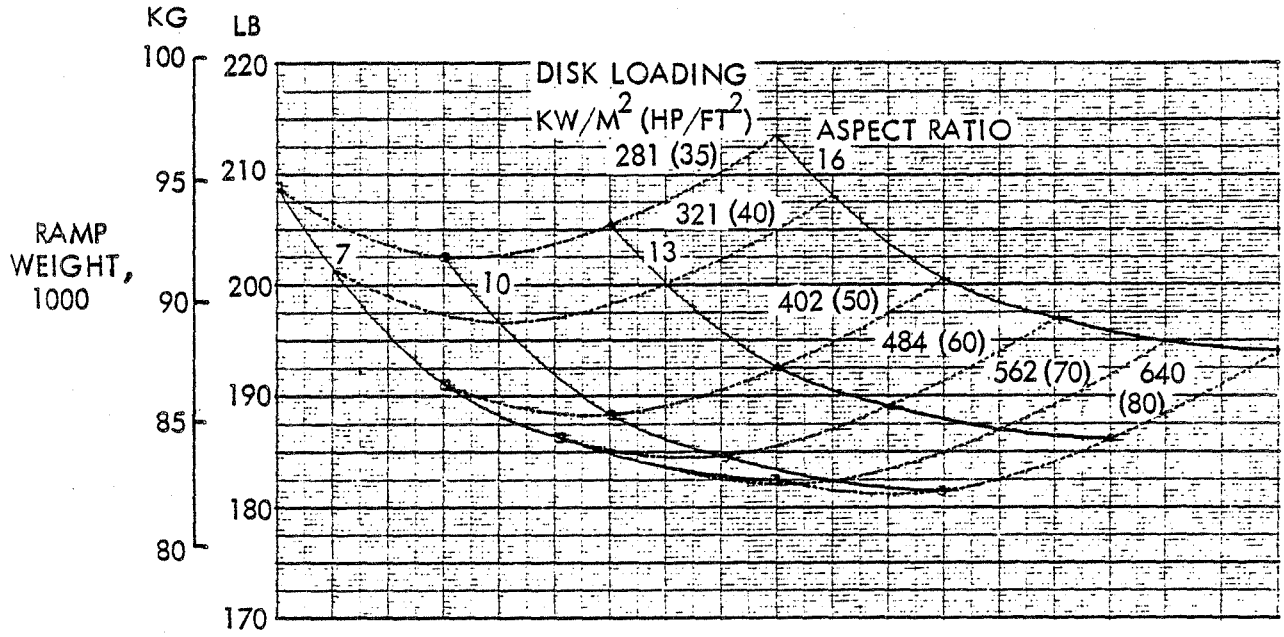

Figure F-1. Ramp Weight Variation for Turboprop Parametric Example

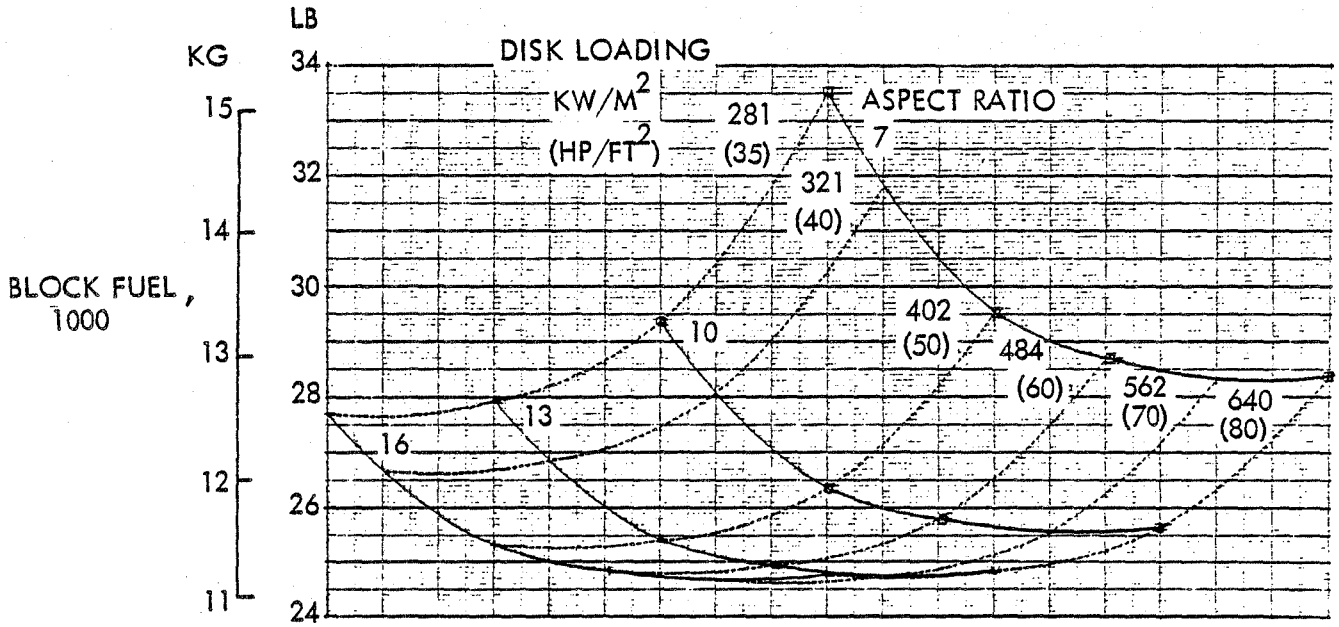

Figure F-2. Block Fuel Variation for Turboprop Parametric Example

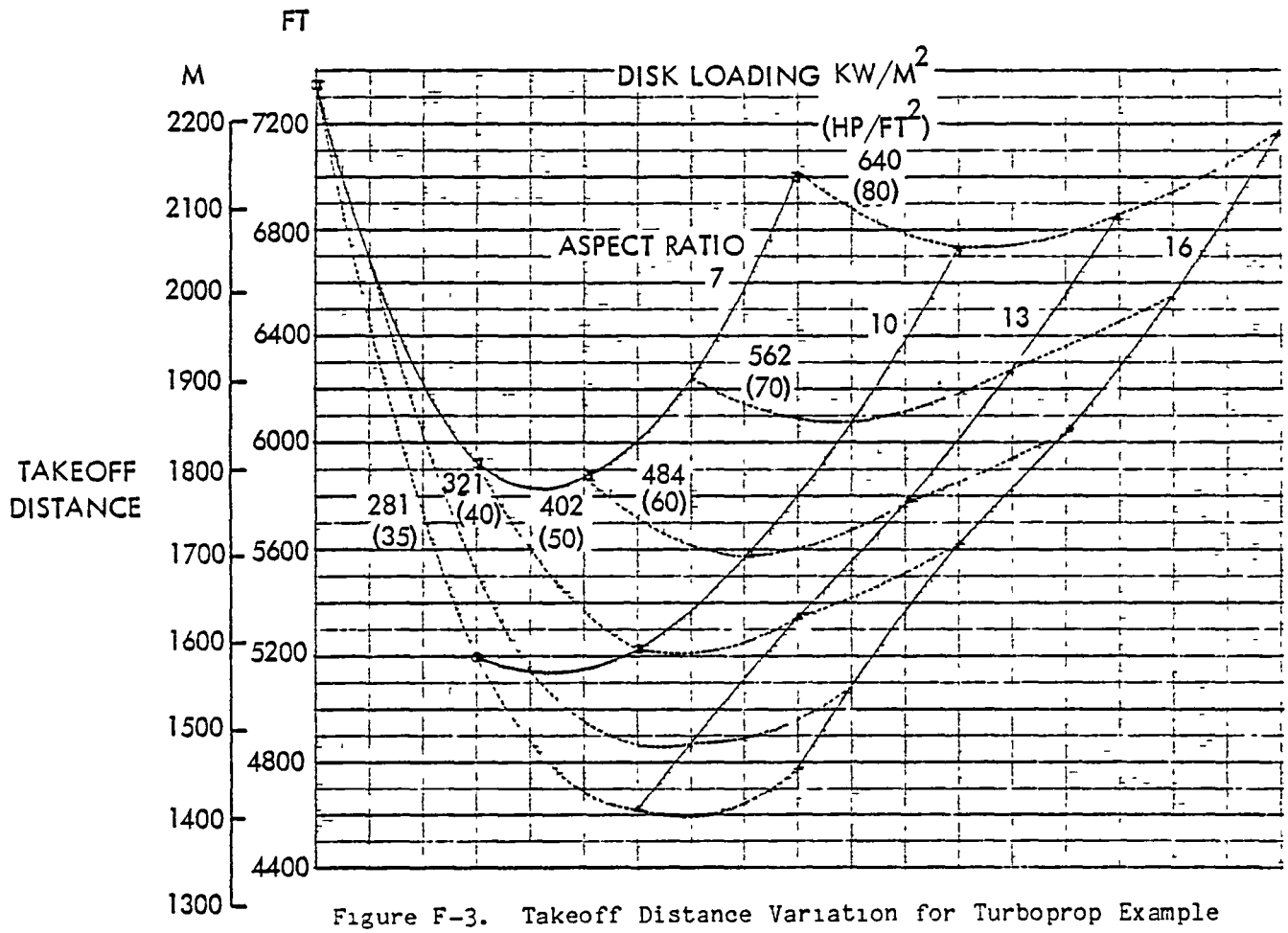

Figure F-3. Takeoff Distance Variation for Turboprop Example

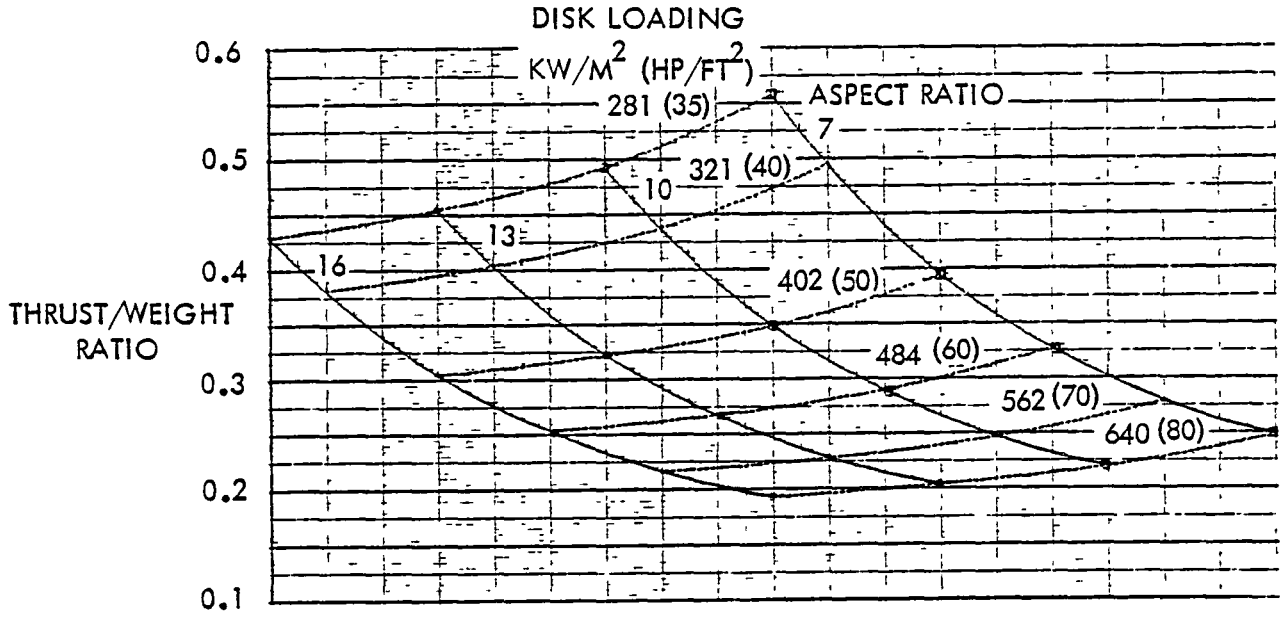

Figure F-4. Thrust/Weight Variation for Turboprop Parametric Example

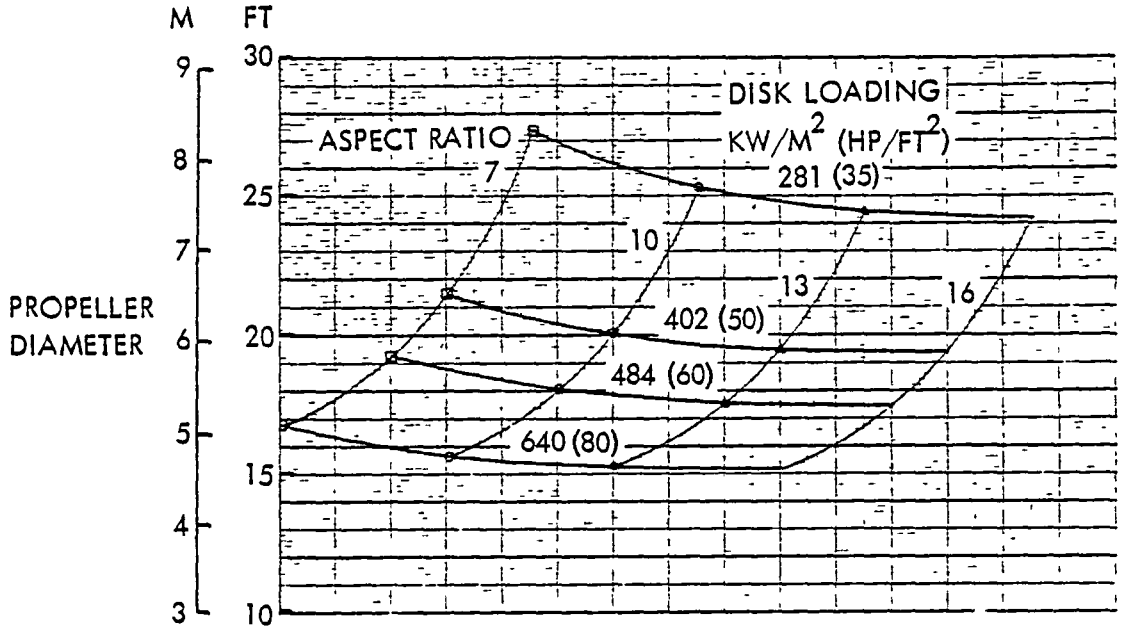

Figure F-5. Propeller Diameter Variation for Turboprop Parametric Example

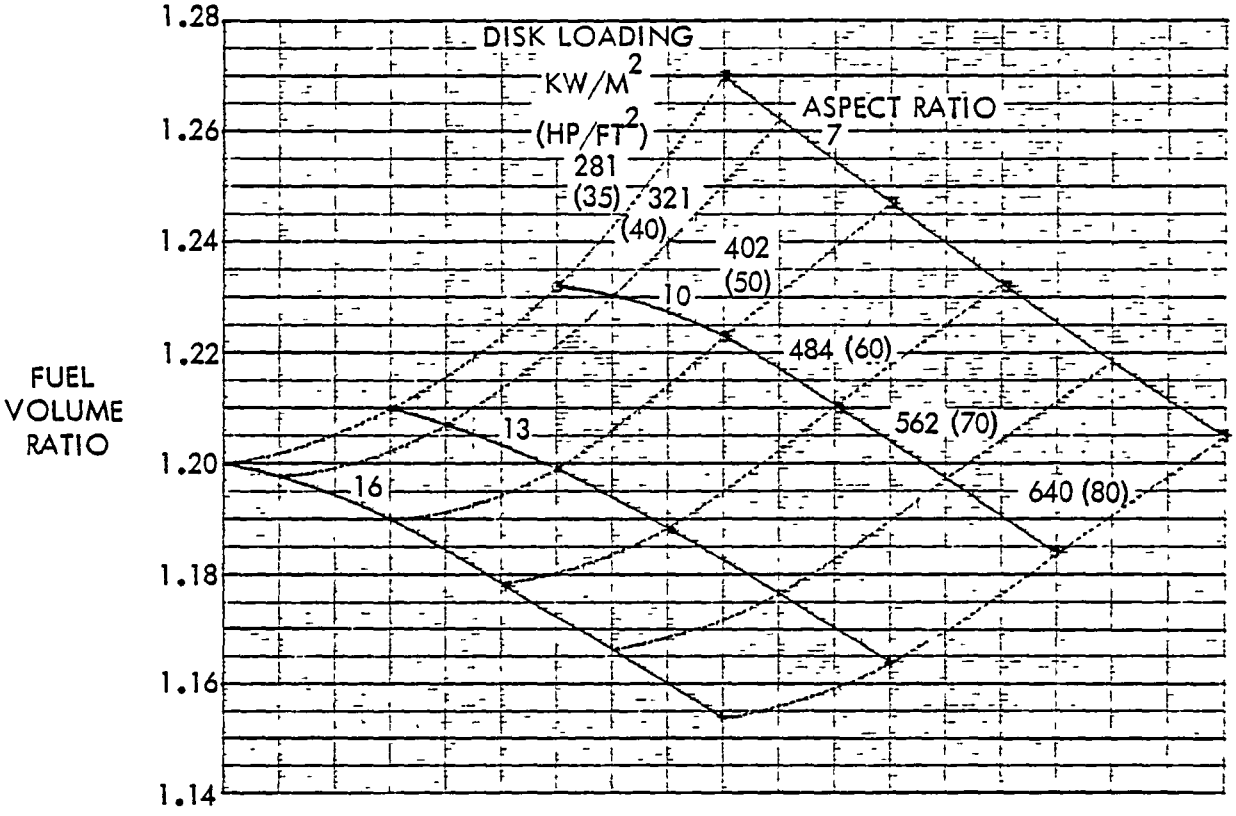

Figure F-6. Fuel Volume Ratio Variation for Turboprop Parametric Example

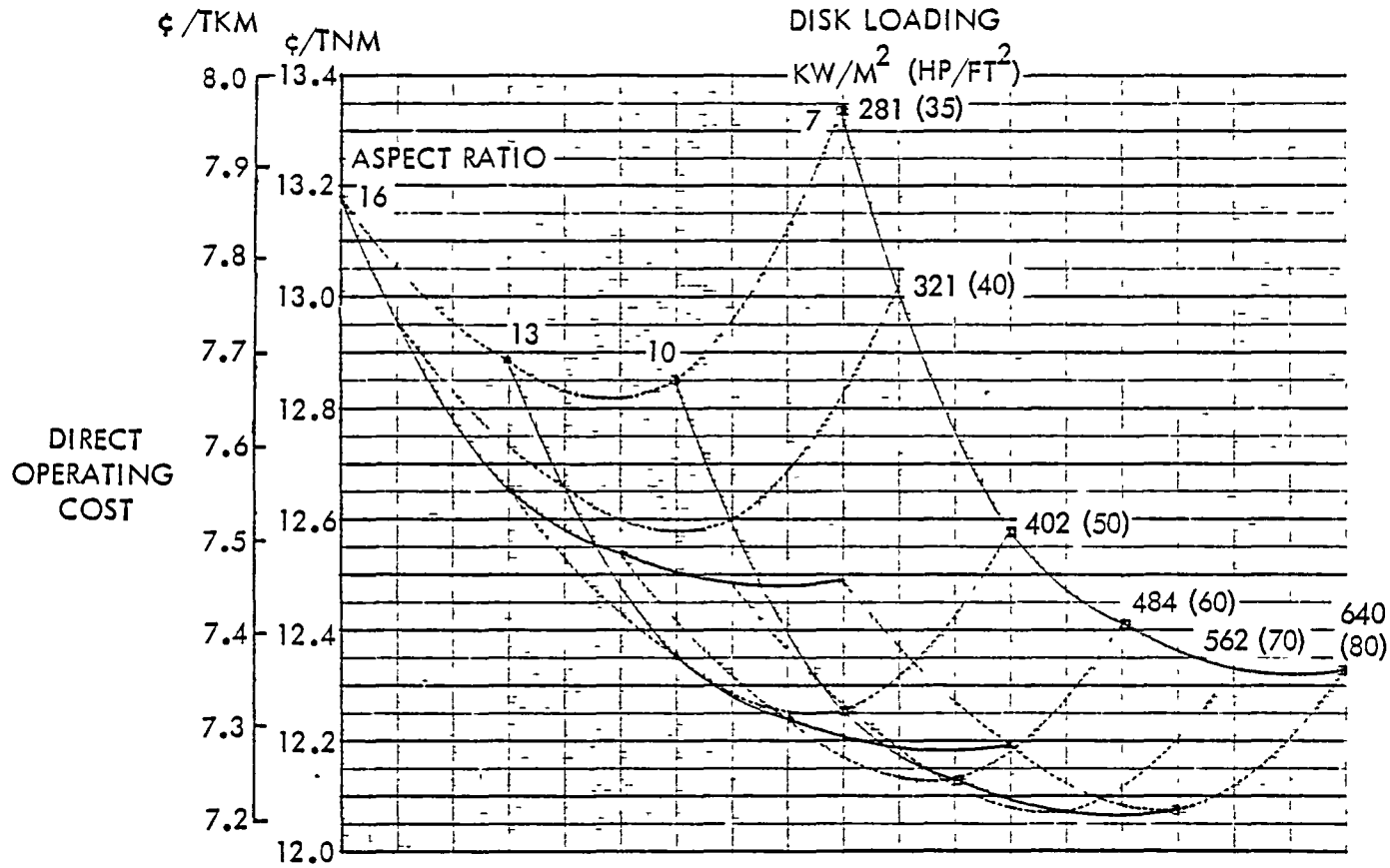

Figure F-7. Direct Operating Cost Variation for Turboprop Parametric Example. Fuel at 132 $/m^3 (50 ¢/gal)

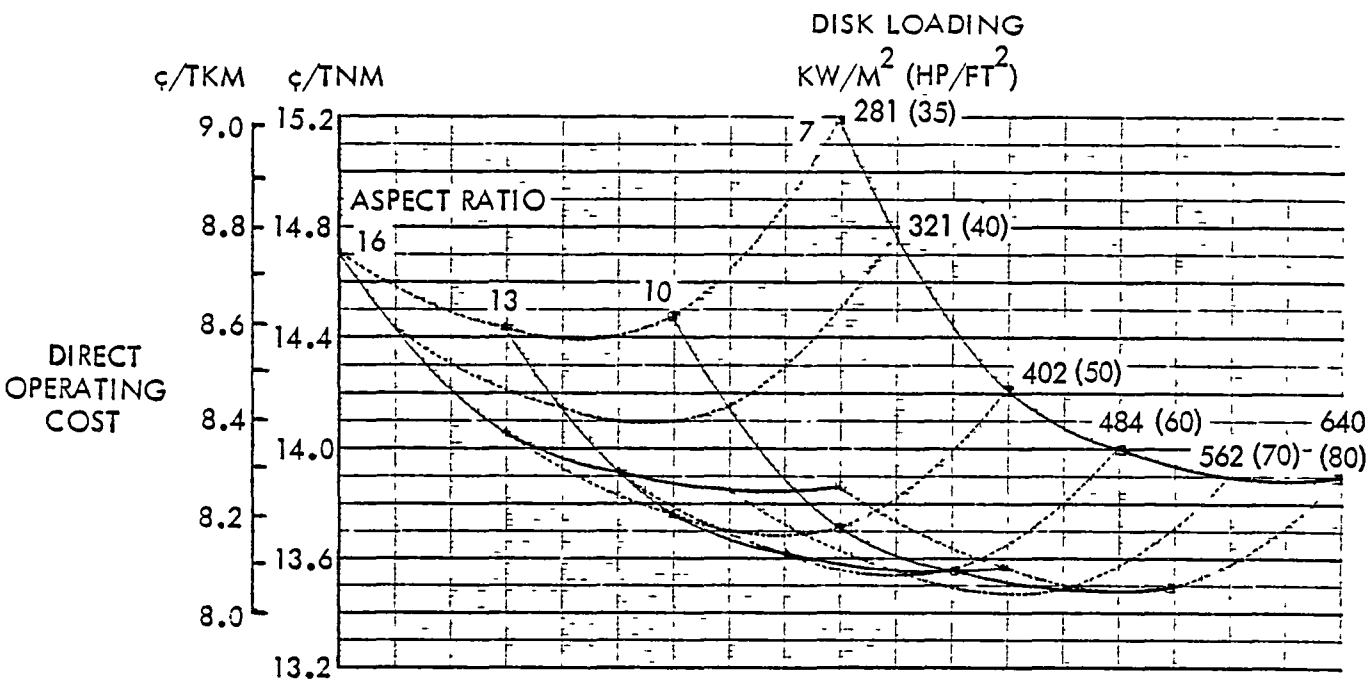

Figure F-8. Direct Operating Cost Variation for Turboprop Parametric Example. Fuel at 198 $/m^3 (75 ¢/gal)

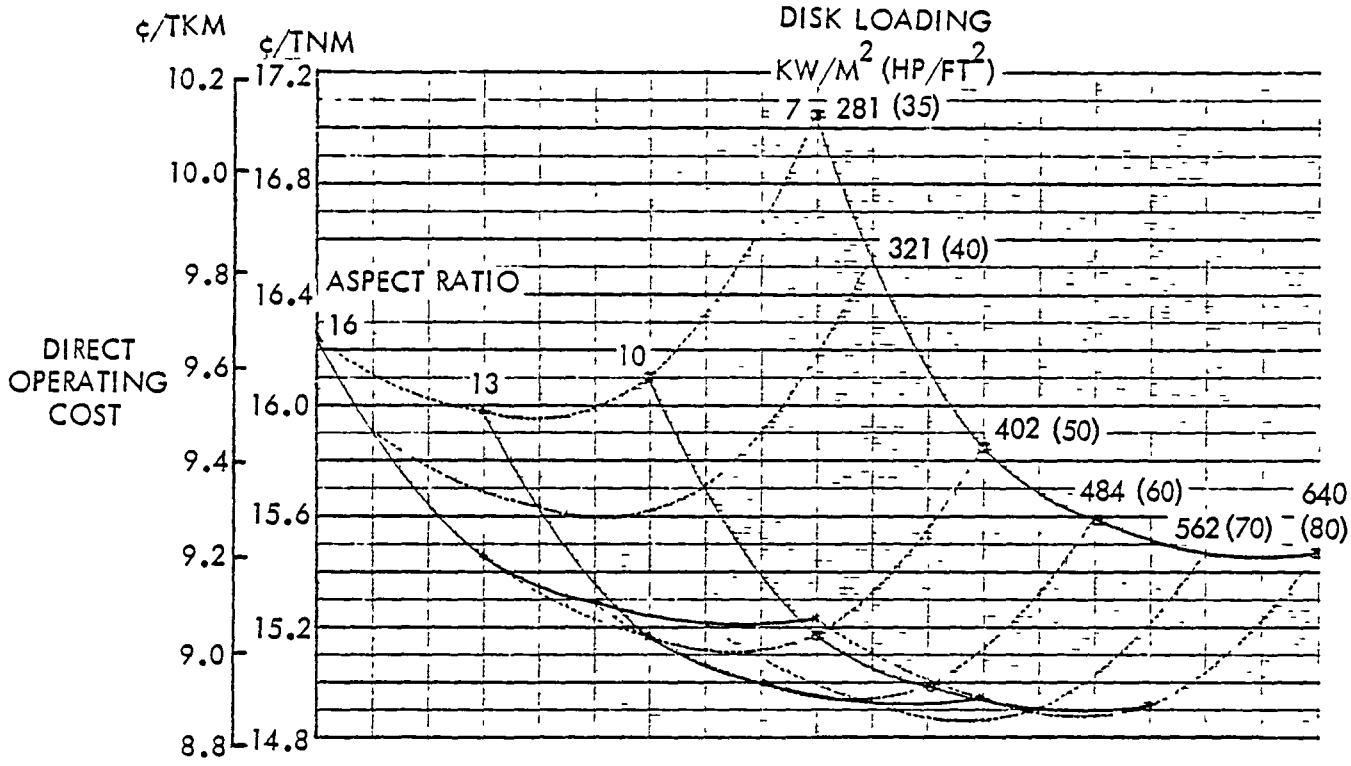

Figure F-9. Direct Operating Cost Variation for Turboprop Parametric Example. Fuel at 264 $/m³ (100 ¢/gal)

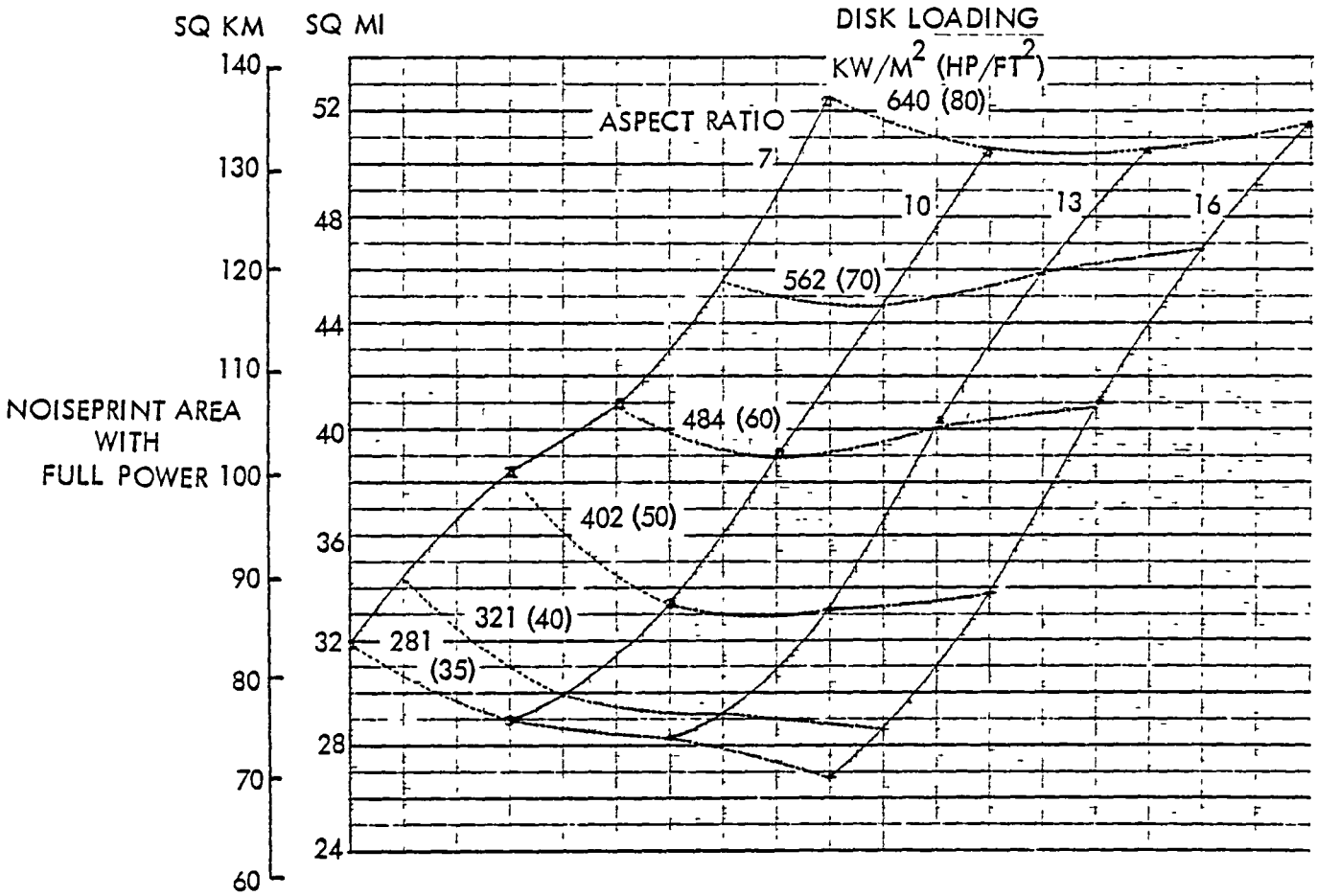

Figure F-10. Noiseprint Area at Full Power for Turboprop Parametric Example.

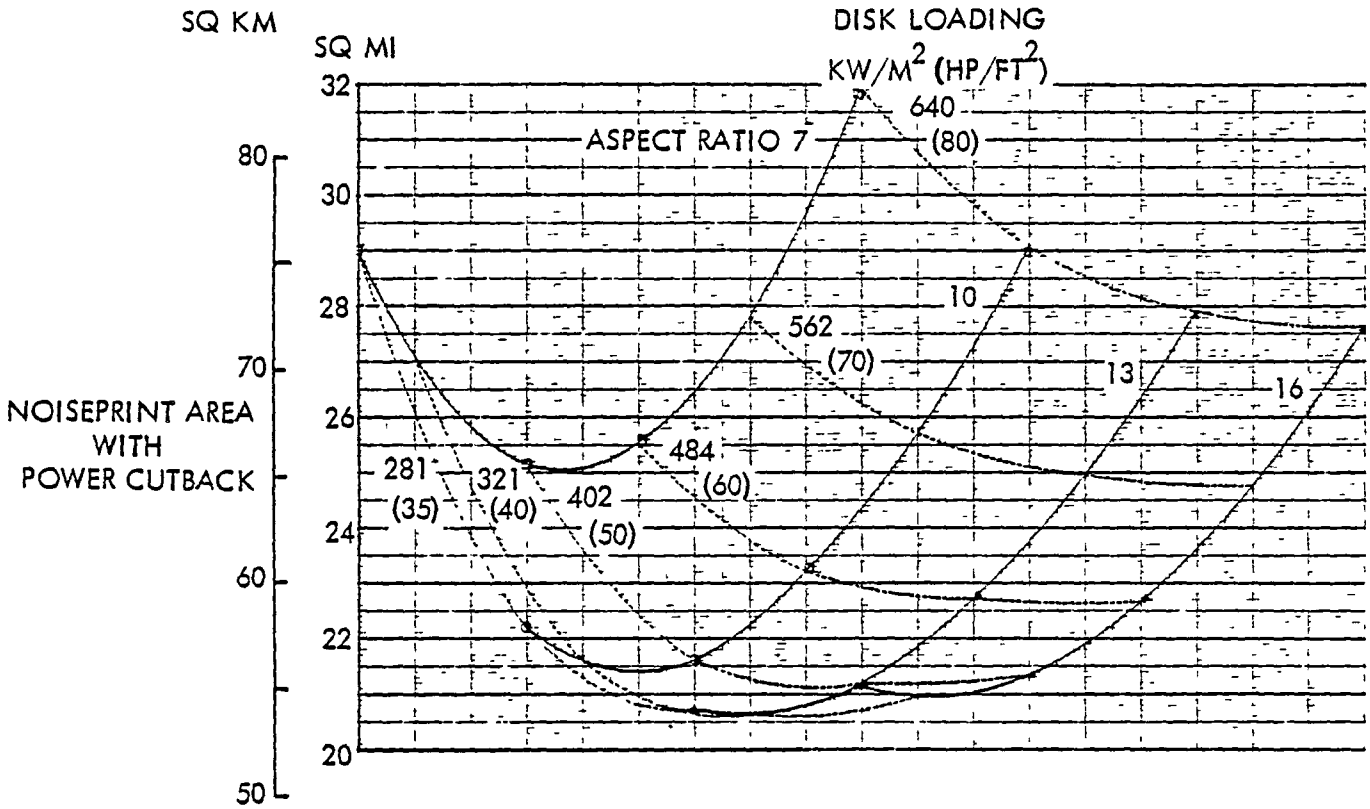

Figure F-11. Noiseprint Area with Cutback Power for Turboprop Parametric Example.

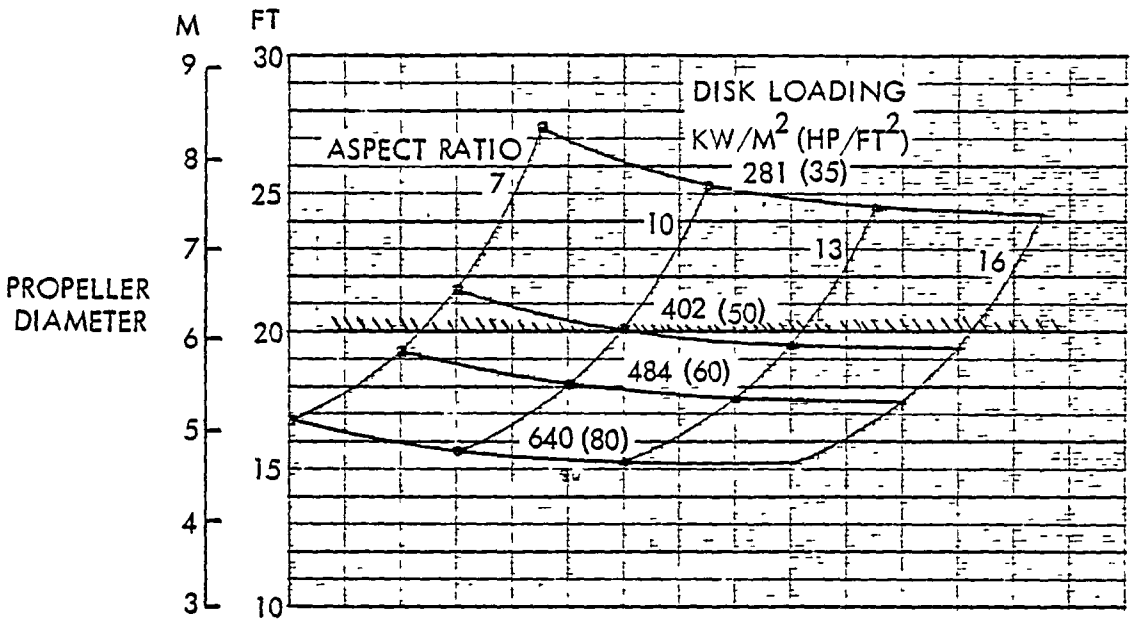

Figure F-12. Limit Imposed by Propeller Diameter

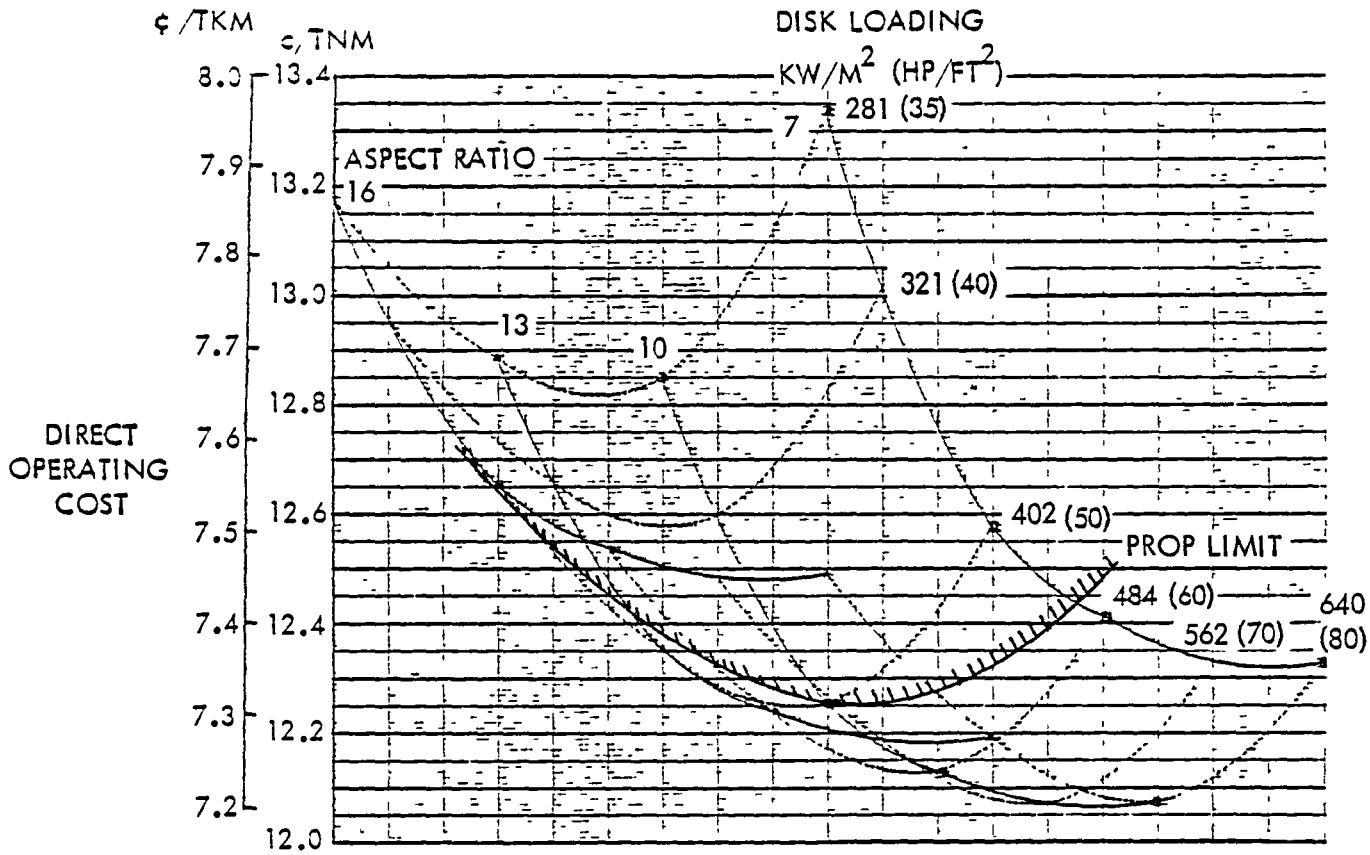

Figure F-13. Propeller Limit Applied to Direct Operating Cost

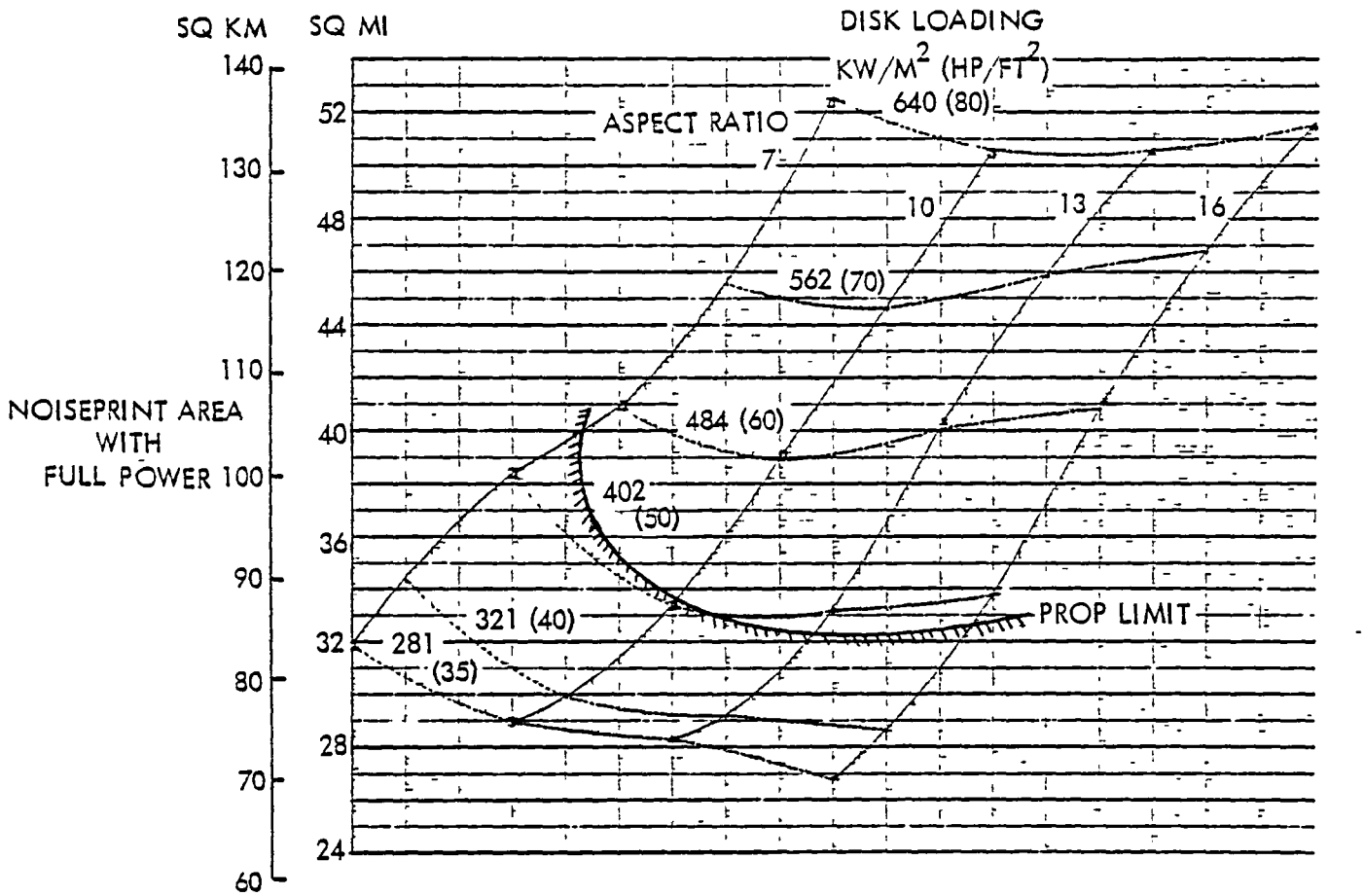

Figure F-14. Propeller Limit Applied to Noiseprint Area for Full Power

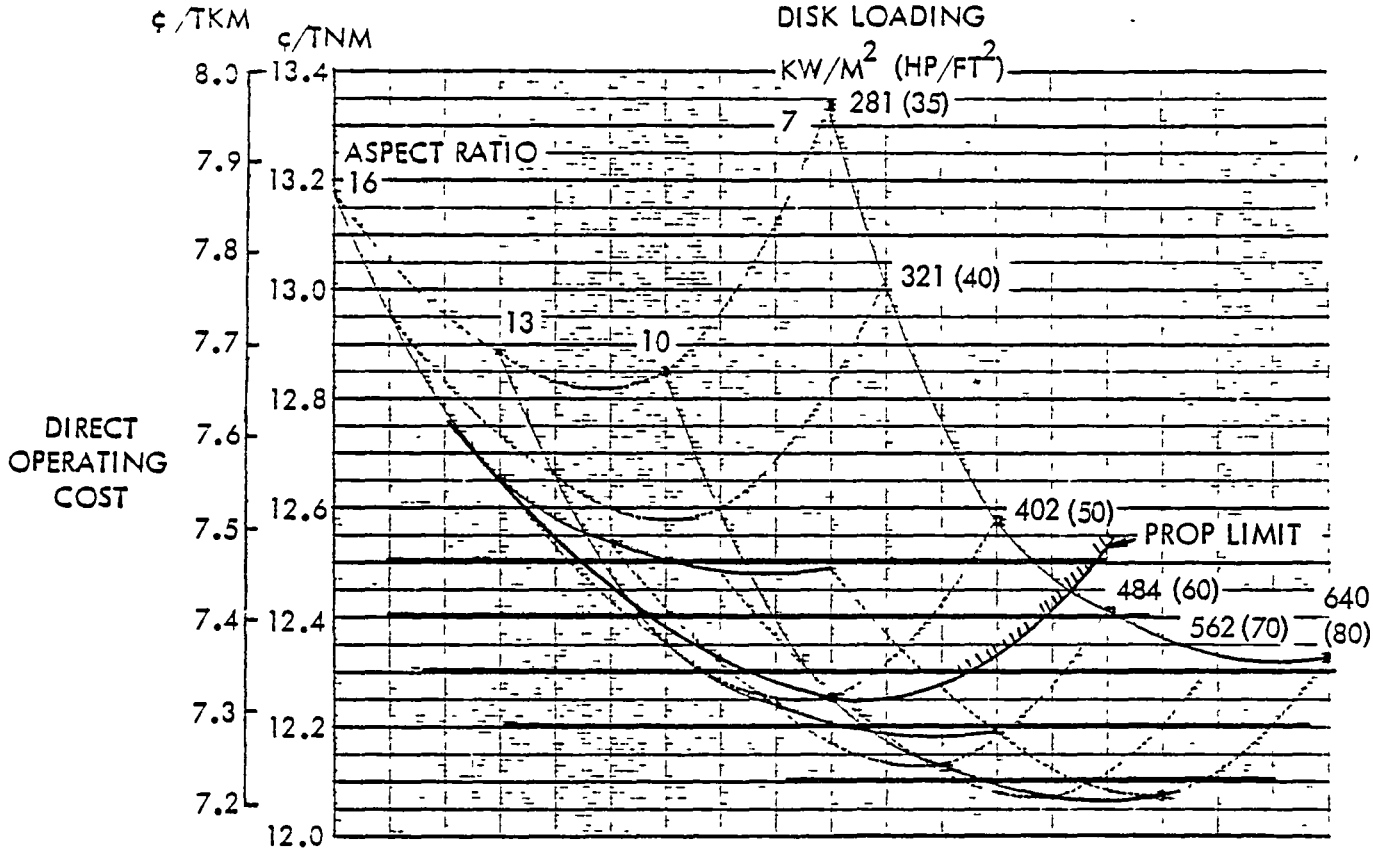

Figure F-15. Direct Operating Cost with Lines of Constant Cost Indicated for Transfer

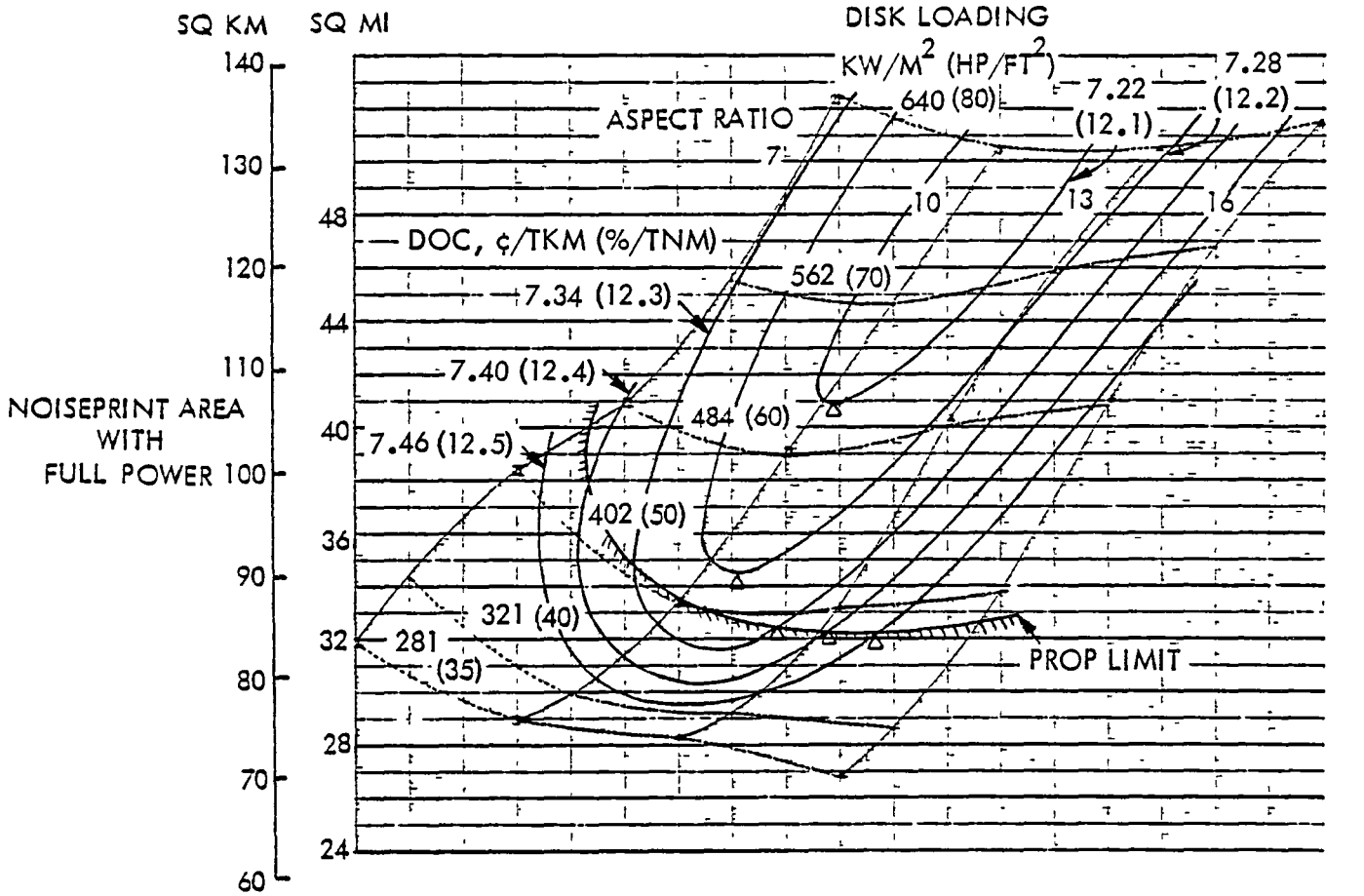

Figure F-16. Noiseprint Area with Lines of Constant Cost Superimposed

Table F-I. Sample Data Compilation for Optimization of 4-Container Payload, 0.8 Mach Number Turboprop Aircraft

DOC, ¢ TKM, FUEL AT $3 132 $ M^3	NUMBER OF BLADES	NOISEPRINT AREAS (SQ KM) FOR TIP SPEEDS (MPS) OF		
		204	229	256
7 28	6	*	248 5	631 7
	8	*	179 9	387 0
	10	*	89 6	216 9
7 34	6	*	235 6	639 5
	8	*	154 0	374 1
	10	72.5	94 7	214 9
7 40	6	86 0	230 4	655 0
	8	85 7	145 8	370 2
	10	67 6	84.7	214 4
7 46	6	81 5	230 4	655 0
	8	76 9	145 0	370 2
	10	66 5	83 9	214 4
DOC, ¢/TNM, FUEL AT 50 ¢ GAL	NUMBER OF BLADES	NOISEPRINT AREAS (SQ MI) FOR TIP SPEEDS (FPS) OF		
		670	750	840
12 2	6	*	96 0	244 0
	8	*	69 5	149 5
	10	*	34 6	83 8
12 3	6	*	91 0	247 0
	8	*	59 5	144 5
	10	28 0	32 7	83 0
12 4	6	33 2	89 0	253 0
	8	33 1	56 3	143 0
	10	26 1	32 4	82 8
12 5	6	31 5	88 0	253 0
	8	29 7	56 0	143 0
	10	25 7	32 4	82 8

* NO AIRCRAFT OBTAINABLE FOR CONDITIONS

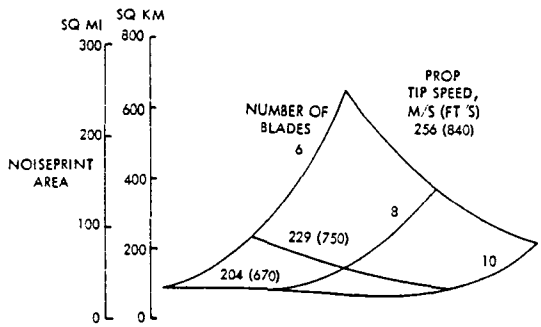

Figure F-17. Noiseprint Area for Variations in Propeller Tip Speed and Number of Blades at Constant DOC

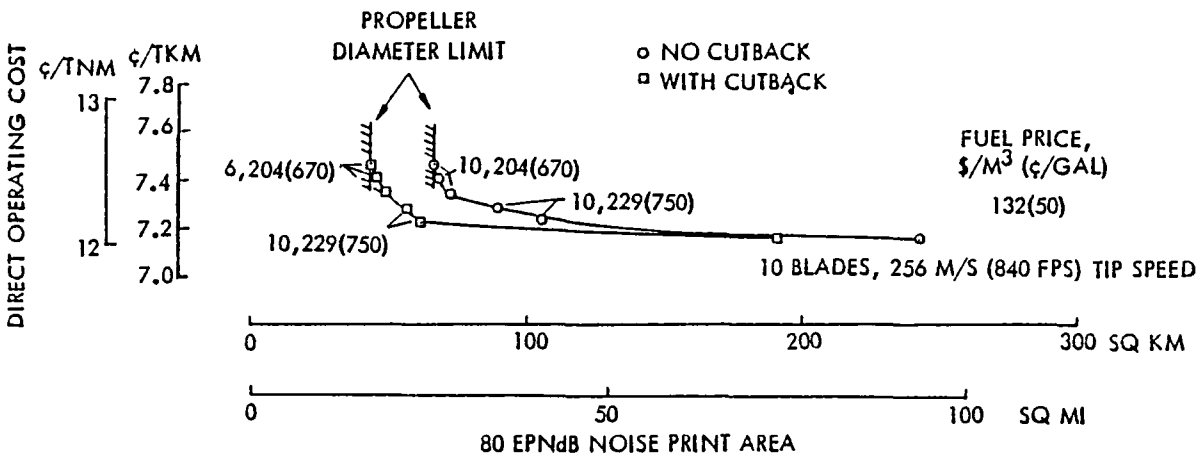

Figure F-18. Cost of Quietness as a Function of Tip Speed and Number of Blades

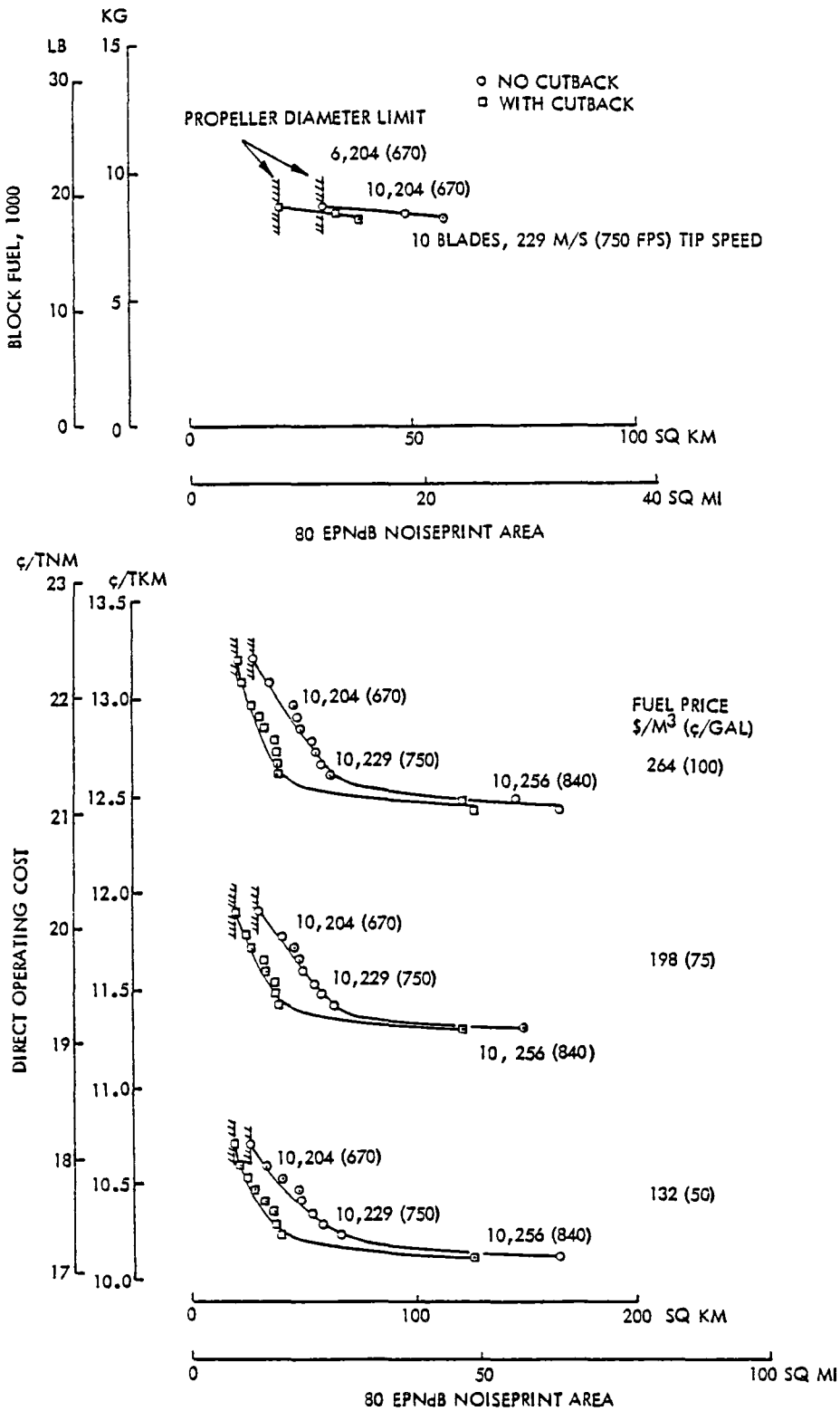

Figure F-19. Cost of Quietness for 0.8 Mach Number and 2-Container Payload

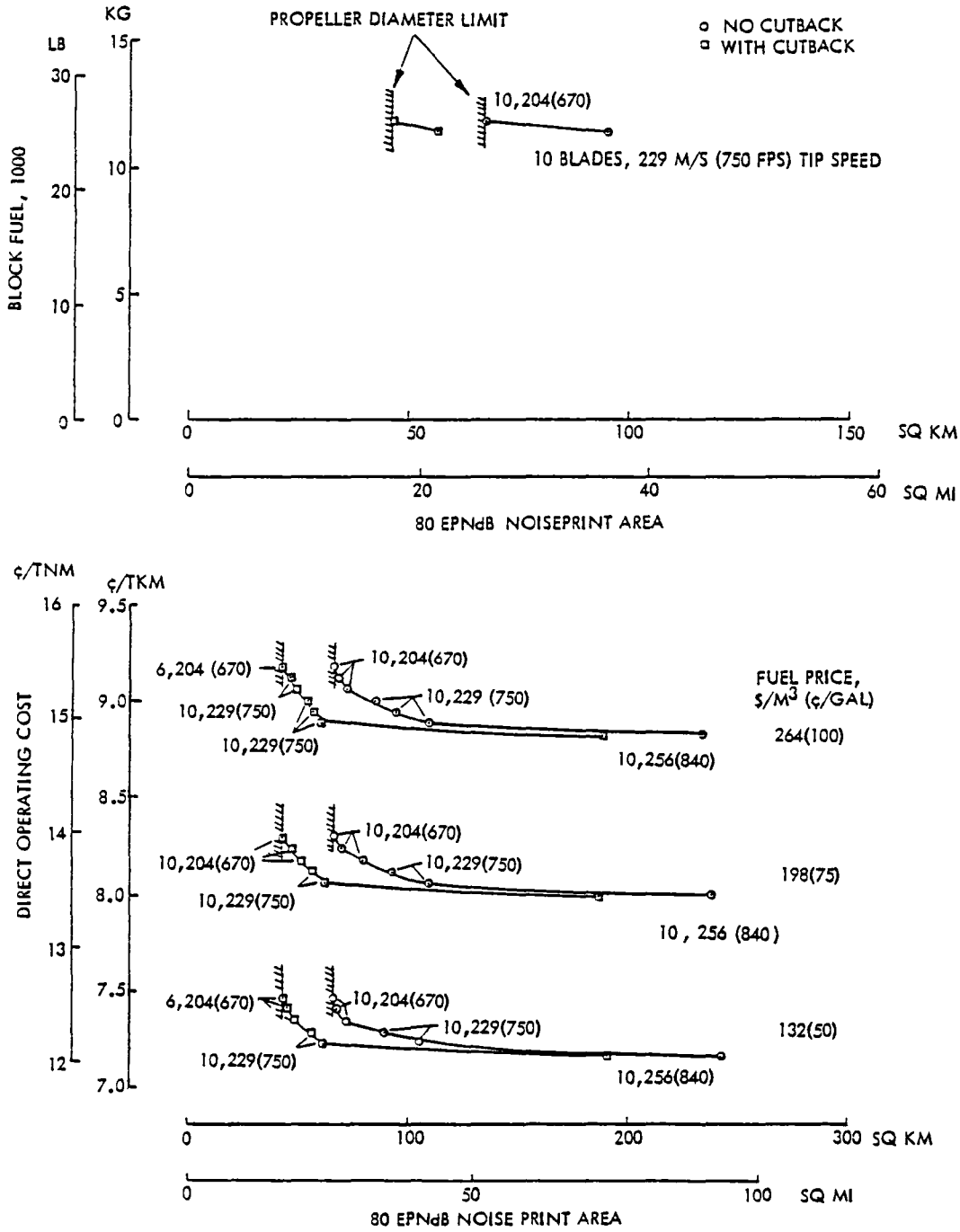

Figure F-20. Cost of Quietness for 0.8 Mach Number and 4-Container Payload

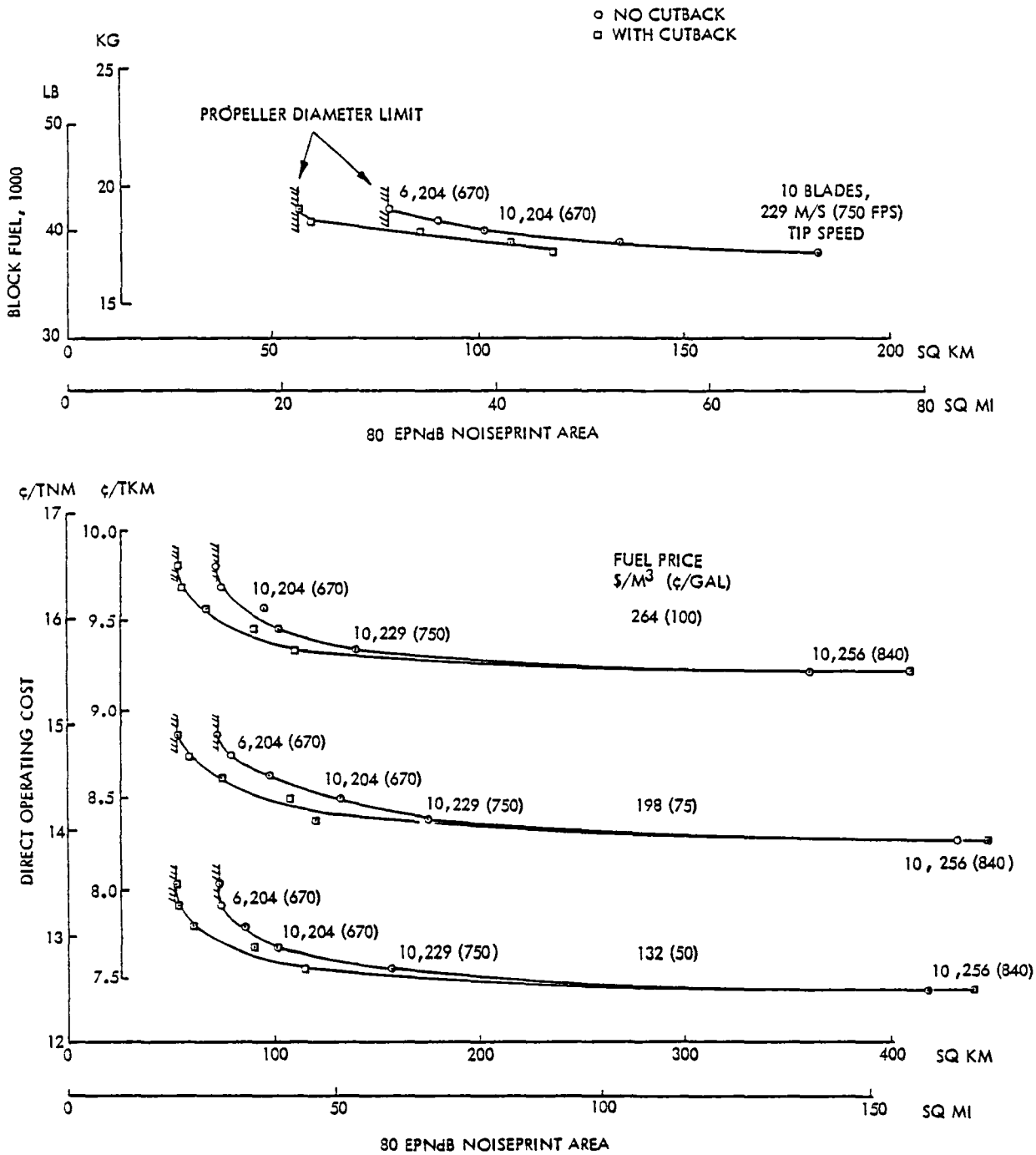

Figure F-21. Cost of Quietness for 0.8 Mach Number and 6-Container Payload

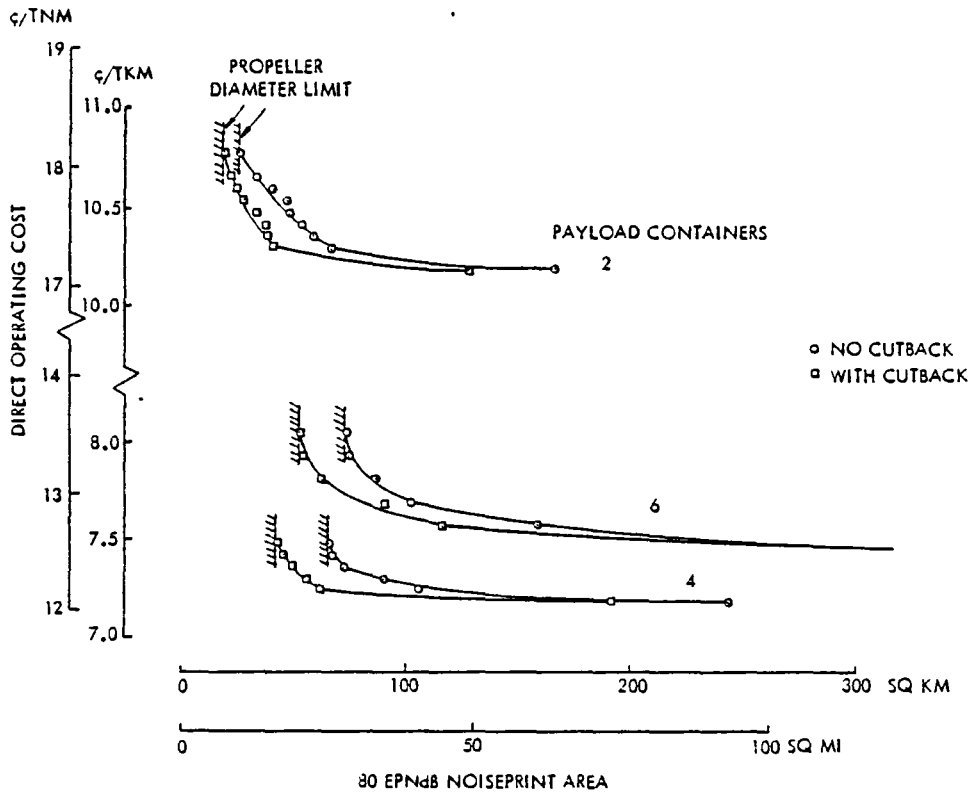

Figure F-22. Effect of Payload on Cost of Quietness for Fuel at 132 $/m^3$ (50 ¢/gal)

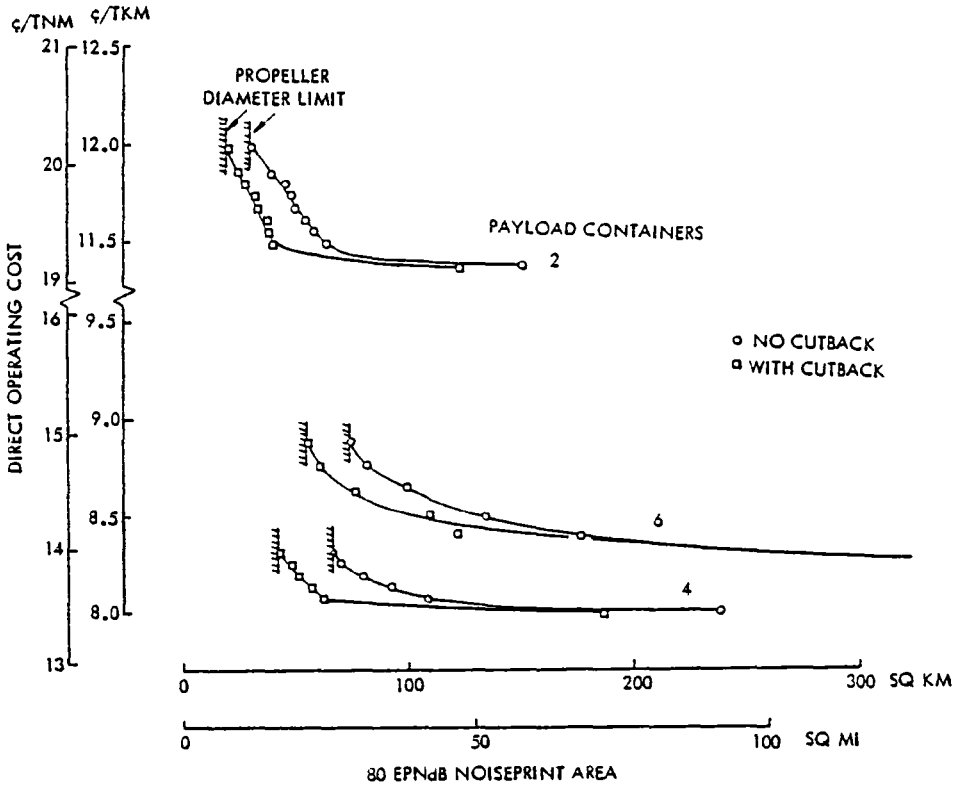

Figure F-23. Effect of Payload on Cost of Quietness for Fuel at 198 $/m^3$ (75 ¢/gal)

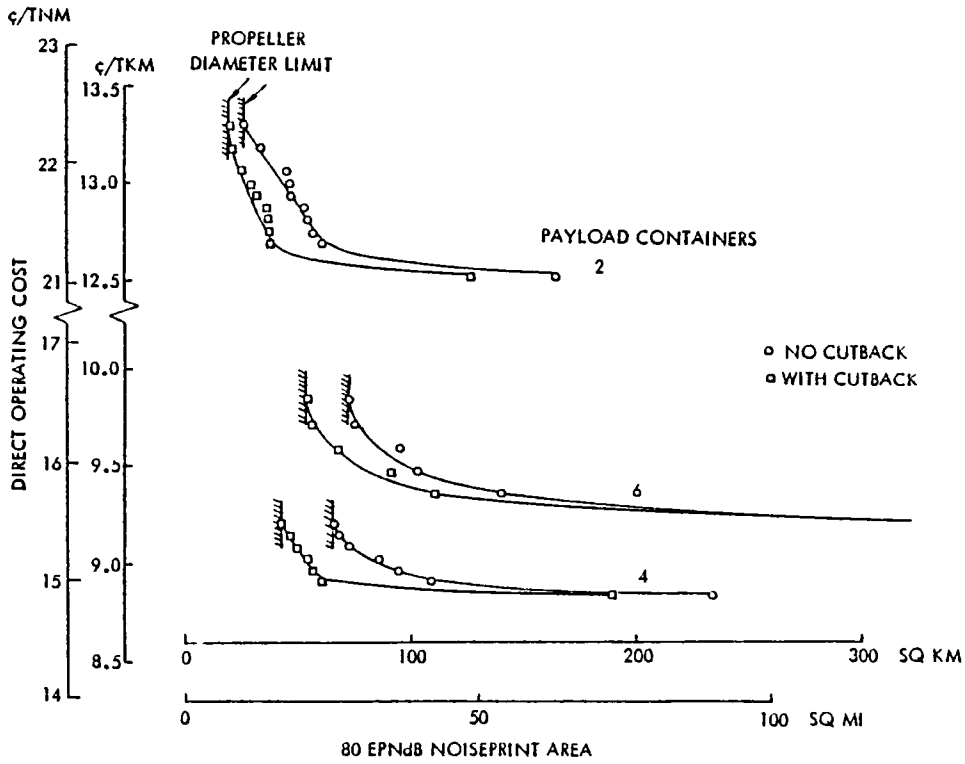

Figure F-24. Effect of Payload on Cost of Quietness for Fuel at 264 $\$/m^3$ (100 ¢/gal)

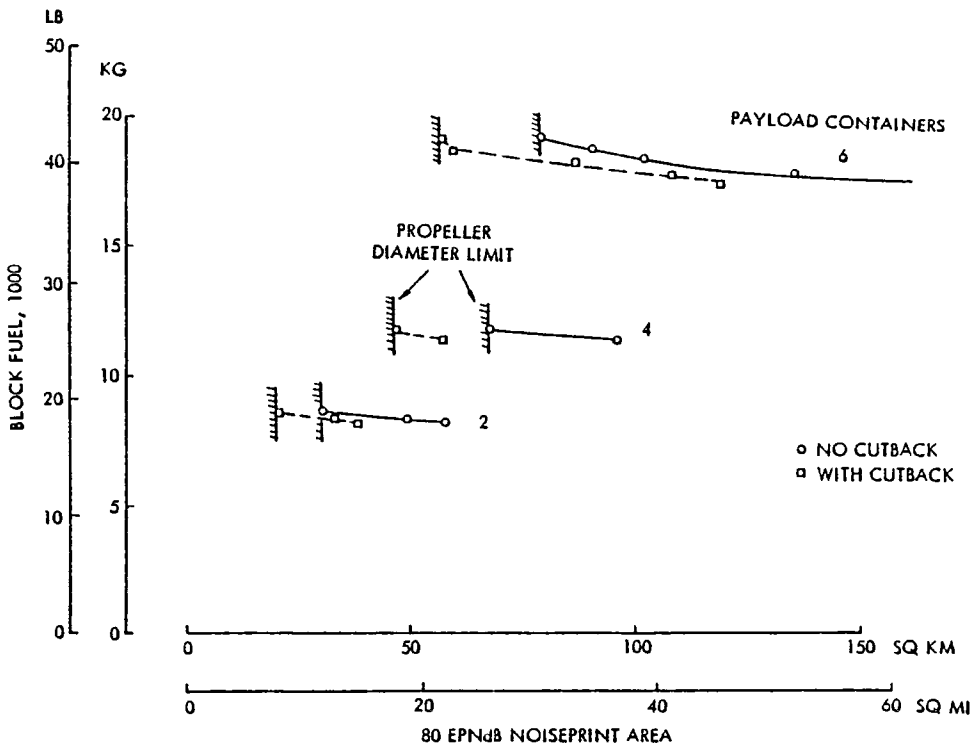

Figure F-25. Effect of Payload on Block Fuel Cost of Quietness

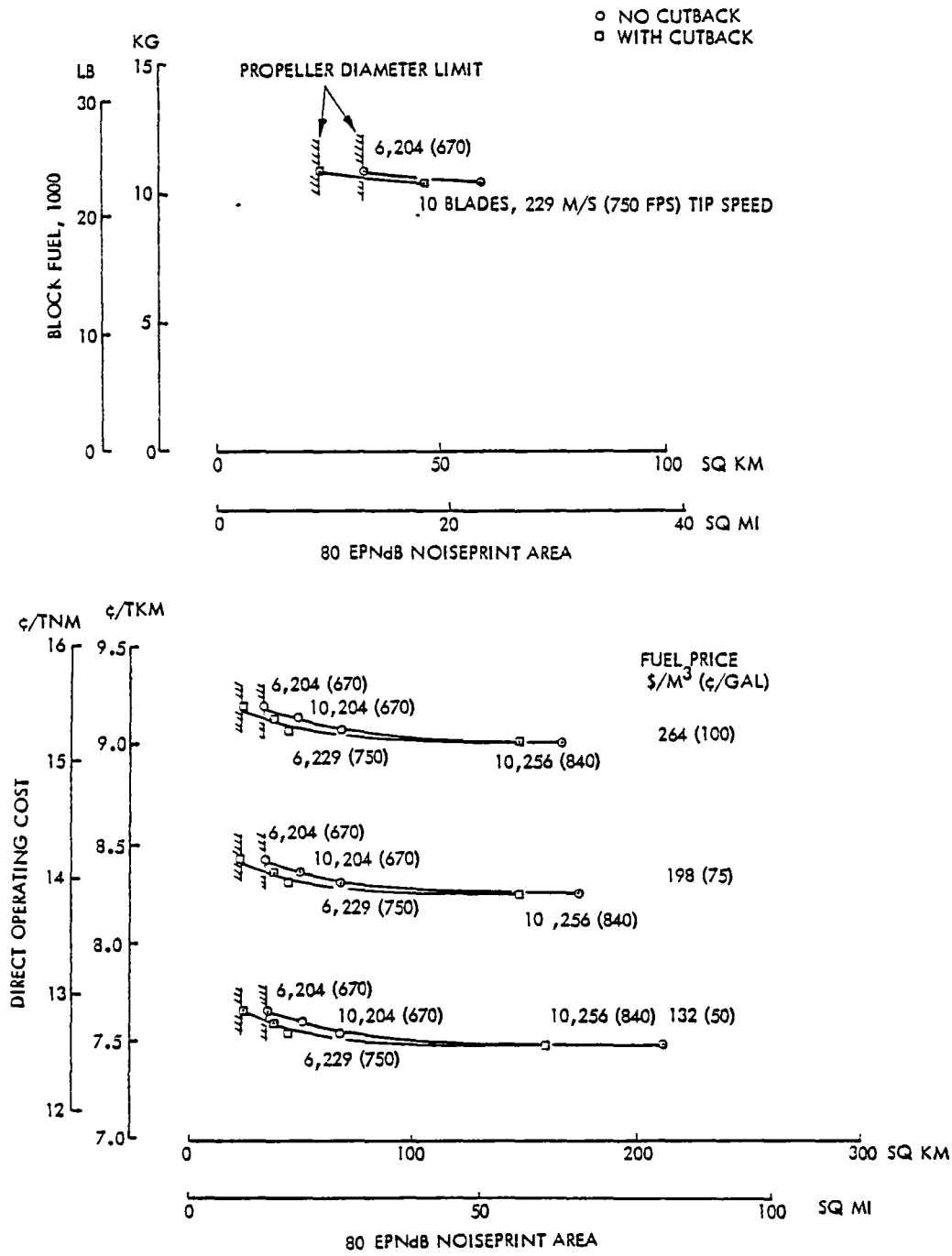

Figure F-26. Cost of Quietness for 0.6 Mach Number and 4-Container Payload

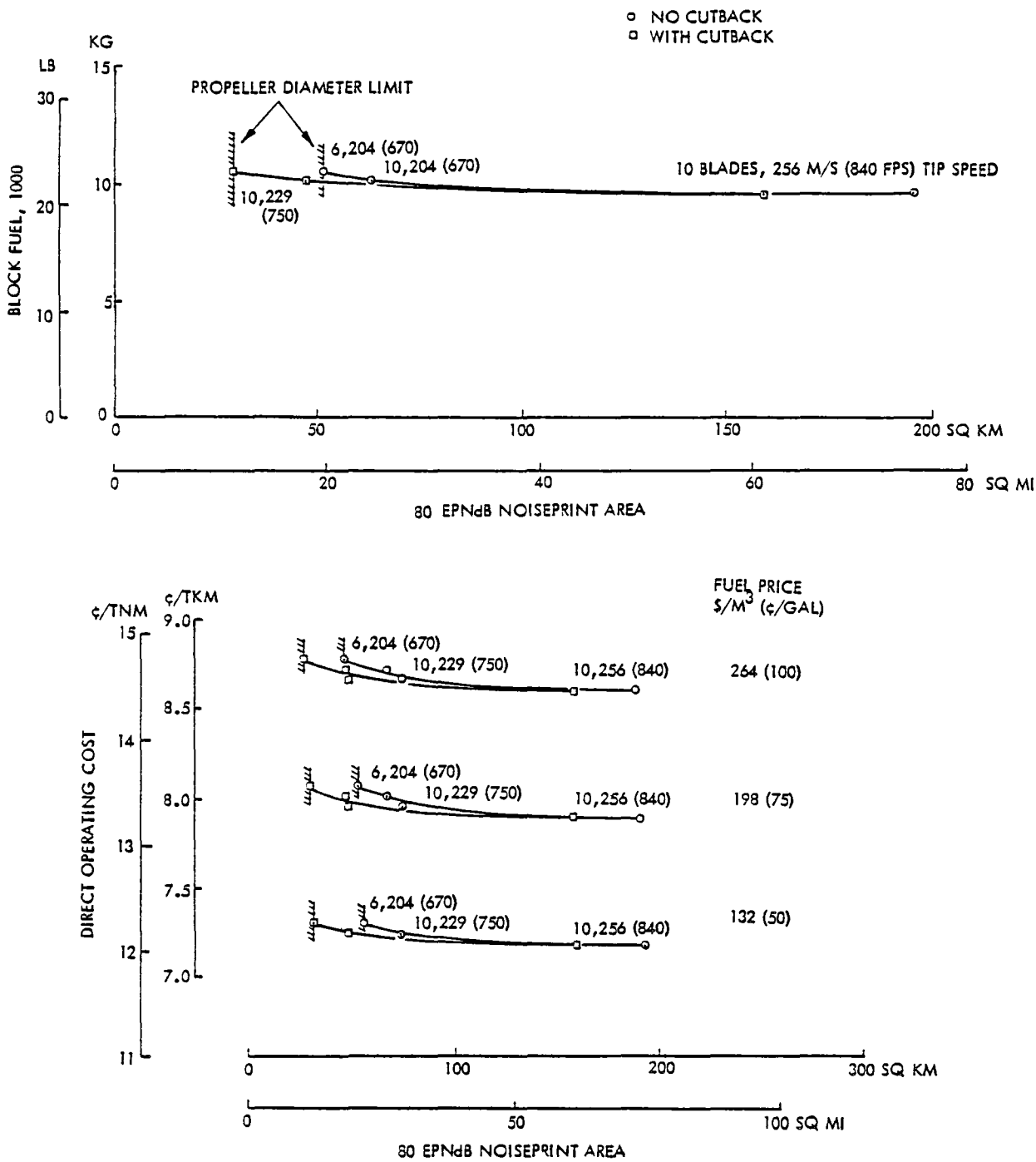

Figure F-27. Cost of Quietness for 0.7 Mach Number and 4-Container Payload

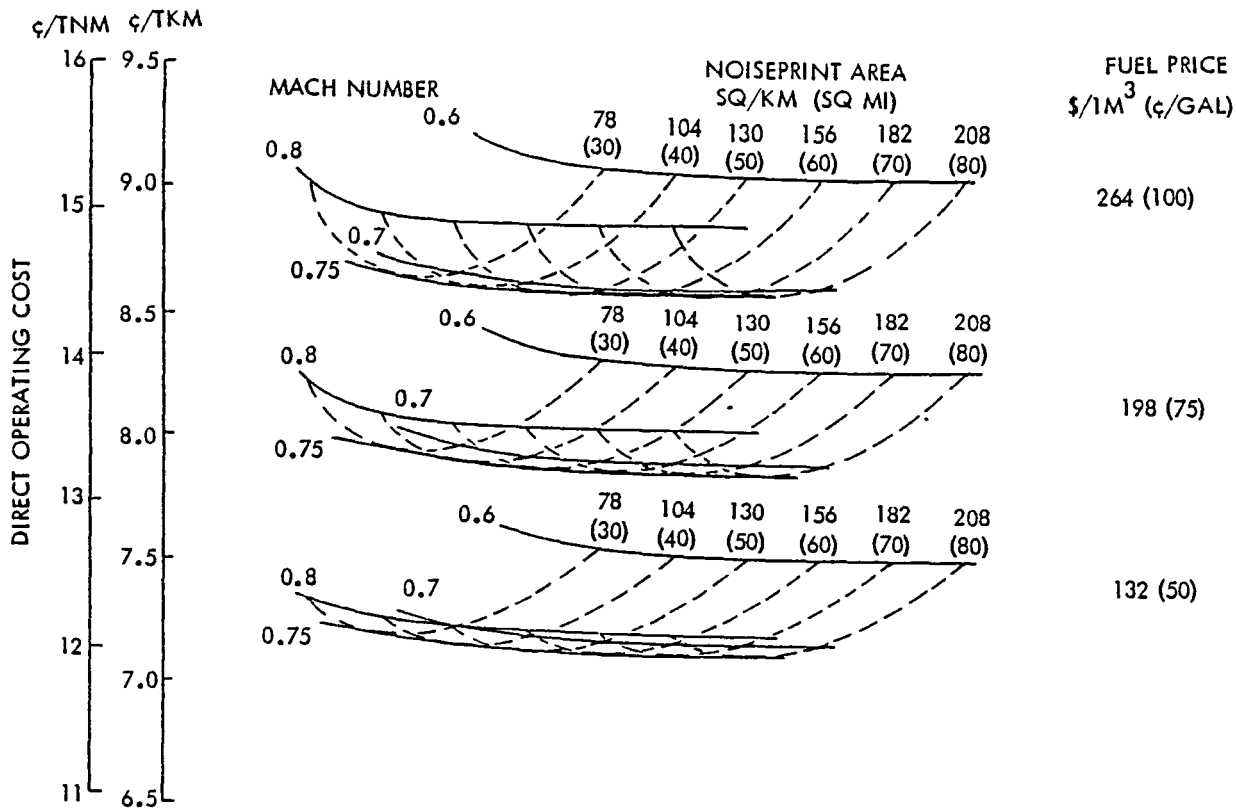

Figure F-28. Effect of Speed on Cost of Quietness for 4-Container Payload Aircraft at Full Power

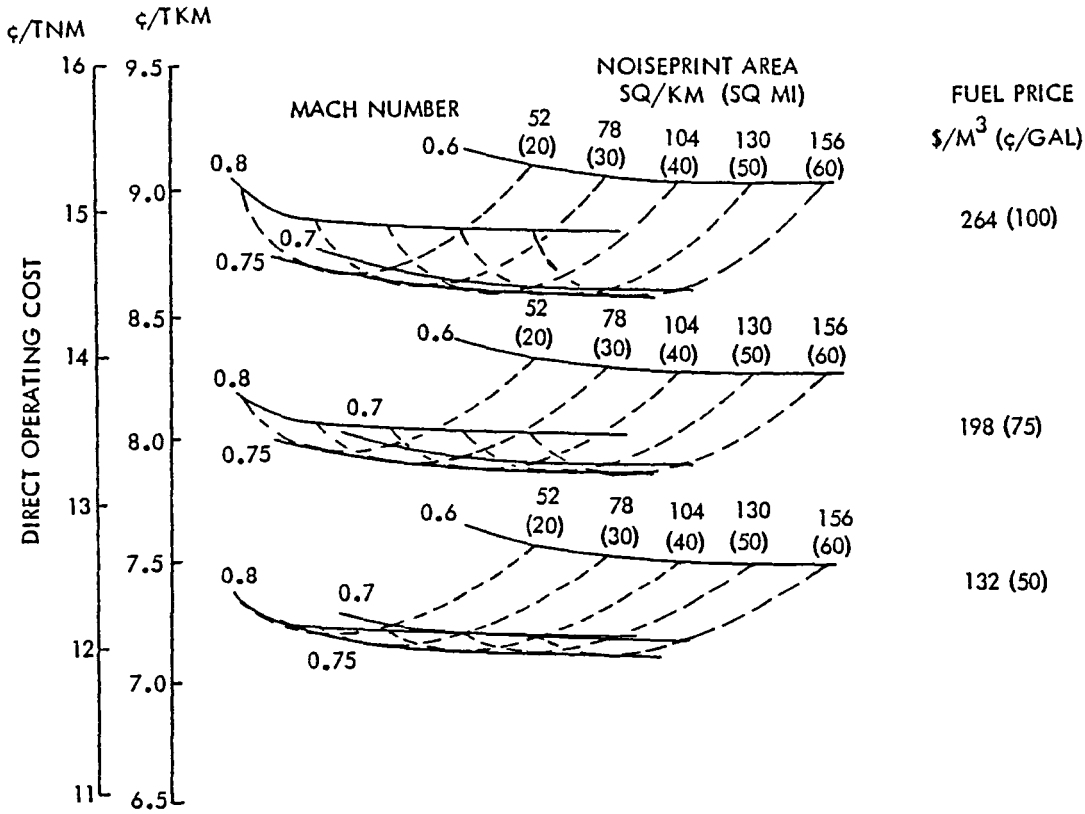

Figure F-29. Effect of Speed on Cost of Quietness for 4-Container Payload Aircraft at Cutback Power

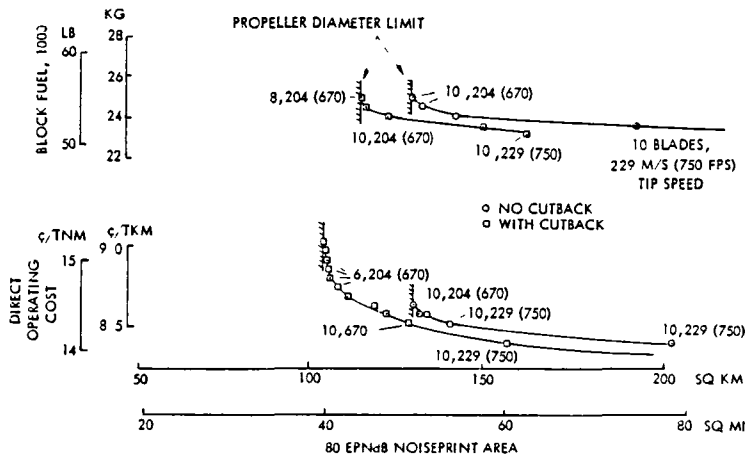

Figure F-30. Cost of Quietness for 0.8 Mach Number and 9-Container Payload

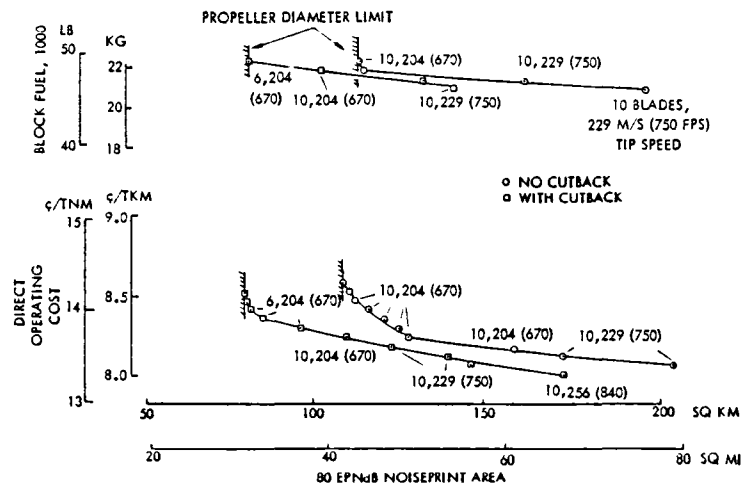

Figure F-31. Cost of Quietness for 0.75 Mach Number and 9-Container Payload

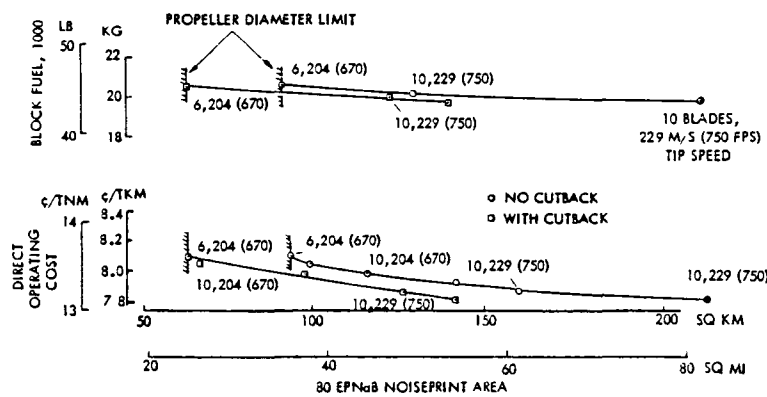

Figure F-32. Cost of Quietness for 0.7 Mach Number and 9-Container Payload

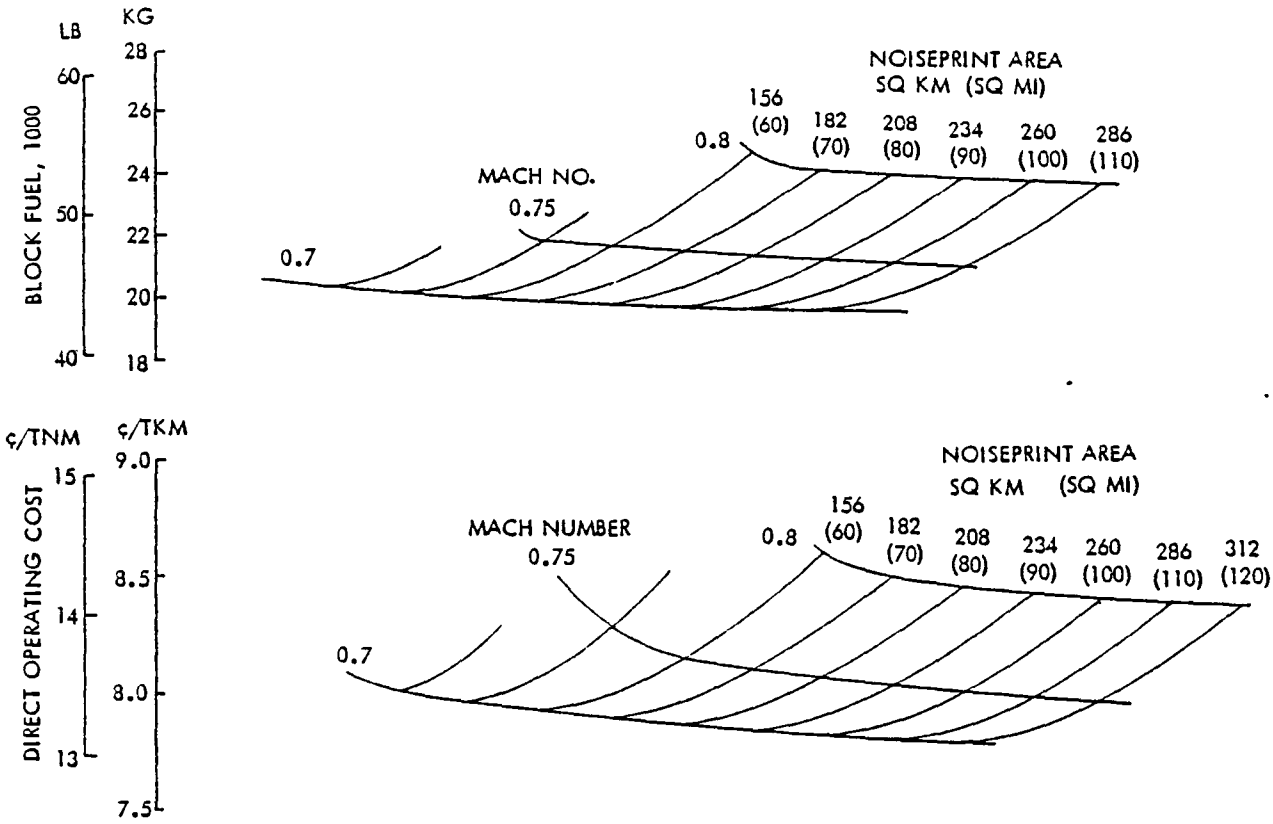

Figure F-33. Effect of Speed on Cost of Quietness for 9-Container Payload Aircraft at Full Power

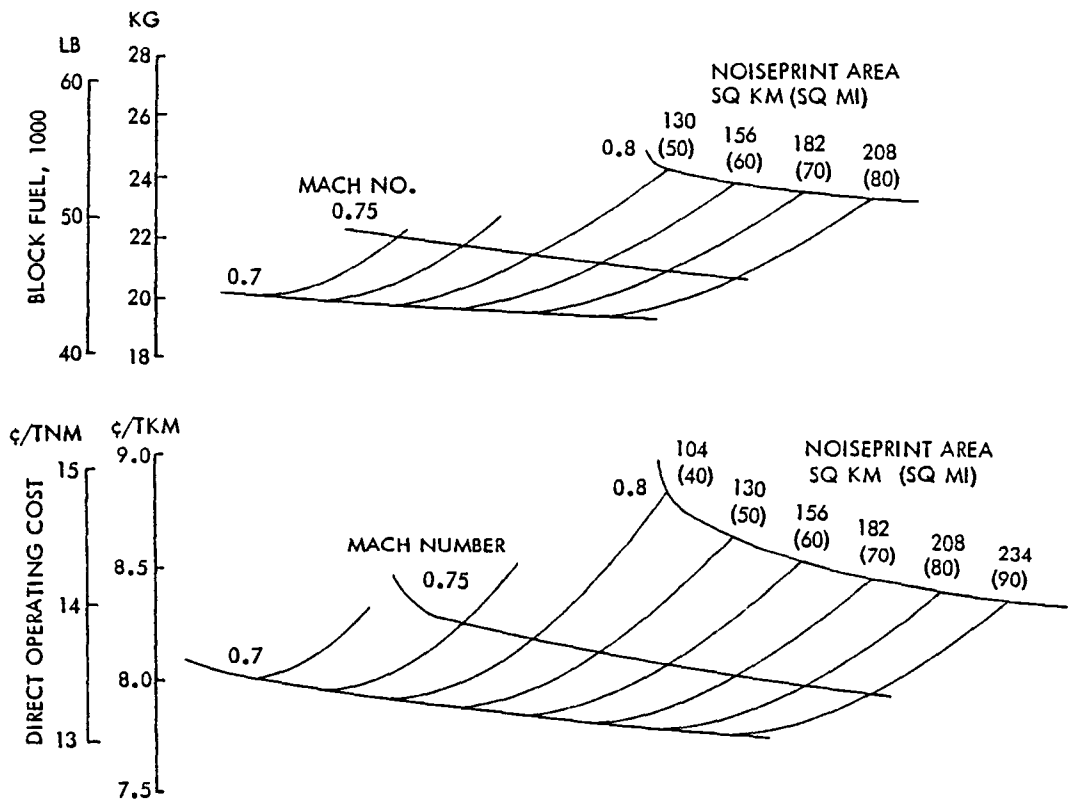

Figure F-34. Effect of Speed on Cost of Quietness for 9-Container Payload Aircraft at Cutback Power

APPENDIX G. PROPELLER NOISE CORRELATION

Much of the thrust of this study is to assess the effect of advanced turboprops on aircraft noiseprint areas. To enhance the credibility of the calculated areas, the major segment of the noiseprint was identified, and the accuracy of the predicted noise was checked for the predominate noise contributor to that segment.

Visual inspection of the noiseprints shown previously in the main portion of this report for the three turboprop aircraft reveals that the takeoff portion of the noiseprint is three to four times that for approach. An indication of the main noise sources contributing to the size of the noiseprint is gained from a check of the noise source distributions over the measuring points. The data shown previously clearly establish that the propeller is the predominate noise source for full power takeoff and sideline conditions, both of which are prime factors related to the size of the takeoff portion of the noiseprint.

The characteristics of the selected aircraft were sent to Hamilton Standard, the developer of the propfan propeller concept, so that they could check the propeller noise predictions with their program. Their predictions of the sound pressure level spectra for the propellers were then combined with the engine and airframe noise predictions of our program (see Appendix C for a description) in a calculation of the equivalent perceived noise levels (EPNL) of the aircraft. Table G-1 compares propeller perceived noise levels (PNLTM) and the resulting EPNLs for the aircraft with the only input difference being that the propeller sound pressure level spectra were predicted by Hamilton Standard* (columns headed H.S.) and Lockheed (LOCK heading) programs. Note that all four conditions are at the FAR 36 measuring points, but the aircraft are flown as specified by FAR 36 for only the cutback takeoff and approach conditions. A normal flight procedure was used for the other two. Also, a constant 3 dB has been added for ground reflection in all cases.

Table G-I. Propeller Noise Prediction Comparison

AIRCRAFT & CONDITION	PROPELLER NOISE PNLTM			AIRCRAFT NOISE, EPNL		
	H S	LOCK	DIFF	H S	LOCK	DIFF
1 COMPROMISE						
NORMAL TAKEOFF	94 65	93 10	1 55	91 90	91 03	0 87
CUTBACK TAKEOFF	87 83	85 42	2 41	89 04	87 21	1 83
SIDELINE	88 00	90 39	-2 39	90 05	91 17	-1 12
APPROACH	97 58	97 73	-0 15	98 58	99 50	0 08
2 QUIETEST						
NORMAL TAKEOFF	95 76	94 89	0 87	92 49	92 28	0 21
CUTBACK TAKEOFF	87 54	84 86	2 68	88 95	87 32	1 63
SIDELINE	86 72	90 96	-4 34	88 92	91 34	-2 42
APPROACH	95 58	92 95	2 63	99 63	99 51	0 12

PROPELLER CHARACTERISTICS

AIRCRAFT	1 COMPROMISE	2 QUIETEST
NUMBER OF BLADES	10	6
TIP SPEED, M S (FT S)	229 (750)	204 (670)
DIAMETER, M (FT)	5 64 (18 5)	6 11 (20 05)
DISK LOADING, KW M^2 (HP FT^2)	402 (50)	345 (43)

NOTE CONDITIONS ARE FAR 36 MEASURING POINTS NORMAL TAKEOFF AND SIDELINE ARE NOT AS PER FAR 36 FLIGHT OPERATIONS

The small difference between the two sets of predictions indicates a much closer correlation between the two methods than was originally anticipated. Lockheed and Hamilton Standard concurred that a better correlation would probably not be obtained within a reasonable level of effort by trying to modify the Lockheed method. Furthermore, the accuracy of the propeller noise prediction methods is thought to be as good or better than that for the engine components and airframe. Consistency in the comparative results of turboprop versus turbofan powered aircraft dictates that further improvements to the propeller noise prediction methods are not warranted without similar efforts on the other noise prediction methods, which is considerably beyond the scope of this study.

---

* Lockheed's propeller noise is predicted by an earlier and less sophisticated version of the Hamilton Standard program. The latest version includes quadrupole and sweep effects that are not in the earlier model, and different approaches are used for ground reflection and unsteady loading.

APPENDIX H. TURBOPROP AIRCRAFT SENSITIVITY STUDIES

This appendix contains the detailed results of the numerous sensitivity studies that were performed for the three selected turboprop aircraft. The particular sensitivity parameters investigated are listed in Table H-I under five general category headings of propulsion system, performance, wing geometry, weight, and economics. Variations of each of the elements under these headings were analyzed to determine the effects on DOC, block fuel, and noiseprint area, which were used as sensitivity indicators, where applicable.*

Unless otherwise noted, only one independent variable is allowed to change in each sensitivity study. In general throughout the sensitivity studies, the DOC variations are for a fuel price of 264 $/m^3$ (100 ¢/gal), and the noiseprint variations are for an 80 EPNdB level. Any exceptions are noted.

PROPULSION SYSTEM

The first four items listed under the propulsion system heading on Table H-I deal exclusively with the propeller subsystem. In contrast, the last parameter is concerned with the performance of the total propulsion system.

* A measure of sensitivity (MOS) for evaluating the impact of each element was defined as the ratio of the percent change realized in one of the indicators divided by the corresponding percent change in the sensitivity parameter. For evaluation purposes, the numerical MOS values are arbitrarily interpreted as follows:

Numerical Evaluation	Qualitative Interpretation
MOS < 1	Negligible
1 ≤ MOS < 2	Marginal
2 ≤ MOS < 5	Significant
MOS > 5	Critical

Table H-I. Turboprop Aircraft Sensitivity Studies

PROPULSION SYSTEM	WEIGHT
o PROP DIAMETER	o PROPULSION SYSTEM
o PROP DISK LOADING	o AIRFRAME
o PROP TIP SPEED	o FUEL
o PROP BLADES	
o THRUST/WEIGHT	ECONOMICS
PERFORMANCE	o STAGE LENGTH
o CRUISE ALTITUDE	o UTILIZATION
o DRAG	o LOAD FACTOR
o FIELD LENGTH	o FUEL PRICE
o APPROACH SPEED	o PROP COST
o GLIDESLOPE	o ENGINE COST
o NOISE LEVEL	o AIRFRAME COST
WING GEOMETRY	o FLYAWAY COST
o ASPECT RATIO	o MAINTENANCE COST
o WING LOADING	

Propeller Diameter

A maximum propeller diameter limit of 6.1 m (20 ft) was adopted because of the following aircraft geometrical considerations. The centerline of the engines, when mounted in aerodynamically optimum positions beneath the wing, is approximately 4.1 m (13.5 ft) above the ground for the three selected aircraft. With a 6.1 m (20 ft) diameter propeller this would leave only a marginal clearance of 1 m (3.5 ft) between the ground and the propeller tip. If a greater clearance is required to avoid propeller damage, then smaller propeller diameters are mandatory, assuming no changes to the aircraft configuration.

The propeller diameter for the No. 2 aircraft is at the limiting value of 6.1 m (20 ft), while the diameters for the other two are below the limit at about 5.6 m (18.5 ft). Figure H-1 shows the effects on the three aircraft of changing the propeller diameter, which may be necessary if other limitations are imposed, such as those indicated.

Of the three aircraft, the noiseprint area for the No. 2 aircraft is much more sensitive to changes in

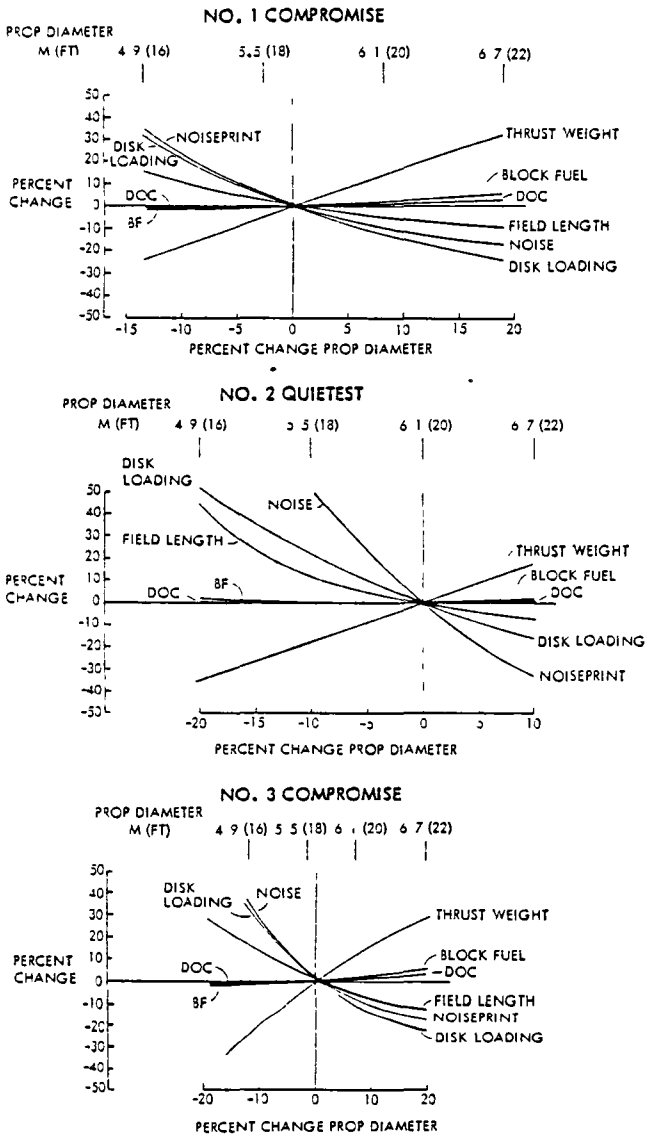

Figure H-1. Propeller Diameter Sensitivity Results for Turboprop Aircraft

propeller diameter than for the other two. There are two reasons for this. First, the No. 2 aircraft has the longest field length of the three, which directly impacts the noiseprint area. It suffers greater increases in field length with decreasing propeller diameter because the tip speed is lower and the takeoff performance is poorest for this aircraft. In fact, if the propeller diameter is decreased by more than 18 percent, the aircraft is not able to comply with the 2440 m (8000 ft) field length limitation. The second reason for the stronger noise sensitivity of the No. 2 aircraft is that it has by far the smallest noiseprint of the three aircraft, and a unit change in area has a more profound effect. For example, a 2.56 sq km (1 sq mi) variation in noiseprint area produces a 5 percent change for the No. 2 aircraft, a 3 percent change for the No. 1 aircraft, and a 1.5 percent change for the No. 3 aircraft.

Some other observations are noteworthy. Variations of the propeller diameter over the ranges shown produce less than a two percent change in direct operating costs. Similarly, less than a four percent change in block fuel is experienced. Exceeding the 6.1 m (20 ft) limit appears to be very beneficial in reducing the noiseprint area for the No. 2 aircraft; in particular, enlarging the propeller diameter by 0.6 m (2 ft) reduces the noiseprint area by 33 percent. This assumes that 0.76 m (2.5 ft) is adequate clearance between the ground and the propeller tip. If it is not, then some modifications to the aircraft will be required, such as a longer landing gear or mounting the engines above the wing, which will penalize the aircraft design and performance.

The large variation in disk loading merely reflects the change in propeller diameter. Recall that disk loading is the ratio of engine power to the square of the propeller diameter. With the engine power held approximately constant, as in these cases, the disk loading curve has a quadratic shape due to the square of the changing propeller diameter.

On the measure-of-sensitivity scale, changing the propeller diameter has a negligible effect on the DOC and block fuel for all three aircraft. The noiseprints of the No. 1 and No. 3 aircraft are, however, significantly affected by changing the propeller diameter, and that for the No. 2 aircraft is critically impacted.

Disk Loading

An alternate approach for showing the effects of variations in propeller diameter is through the propeller disk loading, which is inversely proportional to diameter squared. Thus, the results outlined in the preceding section

are presented in Figure H-2 as a function of the sea-level disk loading for the three aircraft. Increasing the disk loading means that the propeller diameter becomes smaller for a given power level, and, as a result, field lengths are longer and noiseprint areas are larger. Both direct operating costs and block fuel were found to be relatively insensitive to changes in propeller diameter and are likewise insensitive to changes in disk loading.

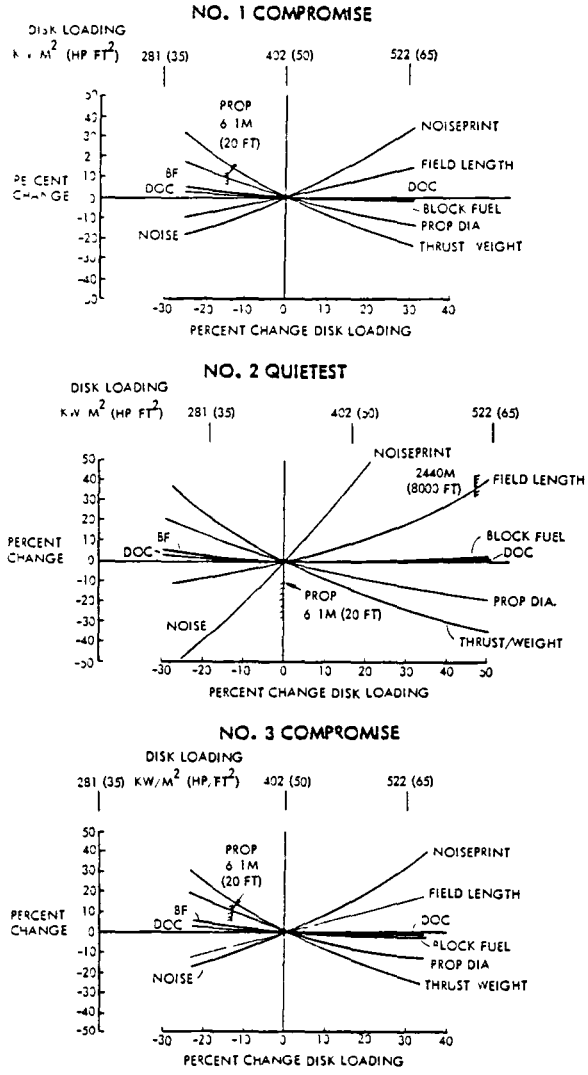

Figure H-2. Disk Loading Sensitivity Results for Turboprop Aircraft

Study limitations on field length and propeller diameter have been noted on the figures, where applicable. The propeller diameter limit restricts the No. 1 and No. 3 aircraft to a maximum reduction in disk loading of about 12 percent, while no reduction is permitted for the No. 2 aircraft. The field length limit is much less restrictive because it impacts only the No. 2 aircraft, and then, only after the disk loading has increased by 47 percent.

The measure of sensitivity for the effect of disk loading on DOC and block fuel is negligible for all three aircraft. Marginal ratings are given to the effect on noiseprints for the No. 1 and No. 3 aircraft, while a significant rating applies to the effect on the No. 2 aircraft.

Propeller Tip Speed

The effects on the three aircraft of changing propeller tip speed are presented in Figure H-3. In all cases, varying the tip speed over the range shown produces less than a 5 percent change in aircraft block fuel, DOC, propeller diameter, or ramp weight. The major effects are on the thrust/weight ratio and the noiseprint area. For the No. 1 and No. 3 aircraft, the thrust/weight ratio changes by up to $\pm$ 20 percent, and correspondingly, the noiseprints change by more than $\pm$100 percent.

Tip speed has a greater effect on the No. 2 aircraft, which experiences more than a 40 percent increase in the thrust/weight ratio and almost an order of magnitude increase in the noiseprint area. In this case, as for the other two, the noiseprint increases at a greater rate at the higher tip speeds than at the lower values.

The measure-of-sensitivity ratings for all three aircraft to changing propeller tip speed indicates negligible effects on DOC and block fuel, but critical impact on the noiseprints.

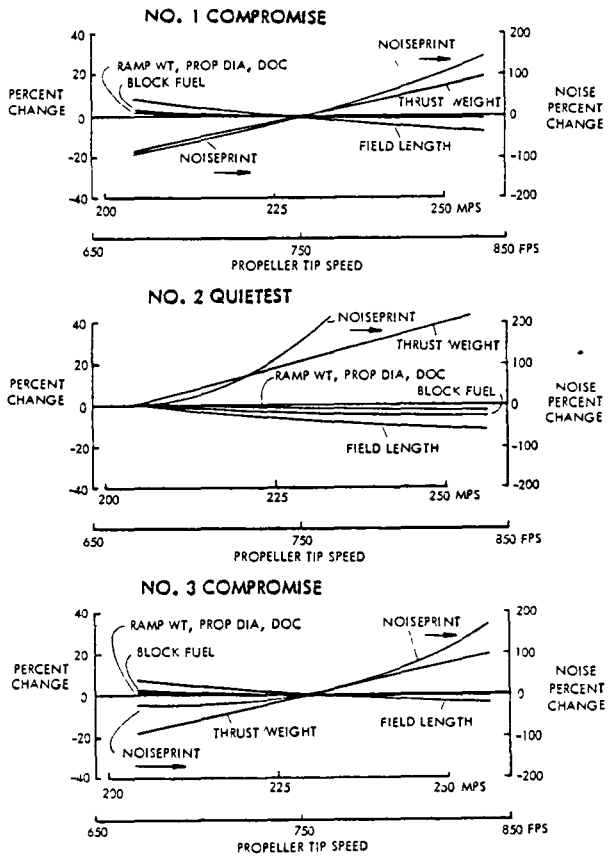

Figure H-3. Propeller Tip Speed Sensitivity Results for Turboprop Aircraft

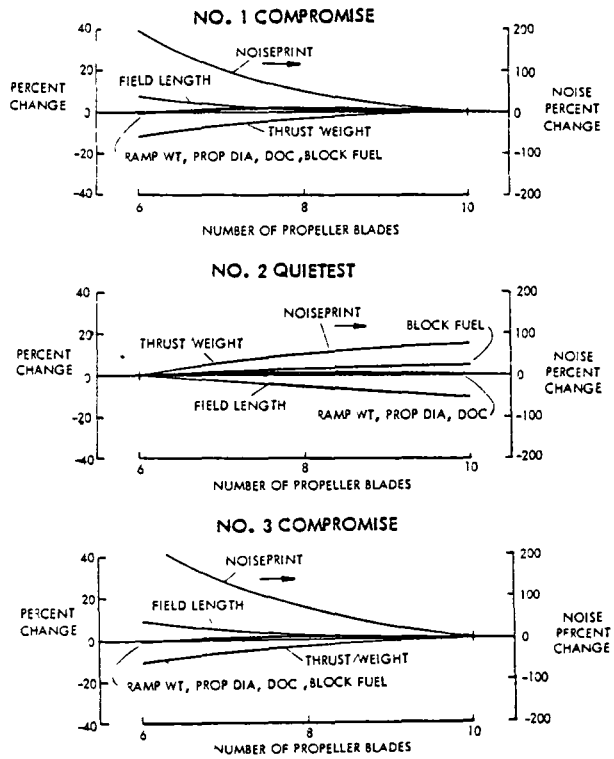

Figure H-4. Propeller Blade Count Sensitivity Results for Turboprop Aircraft

Number of Propeller Blades

Changing the number of propeller blades, as shown in Figure H-4, has only a minimal effect on the ramp weight, block fuel, DOC, and propeller diameter of the three aircraft. Reducing the number of blades on the No. 1 and No. 3 aircraft does, however, cause the thrust/weight ratio to drop, which in turn causes a small increase in field length but a significant increase in noiseprint area due to the poorer climb capabilities. Conversely, increasing the number of blades on the No. 2 aircraft provides a greater thrust/weight ratio and a shorter field length. The noise corresponding to the increased engine size is offset by the greater climb capability so that the net effect is essentially no change in the noiseprint area.

Changing the number of propeller blades has a critical effect on the noiseprints of the No. 1 and No. 3 aircraft, but a negligible effect for the No. 2 aircraft, according to the measure-of-sensitivity ratings. Negligible ratings apply to all three aircraft when evaluating the effect of the number of propeller blades on DOC and block fuel.

Thrust/Weight Variation

Figure H-5 presents the same results as shown previously in Figure H-1 except that now thrust/weight is the abscissa instead of propeller diameter. In all three cases, aircraft block fuel and DOC are insensitive to changes in the thrust/weight ratio. Field length is slightly affected by thrust/weight, but the most significant change occurs to the noiseprint, which is sensitive

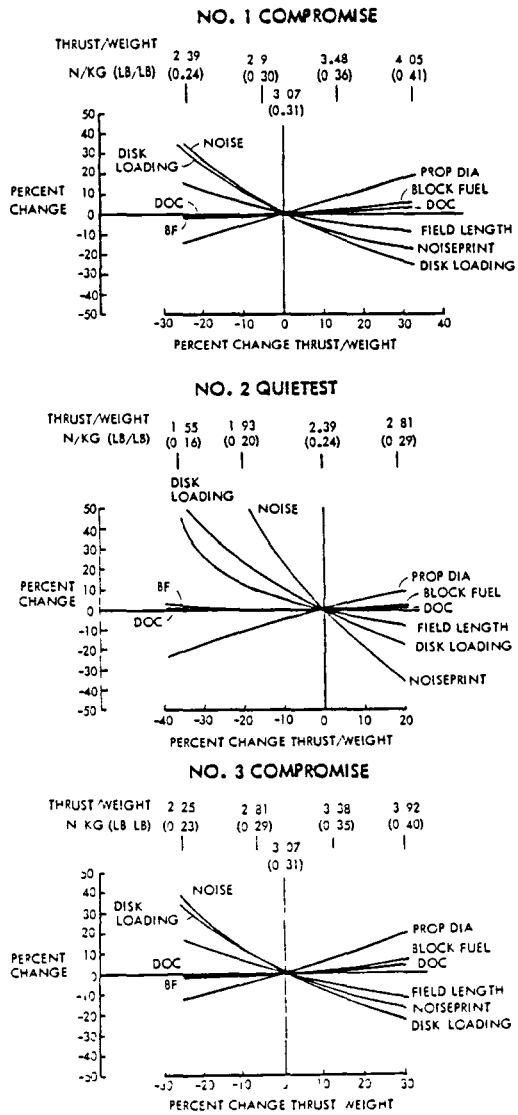

Figure H-5. Thrust/Weight Sensitivity Results for Turboprop Aircraft

to the aircraft thrust level and capability to climb.

The measure-of-sensitivity ratings for the effects of thrust/weight on noiseprints are marginal for the No. 1 and No. 3 aircraft and significant for the No. 2 aircraft. Negligible ratings are indicated for the effect on DOC and block fuel for all three aircraft.

PERFORMANCE

Six performance-related areas were considered as part of the effort to identify those parameters that have the greatest impact on the design of the three selected turboprop aircraft. In particular, variations in initial cruise altitude, aircraft drag, field length, approach speed, glideslope on approach, and noise level were addressed.

Cruise Altitude

Sizing the turboprop aircraft for an initial cruise altitude other than the base value of 10.1 km (33,000 ft), produces the effects illustrated in Figure H-6. The most important result

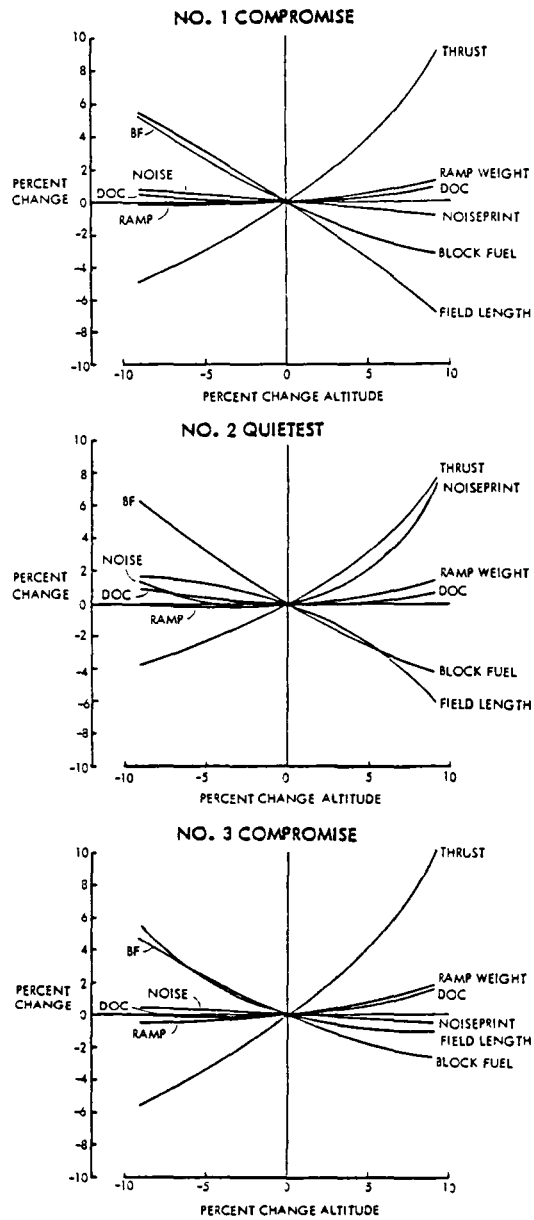

Figure H-6. Altitude Sensitivity Results for Turboprop Aircraft

is that in all three cases, the base altitude provides either the minimum value or is within 0.8 percent of the minimum value for DOC, noiseprint, and ramp weight.

The sea-level-rated thrust of the engines varies somewhat proportionately with altitude because of the lapse rate effect, and as the rated thrust changes, so does the field length. Block fuel follows the expected trend of decreasing with higher altitude. It tends toward a definite minimum at some higher altitude greater than that which minimizes DOC or ramp weight.

In terms of the measure-of-sensitivity ratings, altitude changes have a negligible effect on the noiseprint, DOC, and block fuel for all three aircraft.

Aircraft Drag

Like others in the industry, we are concerned by the limited data on propeller swirl and propeller/wing interference drag effects. Some other features of an aircraft also pose problems in calculating its total drag. For example, calculating the drag contributions for the wing/fuselage fillet, the fuselage afterbody, and the landing gear pod are as much an art as a science. Only through expensive and time-consuming wind tunnel tests can an accurate measure be obtained for the actual drag of a particular design. Such an approach is obviously not suitable for a parametric aircraft preliminary design study; empirical methods for estimating the drag must necessarily be employed.

Recognizing that these methods are approximate, variations were considered for the drag estimates of the selected aircraft. Figure H-7 shows the effects of changing the drag for reductions of up to 20 counts* and for increases of up to 40 counts. The only positive benefit of increased drag is that the larger engine size required does shorten the field length and thereby helps to minimize the effect on the noiseprint. Of the other two major measures, the block fuel changes at nearly twice the rate of the DOC for a unit change in drag. For a one percent change in drag, the block fuel changes by slightly more than one percent, while the DOC changes by about two-thirds of one percent.

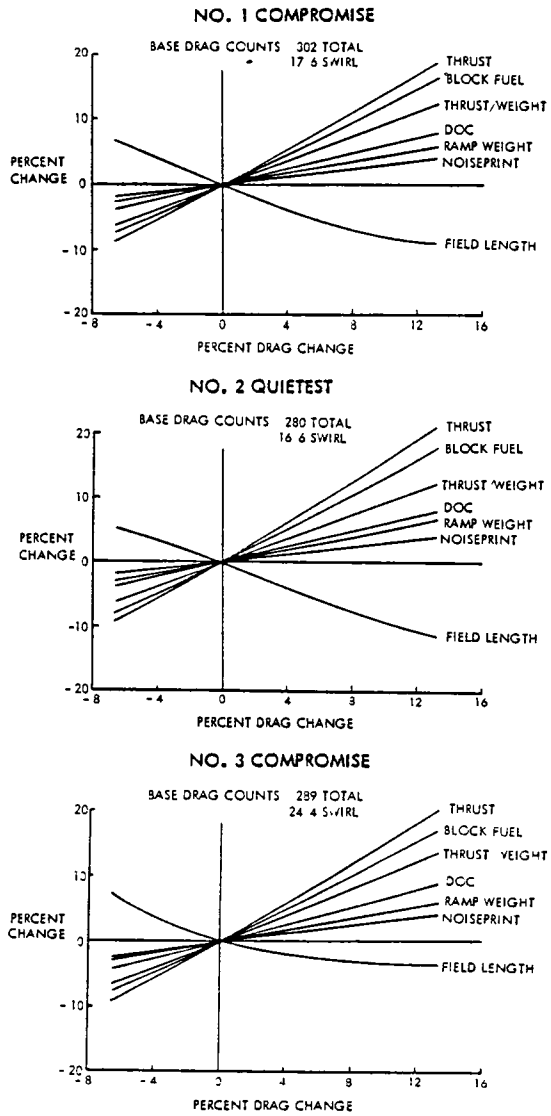

Figure H-7. Aircraft Drag Sensitivity Results for Turboprop Aircraft

Of the three aircraft, the No. 2 aircraft is most noticeably affected by changing the drag, and the No. 3 aircraft is least affected. Generally, there is not a lot of difference among the three aircraft in the drag effects

* One count is 0.0001

on a particular parameter with the exception of the field length. The reason for the different field length trends is that the field length for each aircraft is the longer of the balanced field length and the FAA factored field length. The No. 3 aircraft has the factored field length, while the other two aircraft have their field lengths defined by balanced field conditions.

Drag changes to the three aircraft have a marginal effect on the block fuel and a negligible effect on the noiseprint and DOC, according to the measure-of-sensitivity ratings.

Field Length

All three aircraft take off in field lengths considerably shorter than the limit imposed for this study. Figure H-8 shows the effects of designing these aircraft for other field lengths by allowing the disk loading to change. Note that the propeller diameter limit precludes any reduction in field length of the No. 2 aircraft. For the other two aircraft, some reduction in field length is permitted before the propeller limit is reached.

Both DOC and block fuel are only negligibly affected by changing the field length performance through variation of the disk loading. The noiseprint, however, is significantly altered by these changes.

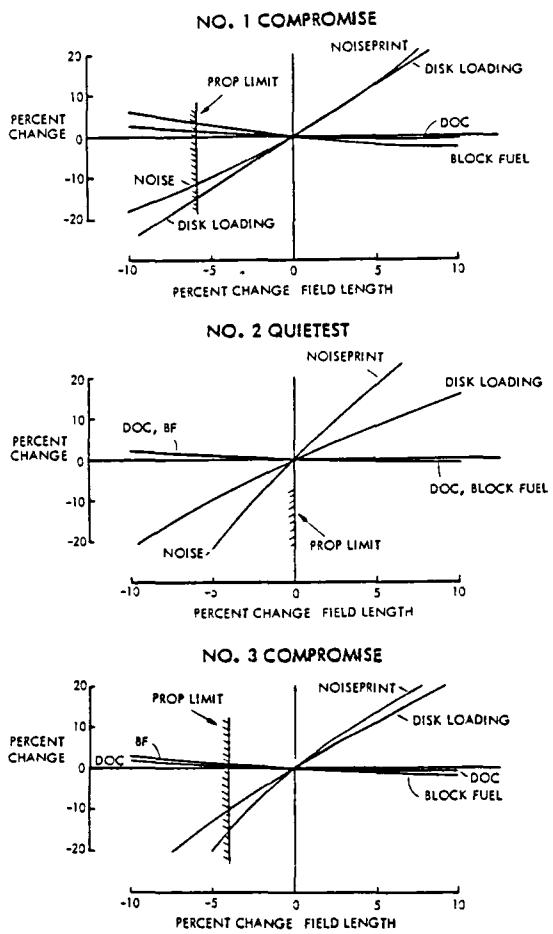

Figure H-8. Field Length Sensitivity Results for Turboprop Aircraft

Approach Speed

All three aircraft are designed for the limiting approach speed of 69 m/s (135 kt). The effects of changing this limit are shown in Figure H-9. Only a four percent increase in approach speed is permitted before all three aircraft become constrained by the projected limit on available lift technology. Even if the lift limit is relaxed, the No. 1 and No. 2 aircraft quickly collide with the fuel volume limit after an additional two percent increase in approach speed; that is, the wings do not have enough volume to carry the fuel needed for the specified range.

Several things occur as the approach speed limit is lowered. The most obvious is that the wing loading decreases rapidly, thereby promoting a proportionately large increase in wing area. This area becomes even larger during the reiterative design process as the aircraft structure, propulsion system, and block fuel grow to accommodate the larger wing size. Simultaneously, the propeller diameter increases with the requirement for more thrust to fly the larger aircraft. Although not shown in the figures, the No. 1 and No. 3 aircraft reach the 6.1 m (20 ft) propeller diameter limit for decreases in approach speed of more than 20 percent.

Over the range of approach speed variations that produce valid aircraft, the No. 1 aircraft experiences negligible effects on DOC, block fuel, and noiseprint due to changing the approach speed. The No. 2 and No. 3 aircraft, however, undergo marginally

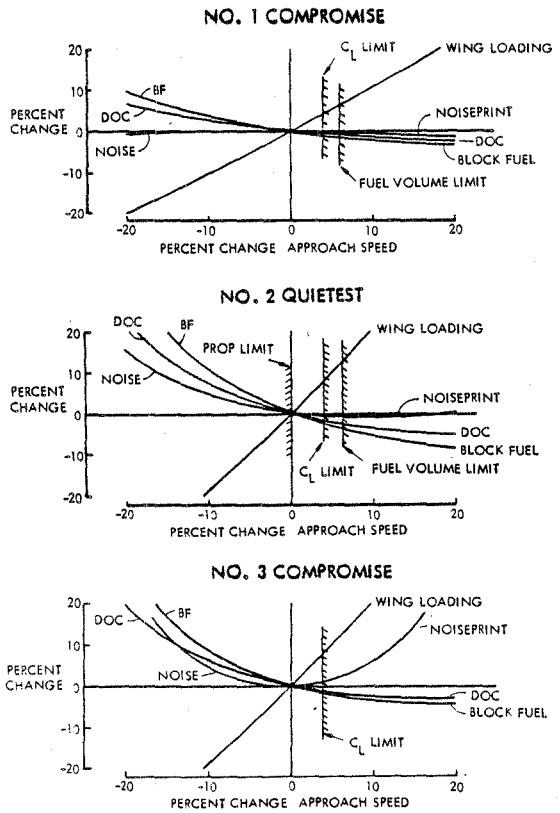

Figure H-9. Approach Speed Sensitivity Results for Turboprop Aircraft

significant changes in both DOC and block fuel.

Glideslope

All of the noiseprints were calculated for an approach flight profile that is in accord with the FAR standard 0.05-rad (3-deg) glideslope. The sensitivity of the noiseprints for the base aircraft was investigated when they are operated on a 0.1-rad (6-deg) glideslope. As indicated by the results in Figure H-10, this 0.05-rad (3-deg) change in glideslope produces less than a 3-percent reduction in noiseprint area. There are two reasons for this small effect. The most significant is that approach contributes only 20 to 30 percent of the total noiseprint. The second reason is related to the effect of the changing glideslope on aircraft altitude and speed. On the 0.1-rad (6-deg) glideslope, the aircraft altitude is twice that for a 0.05-rad (3-deg) glideslope at a particular distance from the airport threshold. Although this increased altitude has a positive effect on reducing the noiseprint, the amount of the reduction is essentially cancelled because the aircraft's higher speed results in a louder noise source.

The effect of glideslope on the noiseprint for all three aircraft is rated negligible in terms of the measure of sensitivity.

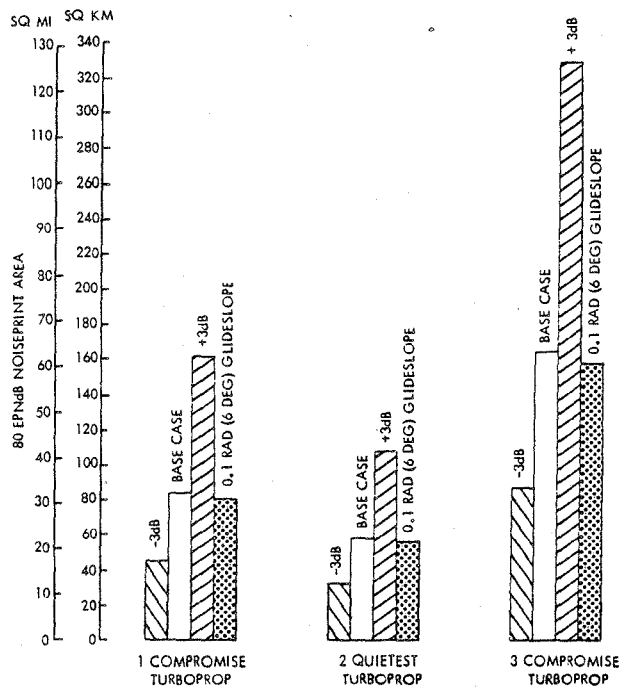

Figure H-10. Glideslope and Noise Source Level Sensitivity Results for Turboprop Aircraft

Noise Source Level

Figure H-10 also shows what the effect will be if the predicted level for the noise source is off by ± 3 dB. This amount of variation causes the 80 EPNdB noiseprint area to change by approximately a factor of two for all three turboprop aircraft. In terms of percentages, a 3-dB increase in the noise source produces nearly a 100 percent increase in the noiseprint area, while a 3-dB noise reduction decreases the noiseprint by about 50 percent.

According to the measure-of-sensitivity ratings, the noiseprints of

the three aircraft are critically affected by a 3-dB variation in the noise source level.

WING GEOMETRY

The two parameters used to determine the sensitivity of the selected aircraft to changes in wing geometry are the wing loading and aspect ratio.

Aspect Ratio

Variations in wing aspect ratio were considered with the disk loading of each aircraft held constant. As noted on Figure H-11, attempts to reduce the aspect ratio are restricted by the propeller diameter limit. In fact, for the No. 2 aircraft no reductions are permitted unless the limit is relaxed.

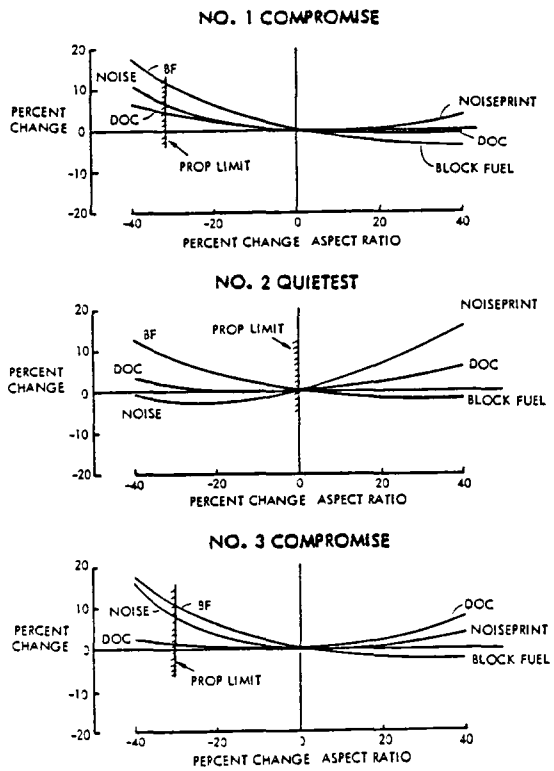

Figure H-11. Wing Aspect Ratio Sensitivity Results for Turboprop Aircraft

The sensitivity study results confirm that the aspect ratio for each aircraft gives the minimum DOC and noiseprint. Changing the aspect ratio merely penalizes the aircraft by a small amount. The effect is rated negligible for the measure of sensitivity.

Wing Loading

Figure H-12 shows that the three aircraft are relatively insensitive to changes in wing loading. Due to the approach speed limit, only lower wing loadings are valid, and they are not desirable because of the penalties incurred. The penalties are sufficiently small to be rated negligible on the measure-of-sensitivity scale.

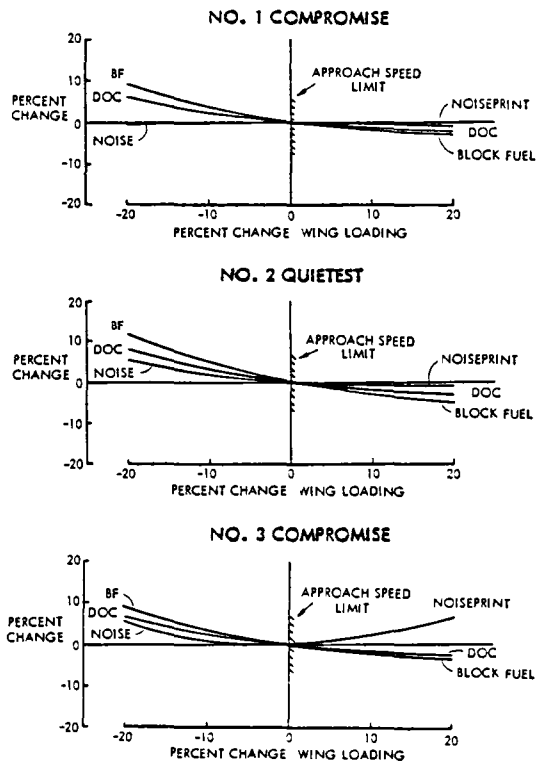

Figure H-12. Wing Loading Sensitivity Results for Turboprop Aircraft

WEIGHT

The sensitivities of the direct operating costs for the selected aircraft were assessed for variations in the weight estimates for three major categories of propulsion, airframe, and fuel. For this assessment, the aircraft ramp weights were held constant.

Changes in the weights of particular categories were compensated for by equivalent, but opposite, changes in payload.

The results of the weight sensitivities are depicted in Figure H-13. The changes in DOC reflect changes in the payload as well as in the costs of the propulsion system, airframe, or fuel commensurate with the particular weight changes. As indicated by the results, a given percent change in airframe weight has a significant impact on the percent DOC change for all three aircraft. In comparison, equal percent changes in fuel and propulsion weights tend to have a much smaller effect on the percent change in DOC.

Another observation of interest is that nearly equal percent changes in DOC are realized for all three aircraft for an equivalent percent change in propulsion weight. A similar effect occurs for variations in percent fuel. In contrast, different changes in percent DOC are experienced for the three aircraft for a given percent change in airframe weight.

A negligible measure-of-sensitivity rating describes the effect of propulsion and fuel weight changes on DOC for all three aircraft. Changing the airframe weight has a marginal effect on DOC for the No. 1 and No. 3 aircraft and is barely significant for the No. 2 aircraft.

ECONOMICS

A number of economic sensitivity studies were conducted to determine the effects of varying stage length, annual utilization rate, load factor, and fuel price. Effects were also estimated for varying the costs of the propeller, engine, airframe, total aircraft, and maintenance.

Stage Length

Flying the selected aircraft over stage lengths shorter than the design range of 4250 km (2295 n.mi.) produces the effects shown in Figure H-14. In all cases, the aircraft design and

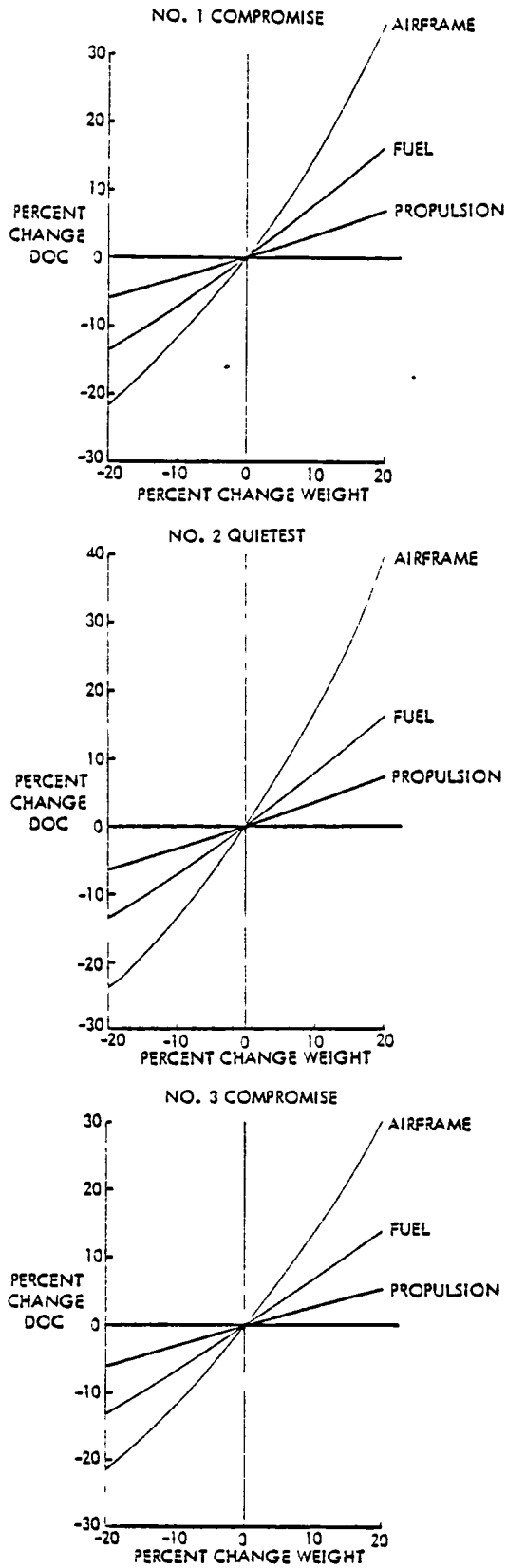

Figure H-13. Weight Sensitivity Results for Turboprop Aircraft

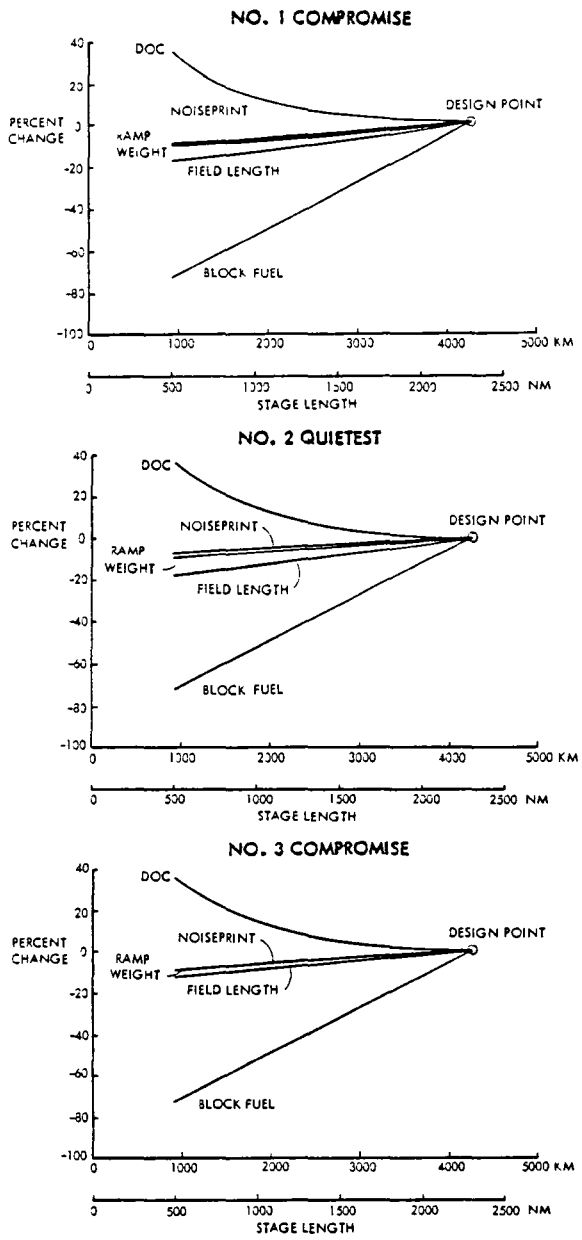

Figure H-14. Stage Length Sensitivity Results for Turboprop Aircraft

payload remain unchanged; only the fuel carried is reduced commensurate with the shorter range to be covered. As a result of the reduction in fuel, the ramp weight goes down, the field length is shortened, and consequently, the noiseprint becomes smaller.

DOC is the only parameter which is adversely impacted by the reduced range. This is as expected because good design practice dictates that minimum DOCs always occur at the design point range.

In terms of our measure of sensitivity, the percent change in DOC and noiseprint are rated negligible, while that for block fuel is between negligible and marginal.

Annual Utilization

Figure H-15 indicates the maximum potential reduction in DOC due to increasing the annual unit utilization from 3000 to 6000 hours. To understand

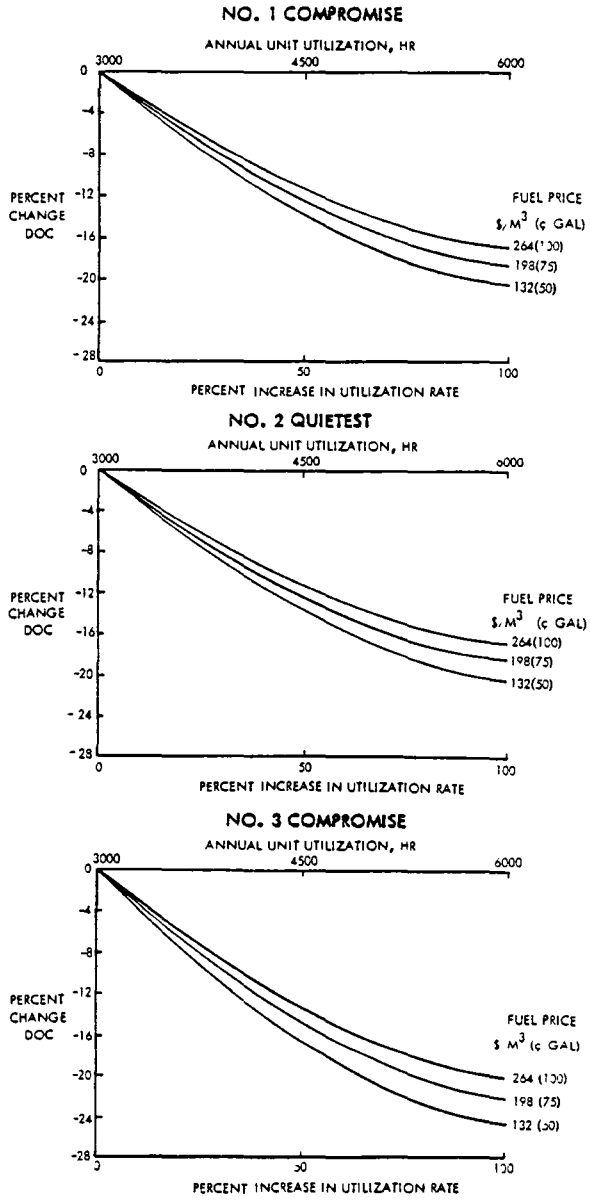

Figure H-15. Utilization Sensitivity Results for Turboprop Aircraft

why the data presented form an upper bound on the amount of DOC reduction, two simplifying assumptions must be reviewed. First, the fleet size was held constant and the productivity was allowed to increase. To appreciate the significance of this assumption, consider that if the productivity requirement is unchanged, then fewer aircraft would be required for the higher utilization. This would be reflected in a smaller DOC reduction because the unit aircraft cost and the depreciation that is included in the DOC would increase due to less benefit from the production learning curve and a larger allotment of the R&D costs to each aircraft.

The second simplifying assumption was that the aircraft have the same 15-year calendar lifetime regardless of the annual utilization. If the 15-year period were treated as an operational lifetime, the aircraft depreciation cost per hour of use would remain constant with increasing annual utilization rather than decreasing, and the DOC reduction would be smaller.

The figures show that, as the fuel price increases, smaller DOC reductions are realized at a particular utilization. This occurs because the fuel cost contribution to DOC increases while the portion due to depreciation decreases.

Greater percent reductions in DOC are experienced by the No. 3 aircraft than by the other two at a given utilization and fuel price because it is more energy efficient. That is, the No. 3 aircraft requires less fuel to carry a unit of payload for a unit distance. Because of this, the portion of DOC contributed by fuel is relatively smaller for the No. 3 aircraft than for the other two, so that depreciation has a stronger effect.

The potential percent change in DOC appears to be substantial; however, when the amount of change in utilization is taken into account, utilization has a negligible effect on DOC according to the measure-of-sensitivity ratings.

Load Factor

A reduction in the load factor from 100 to 85 percent has the effects shown in Figure H-16 for the three aircraft. With a 15-percent reduction in payload, the aircraft requires less fuel to fly the mission range, and the ramp weight is reduced accordingly. This reduced ramp weight results in a shorter field length and a smaller noiseprint. Only the DOC is adversely affected by carrying less than the design payload.

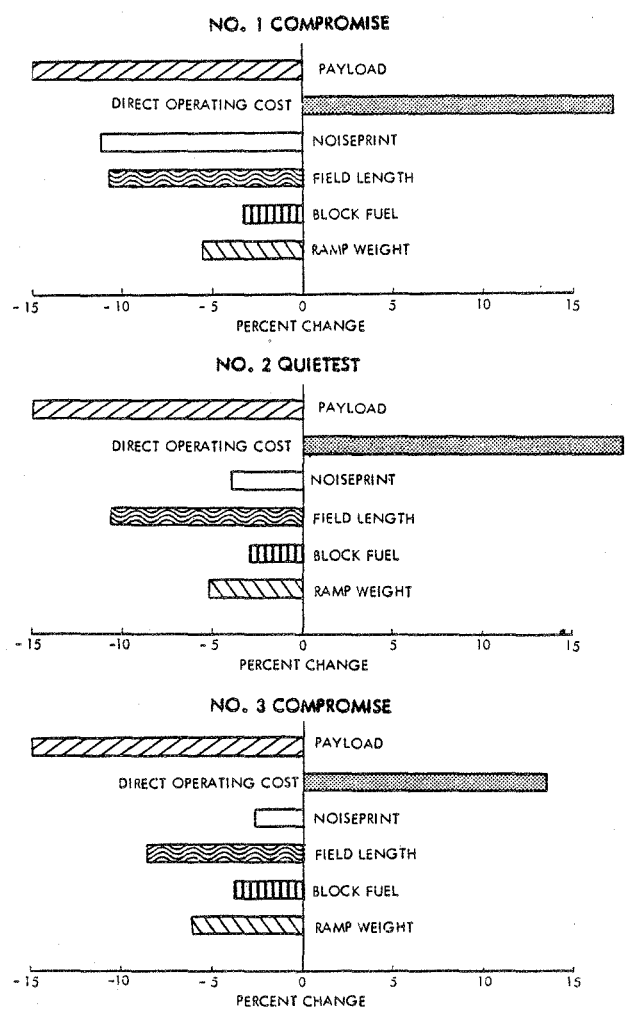

Figure H-16. Load Factor Sensitivity Results for Turboprop Aircraft

The measure-of-sensitivity rating for the reduction in load factor indicates a negligible effect on the block fuel and noiseprint for all three aircraft and a marginal influence on the DOC values.

Fuel Price

Figure H-17 shows the percent change in DOC that results when the fuel price is increased from 264 $/m^3 (100 ¢/gal) up to 792 $/m^3 (300 ¢/gal). Even though substantial changes in DOC are indicated, when the corresponding change in fuel price needed to produce the DOC change is accounted for, the measure-of-sensitivity rating is negligible.

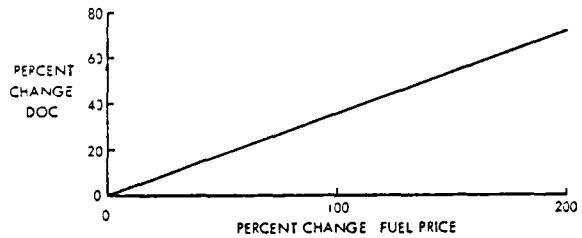

Figure H-17. Fuel Price Sensitivity Results for Turboprop Aircraft

Propeller Cost

Propeller cost changes as great as ± 50 percent were investigated and found to have a negligible effect on the DOCs of the three selected aircraft. For example, a 10-percent change in propeller cost produces less than a 0.1-percent change in DOC. As illustrated in Figure H-18, this result becomes more prominent as fuel price is increased. What happens is that the greater the fuel price, the larger the percentage contribution of fuel to DOC and the smaller that of items that are included in depreciation. Thus, the higher the fuel price, the smaller the percent change in DOC for a given change in propeller cost.

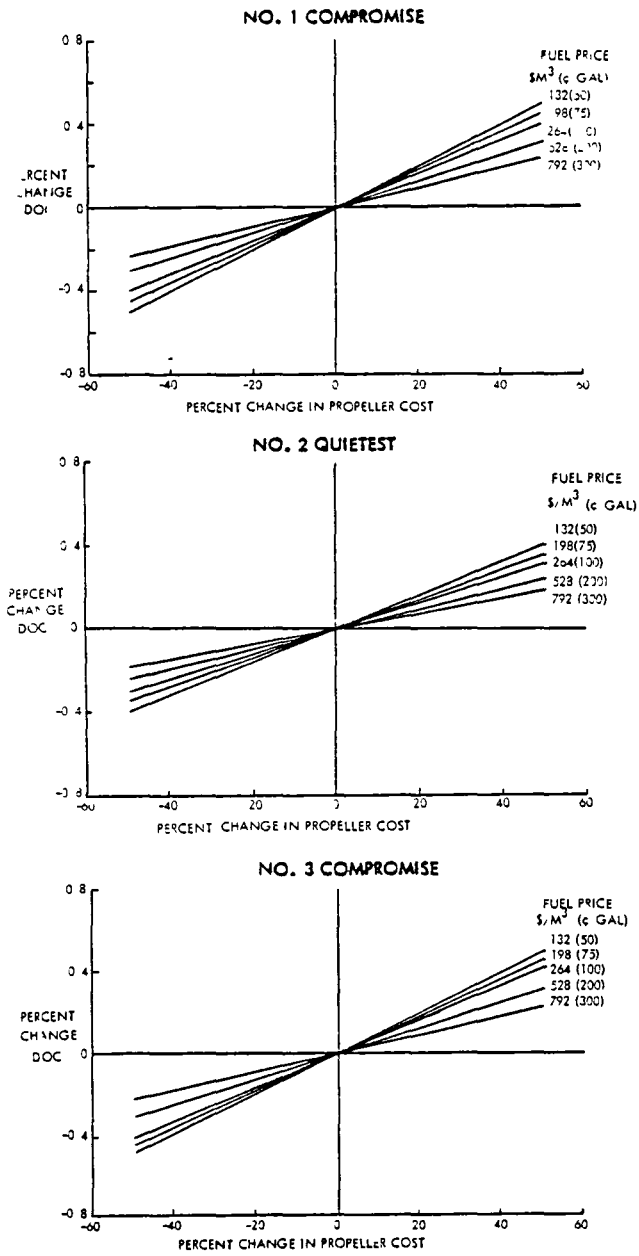

Figure H-18. Propeller Cost Sensitivity Results for Turboprop Aircraft

Engine Cost

Figure H-19 shows the effect of varying the engine cost by ±50 percent for the three aircraft. The changes in DOC per unit change in engine price are negligibly small. For example, a 10-

percent change in engine cost produces less than an 0.8-percent change in DOC. Varying the fuel price has the same effect on these results as it did relative to the propeller.

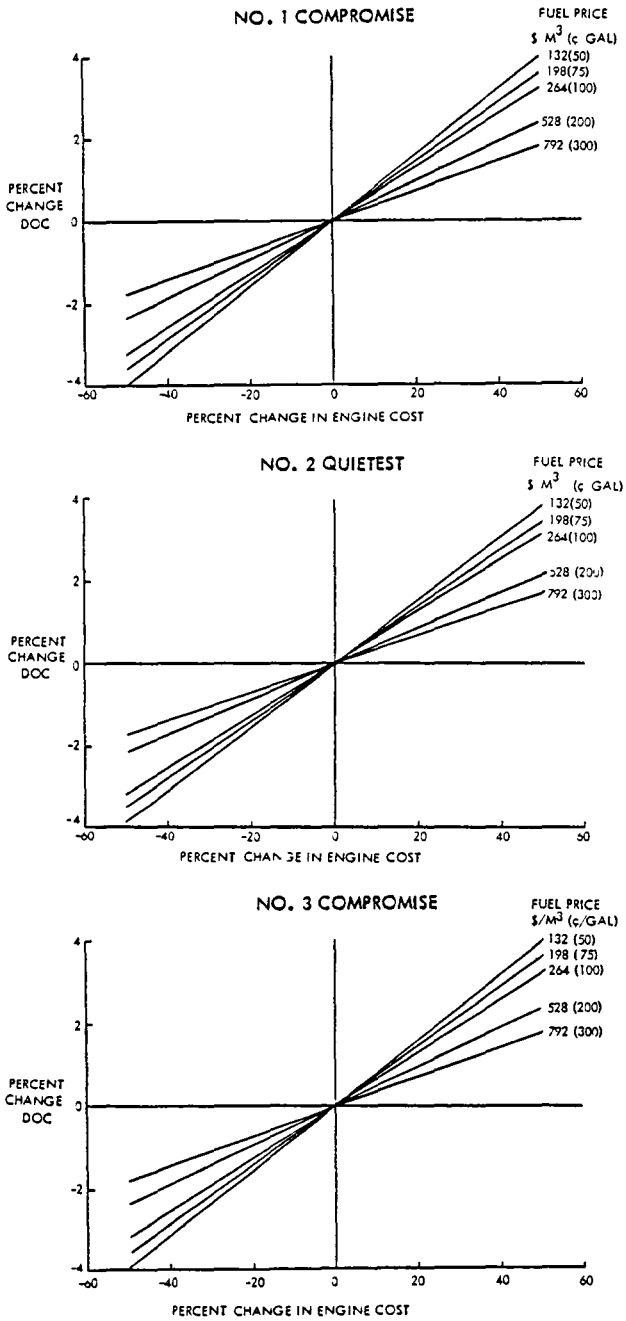

Figure H-19. Engine Cost Sensitivity Results for Turboprop Aircraft

Airframe Cost

Variations in the cost to manufacture the airframe (that is, the aircraft without its propulsion and avionics systems installed) will affect the DOCs of the three aircraft to the extent shown on Figure H-20. Although

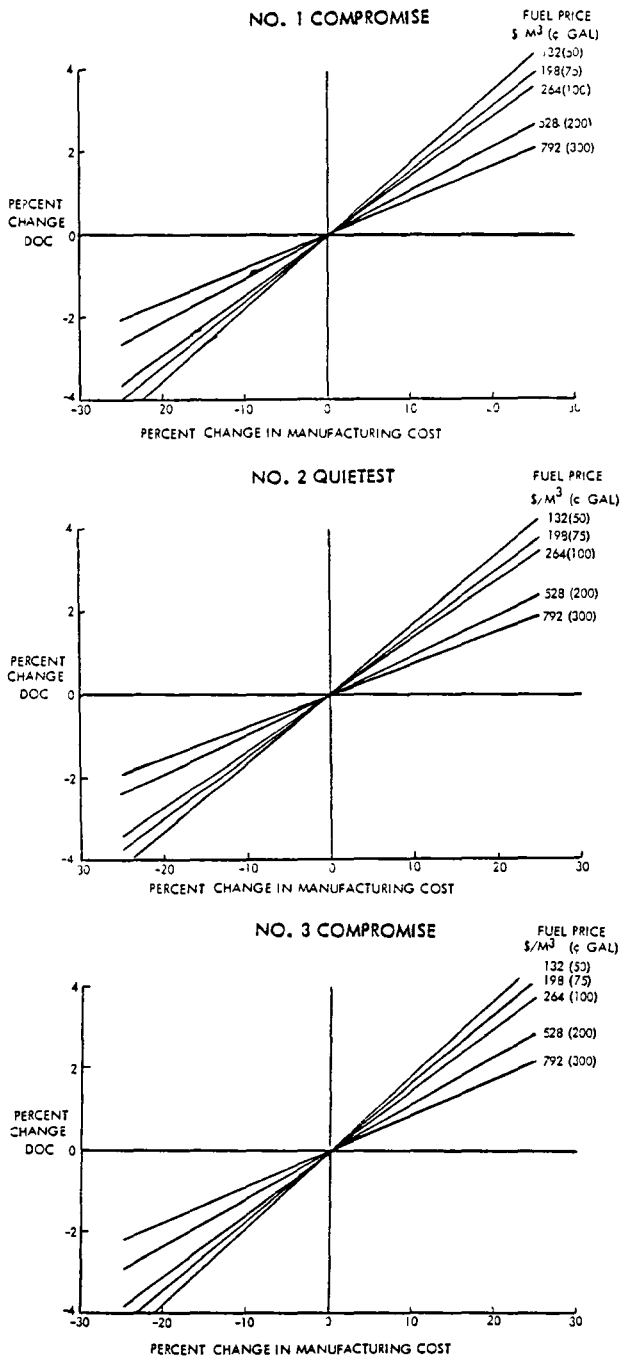

Figure H-20. Airframe Cost Sensitivity Results for Turboprop Aircraft

the percent change in DOC for this case is larger than for the propeller or engine, its measure of sensitivity is still rated negligible. The basis for this is that a 10-percent change in the manufacturing cost causes less than a 2-percent change in DOC. In this case also, fuel price has the same effect as it did relative to the propeller and engine, that is, increasing the fuel price tends to reduce the impact on DOC of changing the manufacturing cost.

Flyaway Cost

As the unit flyaway cost of the aircraft changes, the DOC will be affected as indicated in Figure H-21 for the three aircraft. Although a 10-percent change in flyaway cost will produce between a 2 and 5-percent change in DOC, flyaway cost as a parameter rates as having a negligible measure of sensitivity. Increasing the fuel price tends to minimize the effect of flyaway cost on DOC just as it did for the propeller, engine, and airframe.

Maintenance Cost

Considerable discussion has been voiced concerning the maintenance cost for a turboprop type of propulsion system because of potential problems with the gearbox, propeller, and engine. No attempt was made to analyze or reduce the maintenance requirements for a turboprop propulsion system because that is clearly outside our purview and the scope of this study. However, it is within our realm to assess the effect of arbitrary changes in maintenance cost without regard for the cause of the change.

Figure H-22 shows that negligible changes in DOC can be expected even for relatively large changes in propulsion maintenance cost for all three aircraft. Or, expressed numerically, a ten-percent change in propulsion maintenance cost will cause less than a one-percent change in DOC.

As for the previous cost sensitivities, increasing fuel price reduces the effect of changing maintenance cost on DOC.

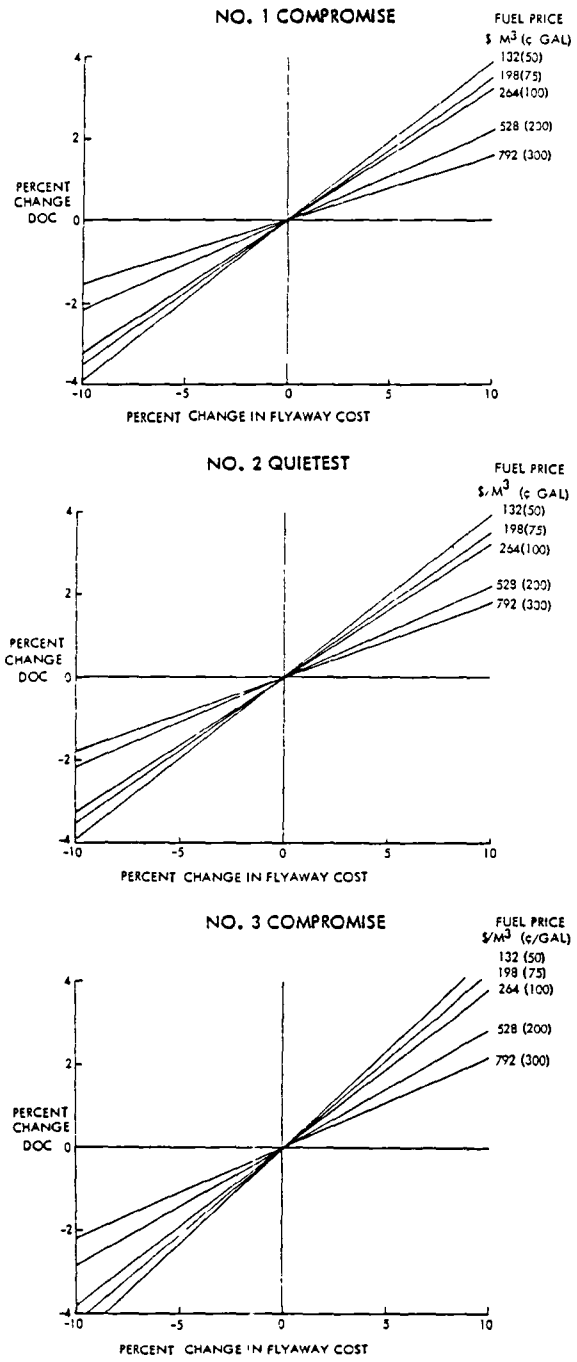

Figure H-21. Flyaway Cost Sensitivity Results for Turboprop Aircraft

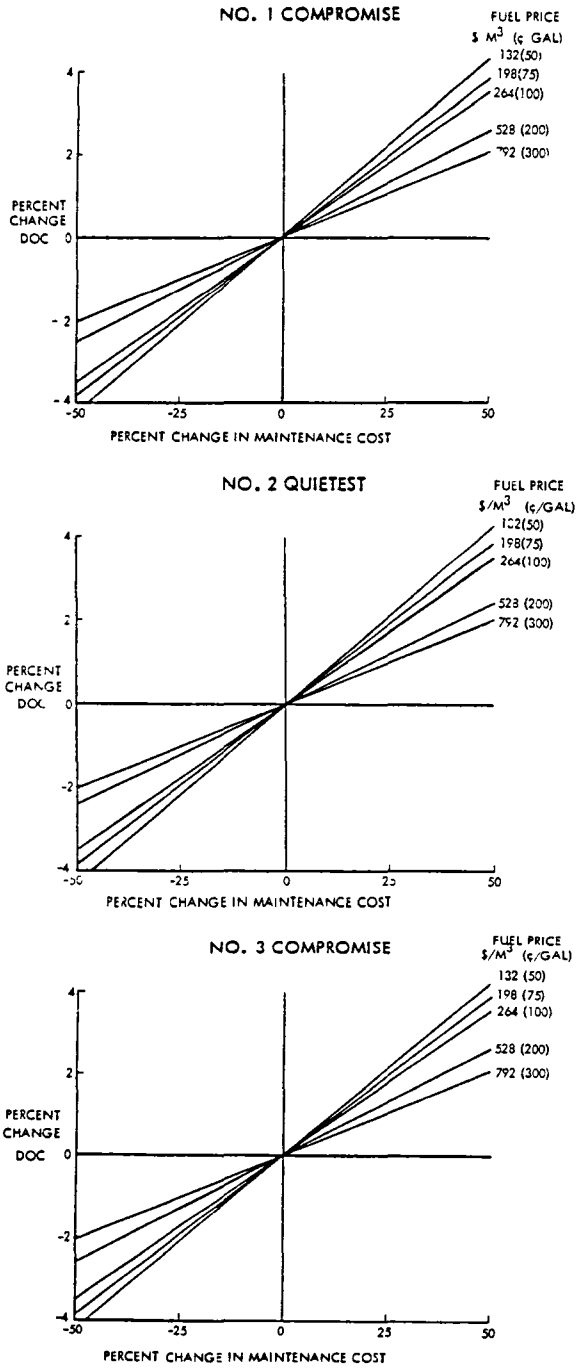

Figure H-22. Maintenance Cost Sensitivity Results for Turboprop Aircraft

APPENDIX J: TURBOFAN PROPULSION SYSTEM DATA AND ANALYSIS

Performance data for the turbofan propulsion system were developed by Lockheed based on the Pratt & Whitney STF477 turbofan engine[22]. Pratt & Whitney are commended for their support and guidance in assisting with the adaptation of their basepoint engine to cover the range of engine performance requirements for this study.

BASELINE ENGINE

The baseline turbofan powerplant is the Pratt & Whitney STF477 engine which was derived* under NASA's program on advanced engines for low energy consumption. Reference 22 presents performance and installation characteristics for this engine with a caution that they should be regarded as maximum target levels because the engine incorporates very aggressive, energy-efficient, advanced-technology concepts with 1990+ operational capabilities. Some of the engine features are: an overall compression ratio of 45:1; a maximum combustor exit temperature of 1700°K (2600°F); an uninstalled, sea-level-rated thrust of 118 kN (26,550 lb) up to 302°K (84°F); and a mass of 1790 kg (3940 lb).

PERFORMANCE

With the STF477 engine as a baseline, a family of 4 engines with discrete bypass ratios of 5.8, 8.4, 13.0 and 18.0 was developed by using

---

* D. E. Gray, "Study of Turbofan Engines Designed for Low Energy Consumption," NASA CR-135002, Pratt & Whitney Aircraft Division, United Technologies Corporation, April 1976 (Ref. 39)

the methodology and background provided by the NASA Ames Short-Haul Systems Study** on thermodynamic cycle trends and engine parameter variations. Installed performance was derived for each of these engines in terms of net pylon thrust and thrust specific fuel consumption for takeoff, climb, and cruise power. The term "net pylon thrust" refers to the engine total thrust minus both engine internal losses and nacelle drag effects. The internal losses reflect typical subsonic transport aircraft airbleed and power extractions of 0.9 kg/s (2 lb/s) and 112 kW (150 hp), respectively, as well as inlet recovery and exhaust duct pressure losses. The nacelle drag is a summation of the freestream scrubbing drag over the fan cowl, the fan exhaust scrubbing drag over the gas generator cowl, the afterbody pressure drag due to boattail effects, and the spillage or additive drag of the nacelle forebody.

Table J-I lists the rated thrusts and bare weights for the four engine point designs. The table also contains the overall dimensions for the engines, nacelles, and pylons for each case. An estimate of the nacelle drag is shown in Figure J-1 for each case as a function of cruise Mach number. This drag is based on both model and flight test results for the C-141, JetStar, and C-5 aircraft. Corrections to the drag levels for other than sea-level, standard-day conditions may be obtained by multiplying by the ratio of standard pressure to actual ambient pressure.

Figures J-2 through J-4 show the net pylon thrust and specific fuel consumption for the 8.4 bypass ratio engine at full power during takeoff,

Table J-I. Characteristics of Base-point Turbofan Engines

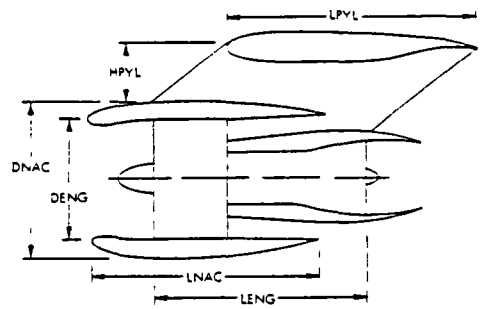

BYPASS RATIO (BPR)		5 8	8 4	13 0	18 0
FAN PRESSURE RATIO (FPR)		1 75	1 537	1 35	1 25
RATED THRUST,	KN	103 4	118 1	144 0	167 8
	LB	23 240	26 550	32 375	37 720
BARE WEIGHT	KG	1438	1791	2594	3547
	LB	3098	3940	5706	7804
DENG,	M	1 67	1 92	2 30	2 73
	FT	5 47	6 30	7 60	8 95
LENG,	M	2 74	2 88	3 08	3 26
	FT	8 98	9 43	10 11	10 68
DNAC	M	1 92	2 23	2 71	3 16
	FT	6 34	7 31	8 88	10 38
LNAC,	M	2 64	3 01	3 57	4 10
	FT	8 66	9 87	11 72	13 45
LPYL	M	4 56	4 92	5 42	5 80
	FT	14 98	16 14	17 77	19 03
HPYL,	M	0 46	0 49	0 54	0 58
	FT	1 50	1 61	1 78	1 90

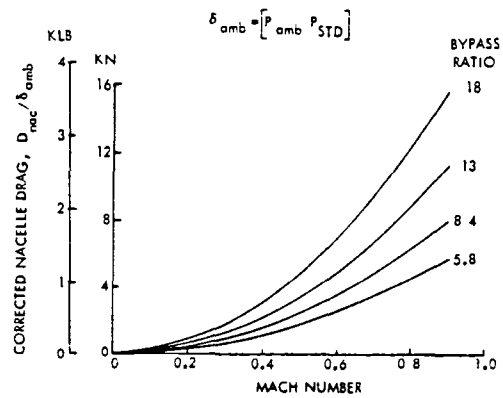

Figure J-1. Nacelle Drag Estimates for STF477 Engine

** T. P. Higgins, et al, "Study of Quiet Turbofan STOL Aircraft for Short Haul Transportation," NASA CR-2355, Lockheed Aircraft Corporation, 1973 (Ref. 40)

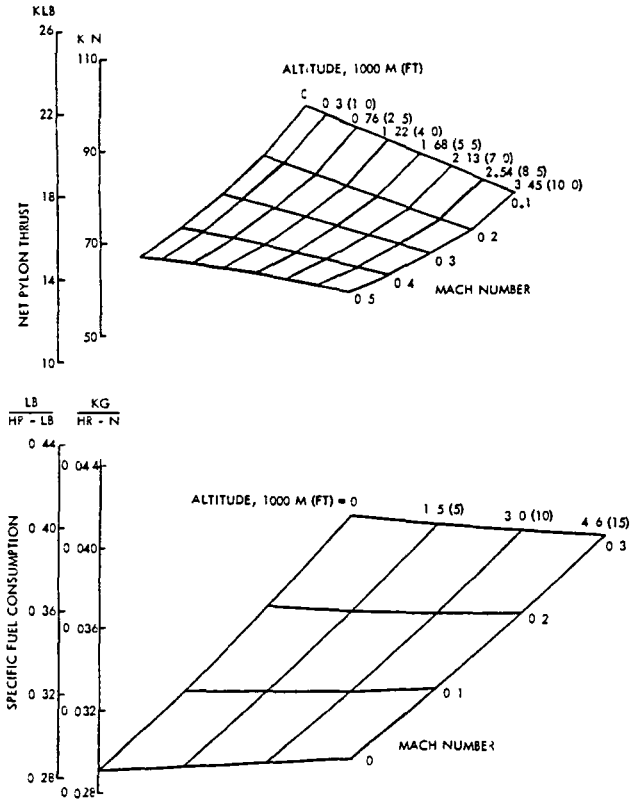

Figure J-2. Takeoff Performance for STF477 Engine. Bypass Ratio = 8.4

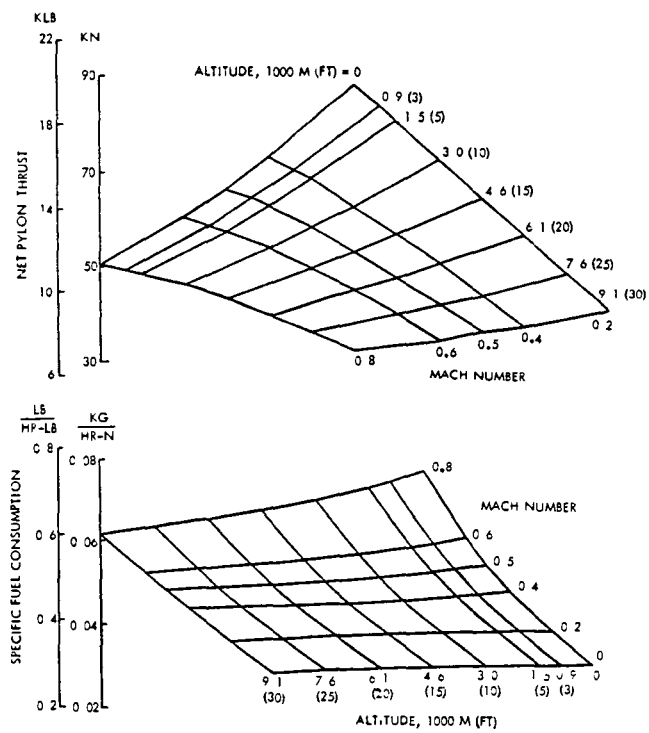

Figure J-3. Climb Performance for STF477 Engine. Bypass Ratio = 8.4

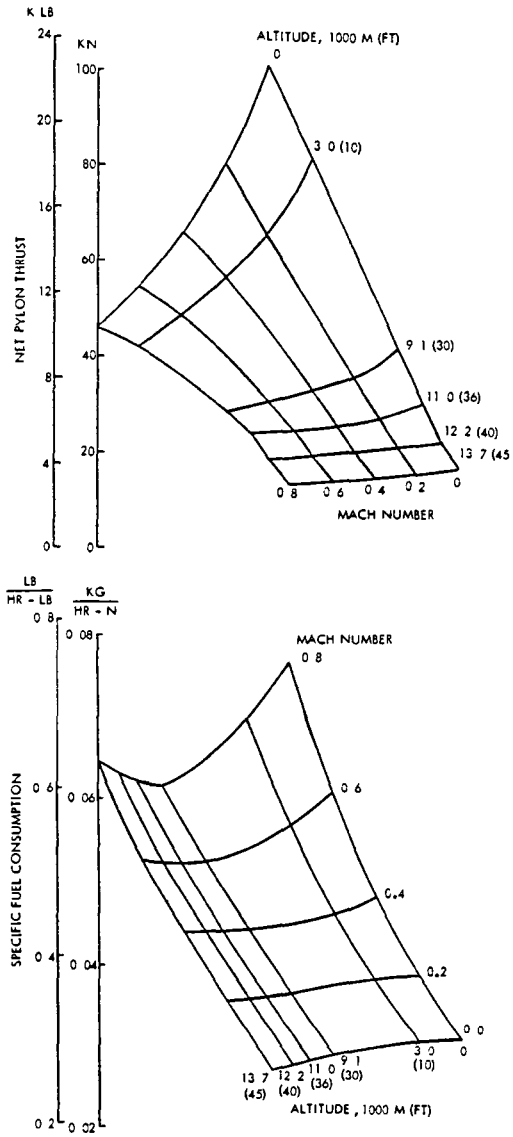

Figure J-4. Cruise Performance for STF477 Engine. Bypass Ratio = 8.4

climb, and cruise. To cover the ranges of the three flight conditions, performance data were generated for altitudes from sea level to 13.7 km (45,000 ft) and for Mach numbers up to 0.8. The effect of operating at part power is illustrated on Figure J-5. These figures are presented as an example of the performance data that were produced for each of the four engines used in the parametric study.

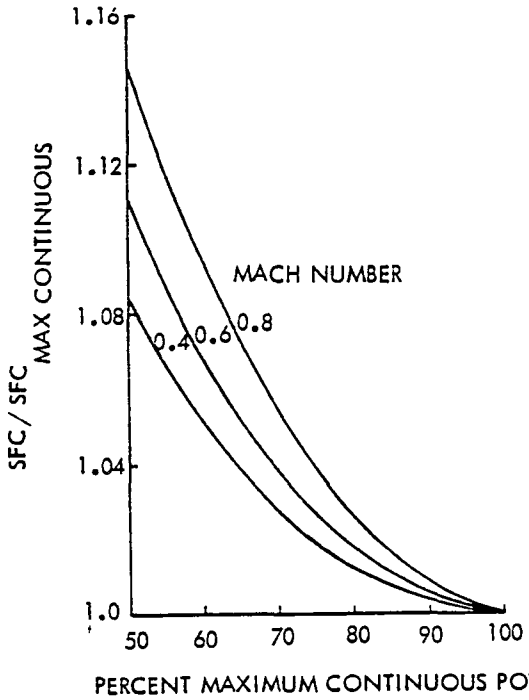

Figure J-5. Part Power Corrections for STF477 Engine. Bypass Ratio = 8.4

SCALING PROCEDURE

All of the performance data for the four turbofan engine design points are for one rated thrust value per engine. In the parametric study and for the selected designs, the aircraft require thrust levels other than those of the basepoint engines. For these alternate thrust levels, the basepoint engine characteristics are scaled in proportion to the ratio of required thrust to available thrust of the basepoint engine at a given power setting, altitude, and flight Mach number. In mathematical notation, the scale factor (SF) is

$$SF = T_{required} / T_{available}$$

or, in terms of subscripts s and b for scaled and base engines, respectively

$$SF = T_s / T_b \qquad (J1)$$

Engine/Nacelle Dimension Scaling

Equations for scaling the engine diameter (DENG) and length (LENG) are those available in Reference 22.

$$DENG_s = DENG_b \ (SF)^{0.5} \qquad (J2)$$

$$LENG_s = LENG_b \ (SF)^{0.43} \qquad (J3)$$

Values for the diameter and length of the base engine were presented earlier in Table J-I.

Nacelle and pylon dimensions are calculated as functions of engine diameter. Once an engine has been scaled to a particular thrust level, the overall sizes of the nacelle and pylon may be determined using the relationships shown in Table J-II.

Table J-II. Sizing Relationships for Nacelles and Pylons with Turbofan Engines

BPR	5 8	8 4	13.0	18 0
DNAC/DENG *	1.16	1 16	1 16	1 16
LNAC/DNAC	1.37	1 35	1.32	1.30
(LNAC/DENG)	1 58	1.57	1 53	1.50
LPYL/LNAC	1.36	1.27	1 13	1 00
(LPYL/DENG)	2.15	1.99	1.73	1.50
HPYL/LPYL	0.10	0 10	0 10	0 10
(HPYL/DENG)	0 22	0 20	0 17	0 15

*REFER TO TABLE J-I FOR DIMENSION DEFINITIONS

Weight Scaling

Reference 22 gives an empirical equation for scaling engine weight (WENG).

$$WENG_s = WENG_b \ (SF)^{1.135} \qquad (J4)$$

The weights of the baseline engines are listed in Table J-I. Weights for the nacelle and pylon are calculated based on their dimensions. Thus, once the correct dimensions are determined, the weights are estimated with standard equations so that no special weight scaling relationships are needed for these two items.

Performance Scaling

Reference 22 graphically depicts the effect of engine scaling on specific fuel consumption. There is no effect when engines are scaled to larger sizes, but there is a penalty in scaling to smaller sizes. The magnitude of the penalty is given by the equation

$$\text{SFC Factor} = 1.117 - 0.214\ SF + 0.096\ SF^2 \qquad \text{(J5)}$$

if SF is less than one.

Technology Scaling

The STF477 engine uses technology levels that are predicted to be consistent with a 1998 commercial engine certification. An earlier introduction of the engine would be accompanied by weight and specific fuel consumption penalties that reflect lower levels of advanced technology. These penalties are presented in Reference 22 for the baseline 8.0 bypass ratio engine. Following consultations with Pratt & Whitney, similar penalties were developed for higher-bypass-ratio engines of 13 and 18 that reflect the additional technology advancements required for the geared fans in these two engines. Estimates of the penalties involved in early introduction of these four basepoint engines are provided on Figure J-6. Early introduction of this engine is also likely to be accompanied by louder noise levels, which are not incorporated directly, but are recognized and partially accounted for indirectly through larger thrust requirements resulting from less technology advancement.

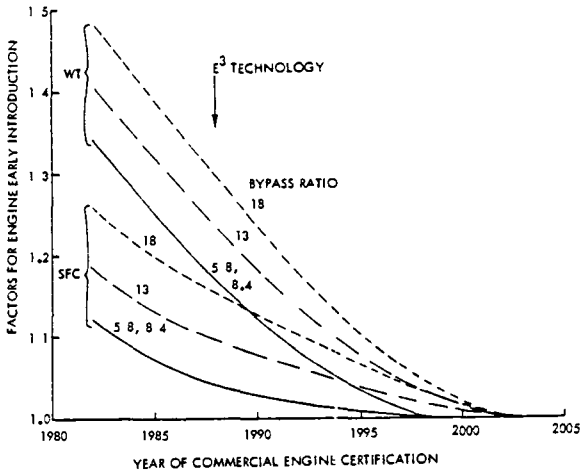

Figure J-6. Estimated Adverse Effects of STF477 Engine Early Introduction

INSTALLATION CONSIDERATIONS

The turbofan engines are mounted on pylons beneath the wing to provide easy access for maintenance with only minimal adverse effects on aircraft structural weight and aerodynamic performance. Engine placement relative to the wing is based on preliminary design guidelines that have evolved from experience in the design of transport aircraft.

Spanwise Location on the Wing

The minimum distance from the side of the fuselage to the centerline of the inboard engine is equal to twice the nacelle diameter. Additional engines are placed outboard on the wing with a minimum spacing between engine centerlines of two nacelle diameters.

Chordwise Location on the Wing

The exit plane of the engine nozzle should be located between the 10 and 20 percent wing chord positions at the particular wing span station.

Vertical Distance from Wing

The vertical distance from the engine centerline to the wing centerline should be between 60 and 80 percent of the nacelle diameter.

Angle of Inclination of the Engine

The engine centerline should be parallel to the fuselage centerline.

APPENDIX K. TURBOFAN PARAMETRIC DATA ANALYSIS

The purpose of this appendix is to provide a step-by-step description of the process that was followed to reduce the turbofan aircraft parametric data for the selection of point designs for further study.

Before describing that process, however, one prior statement merits repeating and its implications explained. The statement is: the selected turbofan aircraft are intended to provide bases for comparing propulsion systems. To allow attention to be focused on just the comparative effects of the two propulsion systems and minimize non-propulsion related effects, each turbofan aircraft has the same delivery capabilities as the corresponding turboprop aircraft. That is, the turbofan and turboprop aircraft to be compared have identical cruise Mach numbers, payloads, cargo compartments, and cruise altitudes. Both types of aircraft are also subject to the same operating constraints on field length, approach speed, and engine-out climb gradients.

The four variables considered in the turbofan aircraft parametric study are listed in Table K-I along with their values. The four bypass ratios identify discrete engine designs, which are scaled based on the thrust required. (Appendix J contains descriptions of these four engines and how they are sized.) The engine power setting is defined as the ratio of thrust required at cruise to the thrust available. It provides a mechanism in the aircraft sizing program for increasing engine size to improve takeoff performance.

For each combination of values in the table, an aircraft design was produced along with estimates of its performance, noise, and cost characteristics. All of the resulting designs were then compared so that optimum designs could be identified for various criteria. This very general description of what was done with the parametric data will now be expanded by presenting an example.

Table K-I. Turbofan Aircraft Parametric Variables

ENGINE	
BYPASS RATIO	5.8, 8.4, 13.0, 18.0
POWER SETTING	70 TO 90 PERCENT
WING	
ASPECT RATIO	8, 12, 16
LOADING, KN/M^2	3.3 TO 6.2
LB/FT^2	70 TO 130

For this example, one set of aircraft designs with variations in wing loading and aspect ratio has been chosen with these characteristics:

o	Cruise Mach Number	0.75
o	Payload	4 Containers
o	Range	4250 km (2295 n.mi.)
o	Cruise Altitude	10.1 km (33,000 ft)
o	Wing Sweep Angle	0.35 rad (20 deg)
o	Engine Bypass Ratio	13
o	Engine Power Setting	0.80

Figures K-1 through K-8 display the effects of variations in wing loading and aspect ratio on ramp weight, block fuel, takeoff distance, approach speed, fuel volume ratio, direct operating cost (DOC) for fuel at 264 $\$/m^3$ (1 \$/gal), and 80-EPNdB noiseprint areas for full power and cutback conditions.

Three limitations tend to be significant in establishing the optimum designs. These limitations are that the aircraft take off in less than 2440 m (8000 ft), land at approach speeds below 69 m/s (135 kts), and have sufficient wing volume to carry the fuel required for the specified range. The first step in the analysis is to

illustrate these limits, as shown on Figures K-9, K-10, and K-11, which are the respective graphs of takeoff distance, approach speed, and fuel volume ratio. To show these limits on the other figures, those combinations of wing loading and aspect ratio values are identified that lie on the limit lines and are transferred to the other figures. For this example, Figures K-12 and K-13 (reproductions of Figures K-6 and K-7) are included with the limits noted.

The next step is to superimpose a regular pattern of constant cost lines on the DOC graph, as shown in Figure K-14. These lines are then transferred to the noiseprint area graph in Figure K-15, and the minimum area values are read for each constant cost line. This procedure is repeated for the other combinations of engine bypass ratio and power setting to complete a table similar to Table K-II. For each subset in the table, that is for each DOC value, a minimum value is evident from a visual inspection. By combining the minimum values at each DOC level, the desired end result is obtained in the form of Figure K-16. Similar figures can be obtained by repeating the process if block fuel or DOC at another fuel price is preferred as the ordinate on the graph.

During this study, the following correlation was recognized. The optimum aircraft for minimizing noiseprint area are obtained at those engine power settings for which the combinations of wing loading and aspect ratio values coincide with those along both the approach speed and field length limits.

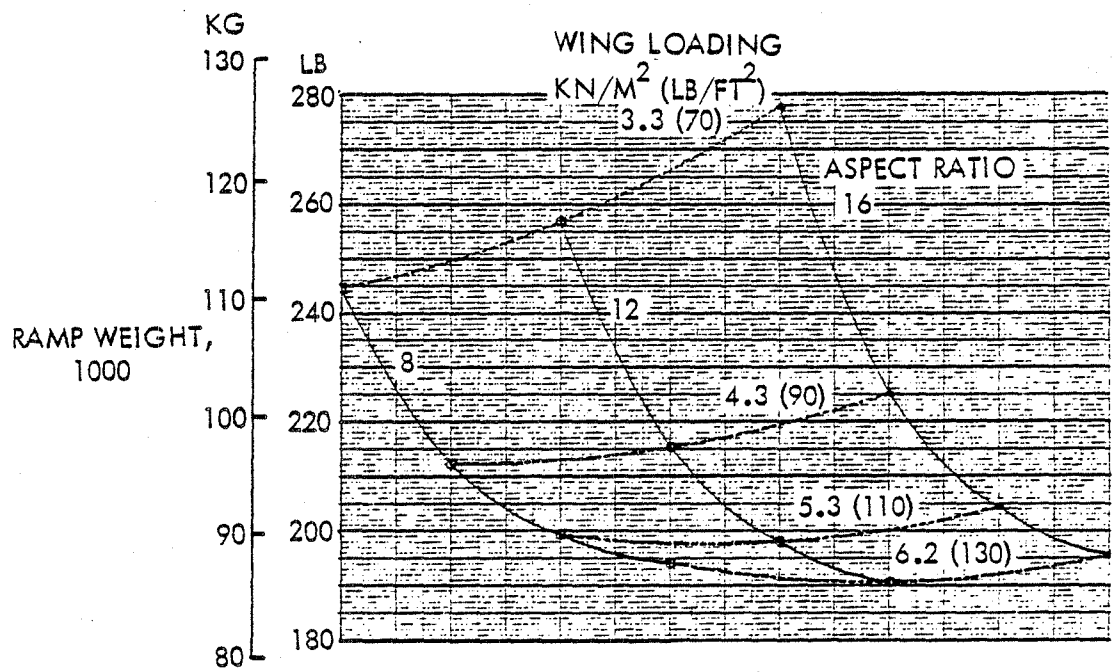

Figure K-1. Ramp Weight Variation for Turbofan Parametric Example

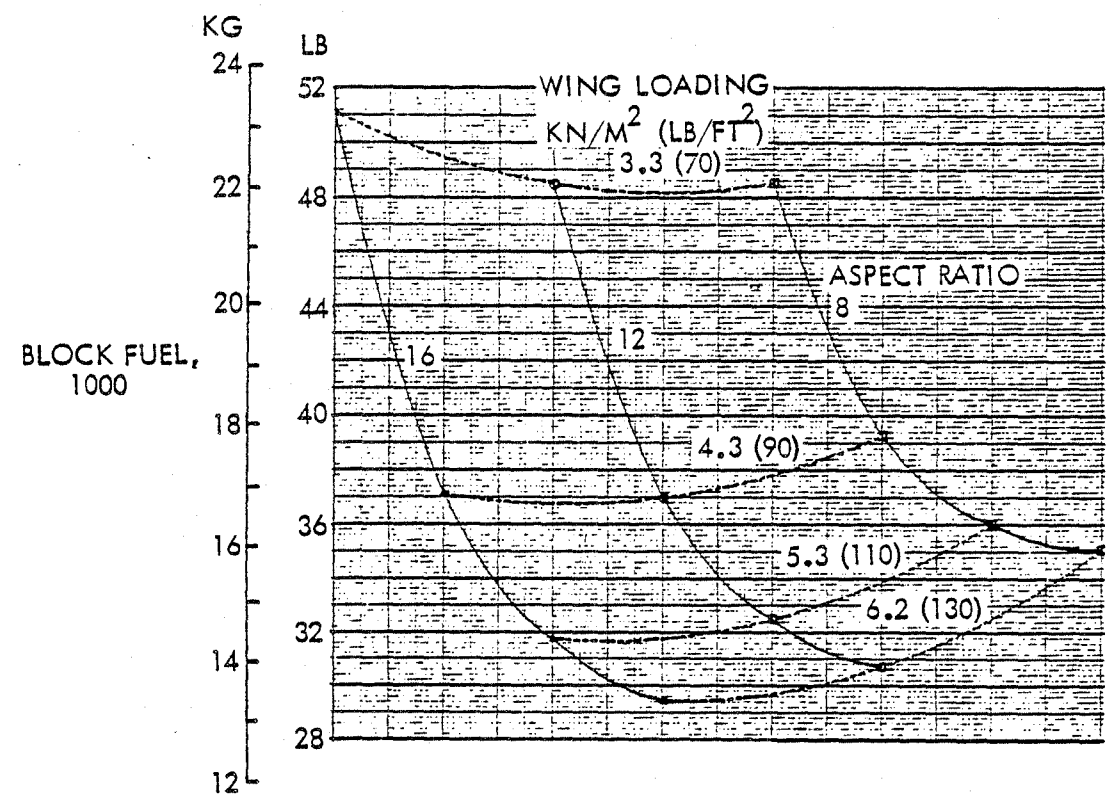

Figure K-2. Block Fuel Variation for Turbofan Parametric Example

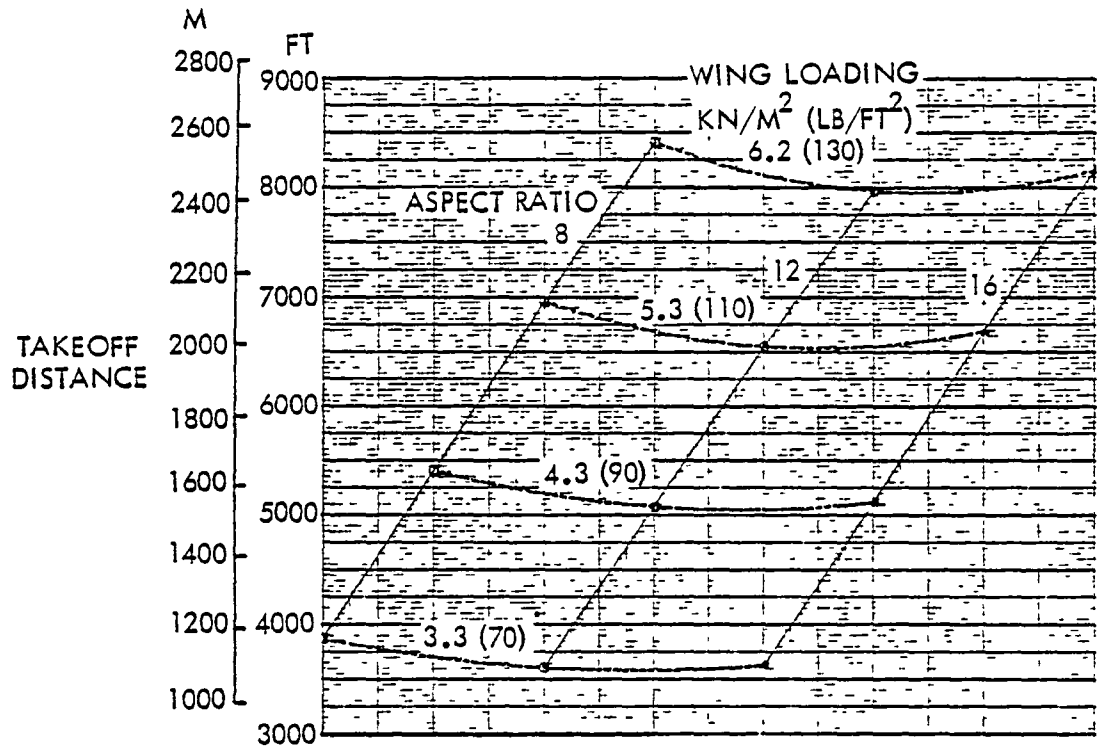

Figure K-3. Takeoff Distance Variation for Turbofan Parametric Example

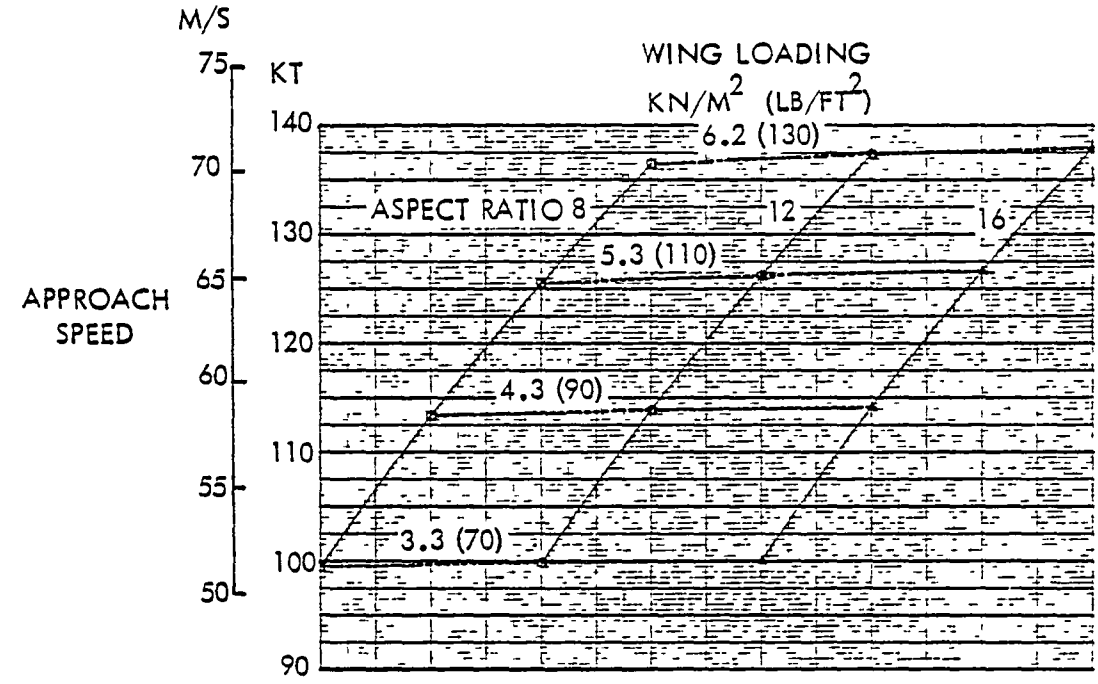

Figure K-4. Approach Speed Variation for Turbofan Parametric Example

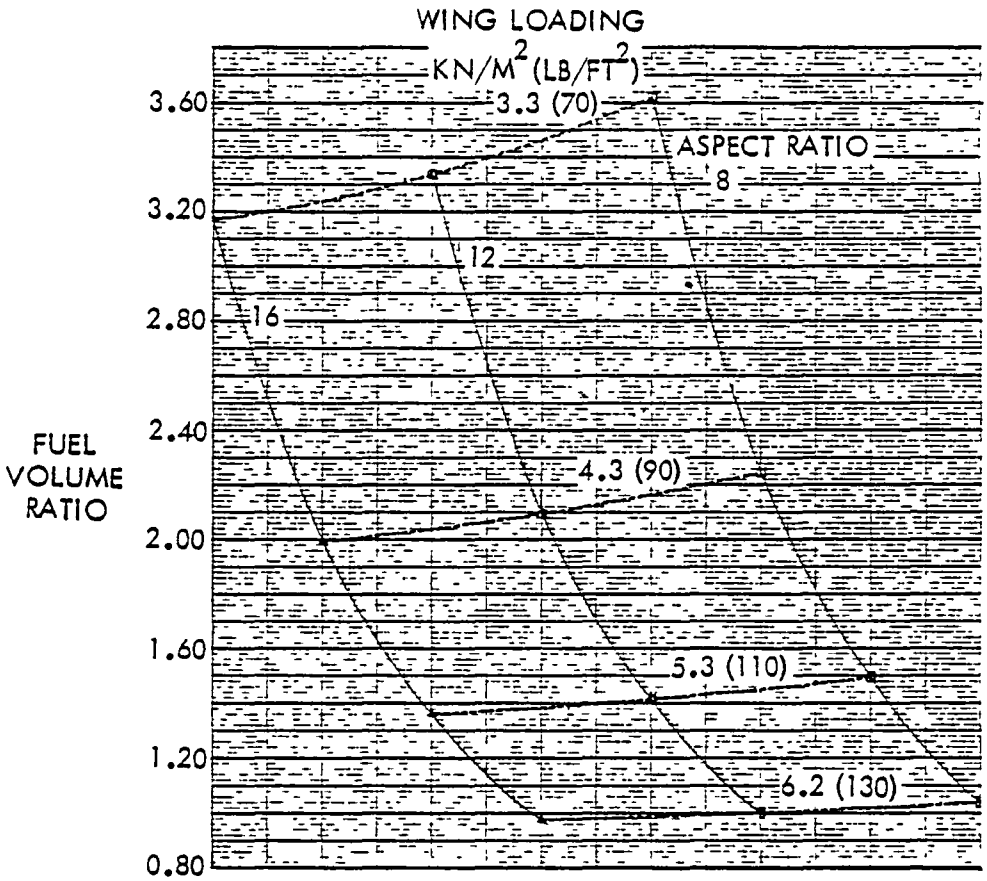

Figure K-5. Fuel Volume Ratio Variation for Turbofan Parametric Example

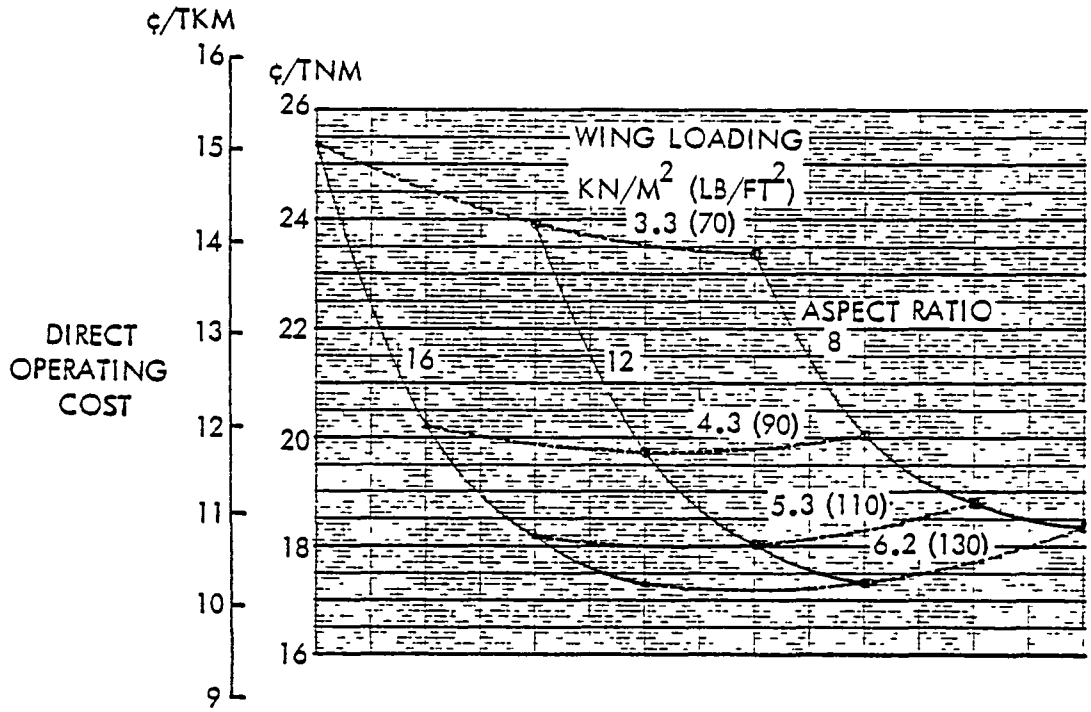

Figure K-6. Direct Operating Cost Variation for Turbofan Parametric Example

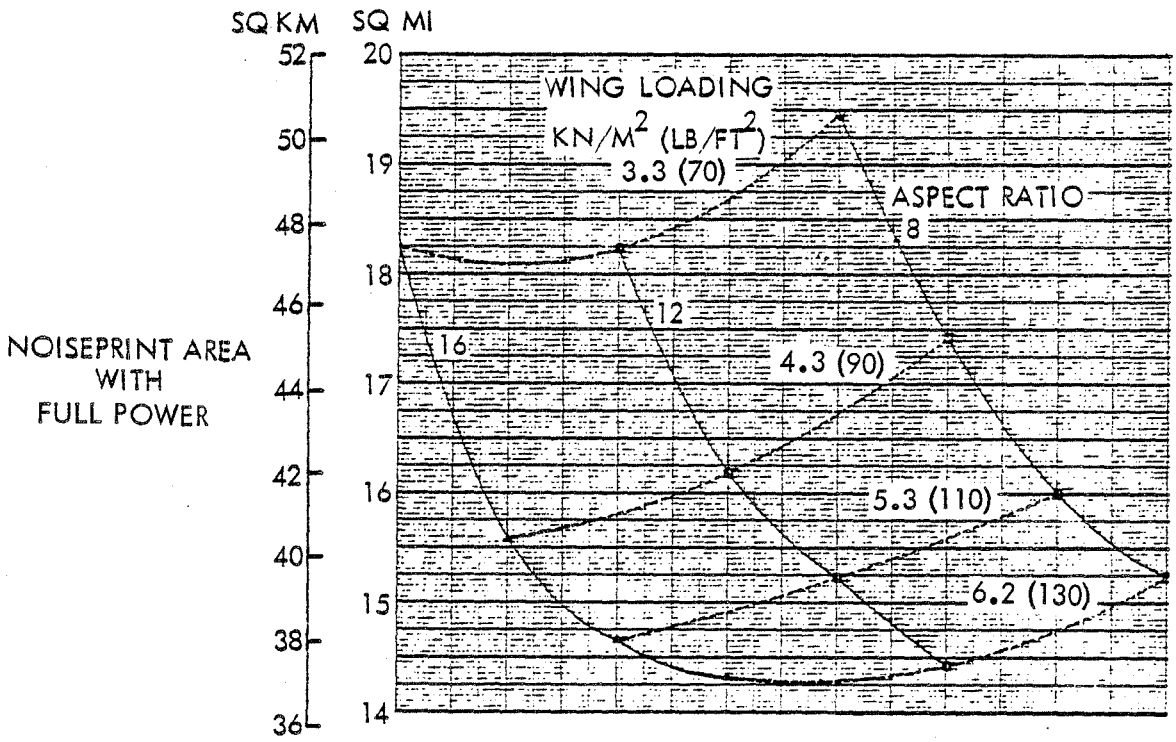

Figure K-7. Noiseprint Variation at Full-Power for Turbofan Parametric Example

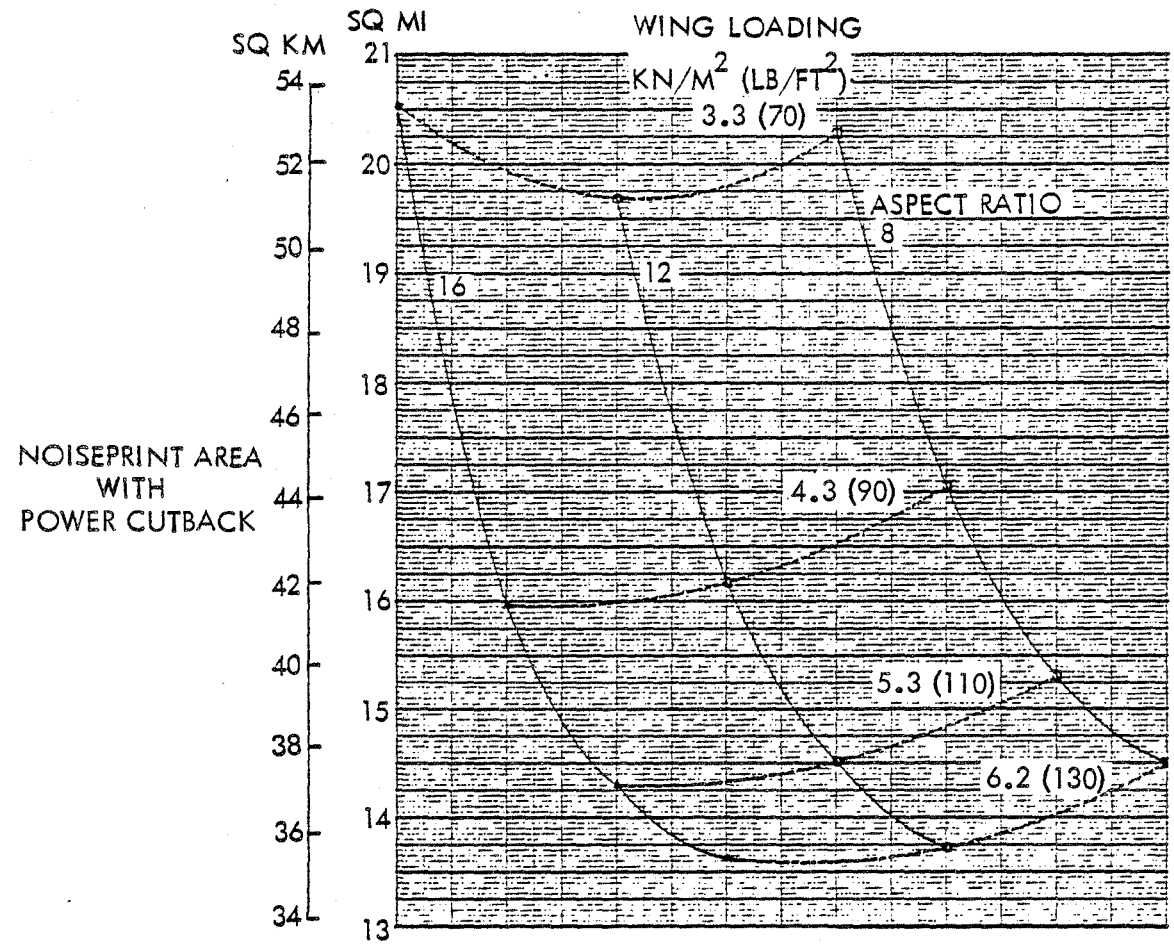

Figure K-8. Noiseprint Variation at Cutback for Turbofan Parametric Example

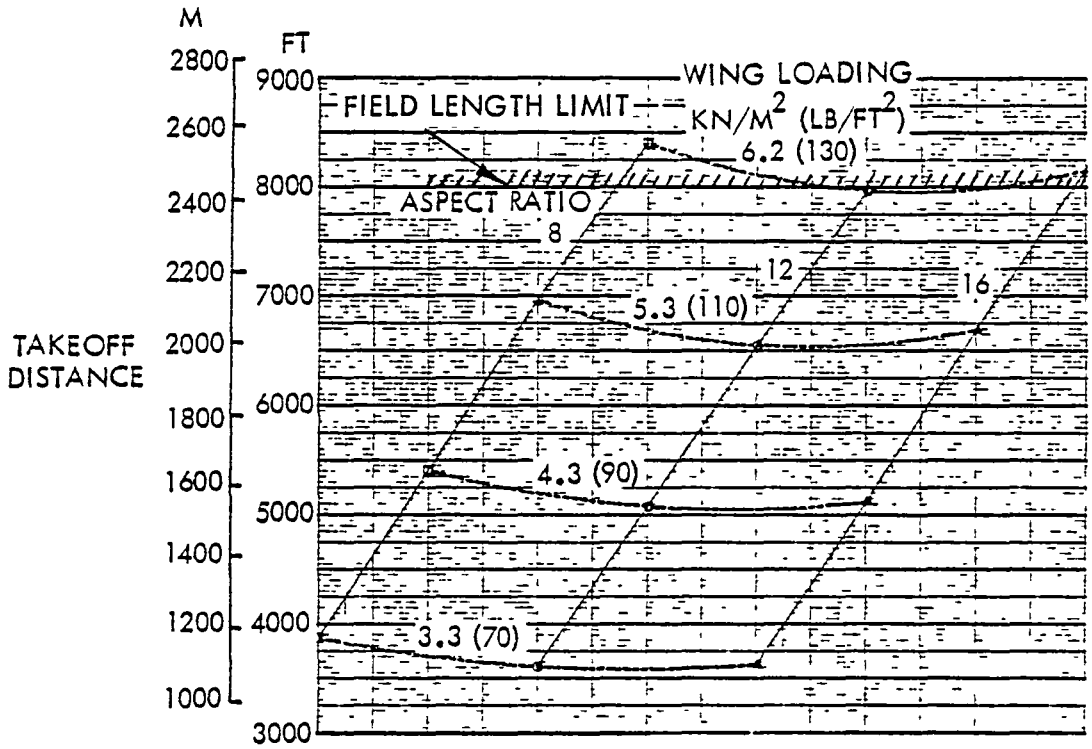

Figure K-9. Takeoff Distance Limit Imposed for Turbofan Parametric Example

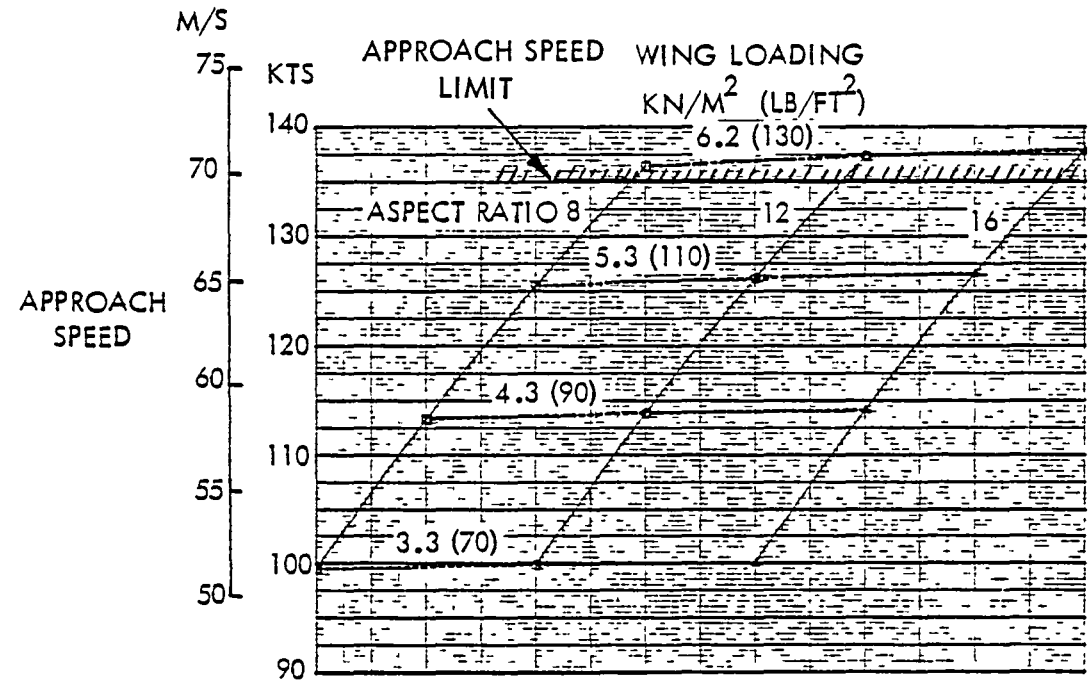

Figure K-10. Approach Speed Limit Imposed for Turbofan Parametric Example

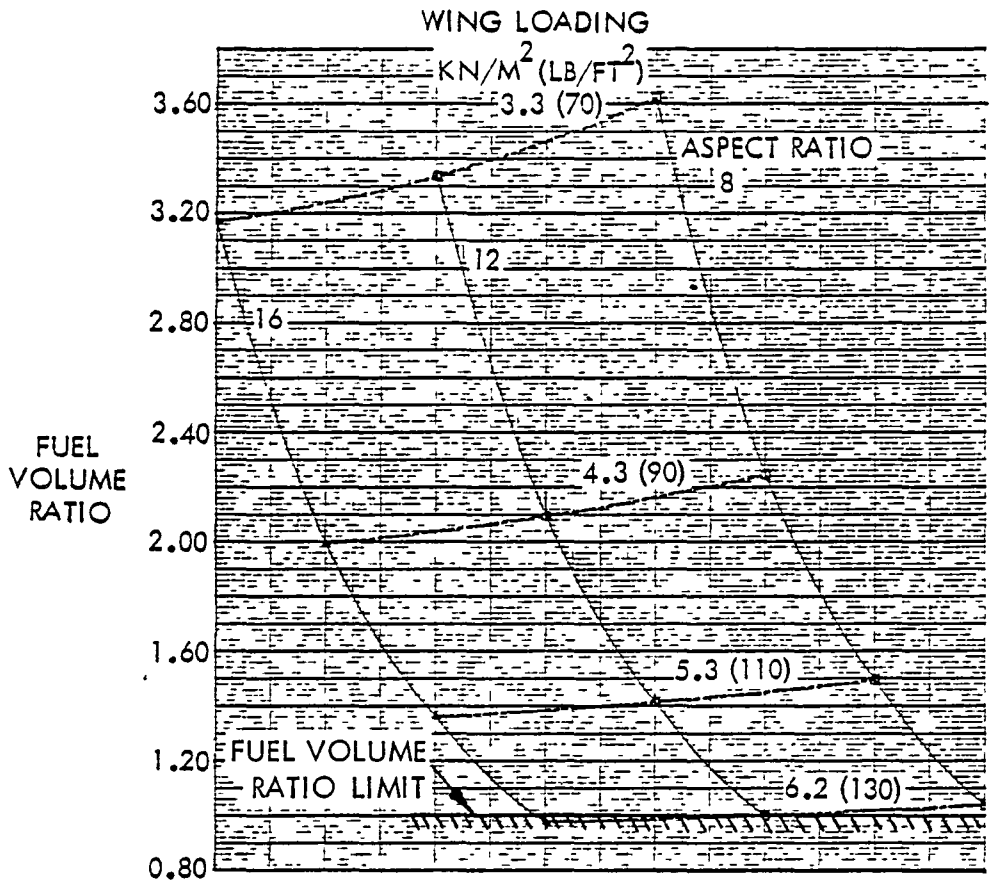

Figure K-11. Fuel Volume Ratio Limit Imposed for Turbofan Parametric Example

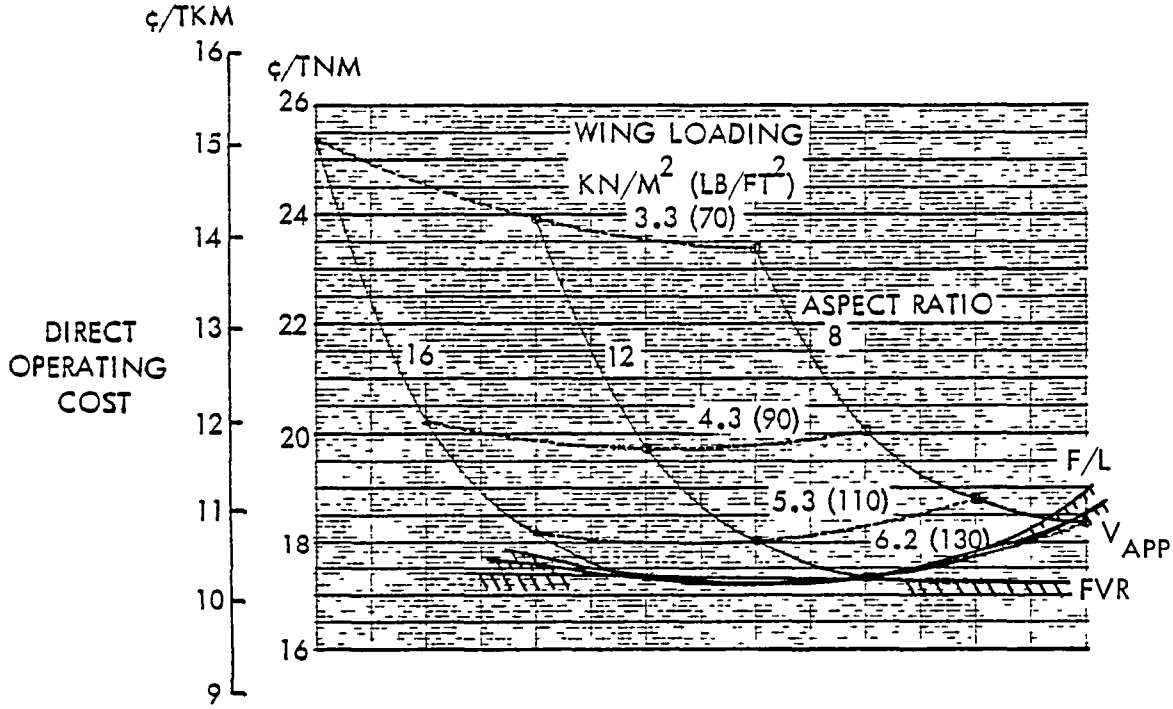

Figure K-12. Direct Operating Cost Variations with Limits Applied for Turbofan Parametric Example

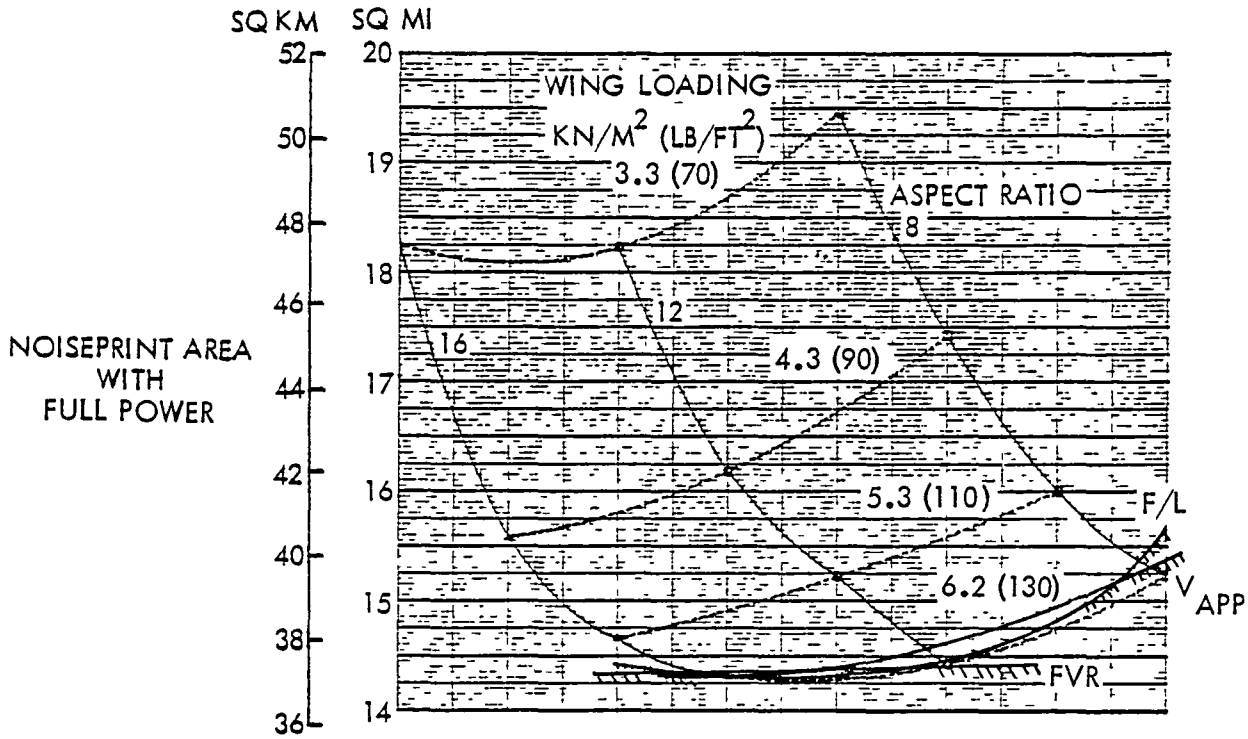

Figure K-13. Noiseprint Variations with Limits Applied for Turbofan Parametric Example

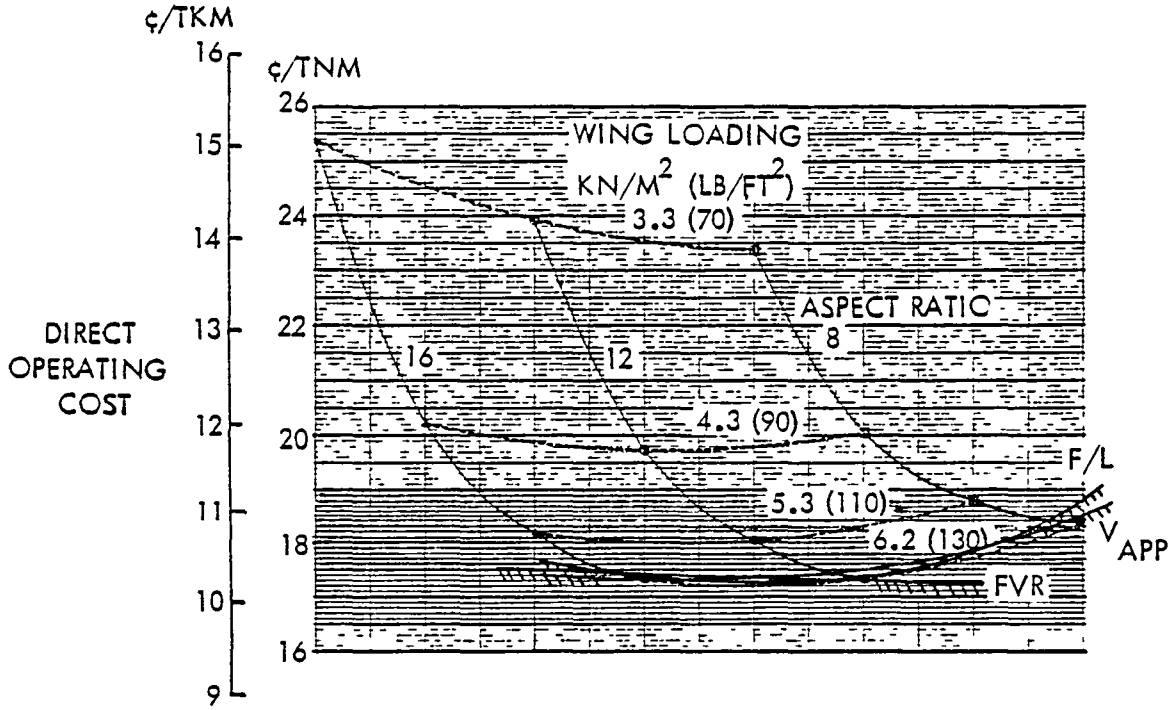

Figure K-14. Constant Cost Lines Used in Analysis Applied to DOC Graph

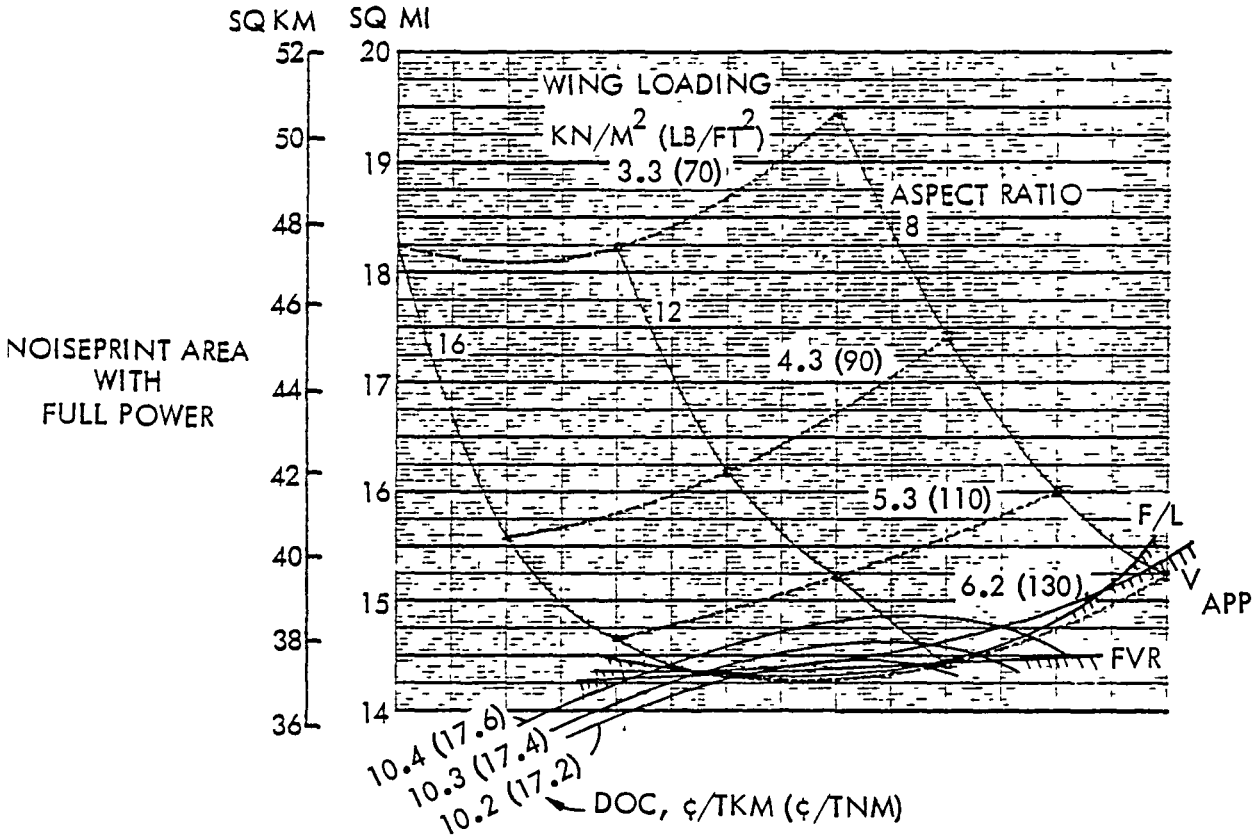

Figure K-15. Constant Cost Lines Used in Analysis Applied to Noiseprint Graph

Table K-II. Sample Data Compilation for Turbofan Aircraft Parametric Study

DOC, ¢/TKM FUEL AT 264 $/M³	ENGINE BYPASS RATIO	NOISEPRINT AREA (SQ KM) FOR ENGINE POWER SETTINGS (PERCENT) 95	90	85	80	75	70
10 2	5 8	*	*	*	85 2	81 8	80 0
	8 4	*	*	67 8	66 0	64 2	62 4
	13 0	*	*	37 8	*	*	*
	18 0	*	*	*	*	*	*
10 3	5 8	*	*	*	85 2	82 8	81 0
	8 4	*	69 1	68 6	66 8	64 7	62 9
	13 0	*	38 6	38 1	37 0	*	*
	18 0	*	*	*	*	*	*
10 4	5 8	*	*	87 8	86 2	83 9	82 1
	8 4	*	69 6	69 4	67 8	65 5	63 4
	13 0	39 6	38 8	38 1	37 3	*	*
	18 0	*	*	*	*	*	*

DOC, ¢ TNM FUEL AT 1 $/GAL	ENGINE BYPASS RATIO	NOISEPRINT AREA (SQ MI) FOR ENGINE POWER SETTINGS (PERCENT) 95	90	85	80	75	70
17 2	5 8	*	*	*	32 9	31 6	30 9
	8 4	*	*	26 2	25 5	24 8	24 1
	13 0	*	*	14 6	*	*	*
	18 0	*	*	*	*	*	*
17 4	5 8	*	*	*	32 9	32 0	31 3
	8 4	*	26 7	26 5	25 8	25 0	24 3
	13 0	*	14 9	14 7	14 3	*	*
	18 0	*	*	*	*	*	*
17 6	5 8	*	*	33 9	33 3	32 4	31 7
	8 4	*	26 9	26 8	26 2	25 3	24 5
	13 0	15 3	15 0	14 7	14 4	*	*
	18 0	*	*	*	*	*	*

* NO DESIGNS OBTAINABLE AT SPECIFIED CONDITIONS WITHIN CONSTRAINTS

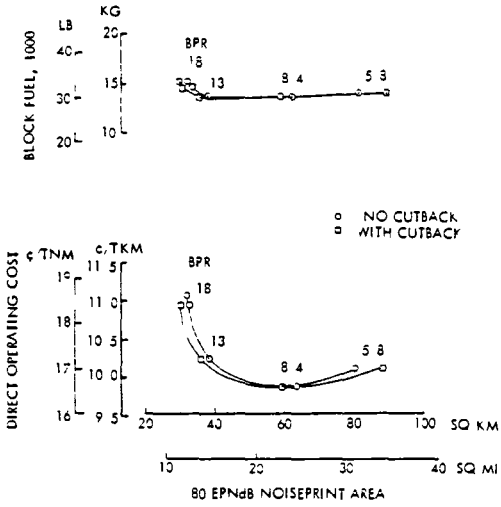

Figure K-16. DOC - Noiseprint Results for Use in Aircraft Selection

APPENDIX L: TURBOFAN SENSITIVITY STUDIES

The three turbofan aircraft served as baseline vehicles in a series of sensitivity studies, which are presented in this appendix. Table L-I lists all of the sensitivity parameters that were investigated, which fall under four major headings of performance, weight, wing geometry, and economics.

Using the same approach as for the turboprop aircraft sensitivity studies, percent variations in noiseprint, DOC, and block fuel were used as indicators, where applicable, of the effect of the various sensitivity parameters. To determine which factors have the greatest impact on these indicators, the previously defined measure of sensitivity (MOS)* was used.

Further details on the individual sensitivity studies are provided in subsequent sections. Unless otherwise noted, only one independent variable is allowed to change in each case. In general throughout these studies, the DOC variations are for a fuel price of 264 $/m^3$ (100 ¢/gal), and the noiseprint variations are for an 80 EPNdB level. Any exceptions are noted.

PERFORMANCE

Six performance-related sensitivity studies were performed to assess the effect of varying the initial cruise altitude, aircraft drag estimate, field length limit, maximum approach speed, glideslope on approach, and predicted noise source level.

* The measure of sensitivity (MOS) is the ratio of the percent change that occurred in one of the indicators to the percent change in the sensitivity parameter. For qualitative evaluation purposes, the numerical MOS values are arbitrarily interpreted as follows:

Numerical Evaluation	Qualitative Interpretation
MOS < 1	Negligible
1 ≤ MOS < 2	Marginal
2 ≤ MOS ≤ 5	Significant
MOS > 5	Critical

Table L-I. Turbofan Aircraft Sensitivity Studies

PERFORMANCE	WING GEOMETRY
o CRUISE ALTITUDE	o ASPECT RATIO
o DRAG	o WING LOADING
o FIELD LENGTH	ECONOMICS
o APPROACH SPEED	o STAGE LENGTH
o GLIDESLOPE	o UTILIZATION
o NOISE LEVEL	o LOAD FACTOR
	o FUEL PRICE
WEIGHT	o ENGINE COST
o PROPULSION SYSTEM	o AIRFRAME COST
o AIRFRAME	o FLYAWAY COST
o FUEL	o MAINTENANCE COST

Cruise Altitude

Varying the initial cruise altitude from the base value of 10.1 km (33,000 ft) has a negligible effect on the noiseprint, DOC, and block fuel of the three turbofan aircraft. This conclusion is reached based on the sensitivity results in Figure L-1. These results confirm that the No. 2 quietest aircraft is at the best altitude for minimum noise and minimum DOC. Likewise, the base altitude for the No. 1 and No. 3 compromise aircraft gives minimum DOCs and block fuels within the field length constraint. A small reduction in noiseprint could be achieved for the two compromise aircraft by increasing the altitude which, because of the lapse rate effect, substantially increases the sea-level-rated thrust of the engines and, as a result, shortens the field length.

Aircraft Drag

Figure L-2 shows that there are some marginally significant effects produced by aircraft drag variations

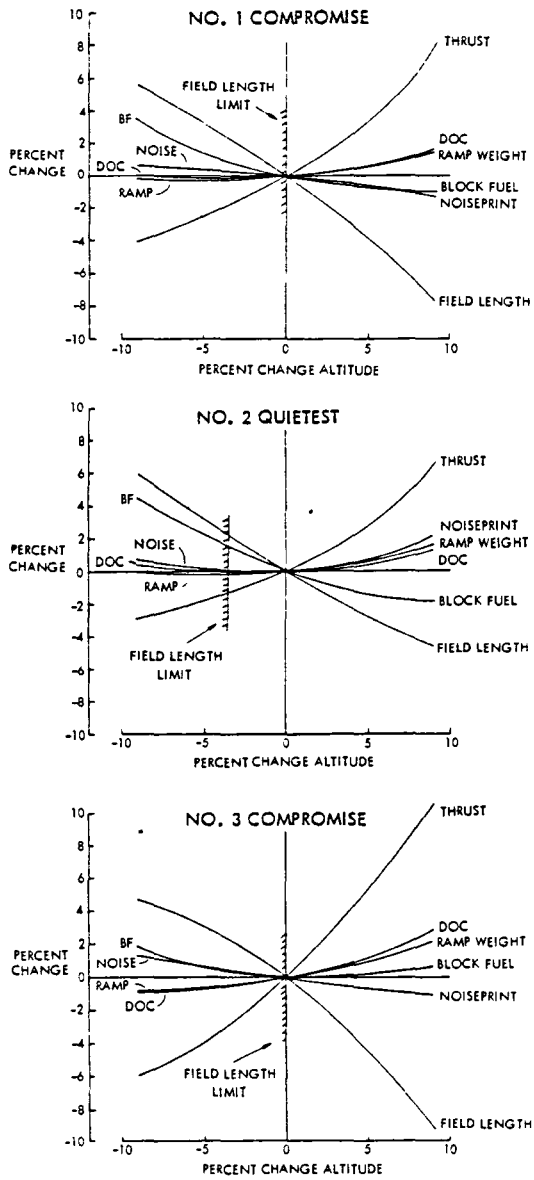

Figure L-1. Altitude Sensitivity Results for Turbofan Aircraft

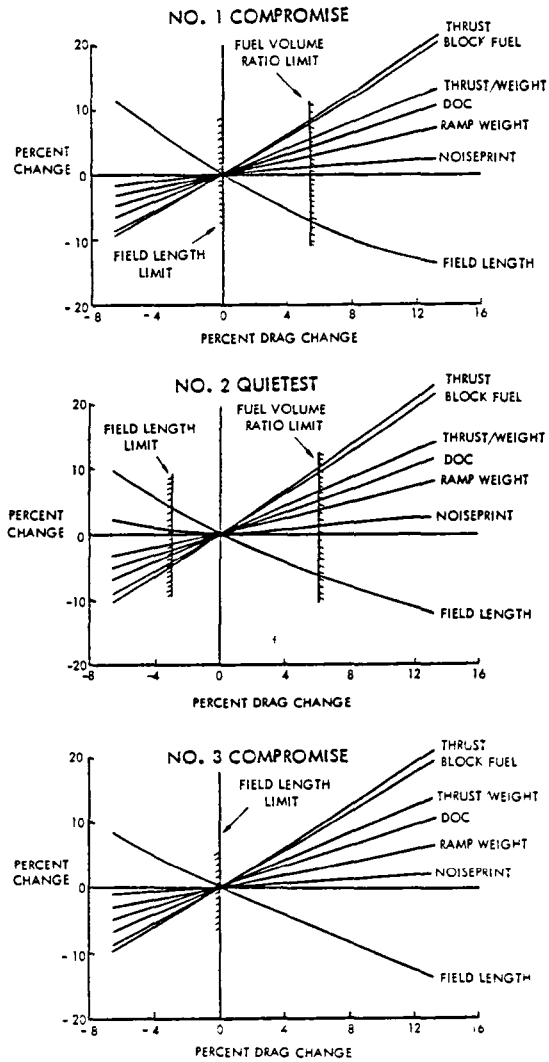

Figure L-2. Aircraft Drag Sensitivity Results for Turbofan Aircraft

that range from reductions of 20 counts to increases of 40 counts. In general, all three aircraft exhibit very similar effects from drag variations. The parameters most noticeably affected are engine thrust and field length. Engine thrust changes in direct proportion to drag and has an inverse effect on field length. These two changes counteract each other and tend to minimize their influence on the noiseprint.

Of the other two major indicators, the block fuel varies by 1.5 percent for each 1.0 percent change in drag. This is roughly twice the rate of change experienced by DOC.

Field Length

All three aircraft take off in field lengths that are either at the maximum length permitted or are close to it. Figure L-3 shows the effects of designing these aircraft for other field lengths by allowing the wing loading to change. In every case, requiring shorter field lengths would

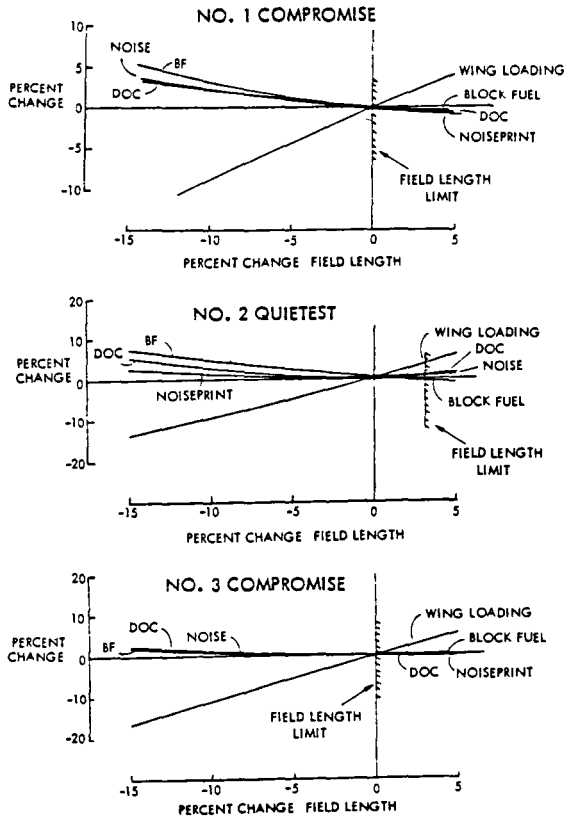

Figure L-3. Field Length Sensitivity Results for Turbofan Aircraft

have only negligible effects in terms of the measure of sensitivity on the noiseprints, DOCs, and block fuels of these aircraft.

Approach Speed

All three aircraft are designed for the limiting approach speed of 69 m/s (135 kt). The effects of changing this limit by varying the wing loading are shown in Figure L-4.

Any attempts to increase the approach speed are quickly squelched because of the field length and fuel volume constraints that become applicable. No such restrictions exist that mitigate against lowering the approach speed; however, there is a practical consideration. Substantial reductions in wing loading are required to lower the approach speed because the wing area is inversely proportional to the wing loading. Also, lower approach speeds mean that the aircraft become heavier, consume more fuel, cost more to operate, and make more noise. All of these effects are adverse with marginal to negligible ratings in terms of the measure of sensitivity. Thus, within the constraints and considerations of this study, there is no apparent reason for seeking a lower approach speed.

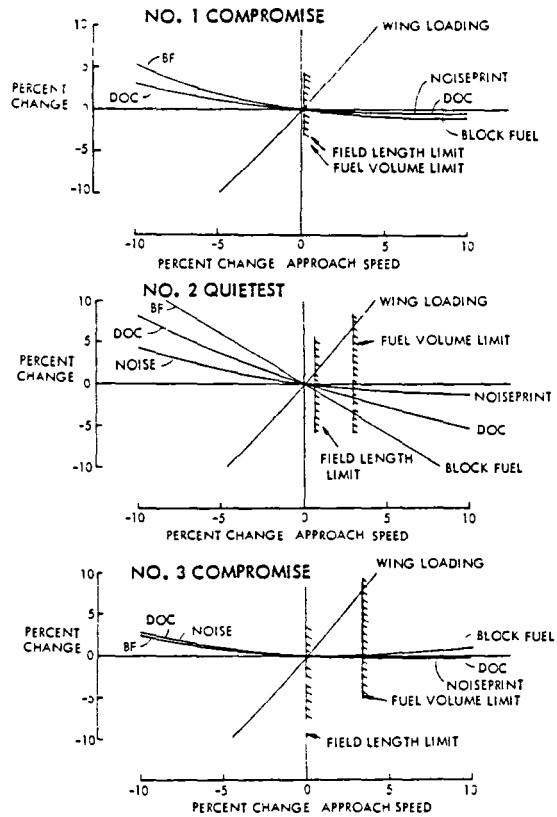

Figure L-4. Approach Speed Sensitivity Results for Turbofan Aircraft

Glideslope

All of the noiseprints were calculated for an approach flight profile that is in accord with the FAR standard 0.05-rad (3-deg) glideslope. An alternate 0.1-rad (6-deg) glideslope was investigated for the three turbofan aircraft. As indicated by the results in Figure L-5, this 0.05-rad (3-deg) change in glideslope produces about a 10-percent reduction in noiseprint area. This effect is three times what

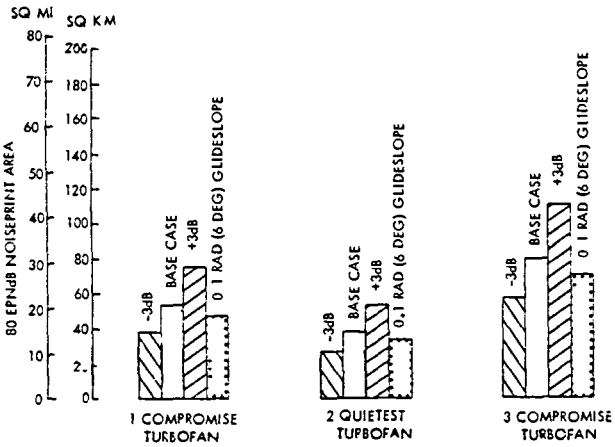

Figure L-5. Glideslope and Noise Source Level Sensitivity Results for Turbofan Aircraft

it was for the turboprop aircraft. The reason for the difference is apparent following an examination of the noiseprints for comparable turboprop and turbofan aircraft. Visual inspection of the noiseprint shown in the main section of this report for the turboprop aircraft reveals that the approach portion of the noiseprint is about one-fifth of the total area. In contrast, approach is responsible for one-third to one-half of the total noiseprint for the turbofan.

The turbofan aircraft also benefits more from a steeper glideslope than does the turboprop aircraft because the turbofan aircraft is not subject to the combination of tip speed and forward speed effects at altitude that plague its counterpart. However, in terms of the measure-of-sensitivity ratings, the effect of varying the glideslope is negligible.

Noise Source Level

Figure L-5 also shows what the effects are if the predicted level for the noise source is off by ± 3 dB. Every 3-dB increase in noise level produces approximately a 40-percent increase in noiseprint. Relative to the 80-EPNdB level of the base cases, the effect of changing the noise source level is critical to the size of the noiseprint.

WEIGHT

Sensitivities of the direct operating costs for the turbofan aircraft were assessed for variations in the weight estimates for three major categories of propulsion, airframe, and fuel. For this assessment, the aircraft ramp weights were held constant. Changes in the weights of one of the three categories were compensated for by equivalent, but opposite, changes in payload.

Figure L-6 displays the results of these weight sensitivity studies. The changes in DOC reflect the adjusted payload weight as well as different costs for the propulsion system, airframe, or fuel which resulted from changing the weight of the particular category. As indicated by the results, the No. 2 quietest aircraft is more sensitive to the weight changes than either of the compromise aircraft. For all three aircraft, propulsion and fuel weight changes have a negligible effect. Airframe weight variations have a significant effect on the No. 2 aircraft, but the impact on the No. 1 and No. 3 aircraft is lower, having only a marginal effect.

WING GEOMETRY

The two parameters used to determine the sensitivity of the selected aircraft to changes in wing geometry are the wing loading and aspect ratio.

Aspect Ratio

Variations in wing aspect ratio were investigated with the wing loading held constant for each aircraft. As noted in Figure L-7, approach speed and field length limits preclude going to higher aspect ratio values. Decreasing the aspect ratio from the base value for each aircraft produces only adverse effects on the three sensitivity indicators, even though the amount is negligible on the sensitivity rating scale. In every case, the sensitivity study results confirm that the aspect ratio chosen for each aircraft gives the minimum noiseprints, DOCs, and block fuels.

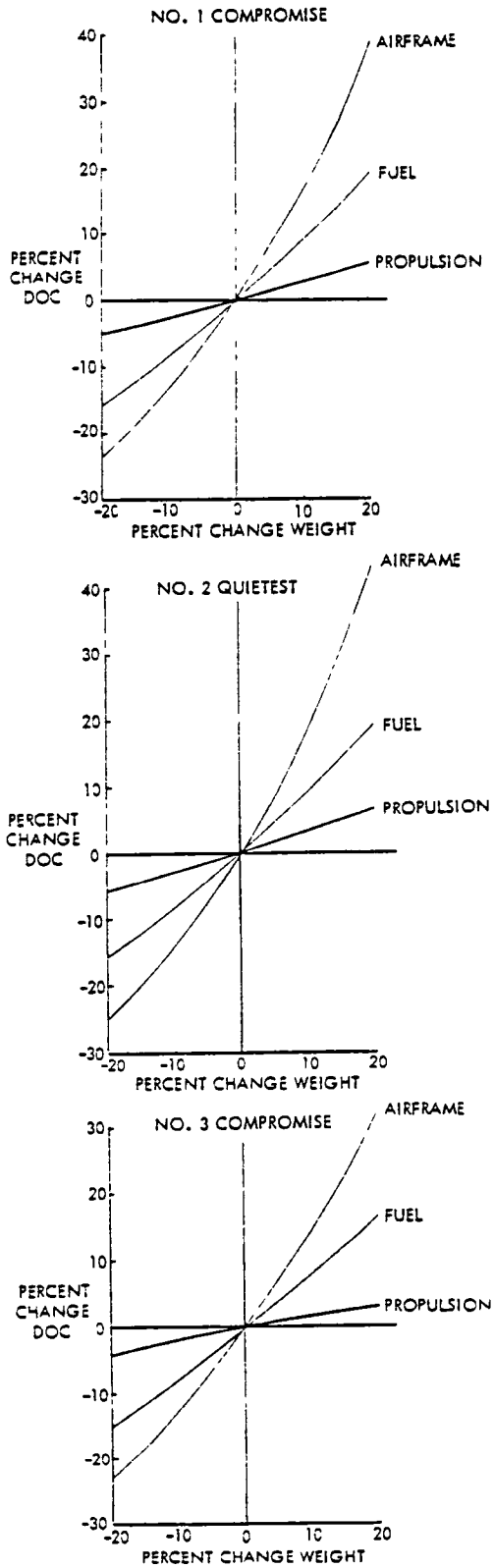

Figure L-6. Weight Sensitivity Results for Turbofan Aircraft

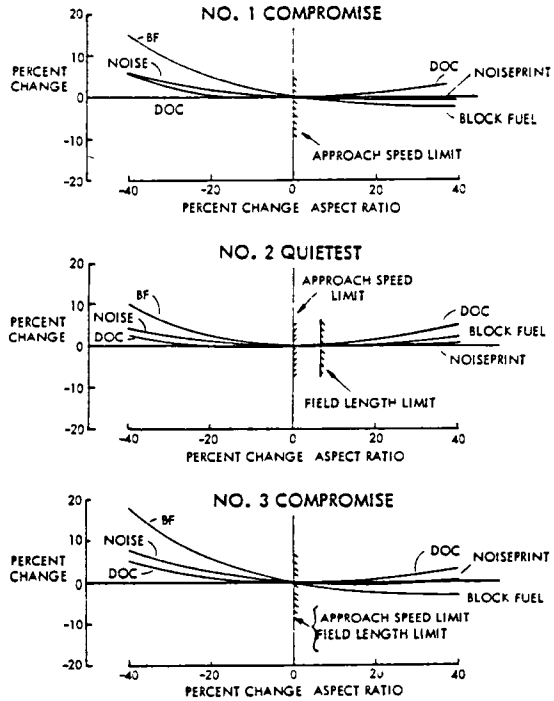

Figure L-7. Wing Aspect Ratio Sensitivity for Turbofan Aircraft

Wing Loading

Figure L-8 shows that the three aircraft are relatively insensitive to changes in wing loading. Due to approach speed, field length, and fuel volume limits, only lower wing loadings are valid, and they are not desirable because of the penalties incurred, even though they are negligibly small.

ECONOMICS

Sensitivity studies were conducted to determine the effects of such economic related parameters as stage length, annual utilization rate, load factor, and fuel price. The effects of varying the costs of the engine, airframe, total aircraft, and maintenance were also assessed.

Stage Length

Operating the turbofan aircraft over stage lengths that are shorter than the 4250 km (2295 n. mi.) design range produces the effects shown in

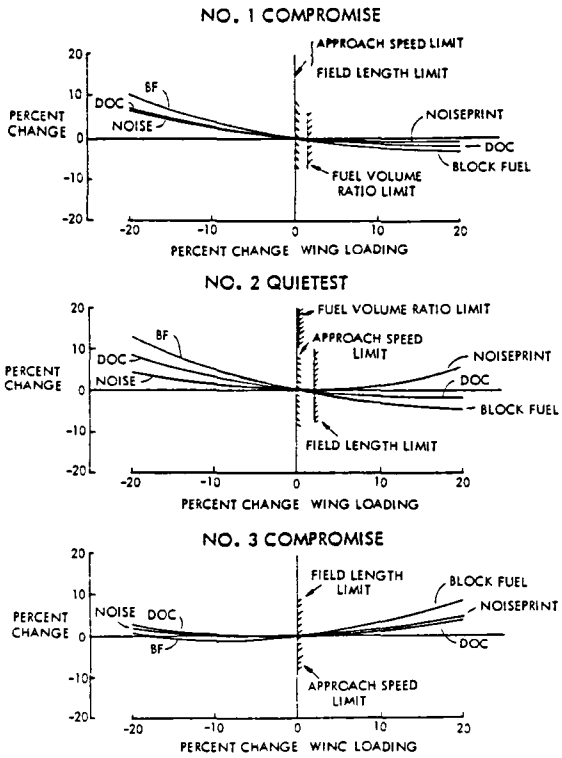

Figure L-8. Wing Loading Sensitivity Results for Turbofan Aircraft

Figure L-9. In each case, the aircraft design and payload are unchanged, but the amount of fuel carried is reduced commensurate with the particular stage length to be flown. As a result of the smaller fuel load, the ramp weight is reduced, the field length is shortened, and consequently, the noiseprint becomes smaller. Only DOC is adversely affected by the reduced range, as expected, because minimum DOC always occurs at the design point range for an efficient design.

Even though the total changes in block fuel and DOC appear to be large, when the change in range is accounted for, as in our measure of sensitivity, the effects of varying stage length are perceived to be negligible.

Annual Utilization

Two simplifying assumptions were used in determining the effect on DOC of increasing the annual unit utilization from 3000 to 6000 hours. First, fleet size is constant and productivity is allowed to increase; and second, the

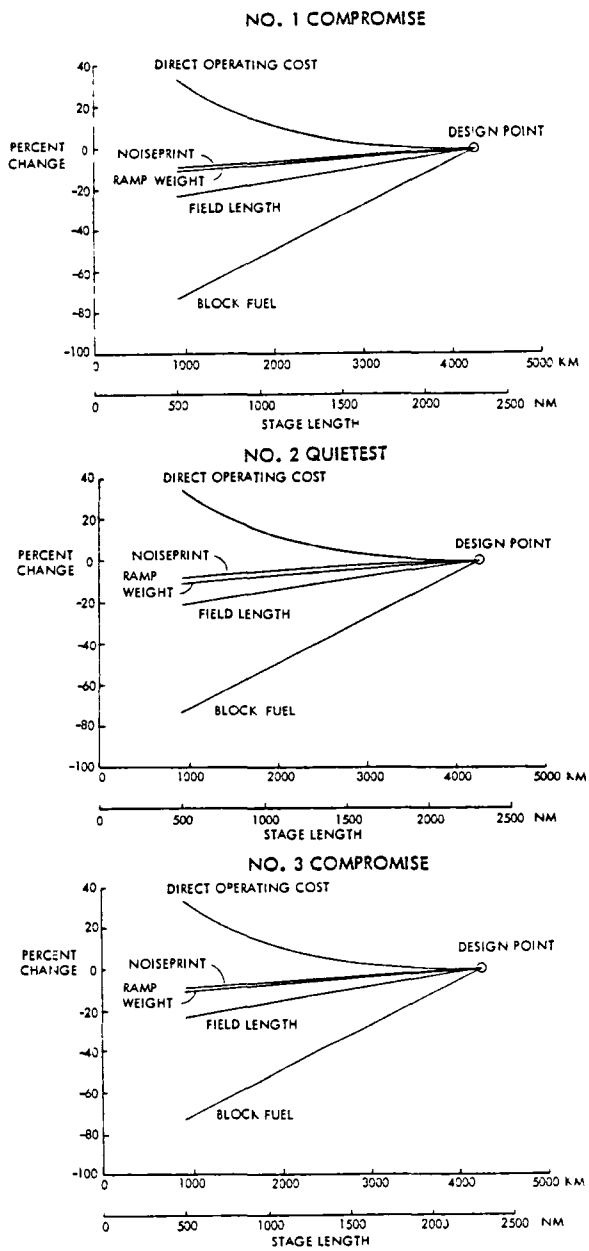

Figure L-9. Stage Length Sensitivity Results for Turbofan Aircraft

aircraft have a 15-year calendar lifetime regardless of utilization. The implications of these assumptions have already been discussed in a comparable section on turboprop aircraft; they will not be reiterated here.

Figure L-10 indicates the maximum potential reduction in DOC due to increased utilization. As fuel price increases, smaller DOC reductions will be realized because the fuel cost contribution to DOC increases, while the

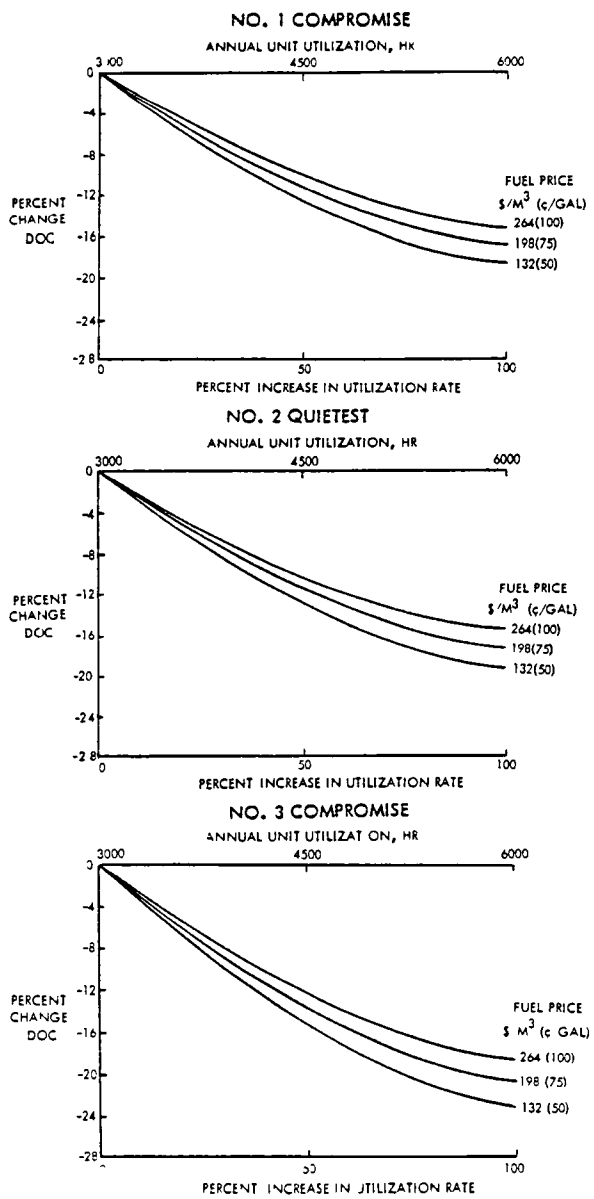

Figure L-10. Utilization Sensitivity Results for Turbofan Aircraft

depreciation portion, which benefits from higher utilization, decreases.

The No. 3 aircraft has the potential for achieving greater DOC reductions with increased utilization than the other aircraft because it is more energy-efficient. That is, the No. 3 aircraft requires less fuel to carry a unit of payload for a unit distance. Because of this, the portion of DOC contributed by fuel for the No. 3 aircraft is relatively smaller than for the other two aircraft. Thus, depreciation has a stronger effect.

The potential percent reduction in DOC is rated as negligible when the required change in utilization is taken into account.

Load Factor

A 15-percent reduction in load factor has the effects shown in Figure L-11. With 15 percent less payload to carry, the aircraft require less fuel to fly the mission range, and the ramp weights are reduced accordingly. As a result, the field lengths are shortened and the noiseprints become smaller. Only the DOCs are penalized by carrying less than the design payload.

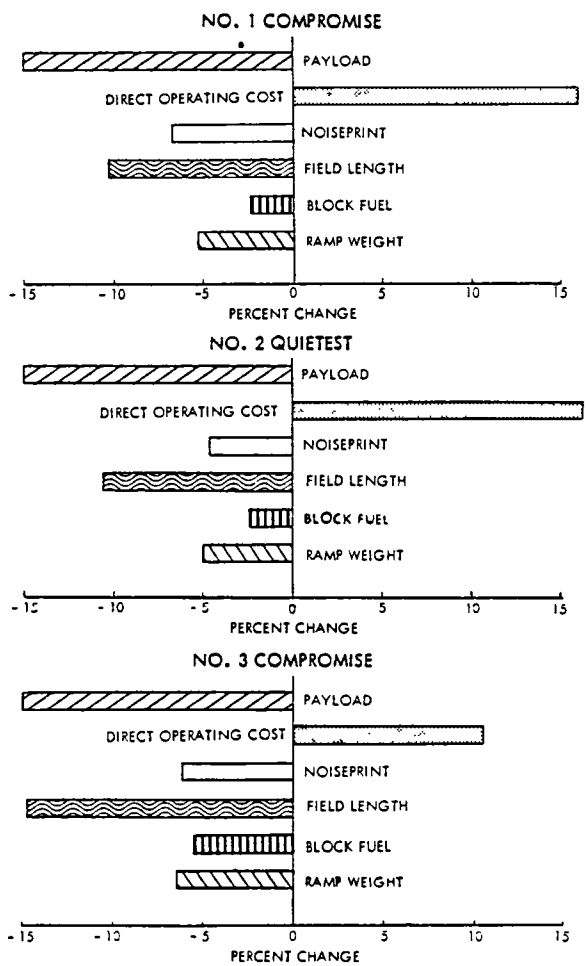

Figure L-11. Load Factor Sensitivity Results for Turbofan Aircraft

As suggested by the figures, the reduced load factor has a negligible effect on the block fuel and noiseprint for the three aircraft. The effect on DOC is barely marginal for the two smaller aircraft and negligible for the larger No. 3 aircraft.

Fuel Price

Figure L-12 shows the percent change in DOC that results when the fuel price is increased from 264 $/m^3$ (100 ¢/gal) to 792 $/m^3$ (300 ¢/gal). Although substantial changes in DOC are indicated, when the corresponding change in fuel price is recognized, the measure-of-sensitivity rating is negligible.

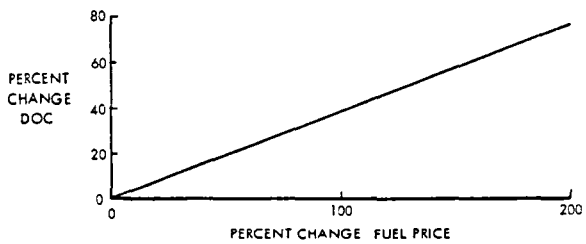

Figure L-12. Fuel Price Sensitivity Results for Turbofan Aircraft

Engine Cost

Varying the engine cost by up to ± 50 percent has negligibly small effects on the DOCs of the three aircraft, based on the results in Figure L-13. For example, a 10-percent change in engine cost produces less than a 0.6-percent change in DOC. As fuel price increases, the effect of engine cost becomes even smaller because fuel contributes a greater percentage of DOC and the share for engine depreciation is less.

Airframe Cost

Variations in the cost to manufacture the airframe (the aircraft without its propulsion and avionics systems) will affect the DOCs of the three aircraft to the extent shown in

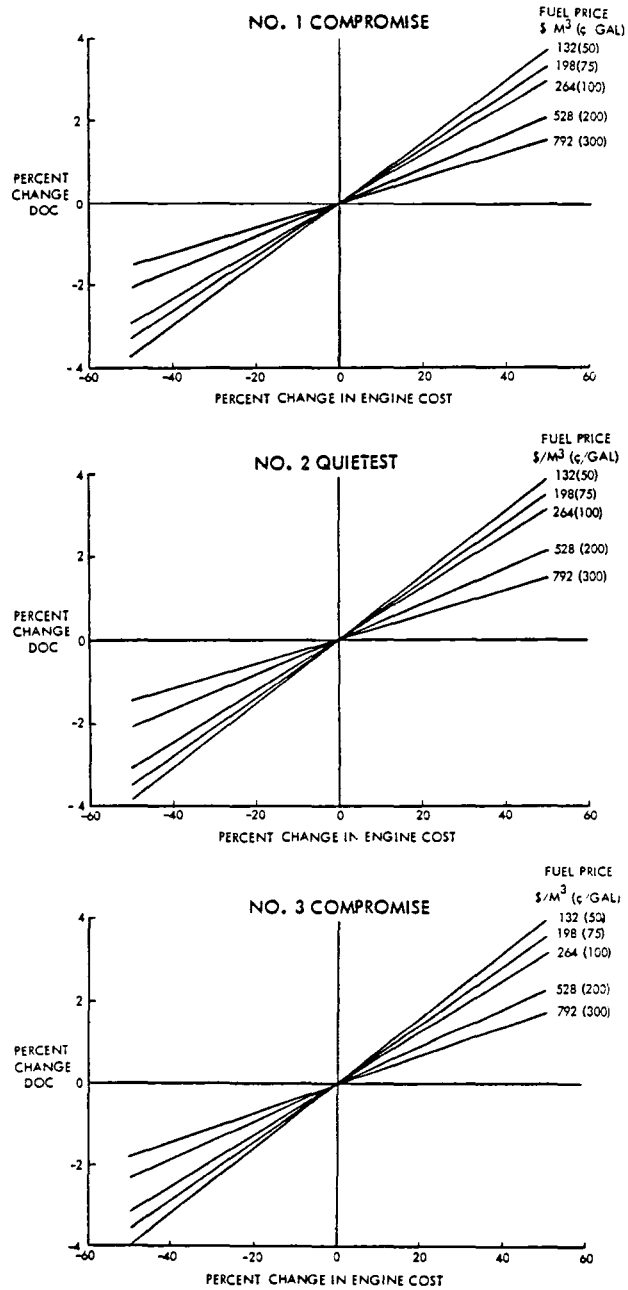

Figure L-13. Engine Cost Sensitivity Results for Turbofan Aircraft

Figure L-14. Although the percent change in DOC for this case is larger than for the engine, the measure of sensitivity is still negligible. The basis for this is that a 10-percent change in the manufacturing cost gives less than a 2-percent change in DOC. In this case also, fuel price has the same effect as it did on the engine, that is, increasing the fuel price

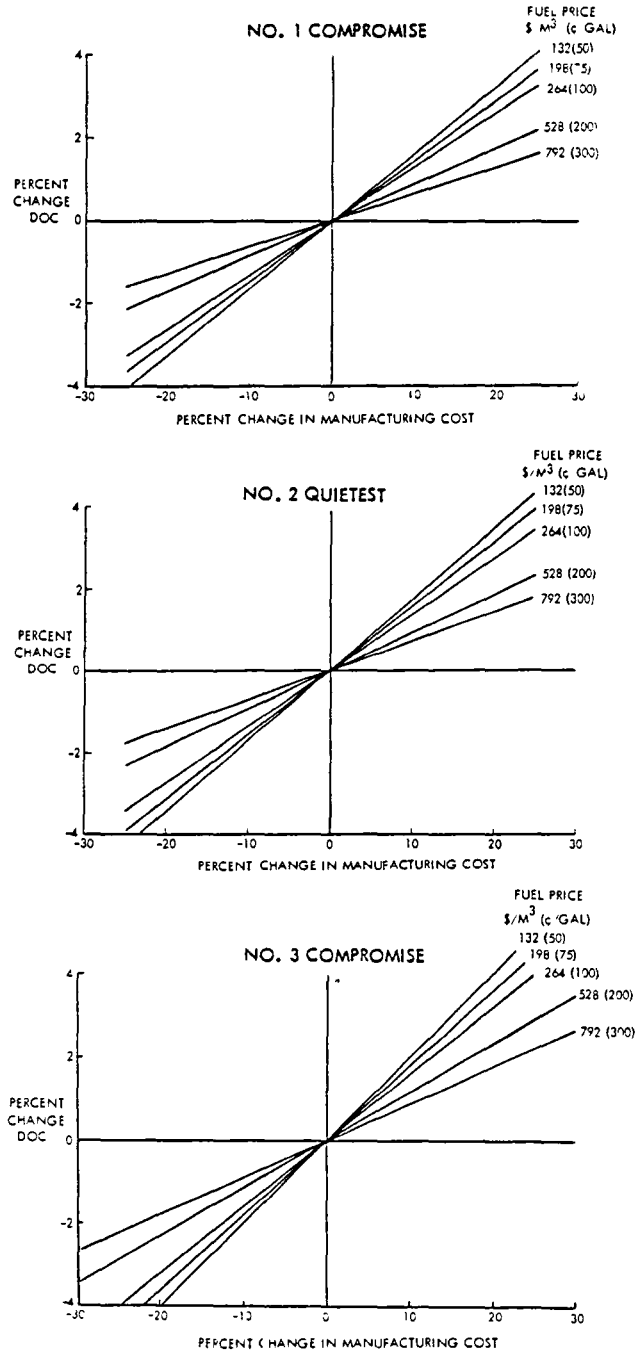

Figure L-14. Airframe Cost Sensitivity Results for Turbofan Aircraft

tends to reduce the impact on DOC of changing the manufacturing cost.

Flyaway Cost

Changing the unit flyaway cost of the aircraft, affects the DOC of the three aircraft to the extent shown in Figure L-15. The DOC variations between 2 and 5 percent that are produced by a 10-percent change in the flyaway cost are negligible on the sensitivity rating scale. Higher fuel prices reduce the effect of flyaway cost on DOC just as they did for the engine and airframe.

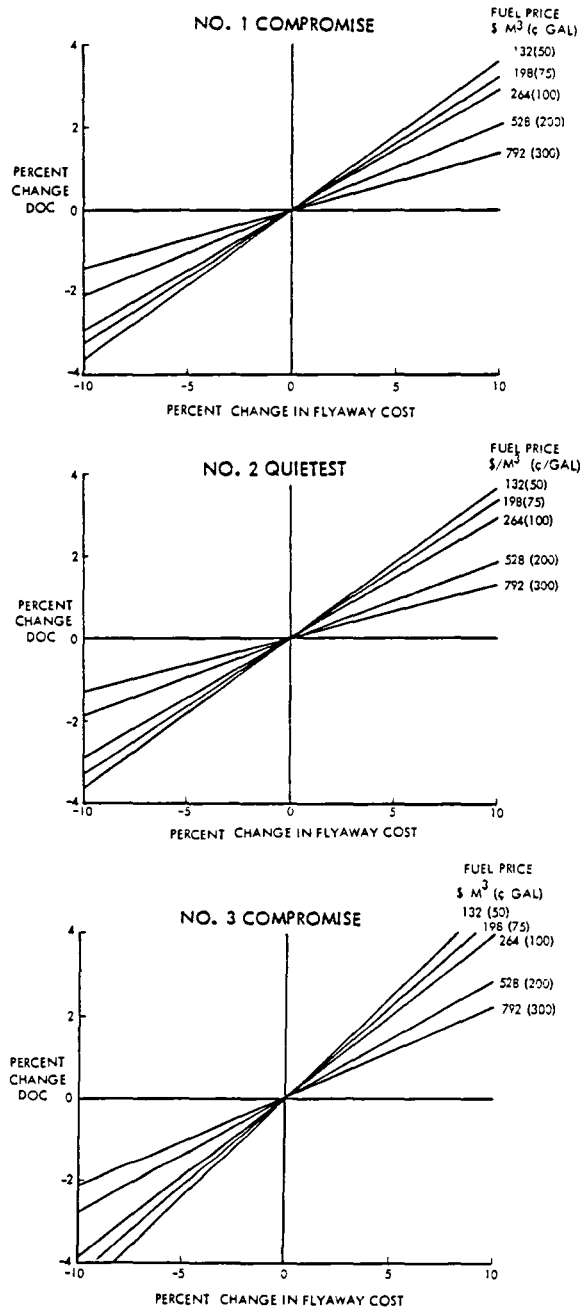

Figure L-15. Flyaway Cost Sensitivity Results for Turbofan Aircraft

Maintenance Cost

To complete this parallel series of studies, a maintenance cost sensitivity study was performed for the turbofan aircraft. Figure L-16 shows that negligible changes in DOC can be expected, even for relatively large changes in propulsion system maintenance for all three aircraft. Expressed numerically, a 10-percent change in propulsion maintenance cost will cause less than an 0.8-percent change in DOC. As for the previous cost sensitivities, increasing fuel price reduces the effect of changing maintenance cost on DOC.

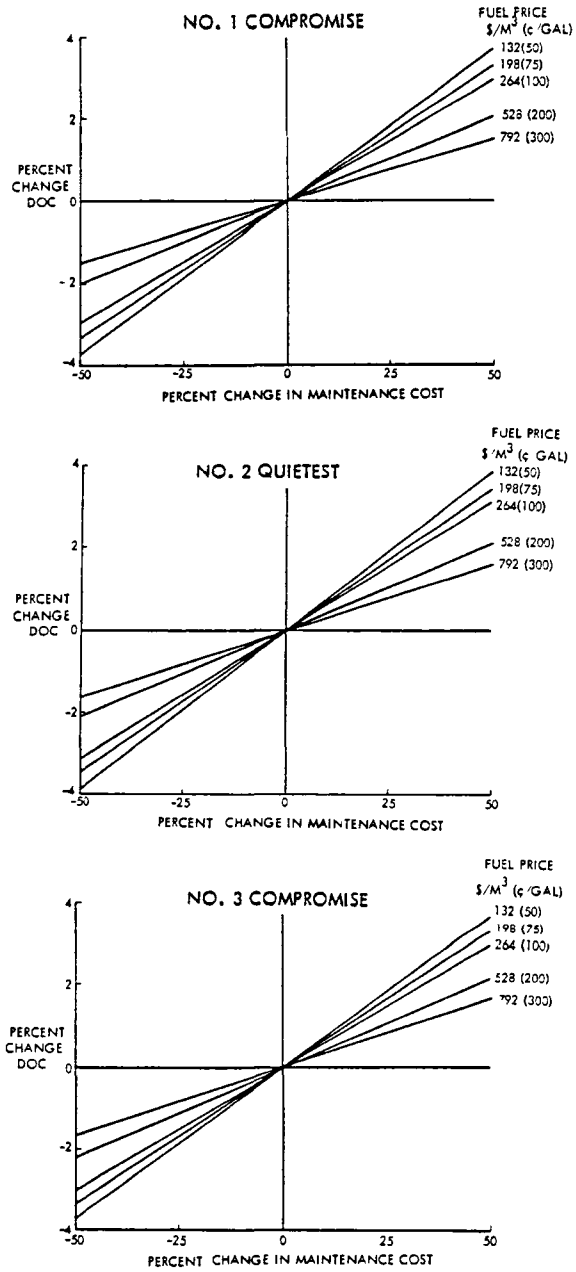

Figure L-16. Maintenance Cost Sensitivity Results for Turbofan Aircraft

APPENDIX M: ADDITIONAL NOISE CONSIDERATIONS

The purpose of this appendix is to document some small noise-related studies that were conducted following the comparison of the turboprop and turbofan powered aircraft.

PROPELLER SLIPSTREAM EFFECTS ON AIRFRAME NOISE

Our results show that airframe noise predominates on approach for the three turboprop aircraft. Furthermore, we note that the airframe noise of the turboprop aircraft is between 2.5 and 3.5 dB noisier than for the turbofan aircraft on approach when both aircraft are at essentially the same conditions (Compare corresponding aircraft in Tables XV and XXVI). The differences in airframe noise at the other measuring points cannot be attributed solely to the propeller slipstream because of the variances in aircraft altitude and speed.

To understand the contribution of the propeller slipstream to airframe noise, the noise levels of the major airframe components* were calculated with and without the slipstream. The results are presented in bar graph form in Figure M-1 for the No. 2 Quietest Turboprop Aircraft at the approach measuring point. In this case, the flaps, which are deflected 0.87 radians (50 degrees), are the major noise source. While the slipstream adds 3.5 dB to the flap noise, the net effect is only an additional 2.6 dB on the total airframe (wing + tail + flaps + gear) because the slipstream does not affect the gear, and it has only a small effect on the wing and tail combination.

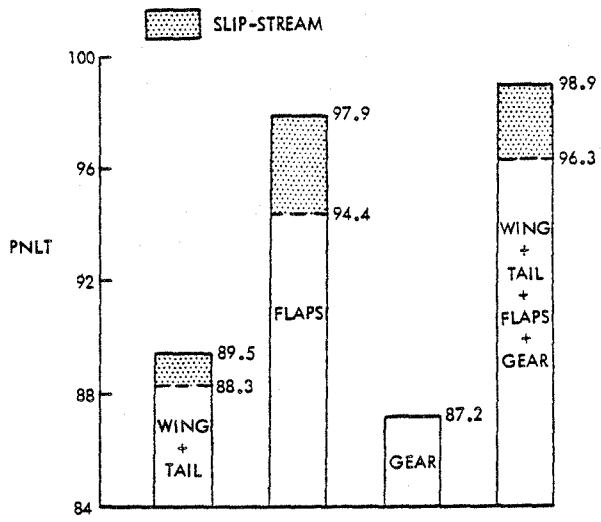

Figure M-1. Propeller Slipstream Effects on Noise

Without the slipstream effects, the noise levels in Figure M-1 should be those expected for a turbofan-powered aircraft of the same geometry. A check of the numbers confirms that this is indeed the case. The 96.3 dB noise level shown for the total airframe (wing + tail + gear) without the slipstream is only 0.2 dB lower than the airframe noise level listed previously in Table XXVI for the No. 2 Turbofan Aircraft. This small difference occurs because the turboprop aircraft is slightly smaller than the turbofan aircraft, having lower values of wing area, wing aspect ratio, and tail area.

ACOUSTIC GROUND REFLECTION EFFECTS

In this report, all of the predicted noise levels include 3 db more than free-field noise levels to account for ground reflection effects. This assumption is based on experience with noise measurements for noise-suppressed turbofan-powered aircraft, where the noise spectra are characterized by broad-band energy contained in the middle and upper frequencies, and where the microphone is pole mounted over a hard surface. This ground reflection effect is not very sensitive to microphone heights above 2 feet.

---

* While the fuselage is a major structural element of the airframe, Reference 31 has shown that the noise level produced by the fuselage is negligible relative to the other structural elements and is not included here.

For an aircraft powered by a propeller where the noise spectra contains low frequency discrete tones, in addition to broad band noise, the ground reflection effect is more complex. The situation is illustrated in Figure M-2 from Reference 41 for the two types of noise sources when they are located directly above a perfectly reflecting surface and the microphone is 4-ft above ground, e.g., FAR 36 microphone locations. As shown, the propeller discrete tones can be subject to large cancellations, or reinforcements of up to 6 dB, depending upon their frequency, while the broad band noise coming from the engine core and airframe is subject to an average increase of 3 dB. The resulting effect, in terms of Δ PNdB and Δ EPNdB, requires detail evaluation; however, through judicious selection of propeller frequencies, tone cancellation can reduce the propeller discrete-frequency noise at the 4-ft high microphone. Any noise reduction obtained by this frequency tuning is, however, sensitive to microphone height and thus does not hold for all points in space. These effects will be diminished if the ground surface were considered to be partially absorbing instead of perfectly reflecting - a more difficult case to analyze.

As an example, estimates of these effects have been evaluated for the No. 2 Quietest Turboprop Aircraft. The propeller fundamental tone is close to 71 Hz, and consequently, the flyover noise is attenuated. But, in contrast, the first harmonic at 142 Hz is subject to a 6-dB increase, and the engine/airframe mid-to-high frequency components are subject to a 3-dB increase. The overall effects on noiseprints are shown in Figure M-3, where a reduction in flyover noise is indicated. For a sideline location, the overall effect is different because of a different source/ground/observer geometry, and a slight increase in sideline noise is shown. In this example, inclusion of propeller-tone ground-reflection

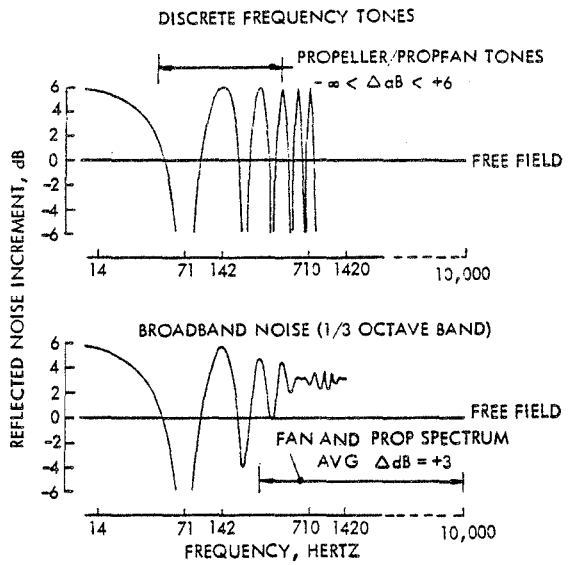

Figure M-2. Ground Reflection Effects

effects provides some reductions in noiseprint areas at the two lower noise levels of 70 and 80 EPNdB.

Based on these results, we must conclude that further study is needed on the influences of ground reflection effects - both ground absorption characteristics and microphone height - on the selection of propeller rotational frequencies for the low-noise design of turboprop-powered aircraft.

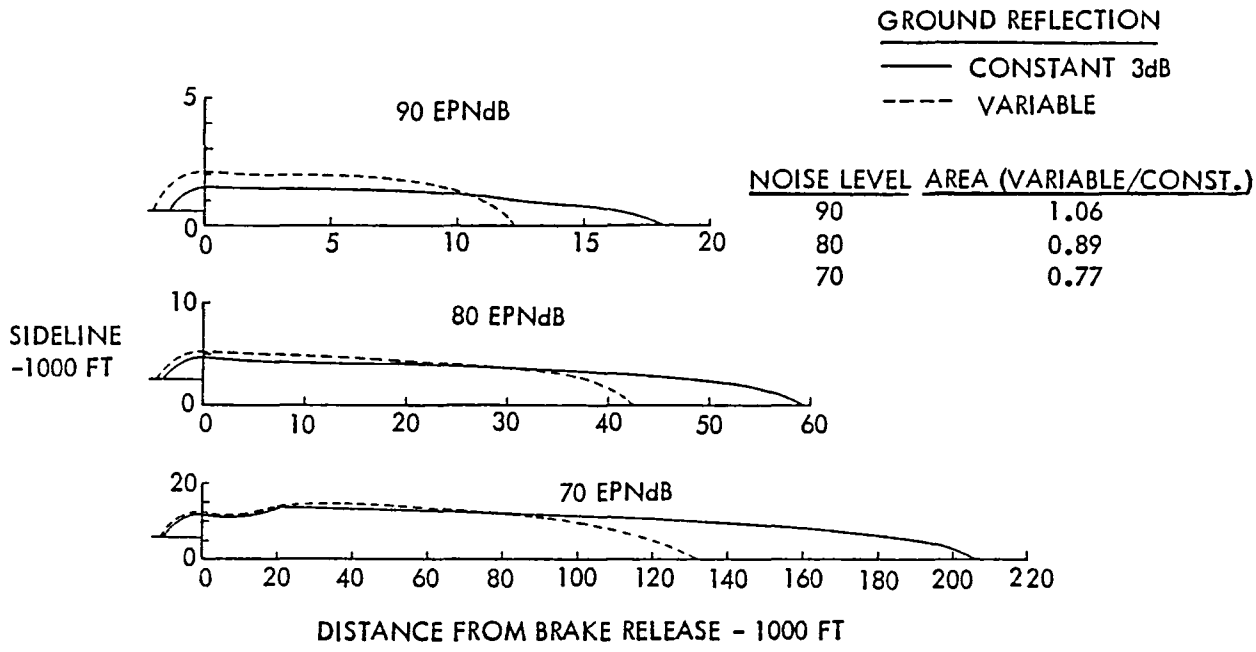

Figure M-3. Noiseprint Sensitivity to Ground Reflection Effects

APPENDIX N. ANALYSIS OF ALTERNATE TAKEOFF AND CLIMB PROFILES

Various changes to the takeoff and climb procedures were investigated in an effort to reduce the noiseprints of the No. 1 and No. 2 Turboprop and Turbofan Aircraft. The final results have already been summarized in the body of this report along with a discussion of the net effects of the changes on the relative comparison of the two types of propulsion. This Appendix presents the details of what individual changes were considered, what the effects were, and how the noiseprint reductions were achieved for each of the four aircraft.

Before proceeding with the detailed report, two points bear repeating so that there is a clear understanding of the base from which the analysis begins and of the assumptions which constrain the results. First, in the base case, all of the aircraft took off with the flaps deflected at 0.35 rad(20 deg) and achieved an obstacle speed 5.1 m/s (10 kt) above the minimum safe speed. Upon reaching an altitude of 122 m (400 ft), the flaps were retracted and the aircraft continued at their maximum rate of climb to cruise altitude. Second, the optimizations were directed toward the 80-EPNdB noiseprints only. The benefits achieved at the 70 and 90 EPNdB levels are merely fallouts and are not suggested to be the minimum noiseprints that can be attained if other takeoff and climb procedures are adopted.

The changes to the takeoff and climb procedure that were investigated were: different flap angles, higher altitudes for flap retraction, increased obstacle speeds, climbing at maximum gradient (altitude gained per unit of horizontal distance travelled) instead of maximum rate of climb (altitude gained per unit of time in flight), and cutback power. Each of these were varied independently and sequentially to minimize the noiseprints, using the following procedure for all four aircraft. Initially, the takeoff flap angle was varied while all other parameters were held constant at their original values. That flap angle which minimized the 80-EPNdB noise print was selected and held constant while the effects of different flap retraction altitudes were then investigated. This type of cycle of varying one parameter, selecting an optimum value, and holding it constant while optimizing another was repeated several times to reach the final results shown in Figure N-1. Presented here are the maximum noiseprint reductions, what variations to the takeoff procedure caused the reductions, and the accompanying block fuel penalties for each of the four aircraft. The remainder of this appendix describes how these results were obtained for each aircraft.

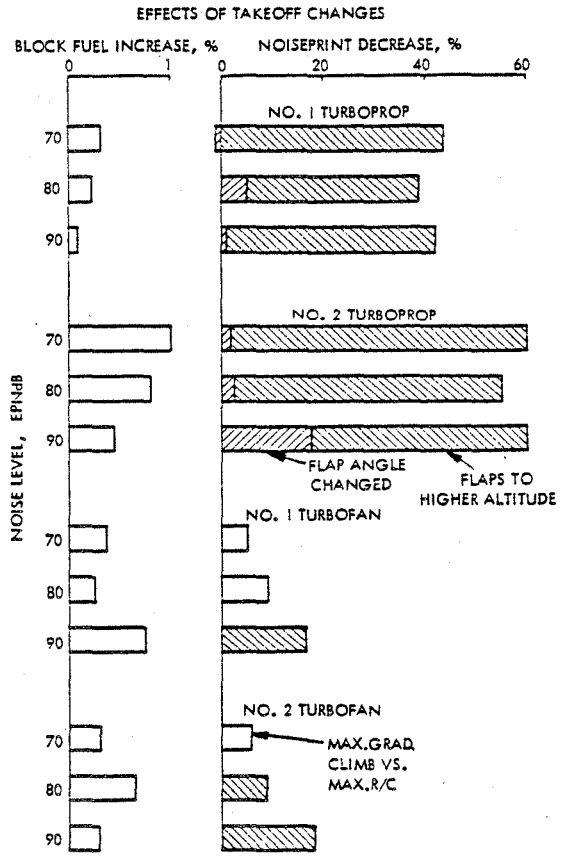

Figure N-1. Summary of Results for Alternate Climb Procedures

NO. 1 TURBOPROP

The initial investigation for this aircraft dealt with variations to the flight profile under conditions of full power and maximum rate of climb. After determining the best combination of flap angle, flap retraction altitude, and obstacle speed, attention was focused on the effects of maximum gradient climb and cutback power.

Maximum Rate of Climb

Figure N-2 graphically depicts the sequential approach that was followed and the noiseprint changes that were obtained for the initial part of this investigation. Figure N-3 contains the corresponding effects on block fuel consumption.

Takeoff Flap Angle - Two factors, which tend to counteract each other, are responsible for the results shown in part a) of Figure N-2. As the flap angle increases, the lift coefficient and area of the wing-flap combination increase, which enhances the climb capability of the aircraft, and thereby tends to reduce the noiseprint. Concurrently, however, the drag also increases, which means that less of the engine thrust is available to accelerate the aircraft. Thus, the portion of lift due to speed is reduced, which causes the aircraft to climb slower and the noiseprint to become larger.

These results show that only very small benefits are obtained for any of the noiseprints from reducing the takeoff flap angle below the base value of 0.35 rad (20 deg), and that only penalties accrue for larger angles. In keeping with the spirit of the optimization process, however, a 0.26 rad (15 deg) flap angle was selected for the subsequent analyses, even though this value gives less than a 0.2 percent decrease in area. A miniscule savings of 0.01 percent in block fuel is realized at this flap angle, as shown in part a) of Figure N-3.

Flap Retraction Altitude - Results from the second step are illustrated in part b) of Figures N-2 and N-3. They show that deploying the flaps to higher altitudes substantially reduces the noiseprints for all three noise levels while increasing the fuel required by a small amount.

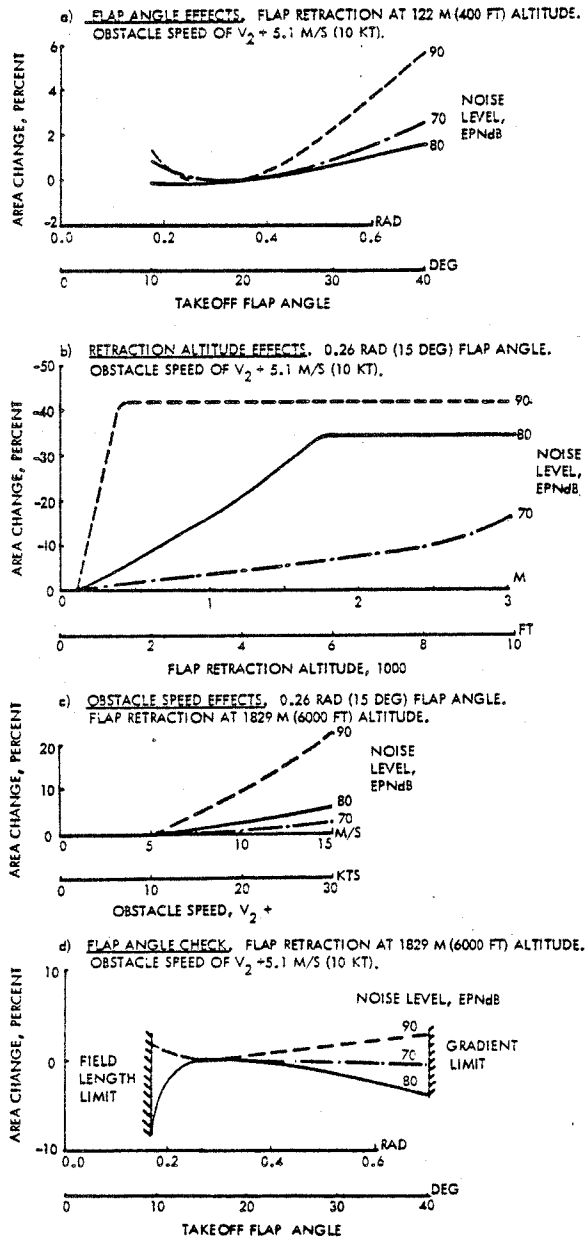

Figure N-2. Noiseprint Variations Due to Alternate Climb Procedures for No. 1 Turboprop Aircraft at Maximum Rate of Climb

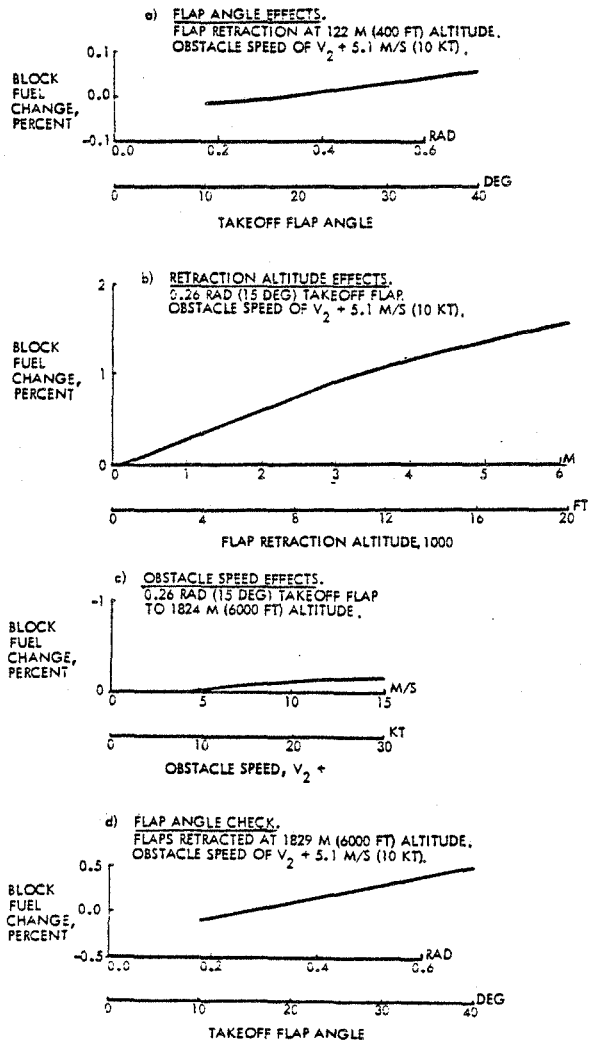

Figure N-3. Fuel Consumption Variations Due to Alternate Climb Procedures for No. 1 Turboprop Aircraft at Maximum Rate of Climb

The noiseprint curve for each level eventually reaches a horizontal plateau where no further reductions in area are possible from keeping the flaps deployed. This plateau is attained when the aircraft altitude is high enough to produce noiseprint closure. That is, as the aircraft climbs, it reaches an altitude at which the noise perceived on the ground is less than the minimum level which establishes the boundary of the noiseprint, and the noiseprint no longer grows in size.

The significance of the noise level used in selecting the takeoff procedures becomes very evident in this case. For a 90-EPNdB level, the flaps need to be deployed only to an altitude of 457 m (1500 ft). For 80 and 70 levels, however, the maximum benefits are realized only if the flaps remain deployed to altitudes of 1829 m (6000 ft) and 3048 m (10,000 ft), respectively. Following the ground rules for this study, the value which minimizes the 80-EPNdB noiseprint was selected for the next step in the analysis.

Obstacle Speed - Increasing the aircraft obstacle speed* above the minimum safe value used as a baseline, adversely impacted the noiseprints at all three noise levels, as illustrated in part c) of Figure N-2. Furthermore, the higher the noise level of the noiseprint, the greater the severity of the penalty.

What causes these two effects? First, when the obstacle speed is increased, the aircraft must accelerate to a higher liftoff speed before leaving the runway. This increases the takeoff distance and keeps the aircraft close to the ground for a longer period of time during takeoff and initial climb. Both of these contribute to enlarging the noiseprint. Second, the typical trend is that the higher the noise level defining the noiseprint, the quicker the noiseprint closes, the smaller its area, and the greater the percentage effect of a unit change in area.

While part c) of Figure N-3 shows small reductions in block fuel at higher obstacle speeds, there are no noiseprint benefits from increasing the obstacle speed, and so, the baseline minimum safe obstacle speed value is retained for the rest of this analysis.

*Obstacle speed is the speed of the aircraft when it reaches an altitude of 10.7 m (35 ft) on takeoff. This corresponds to the height required to clear a possible obstacle at the end of the runway.

Takeoff Flap Angle Check - With the previous results indicating the desirability of deploying the flaps to an altitude of 1829 m (6000 ft) to minimize the 80-EPNdB noiseprint, the takeoff flap angle was reoptimized. The results in part d) of Figures N-2 and N-3 show that a reduction of the flap angle to 0.17 rad (10 deg) is beneficial to both the noiseprint and block fuel consumption.

Interestingly, the 80-EPNdB noiseprint can be reduced by increasing or decreasing the flap angle relative to the 0.26 rad (15 deg) value previously used. This is the result of the lift on the aircraft coming from its speed and the product of the lift coefficient and area of the wing-flap combination, as previously explained. With 0.17 rad (10 deg) flaps, the speed contribution is responsible for the reduced noiseprint, while at 0.7 rad (40 deg) flaps, the area and lift coefficient product is the major contributor. The two extremes of the curve are limited at the lower flap angles by field length restrictions and at the higher angles by engine-out gradient limitations.

Both the 70 and 90-EPNdB noiseprints display a preference for remaining at the 0.26 rad (15 deg) flap angle previously selected.

Maximum Gradient Climb

Figure N-4 shows the effects on noiseprint area and block fuel consumption of climbing at maximum gradient for some portion of the flight profile. Initially, the aircraft follows the baseline procedure of taking off with 0.35 rad (20 deg) flaps, of passing the obstacle with a speed of V_2 + 5.1 m/s (10 kt), and of climbing to 122 m (400 ft) before retracting the flaps. The aircraft then climbs at maximum gradient, instead of maximum rate, from flap retraction to the altitude shown. Once the aircraft reaches each particular altitude value, it reverts to a maximum rate of climb.

The horizontal plateau for each noise level signifies, as discussed before, that the aircraft has attained sufficient altitude so that its noise no longer contributes to the particular noiseprint, that is, the noiseprint has closed. A comparison of these results with those in part b) of Figure N-2 shows that climbing at maximum gradient allows the high-level noiseprints to close when the aircraft is at a lower altitude than when the flaps remain deployed. However, there is a greater percentage reduction in noiseprint area from keeping the flaps deployed. The reason for this is that with the flaps deployed the aircraft speed remains low and the distance travelled horizontally from brake release on takeoff is considerably shorter than for maximum gradient climb.

A comparison of the results in Figure N-4 with those in part b) of Figure N-3 shows that of the two methods, climbing at maximum gradient uses less fuel. This is as expected because when the flaps are deployed they produce a drag penalty which is reflected in the higher fuel consumption.

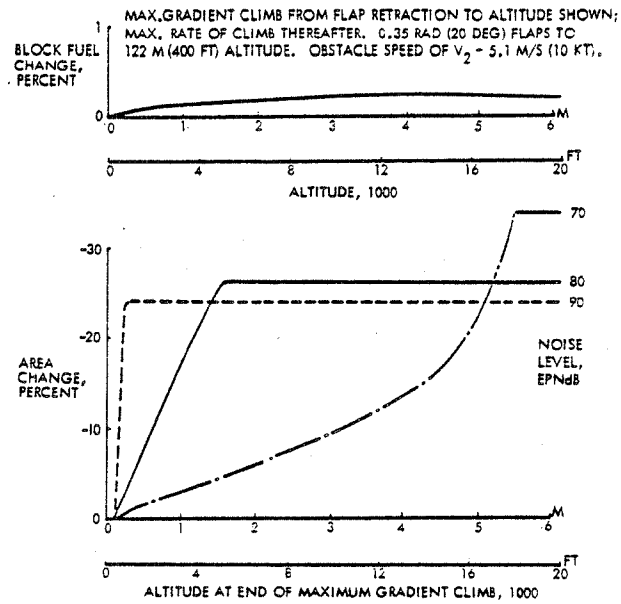

Figure N-4. Maximum Gradient Climb Effects for No. 1 Turboprop Aircraft

Having observed that smaller areas were obtained by climbing with flaps deployed until after the noiseprint closed, rather than by climbing at maximum gradient, attention was directed toward determining if any combination of the two might be more attractive. That is, might greater benefits be achieved by keeping the flaps deployed to an altitude greater than the 122 m (400 ft) standard retraction value and then continuing to climb at maximum gradient until the noiseprints close. Figure N-5 illustrates the results from doing this for each of the three noise levels. This figure also compares this procedure with a similar case of increasing the flap retraction altitude and then climbing at the maximum rate.

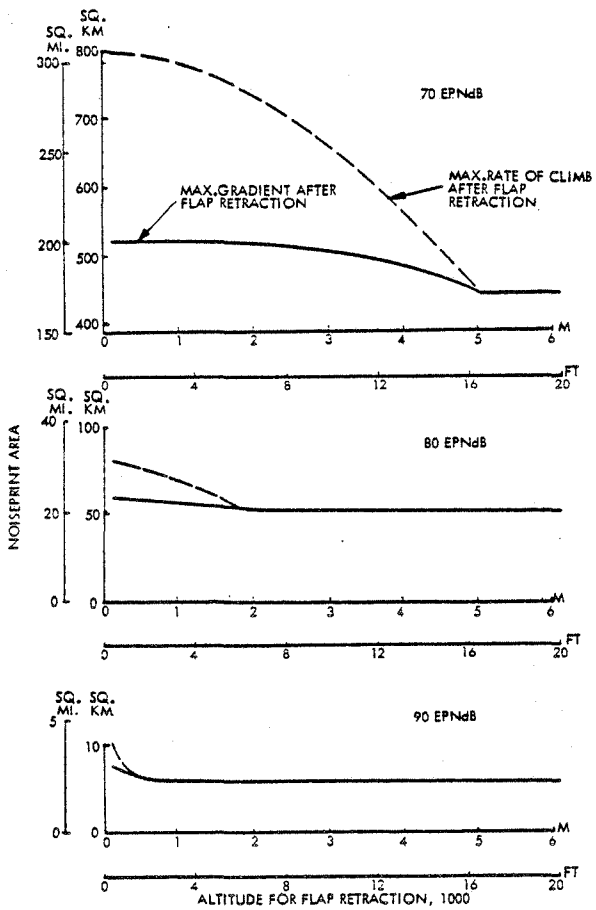

Figure N-5. Comparison of Maximum-Gradient and Maximum-Rate Climb Effects on Noiseprint for No. 1 Turboprop Aircraft

Clearly, increasing the flap retraction altitude before climbing at maximum gradient does reduce the noiseprint, but not below the level achieved by simply leaving the flaps deployed until the noiseprint closes. Also, for a given flap retraction altitude, smaller noiseprint areas are obtained by climbing at maximum gradient instead of maximum rate until the noiseprint closes.

Figure N-6 shows the fuel penalties to be expected when reducing the noiseprints by the amounts indicated in Figure N-5 from deploying the flaps to higher altitudes and then climbing at maximum gradient. Of this penalty, the gradient climb is largely responsible for that incurred up through 610 m (2000 ft) altitude, but thereafter, the additional increases are almost totally due to the flaps.

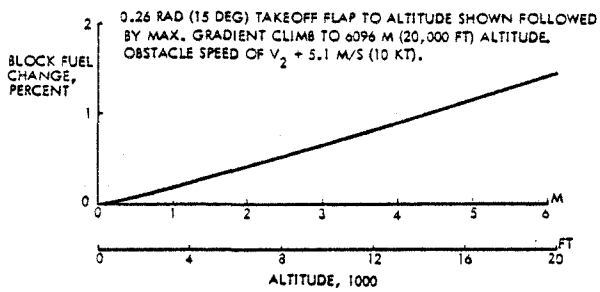

Figure N-6. Comparison of Maximum-Gradient and Maximum-Rate Climb Effects on Fuel Consumption for No. 1 Turboprop Aircraft

Cutback Power

Aircraft having difficulty meeting the FAR 36 noise regulations can be certified by following a procedure that includes reducing engine power just before reaching the takeoff flyover and sideline noise measuring points. The potential effects of following such a procedure to reduce the noiseprints of an aircraft were investigated.

As prescribed by FAR 36 for the cutback case, the flaps remain deployed in the takeoff position while the aircraft climbs to an altitude not less

than 305 m (1000 ft) and reduces engine power to the minimum levels permitted prior to passing the measuring points. This type of profile is then continued until the aircraft is sufficiently past the measuring points so that no higher readings are recorded as the aircraft resumes power and climbs to altitude.

This type of procedure was investigated with variations considered to the takeoff flap angle, obstacle speed, and cutback altitude. Figure N-7 summarizes the results. Parts a) and b) confirm that the previously selected flap angle and obstacle speed are the best values for minimizing the noiseprint. Several observations may be noted based on part c). First, delaying the start of power cutback to higher altitudes is undesirable for the 90 EPNdB noiseprint, but does offer some benefits at the two lower noise levels. Second, the changes for both the 90 and 80 EPNdB noiseprints give evidence of noiseprint closure as indicated by the plateau reached on the right side of each curve. Third, at the 70 EPNdB level there is an optimum cutback altitude, and it occurs well before noiseprint closure, which is not shown on the figure.

Figure N-8 compares the extent to which the base noiseprint area, that was previously listed in Table XXX, has been reduced through flight profile modifications with full and cutback power. The top bar in the figure for each noise level indicates the reduced noiseprint size, as discussed in a previous section, which can be achieved by climbing at full power with some changes to the basic climbout procedures. The second bar depicts the reduced noiseprint size that occurs with power cutback, as reported previously in Table XXX. The last bar reflects the benefits of using the optimum altitude for power cutback.

These results show that power cutback offers only slight benefits relative to those obtained with full power and modified climb-out procedures. While the power cutback is within prescribed safe operating limits,

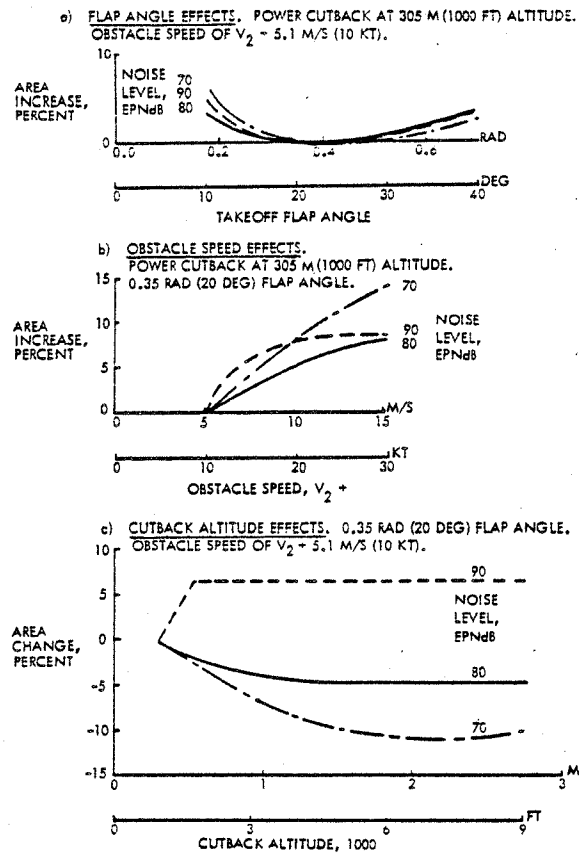

Figure N-7. Effect of Alternate Climb Procedures with Cutback Power for No. 1 Turboprop Aircraft

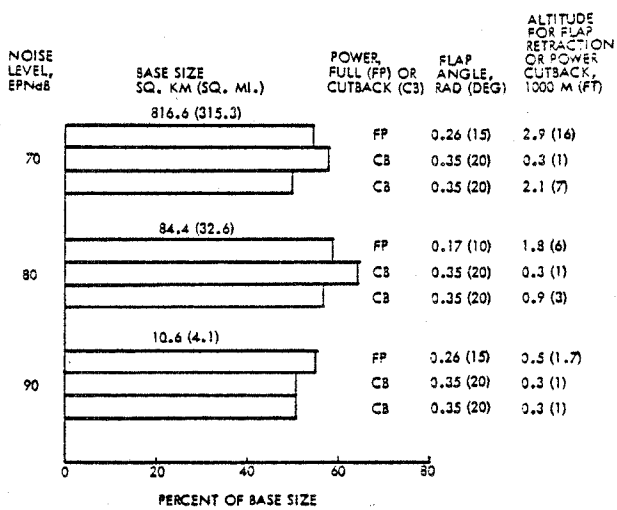

Figure N-8. Comparison of Full and Cutback Power Results for No. 1 Turboprop Aircraft

pilots are not overly enamored with any power reduction during this phase of flight and probably will tend to resist such a procedure. Recognizing that the pilot concerns are likely to preclude universal compliance with a cutback procedure to reduce noiseprint areas in practice, and in view of the relatively small benefits that accrue from the reduced power, we will concentrate our efforts on reducing noiseprints at full power operation.

NO. 2 TURBOPROP

The investigation to reduce the noiseprints of this aircraft paralleled that for the No. 1 aircraft. To limit repetition, the results will be presented for this case without extensive explanations unless there is some radical change in the trends.

Maximum Rate of Climb

Figure N-9 illustrates the sequential approach that was followed and the noiseprint changes that were obtained from varying the takeoff flap angle, the flap retraction altitude, and the obstacle speed in conjunction with takeoff and climb at the maximum rate. Figure N-10 displays the corresponding effects on block fuel consumption.

Part a) of Figure N-9 shows that the noiseprints are insensitive to decreasing the flap angle for all three noise levels and only slightly sensitive to increasing the angle for the 70 and 80 EPNdB levels. The 90 EPNdB level noiseprint experiences a substantial reduction in size from increasing the flap angle to 0.67 rad (39 deg) because with the larger value, the aircraft is at higher altitudes and lower speeds for almost the entire takeoff portion of this relatively small noiseprint. While larger angles might prove more beneficial in reducing the noiseprints, at angles greater than 0.68 rad (39 deg) the aircraft is unable to comply with the minimum limits of FAR 25 for engine out during second segment climb. Based on the favorable results at this

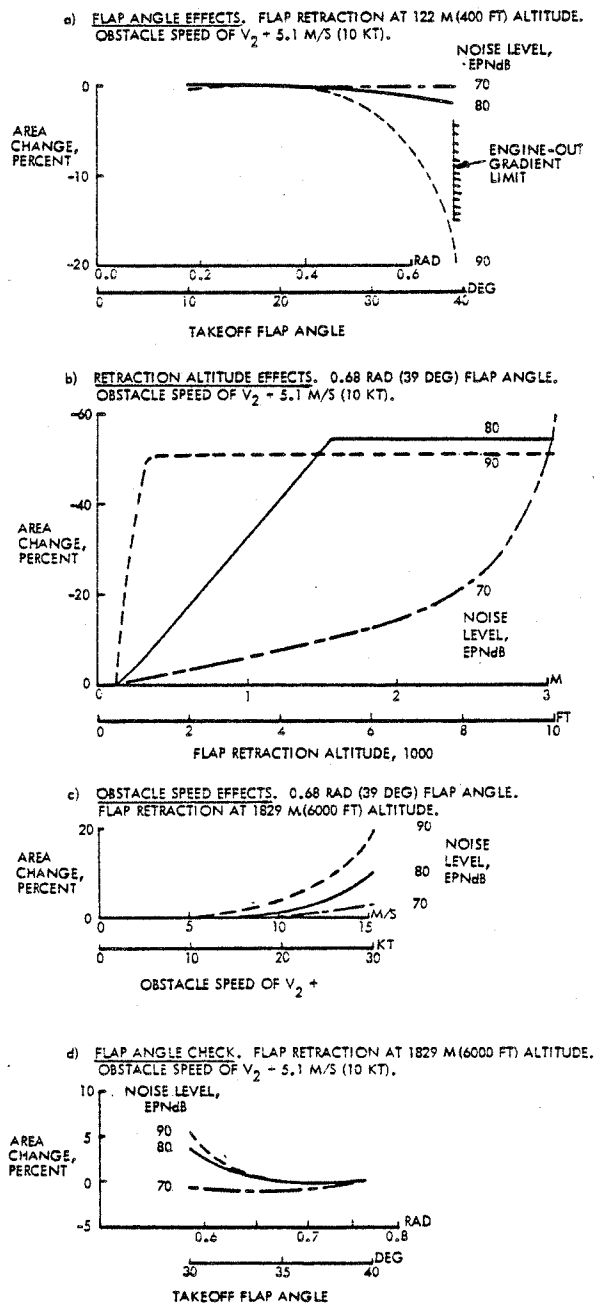

Figure N-9. Noiseprint Variations Due to Alternate Climb Procedures for No. 2 Turboprop Aircraft at Maximum Rate of Climb

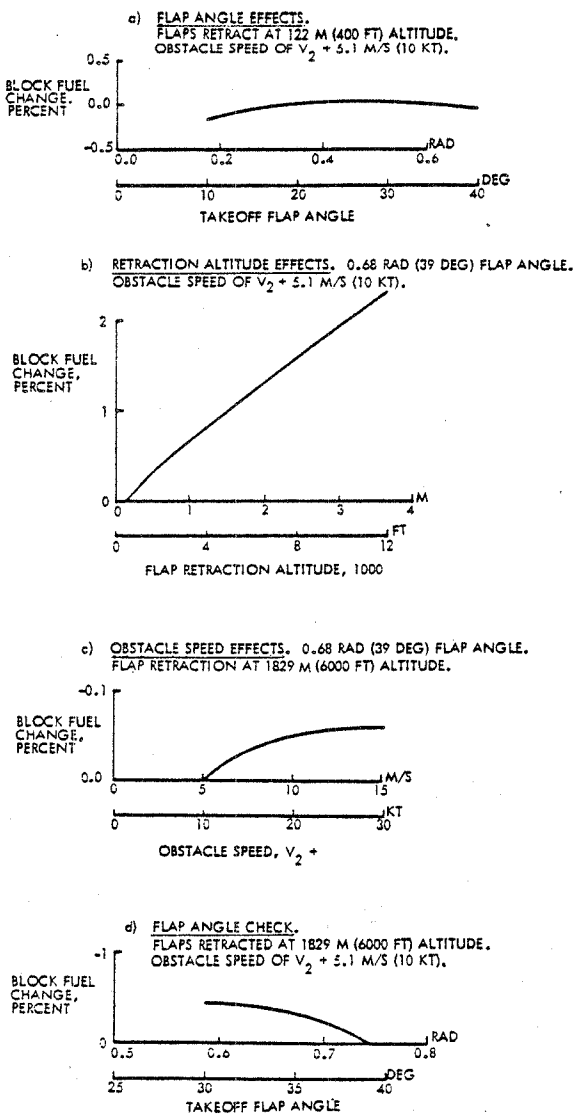

Figure N-10. Fuel Consumption Variations Due to Alternate Climb Procedures for No. 2 Turboprop Aircraft at Maximum Rate of Climb

angle for all three noise levels, it was selected for use in the subsequent steps.

Results similar to those for the No. 1 Turboprop aircraft were obtained from the investigation of varying flap retraction altitude and obstacle speed. That is, a flap retraction altitude of 1829 m (6000 ft) minimizes the 80-EPNdB noiseprint, and increasing the obstacle speed above the minimum safe value of the baseline has no positive effects.

Flap angle variation was reconsidered for the 1829 m (6000 ft) altitude flap retraction case. The results in part d) of Figures N-9 and N-10 show that both 0.61 rad (35 deg) and 0.68 rad (39 deg) flap angles are equally effective in reducing the 80-EPNdB noiseprint, but that the lower value imposes a smaller fuel penalty, and therefore, is preferred.

Maximum Gradient Climb

Figure N-11 ilustrates the reductions in noiseprint area and the fuel consumption penalties that occur in climbing at maximum gradient, instead of maximum rate, over a portion of the flight profile. In particular, the aircraft climbs at maximum gradient between the altitudes of 122 m (400 ft), where the flaps are retracted, and the values listed along the abscissa of the graph.

The data that contributed to Figure N-11 have been combined with those from part b) of Figure N-9 to obtain the comparative results in Figure N-12. This comparison shows that smaller noiseprints are obtained for the No. 2

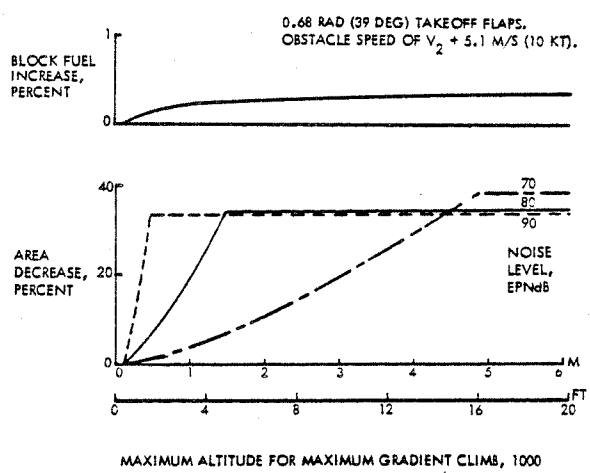

Figure N-11. Maximum Gradient Climb Effects for No. 2 Turboprop Aircraft

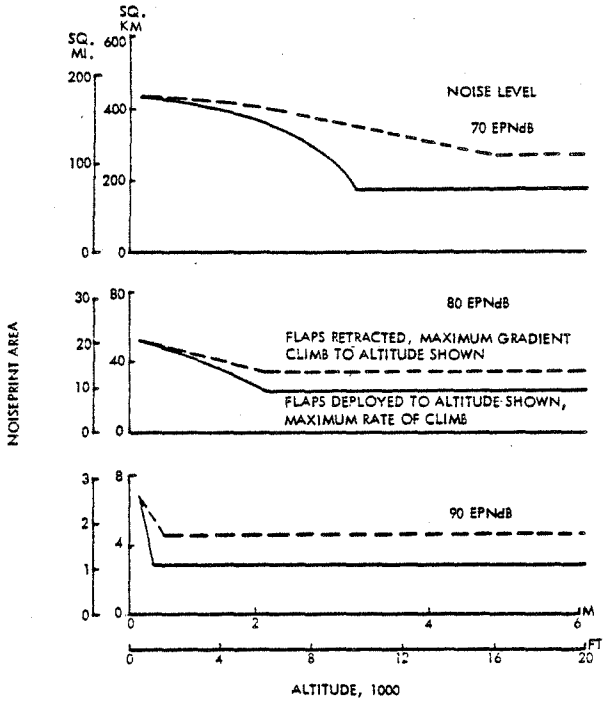

Figure N-12. Comparison of Maximum - Gradient and Maximum-Rate Climb Effects on Noiseprints for No. 2 Turboprop Aircraft

Turboprop Aircraft by keeping the flaps deployed until the aircraft climbs to an altitude which closes the noiseprint, as opposed to simply climbing at maximum gradient until the noiseprint closes.

Cutback Power

Figure N-13 presents the results of studies related to cutback power following takeoff. The initial set of results indicates that the original takeoff flap angle of 0.35 rad (20 deg) is more effective with cutback power than the 0.68 rad (39 deg) angle that is best for the full power case. The middle set confirms that the minimum obstacle speed is preferred. The last set suggests two divergent conclusions. For the 90 EPNdB noiseprint, increasing the cutback altitude above the 305 m (1000 ft) minimum is to be avoided, mainly, because this noiseprint closes when the aircraft reaches an altitude of about 430 m (1400 ft). For the other two cases, delaying power cutback to a higher altitude is beneficial because the aircraft must climb to a relatively much higher altitudes before the noiseprints close. Specifically, the closure altitudes are about 1340 m (4400 ft) for the 80 EPNdB noiseprint and 3290 m (10,800 ft) for the 70 contour.

Figure N-14 compares the extent to which the base noiseprint area, that was previously listed in Table XXX, has been reduced through flight profile

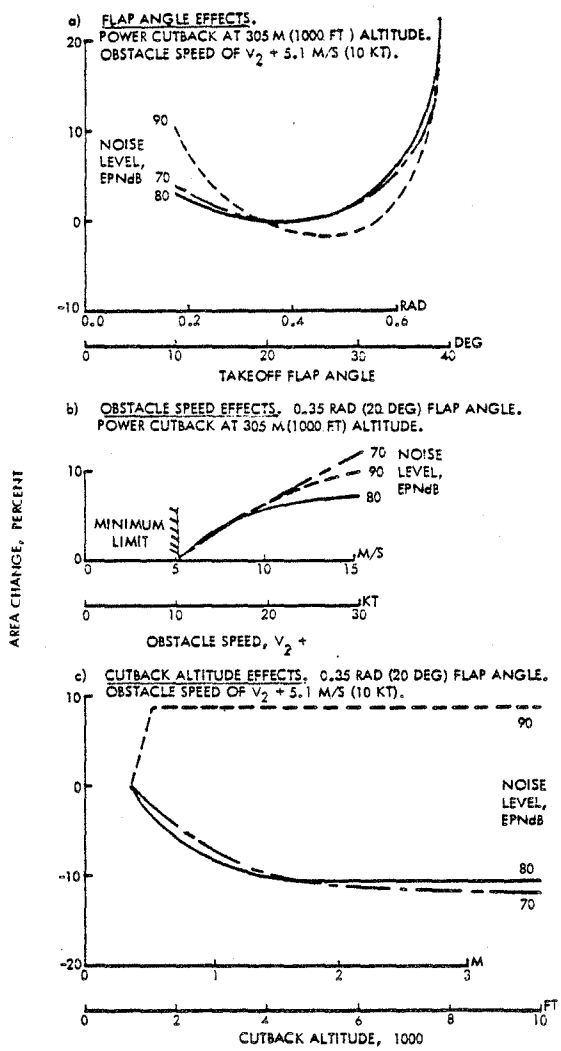

Figure N-13. Effect of Alternate Climb Procedures with Cutback Power for No. 2 Turboprop Aircraft

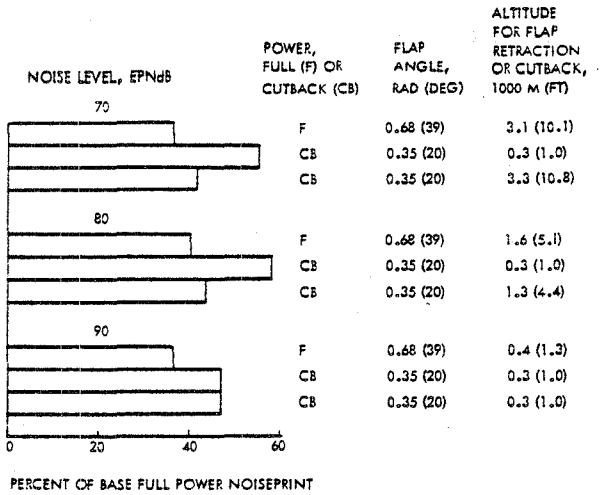

Figure N-14. Comparison of Full and Cutback Power Results for No. 2 Turboprop Aircraft

modifications with full and cutback power. The top bar in the figure for each noise level indicates the reduced noiseprint size, from a previous section, which can be achieved by climbing at full power with some changes to the basic climb-out procedure. The second bar shows the reduced noiseprint size that occurs with power cutback, as reported before in Table XXX. The last bar reflects the benefits of using the optimum altitude for power cutback.

These results show that power cutback offers advantages over the full power base case in reducing the noiseprints. Modifying the flight profile while maintaining full power provides the greatest noiseprint reduction, however.

NO. 1 TURBOFAN

Analysis of alternative flight profiles for the two competitive turbofan aircraft followed the same sequence as for the turboprop aircraft. That is, the initial variations were in conjunction with a maximum rate of climb, while the subsequent ones were for a maximum gradient climb. Because of the comparative characteristic of turbofans, relative to turboprops, of being takeoff thrust limited, and in view of the marginal to negative results listed in Table XXX for cutback power on the baseline aircraft, no consideration was given to cutback power as part of the flight profile alternatives for the two turbofan aircraft in this study.

Maximum Rate of Climb

Figure N-15 shows the noiseprint changes that were obtained and the sequential approach that was followed in analyzing different takeoff flap angles, flap retraction altitudes, and obstacle speeds. The corresponding effects on block fuel are presented in Figure N-16.

As indicated in part a) of Figure N-15, the No. 1 Turbofan Aircraft has very little flexibility in its takeoff flap angle. If the flaps are set greater than 0.35 rad (20 deg), the aircraft cannot meet the minimum gradient requirements of FAR 25 with an

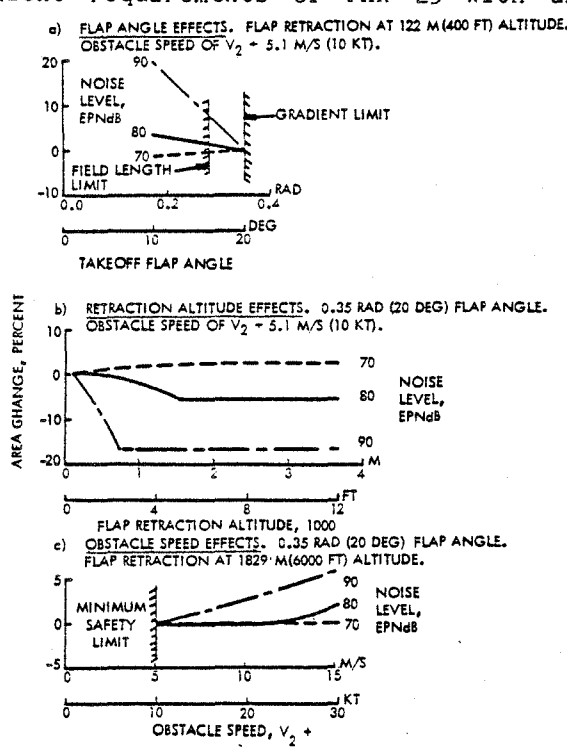

Figure N-15. Noiseprint Variations Due to Alternate Climb Procedures for No. 1 Turbofan Aircraft at Maximum Rate of Climb

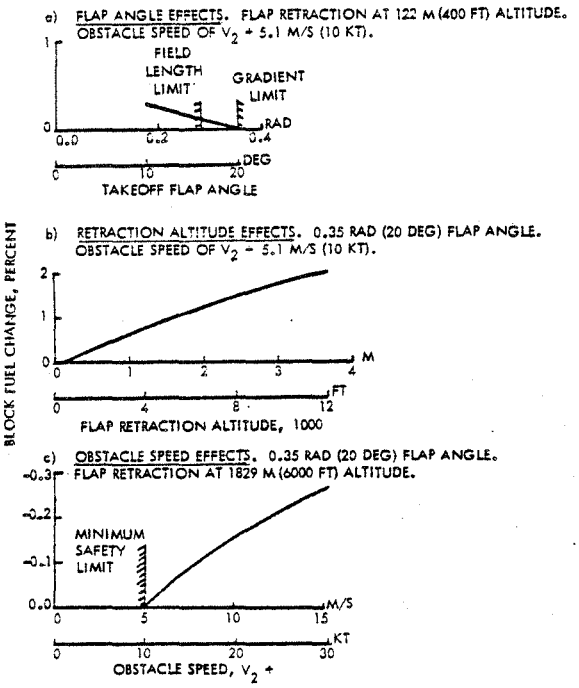

Figure N-16. Fuel Consumption Variations Due to Alternate Climb Procedures for No. 1 Turbofan Aircraft at Maximum Rate of Climb

engine out during second segment climb. Alternatively, if the flap angle is less than 0.28 rad (16 deg), the aircraft cannot takeoff within the 2440 m (8000 ft) field length limit. Within these two constraints, the smallest noiseprint occurs at a 0.35 rad (20 deg) angle for the 80 EPNdB base level. This angle is also best for the 90 EPNdB level, and it penalizes the 70 EPNdB noiseprint by less than one half of one percent.

Leaving the flaps deployed to higher altitudes is beneficial in reducing the noiseprints for both the 80 and 90 EPNdB noise levels, as shown in part b) of Figure N-15. However, the trend is that the lower the desired noise level, the less beneficial is prolonged flap deployment likely to be. In fact, for the quietest level of 70 EPNdB, the noiseprint area is increased when the flaps stay deployed. This trend reflects the relatively limited takeoff thrust characteristic of turbofan powered aircraft. Once the aircraft gains its initial increment of altitude on takeoff, continued flap deployment limits subsequent climb because the drag of the flaps retards aircraft acceleration, thereby negating the more extensive climb capability that can be achieved through higher speed.

As determined for the turboprop aircraft, increasing the obstacle speed was detrimental to attempts to decrease the noiseprints.

Maximum Gradient Climb

Figure N-17 shows the reductions in noiseprint area and the fuel consumption penalties that occur in climbing at maximum gradient, instead of maximum rate, over a portion of the flight profile. In particular, the aircraft climbs at maximum gradient between the altitudes of 122 m (400 ft), where the flaps are retracted, and the values listed along the abscissa of the graph.

The data that contributed to Figure N-17 have been combined with those from part b) of Figure N-15 to obtain the comparative results in Figure N-18. This comparison shows that smaller noiseprints are obtained at 70 and 80 EPNdB for the No. 1 Turbofan Aircraft

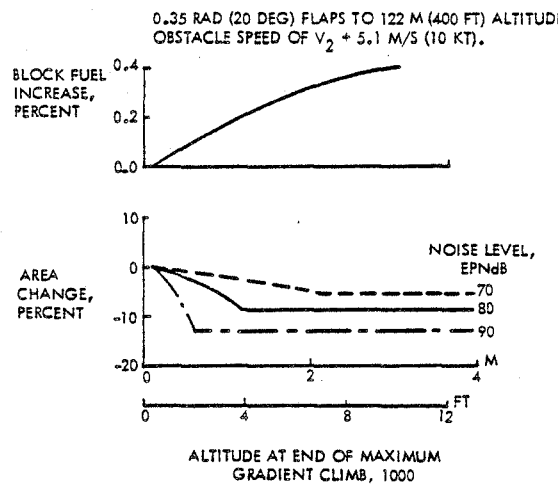

Figure N-17. Maximum Gradient Climb Effects for No. 1 Turbofan Aircraft

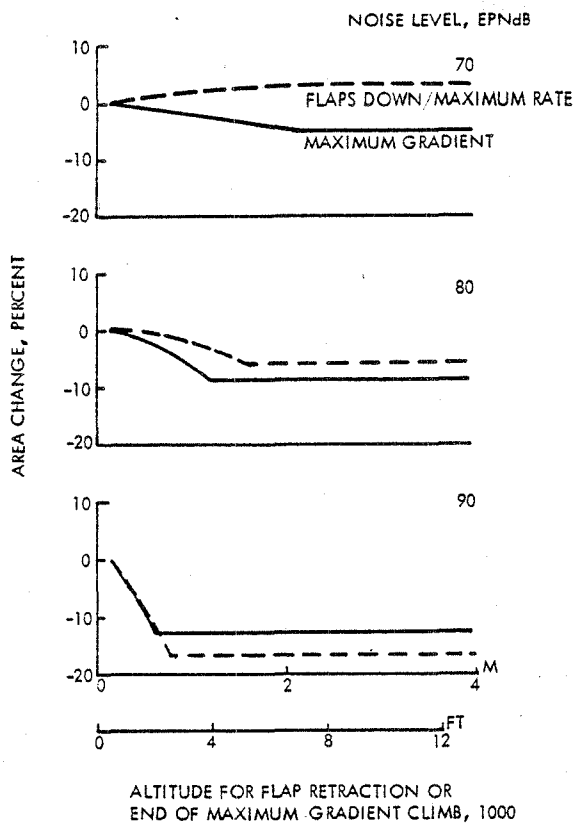

Figure N-18. Comparison of Maximum - Gradient and Maximum - Rate Climb Effects on Noiseprints for No. 1 Turbofan Aircraft

by retracting the flaps at 122 m (400 ft) altitude and climbing at maximum gradient until the noiseprint closes, rather than by leaving the flaps deployed and climbing at the maximum rate. At the 90 EPNdB level the reverse occurs; maximum benefits are achieved by leaving the flaps deployed until the noiseprint closes.

NO. 2 TURBOFAN

As in the previous cases, the analysis was done first for maximum rate of climb and then for maximum gradient climb. Flap angle variations were not investigated because this aircraft was sized by the field length and engine-out gradient limitations.

Maximum Rate of Climb

Changes to the noiseprint area that can be obtained by varying the flap retraction altitude or obstacle speed are presented in Figure N-19. Figure N-20 shows the associated changes in block fuel consumption.

The trends for this aircraft are very similar to those for the No. 1 Turbofan Aircraft. Thus, the discussion of the trends in the previous section is equally applicable here.

Maximum Gradient Climb

Figure N-21 shows the reductions in noiseprint area and the fuel consumption penalties that occur in climbing at maximum gradient, instead of maximum rate, between flap retraction at 122 m (400 ft) altitude and the altitude

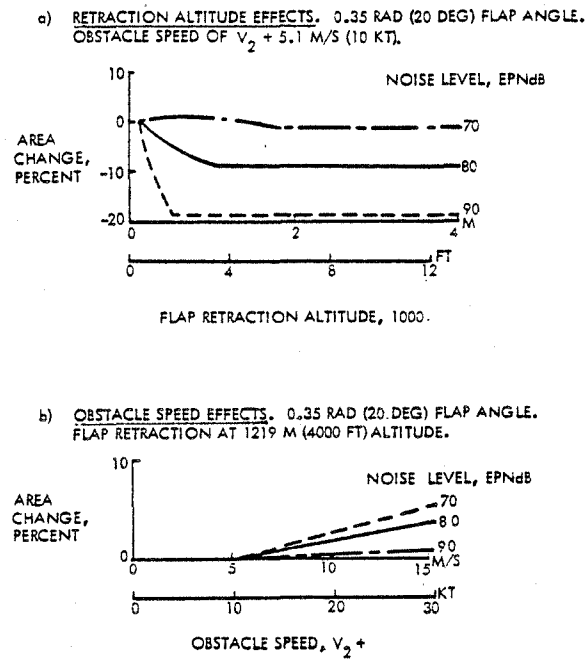

Figure N-19. Noiseprint Variations Due to Alternate Climb Procedures for No. 2 Turbofan Aircraft at Maximum Rate of Climb

a) RETRACTION ALTITUDE EFFECTS. 0.35 RAD (20 DEG) FLAP ANGLE. OBSTACLE SPEED OF V_2 + 5.1 M/S (10 KT).

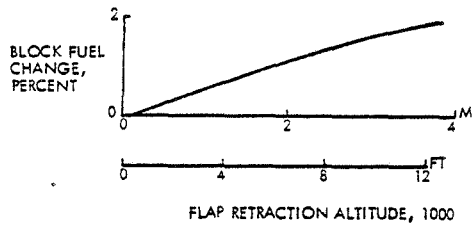

FLAP RETRACTION ALTITUDE, 1000

b) OBSTACLE SPEED EFFECTS. 0.35 RAD (20 DEG) FLAP ANGLE. FLAP RETRACTION AT 1219 M (4000 FT) ALTITUDE

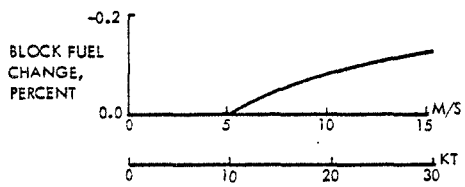

OBSTACLE SPEED, V_2 +

Figure N-20. Fuel Consumption Variations Due to Alternate Climb Procedures for No. 2 Turbofan Aircraft at Maximum Rate of Climb

0.35 RAD (20 DEG) FLAPS TO 122 M (400 FT) ALTITUDE. OBSTACLE SPEED OF V_2 + 5.1 M/S (10 KT).

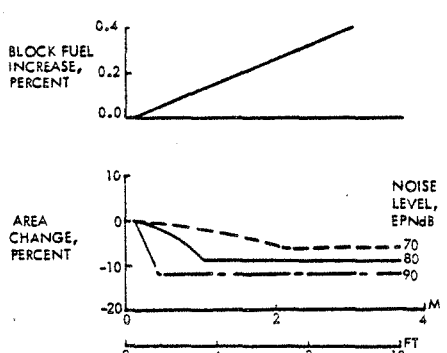

ALTITUDE AT END OF MAXIMUM GRADIENT CLIMB, 1000

Figure N-21. Maximum Gradient Climb Effects for No. 2 Turbofan Aircraft

values on the graph. These results have been combined with those of Figure N-19 to obtain the comparisons in Figure N-22. The same trend is obtained as for the No. 1 Turbofan Aircraft but with a slight shift. At the 90 EPNdB noise level, continued flap deployment is still the best way to minimize the noiseprint. Also, at the 70 EPNdB level, climbing at the maximum gradient is still the best. However, at the 80 EPNdB level, both methods are now equally effective.

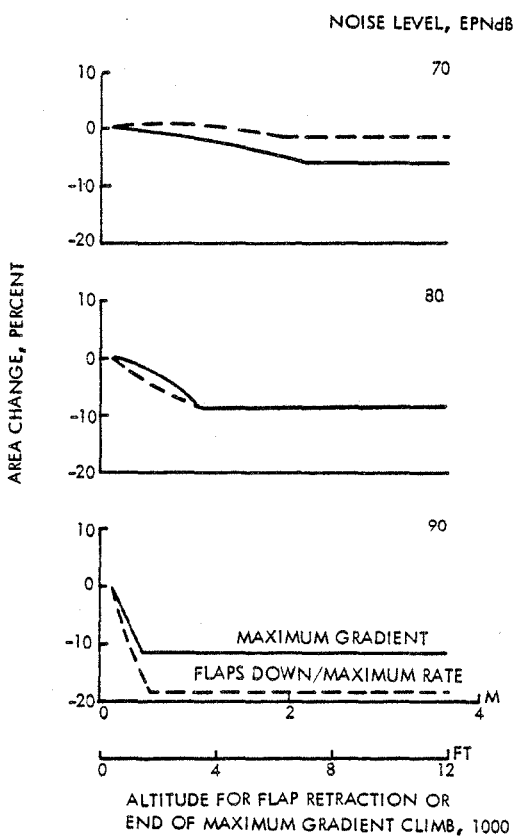

ALTITUDE FOR FLAP RETRACTION OR END OF MAXIMUM GRADIENT CLIMB, 1000

Figure N-22. Comparison of Maximum-Gradient and Maximum-Rate Climb Effects on Noiseprints for No. 2 Turbofan Aircraft

APPENDIX O. SUMMARY OF C-X REQUIREMENTS FOR APPLICATION STUDY

MISSIONS

Mission fuel loads are to be computed assuming a 1962 U.S. Standard Atmosphere and military reserves.

1. Maximum Payload Mission. Carry 59,090 kg (130,000 lb) or more at 2.25 g's over an unrefueled range that is to be determined (TBD). Carry the maximum 2.25-g payload over an unrefueled range of 4445 km (2400 NM); the initial portion may be flown at less than 2.25 g's but not less than 2.0 g's.

2. Heavy Logistics Mission. Carry the larger of 54,545 kg (120,000 lb) or 92 percent of the maximum 2.25-g payload at 2.25 g's over a 4445 km (2400 NM) unrefueled range.

3. Intertheater Logistics Mission. Carry the greater of 45,455 kg (100,000 lb) or 75 percent of the maximum 2.25-g payload at 2.5 g's over a 5185 kg (2800 NM) unrefueled range.

4. High Performance Logistics Mission. Carry the greater of 31,820 kg (70,000 lb) or 50 percent of the maximum 2.25-g payload both directions on a 925 km (500 NM) combat radius mission, unrefueled, at 3 g's.

5. Ferry Range. Have a 9250 km (5000 NM) unrefueled range with no payload at 2.5 g's.

SPEEDS

1. Cruise Speed. Perform the required missions at a cruise speed of at least 0.7 Mach number at an initial cruise altitude of at least 7925 m (26,000 ft).

2. Airdrop Speed. As a design goal, the maximum airdrop speed shall be 129 m/s IAS (250 KIAS). In stabilized level flight, airdrops will be made at speeds between 1.2 times the stall speed (not to exceed 67 m/s IAS (130 KIAS) and 120 m/s IAS (235 KIAS), for altitudes between sea level and 7620 m (25,000 ft), and for the aircraft gross weights required by the missions.

3. Low Altitude Speed. Have a cruise airspeed of at least 154 m/s IAS (300 KIAS) and a maximum level flight speed of 180 m/s IAS (350 KIAS) between sea level and 4570 m (15,000 ft) altitudes for the specified missions.

NOISE

Comply with FAR 36, stage 3.

FIELD PERFORMANCE

The aircraft shall be capable of performing the following takeoff, landing, and ground operations at sea level on a 32°C (90°F) day.

1. Maximum Gross Weight Takeoff. At the maximum weight for the required missions, be capable of safe and routine takeoffs from a 2590-m (8500-ft) paved runway with a load classification group (LCG) III rating.

2. Small Austere Airfield Takeoff. At the midpoint takeoff gross weight for the High Performance Mission, be capable of safe and routine takeoffs from a 915-m (3000-ft) long by 27-m (90-ft) wide load classification number (LCN) 40 paved runway.

3. Critical Engine Inoperative Takeoff. With the most critical engine inoperative, be capable of takeoff from a 915-m (3000-ft) long by 27-m (90-ft) wide LCN 40 paved runway

with no payload and the fuel required at the midpoint of the High Performance Mission.

4. Blown Tire Takeoff. Be capable of takeoff with one blown tire, no payload, and the fuel required at the midpoint of the High Performance Mission.

5. Normal Landing. Be capable of safe and routine landings on a 1220-m (4000-ft) long by 27-m (90-ft) wide LCG IV paved runway with the maximum 2.25-g payload and fuel to fly a 925 km (500 NM) range mission with zero payload.

6. Maximum Effort Landing. Be capable of maximum effort landings on a 915-m (3000-ft) long by 27-m (90-ft) wide LCN 40 paved runway with a payload of 45,455 kg (100,000 lb) or 75 percent of the maximum 2.25-g payload, whichever is greater, and fuel to fly a 925 km (500 NM) range mission with zero payload.

7. Maximum Payload Landing. Be capable of maximum effort landings on a 915-m (3000-ft) long by 27-m (90-ft) wide LCG IV paved runway with the maximum 2.25-g payload and the fuel to fly a 555 km (300 NM) range mission with zero payload.

8. Ground Flotation. Have a LCN not greater than 40 when carrying the larger of a 45,455-kg (100,000-lb) payload or 75 percent of the maximum 2.25-g payload, and fuel to fly a 925 km (500 NM) range mission with zero payload. Be capable of operating on designated unpaved, semi-prepared, compacted surface (sand, gravel, etc.) runways.

9. Ground Maneuvering. Must maintain at least a 7.6-m (25-ft) clearance from other aircraft and ramp obstructions. When parked shall not prevent another aircraft from taxiing to or from its parking space. Once parked for loading/unloading will not be moved until loading/unloading is completed. Small austere airfield ramp is 76-m (250-ft) by 91 m (300-ft) with access via 15-m (50-ft) wide taxiway to center of 91-m (300-ft) long side.

10. Turning. It is desired that the C-X be capable of a 3.14 rad (180 degree) turn on a 27-m (90-ft) wide LCN 40 paved runway with not more than three maneuvers and without external assistance.

11. Backing Up. Be capable of backing up a 1.5 percent grade on a LCG IV paved runway with the maximum 2.25-g payload and fuel to fly a 1850 km (1000 NM) range mission.

12. Minimum Runway Width. Be capable of operating from 18-m (60-ft) wide runways when turn areas or access to a parallel taxiway are provided at both ends of the runway.

Note: Landing distance for runways 1220 m (4000 ft) or more will be computed as the horizontal distance from 15 m (50 ft) over the threshold to a complete stop using maximum braking and idle reverse. For runways 915 m (3000 ft) long, landing distance will be computed as the distance from touchdown to a complete stop plus 152 m (500 ft) using maximum braking and idle reverse.

AIRDROP

The aircraft shall be capable of conducting high and low altitude airdrops of paratroopers and equipment under good and adverse weather conditions.

1. Platforms and containers are to be airdropped from a centerline mounted rail/roller system compatible with the 274-cm (108-in.) wide U.S. Army Type II and Type V airdrop platforms. Provisions shall be

made for sequential airdrops of any possible combination of 2.4, 3.7, 4.9, 6.1, 7.3 and 8.5-m (8, 12, 16, 20, 24 and 28-ft) platform lengths totaling up to 45,455 kg (100,000 lb) in gross rigged weight and at least 18 m (60 ft) in platform length. For sequential airdrop, the maximum unit load will not exceed 15,910 kg (35,000 lb). For airdrop and Low Altitude Parachute Extraction System (LAPES) of single platform loads, provisions will be made for payload weights of at least 22,725 kg (50,000 lb). Provisions will be made for airdrop and LAPES of oversize loads up to and including the M551, Armored Reconnaissance Airborne Assault Vehicle, TOE-Line Item A93125, rigged per Army FM 10-515/AF TO 13C7-10-181. As a minimum, the aircraft shall be capable of simultaneous and sequential airdrop of TBD Container Delivery System A-22 supply containers at 1070 kg (2350 lb) each, from high 7620 m (25,000 ft) or low 183 m (600 ft) altitudes.

2. Provisions will be made to airdrop combat equipped paratroops using static line deployed parachutes. The airdrop equipment shall permit at least 100 troops preceded by at least four A7A/A21 equipment bundles to exit the aircraft in 55 seconds.

CARGO COMPARTMENT

The cargo compartment will be sized to permit the loadmaster access around the periphery of the cargo box (front, back, and sides) while the aircraft is in flight with the maximum volume of cargo aboard. While the aircraft is in flight, a single loadmaster will be able to reconfigure the cargo compartment for rolling stock, palletized cargo, troop transport, or aeromedical evacuations. For preplanned aeromedical evacuations, there will be a minimum of 48 litter positions and 54 seats with emergency oxygen for each litter and seat.

CARGO RESTRAINT

Cargo restraint provisions will accommodate ultimate loads acting separately up to:

Longitudinal - 3 g's forward, 1.5 g's aft

Lateral - 1.5 g's

Vertical - 4.5 g's down, 2 g's up

RAMP

The cargo compartment ramp will be capable of being raised from, and lowered to, rear ground level from within the cargo compartment while supporting the cargo load to be carried on the ramp in flight. The ramp, including extensions and/or toes will be capable of making contact with a ground plane 0.3 m (1 ft) below the ground level of the aircraft at any gross weight.

CARGO ITEMS REQUIRING AIRLIFT

The aircraft will be capable of airlift of a large variety of cargo items of rolling stock, containers, and pallets, and airdrop/extraction of platform loads of vehicles and supplies.

1. Rolling Stock. The aircraft will be capable of airlifting significant elements of equipment items of the USAF, USMC, and of U.S. Army Airborne, Airmobile, Armor, or Infantry Divisions. Any items which cannot be carried shall be identified. Clearances between all vehicles are 15.2 cm (6 in.). Clearances between vehicles and sidewalls, bulkheads, overhead, and doors will be at least 15.2 cm (6 in.). Vehicles will not be stacked

or loaded sideways. Vehicles married in the vehicle list will stay together.

2. Containers. Provisions will be made for airlifting vans, shelters, and containers which are configured for interface with a 274-cm (108-in.) wide 463L materials handling rail system. Slave pallets may be used if necesary. For sizing use:

    a. 2.4-m (8-ft) wide by 2.6-m (8.5-ft) high by 6.1-m (20-ft) long ocean container mounted on a 274-cm (108-in.) wide by 8-cm (3-in.) high by 6.1-m (20-ft) long adapter pallet with a total gross weight of 21,365 kg (47,000 lb).

    b. 2.4 m (8-ft) wide by 2.6-m (8.5-ft) high by 12.2-m (40-ft) long ocean container mounted on a 274-cm (108-in.) wide by 2.6-m (8.5-ft) high by 12.2-m (40-ft) long adapter pallet with a total gross weight of 32,725 kg (72,000 lb).

3. Pallets. Be capable of airlifting USAF type HCU-6/E cargo pallets as defined by MIL-P-27443 at maximum gross weights of 4680 kg (10,300 lb) each, including tare weight of pallet and net. Be able to carry at least 75 percent of the maximum 2.25-g payload on pallets so that the pallet density shall not exceed 3000 kg (6,600 lb) per pallet.

AERIAL REFUELING

The Universal Aerial Refueling Receptacle Slipway Installation will be used to provide aerial refueling from the Air Force KC-135 and KC-10 aircraft.

REFERENCES

1. C. Rohrbach and F. B. Metzger, "The Prop-fan - A New Look in Propulsors," AIAA Paper 75-1208, Hamilton Standard, October 1975.

2. A. H. Jackson, Jr. and B. S. Gatzen, "Multi-Mission Uses for Prop-fan Propulsion," AGARD Paper, Hamilton Standard, September 1976.

3. B. S. Gatzen and S. M. Hudson, "Generalized Characteristics of Fuel Conservative Prop-fan Propulsion System," SAE Paper 751085, Hamilton Standard and Detroit Diesel Allison, November 1975.

4. J. F. Dugan, Jr., B. S. Gatzen and W. M. Adamson, "Prop-fan Propulsion, Its Status and Potential," SAE Paper 780995, NASA-Lewis and Hamilton Standard, November 1978.

5. E. F. Kraus and J. C. Van Abkoude, "Cost/Benefit Tradeoffs for Reducing the Energy Consumption of the Commercial Air Transportation System," NASA CR-137923, 137924, 137925, Douglas Aircraft, June 1976.

6. J. P. Hopkins and H. E. Wharton, "Study of the Cost/Benefit Tradeoffs for Reducing the Energy Consumption of the Commercial Air Transportation System," NASA CR-137926 and 137927, Lockheed-California, August 1976.

7. "Energy Consumption Characteristics of Transports Using the Prop-fan Concept," NASA CR-137937 and 137938, Boeing Commercial Airplane Co., October 1976.

8. J. D. Revell and R. H. Tullis, "Fuel Conservation Merits of Advanced Turboprop Transport Aircraft," NASA CR-152096, Lockheed-California, August 1977.

9. C. Rohrbach, "A Report on the Aerodynamic Design and Wind Tunnel Test of a Prop-fan Model," AIAA Paper 76-667, Hamilton Standard, July 1976.

10. D. C. Mikkelson et al, "Design and Performance of Energy Efficient Propellers for Mach 0.8 Cruise," SAE Paper 770458, NASA-Lewis, 1977.

11. J. F. Dugan, Jr., D. P. Bencze, and L. J. Williams, "Advanced Turboprop Technology Development," AIAA Paper 77-1223, NASA-Lewis and Ames, August 1977.

12. J. A. Baum et al, "Prop-fan Data Support Study," NASA CR-152141, Hamilton Standard, February 1978.

13. H. R. Welge and J. P. Crowder, "Simulated Propeller Slipstream Effects on a Supercritical Wing," NASA CR-152138, Douglas Aircraft, June 1978.

14. M. L. Boctor et al, "An Analysis of Prop-fan/Airframe Aerodynamics Integration," NASA CR-152186, Boeing Commercial Airplane Co., October 1978.

15. J. V. Bowles, T. L. Galloway and L. J. Williams, "Turboprop/Propfan Performance and Installation Considerations for Advanced Tranport Aircraft," SAE Paper 780996, NASA-Ames, November 1978.

16. D. P. Bencze, R. C. Smith, H. R. Welge, and J. P. Crowder, "Propeller Slipstream/Wing Interaction at M = 0.8," SAE Paper 780997, NASA-Ames and Douglas Aircraft, November 1978.

17. F. B. Metzger and C. Rohrback, "Aeroacoustic Design of the Prop-fan," AIAA Paper 79-0610, Hamilton Standard, March 1979.

18. D. B. Hanson, "The Influence of Propeller Design Parameters on Far Field Harmonic Noise in Forward Flight," AIAA Paper 79-0609, Hamilton Standard, March 1979.

19. D. B. Hanson, "Near Field Noise of High Tip Speed Propellers in Forward Flight," AIAA Paper 76-565, Hamilton Standard, July 1976.

20. D. B. Hanson and M. R. Fink, "The Importance of Quadrupole Sources in Prediction of Transonic Tip Speed Propeller Noise," Journal of Sound and Vibration, Vol. 62, January 1979.

21. "Noise Standards: Aircraft Type Certification," Federal Aviation Regulations, Part 36 (FAR 36), Federal Aviation Administration, Department of Transportation, November 1976.

22. "Preliminary Performance and Installation Data for the STF477 Turbofan Engine," CDS-6, Pratt & Whitney, February 1976.

23. "Preliminary Performance and Installation Data for the STS487 Turboshaft Engine," CDS-11, Pratt & Whitney, March 1976.

24. "Standard Method of Estimating Direct Operating Costs of Turbine Powered Transport Aircraft," Air Transport Association, 1967.

25. "Airworthiness Standards: Transport Category Airplanes," Federal Aviation Regulations, Part 25 (FAR 25), Federal Aviation Administration, Department of Transportation, 1974.

26. F. R. Stone, "Propfan Data Base for Parametric Aircraft Studies," LG79ER0128, Lockheed-Georgia, August 1979.

27. D. L. Bouquet, "Strategic Airlift Aircraft Design Study, (Issues of Commonality)," Lockheed-Georgia Final Report on Air Force Contract F33615-78-C-0115, December 1979.

28. A. P. Pennock, "EPNL Prediction Program," LG78ER0211, Lockheed-Georgia, September 1978.

29. N. Searle, "A Parametric Method for Predicting the Far-Field Noise and Footprint Area for Propfan-Powered Aircraft," LG79ER0163, Lockheed-Georgia, October 1979.

30. N. Searle, "A Parametric Method for Predicting the Far-Field Noise and Footprint area for Turbofan-Powered Aircraft," LG80ER0023, Lockheed-Georgia, January 1980.

31. G. Swift and P. Mungur, "A Study of the Prediction of Cruise Noise and Laminar Flow Control Noise Criteria for Subsonic Air Transports," NASA CR-159104, -159105, Lockheed-Georgia, November 1979.

32. M. F. Heidemann, "Interim Prediction Method for Fan and Compressor Source Noise," NASA TMX 71763, June 1975.

33. "V/STOL Rotary Propulsion System Noise Prediction and Reduction," FAA-RD-76-49, Hamilton Standard, May 1976.

34. R. K. Matta, G. T. Sanduski, and V. L. Doyle, "GE Core Engine Noise Investigation - Low Emission Engines, FAA-RD-77-4, General Electric, 1977.

35. J. R. Stone, "Interim Prediction Method for Jet Noise," NASA TMX 71618, 1975.

36. M. R. Fink, "Airframe Noise Prediction," FAA-RD-77-29, United Technologies Research Center, March 1977.

37. S. G. Thompson, "Aircraft Life-Cycle Cost Evaluation (ALICE) Model," LG77ER0084, Lockheed-Georgia, April 1977, Revised March 1980.

38. Smelt and Davies, "Estimation of Increase in Lift Due to Slipstream," RAE R&M No. 1788, British A.R.C., February 1937.

39. D. E. Gray, "Study of Turbofan Engines Designed for Low Energy Consumption," NASA CR-135002, Pratt & Whitney, April 1976.

40. T. P. Higgins et al, "Study of Quiet Turbofan STOL Aircraft for Short Haul Transportation," NASA CR-2355, Lockheed Aircraft, 1973.

41. "Acoustic Effects Produced by a Reflecting Plane," SAE Air 1327, Society of Automotive Engineers, January 1976.

42. F. Farassat, "Theory of Noise Generation from Moving Helicopter Blades with an Application to Helicopter Rotors," NASA TR-R-451, NASA, December 1975.

43. F. Farassat, "Linear Acoustic Formulas for Calculation of Rotating Blade Noise," AIAA Journal, Vol. 19, September 1981.

1. Report No.	2. Government Accession No.	3. Recipient's Catalog No.
NASA CR- 165813		

4. Title and Subtitle	5. Report Date
TURBOPROP CARGO AIRCRAFT SYSTEMS STUDY	NOVEMBER 1981
	6. Performing Organization Code

7. Author(s)	8. Performing Organization Report No.
J. C. Muehlbauer; J. G. Hewell, Jr.; S. P. Lindenbaum; C. C. Randall; N. Searle; and R. G. Stone, Jr.	LG81ER0222
	10. Work Unit No.

9. Performing Organization Name and Address	11. Contract or Grant No.
LOCKHEED-GEORGIA COMPANY 86 South Cobb Drive Marietta, Georgia 30063	NAS1-15708
	13. Type of Report and Period Covered

12. Sponsoring Agency Name and Address	13. Type of Report and Period Covered
NATIONAL AERONAUTICS AND SPACE ADMINISTRATION Washington, D.C. 20546	Contractor Report
	14.

15. Supplementary Notes

Contract Monitor: S. J. Morris, NASA Langley Research Center
G.A. Kraft, NASA Lewis Research Center

16. Abstract

Parametric studies determined the effects of advanced propellers (propfan) on aircraft direct operating costs, fuel consumption, and noiseprints. Advanced turboprop aircraft offer these potential benefits, relative to competitive advanced turbofan aircraft: 21-percent fuel saving, 26-percent higher fuel efficiency, 15-percent lower DOCs, and 25-percent shorter field lengths. Fuel consumption for the turboprop is nearly 40 percent less than for current commercial turbofan aircraft.

Aircraft with both types of propulsion satisfy current federal noise regulations. Advanced turboprop aircraft have smaller noiseprints at 90 EPNdB than advanced turbofan aircraft, approximatel y equal noiseprints at 80 EPNdB, but larger noiseprints at 70 EPNdB. The latter levels are usually suggested as quietness goals. The turboprop aircraft easily satisfies the Air Force's C-X requirements with minimal modifications and penalties.

Accelerated development of advanced turboprops is strongly recommended to permit early attainment of the potential fuel saving. Several areas of work have been identified which may produce quieter turboprop aircraft.

17. Key Words (Suggested by Author(s))	18. Distribution Statement
Advanced Turboprops, Prop-fans, Energy Conservation, Energy Efficient Aircraft, Quiet Aircraft, Propeller Noise C-X Aircraft	Unclassified - Unlimited

19. Security Classif. (of this report)	20. Security Classif. (of this page)	21. No. of Pages	22. Price*
Unclassified	Unclassified	234	

*For sale by the National Technical Information Service, Springfield, Virginia 22161

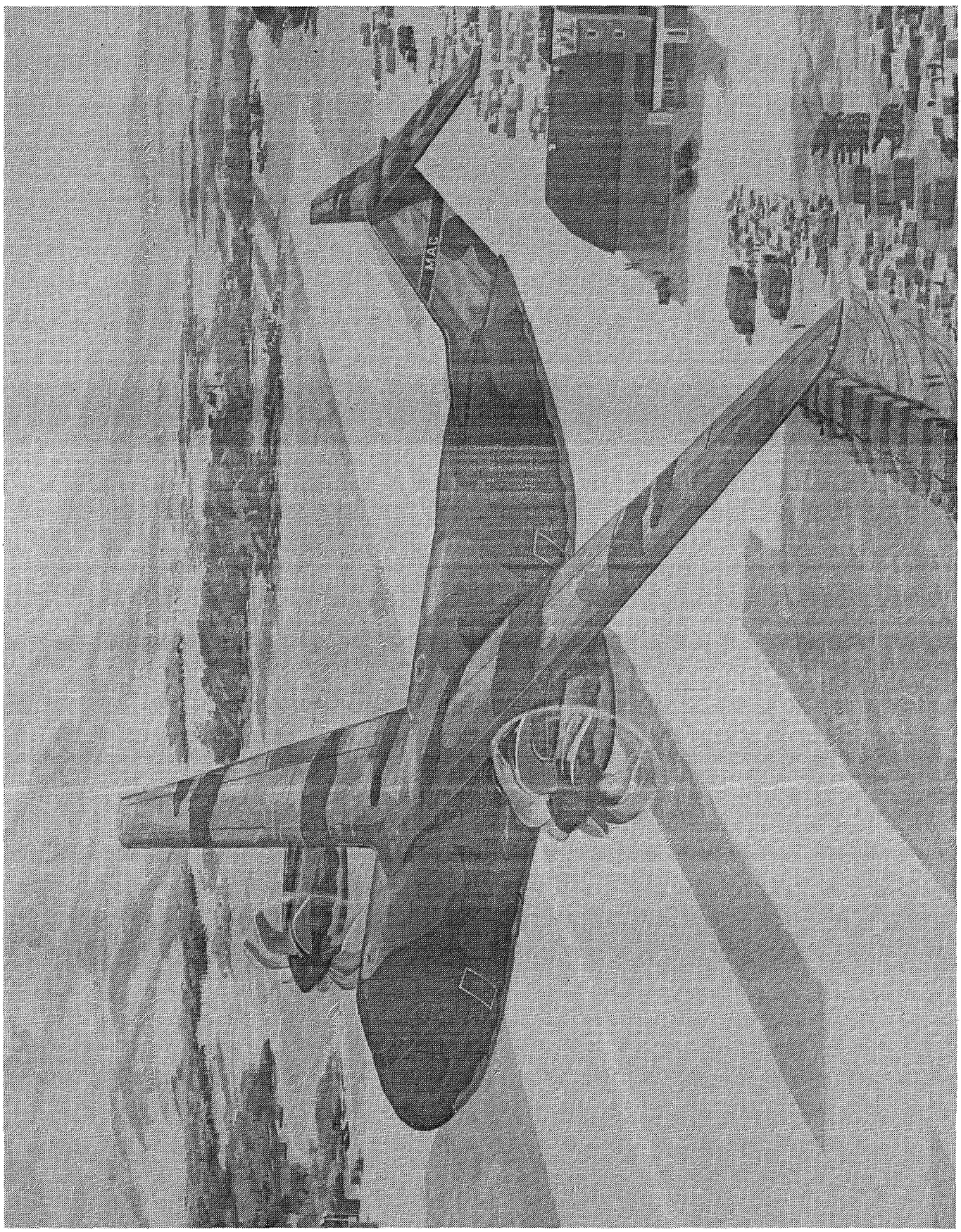

End of Document